LOUGHBOROUGH
UNIVERSITY OF TECHNOLOGY
LIBRARY

AUTHOR
MARTIN, D

COPY NO. 0030402/01

VOL NO. CLASS MARK

ARCHIVES
COPY

FOR REFERENCE ONLY

"THE MECHANICAL BEHAVIOUR OF CARBON FIBRE COMPOSITES AT HIGH RATES OF LOADING"

by

DAVID JOHN MARTIN, BSc (MANCHESTER)

A Doctoral Thesis, submitted in partial fulfilment of the requirements for the award of doctor of philosophy of the Loughborough University of Technology.

AUGUST 1973

Supervisor: L.J. GRIFFITHS, BSc, PhD, M Inst P,
Department of Physics.

© by DAVID JOHN MARTIN, 1973.

Loughborough University
of Technology Library
Date Nov. 73
Class
Acc. No. 030402/01

ACKNOWLEDGEMENTS

The author wishes to thank Dr. L.J. Griffiths for his constant advice and encouragement through the period of study, and Professor J.F. Raffle for his provision of facilities in the Physics Department.

Thanks are also extended to Mr. F.P. Mallinder, formerly of Rolls-Royce Ltd., for his help in initiating the research, and to Mr. C. Hannah, of the Composite Materials Laboratory, Rolls-Royce (1971) Ltd. Derby, for his continued interest and technical assistance, particularly in the supply of carbon fibre materials.

The author was a recipient of an ASSIST post-graduate award, sponsored jointly by Rolls-Royce (1971) Ltd. and the Science Research Council.

ABSTRACT

This thesis describes an investigation of stress wave propagation in solids in order to study the behaviour of materials under simulated impact conditions. The dynamic stress-strain response of carbon fibre composites has been investigated experimentally for a compressive loading of about 40μs duration. The split Hopkinson pressure bar has been used for these measurements, in which cylindrical specimens are sandwiched between two steel rods and deformed under a compressive stress wave induced by impacting the free end of one rod with a 0.22" bullet. An optical recording has been employed, in which the displacement of a metal shutter attached to each steel rod has been monitored during the passage of the pulse. Results have been obtained for several fibre volume fractions, two fibre lay-ups and two fibre directions relative to the impact.

An empirical relation has been proposed for the dynamic behaviour of a composite, to which the resin and fibre contribute in different ways. For the initial small strain, the fibres sustain most of the load until the relaxation effects of the viscoelastic resin appear, and the composite undergoes a larger strain. Measurements at 150°C show that the stress response becomes much more dependent on these viscous properties.

The pulse propagation speed and the local stress-strain during the passage of a pulse in a long composite bar have also been measured, and a simple viscoelastic model is used to interpret this behaviour. Certain specimens have broken after a number of loadings, and the fracture surface has been examined using a scanning electron microscope. Observations of the bulk behaviour suggest that the fibre-matrix bond is of particular importance in determining the composite response.

TABLE OF CONTENTS

CHAPTER 1 INTRODUCTION

1.1 PRELIMINARY REMARKS

The feasibility of using fibre reinforced composites for structural applications in preference to conventional metallic materials has received considerable attention in the last few years. It has been known for some time that the theoretical strength of most materials is never reached in practice because of the presence of microscopic defects in the material in bulk form. These defects may be dislocations which allow plastic flow or microscopic sharp cracks which cause brittle failure. The highest strengths have been observed in "whisker" crystals, which have a very small diameter and are grown in controlled conditions of structural and surface perfection. Such whiskers are usually very susceptible to damage, and have the additional disadvantages of high cost and short lengths. The cheaper, continuous fibres which can be manufactured more readily on a large scale have become the practical reinforcements applied to engineering structures. The many advantages of fibre reinforcement, consisting of fibres embedded in a matrix material, compared with conventional isotropic materials are now of significant value in engineering design. In particular, the advantages of weight, strength and ease of fabrication appeal to the designer. Whether whiskers are ever used as a reinforcement on a large scale or not, they appear to set an upper strength limit for the production of high performance materials.

In spite of the inferior bulk properties of these materials, various reinforcing filaments have been proposed, such as boron, carbon, silica and glass fibres, together with a variety of polymer matrices of either the thermosetting or thermoplastic type. Aluminium has also been used as a matrix material. The two components of a fibre reinforced composite - the fibres and the matrix - each have an important function; the fibres are oriented in the

loading direction and hence carry the principal loads applied, whereas the matrix binds the fibres together to provide dimensional stability so that the load is distributed equally amongst the fibres.

Carbon fibre - epoxy resin composites were initially developed by Rolls-Royce Ltd. as the material for the low pressure compressor (the fan blade) of the RB211 aero-engine. This component of the engine is vulnerable to impact damage caused by bird ingestion, and at an early stage of development it became clear that carbon fibre composites were not suitable for this application, as empirical simulations of bird impact on a rotating fan had shown that catastrophic damage occurred. Consequently, it was of interest to Rolls-Royce Ltd. to examine the behaviour of carbon fibre composites at high rates of loading, and to determine the dynamic stress-strain characteristics of these materials.

It has been known for some time that many materials, when deformed at high strain rates, respond in an appreciably different manner from that observed under conditions of static or quasi-static deformation. When a force is applied to a body under dynamic conditions in which the inertia of the body cannot be ignored, the behaviour must be considered in terms of stress waves. There are several types of wave possible, and the three general types of stress wave which can be propagated in a metal are elastic, plastic and shock waves. The level of applied stress and the stress-strain - strain rate relation of a particular metal determine which waves are present. Rubbers and plastics usually behave non-elastically or with very pronounced time dependence, and viscoelastic waves can propagate in these materials.

It is generally accepted that the strain rate is an important parameter for dynamic conditions, and this will be especially so for

the composite materials which contain fibres embedded in a polymeric matrix. It is the purpose of this thesis to describe the experimental techniques involved in the propagation and measurement of stress waves in carbon fibre composites and to indicate how a strain rate of the order of 500 s^{-1} influences the mechanical behaviour of these materials.

Studies at high rates of loading have been useful in providing information on dislocation mechanisms in crystals, on high speed machining and metal rolling processes in engineering production and on the impact behaviour of structures. Hence accurate experimental data relating stress, strain and strain-rate, accompanied by an adequate theory, is required in many fields of applied science.

1.2 COMPOSITE MATERIALS

1.2.1 Manufacture and general properties

The advantages of fibre reinforcement have already been mentioned; the major attractions being the low density, greater strength compared with metals and the ease of fabrication. The mechanical properties under static conditions of fibre reinforced materials, particularly those involving carbon fibres, have been well documented in several conference reports (e.g. American Society of Metals 1964, National Physical Laboratory, 1971) and by several workers in the subject (Phillips 1967, Tsai, Halpin and Pagano 1967, Kelly 1967 and Mallinder 1970). Many grades and types of fibre reinforcement are now commercially available.

Carbon fibres have as their raw material an acrylic precursor fibre, which is pyrolysed in an inert atmosphere, with or without prior oxidative treatment. The precursor fibre is generally in the form of poly-acrylonitrile chains, with other organic groups such as methyl acrylate and itaconic acid occurring periodically along the chain. Continuous lengths of fibre (diameter 5 - 7 μm) can be produced by extrusion from a spinneret. Controlled temperature and pressure conditions produce a ring structure due to breakdown of the C≡N bond, and at temperatures of 1 000°C to 1 500°C hydrogenation of this ring gives an aromatic structure. Further fusion of adjacent chains liberates nitrogen, leaving the planar graphite structure in an oriented crystalline form (Turner and Johnson, 1969). The individual filaments are wound into a larger structure called a tow, with a nominal size of 130 - 150 μm. These tows are then laid together in a laminate form, with an epoxy resin pre-impregnated onto the fibre surface. The epoxy resin is basically a long chain structure, with a molecular weight of about 3 000. A catalytic crosslinking agent is included in the resin system. The curing cycle for forming

laminated fibres into a composite material consists of three stages: precure, curing under pressure, and postcure. Curing temperatures are typically 150°C - 180°C and curing is chemically irreversible due to the crosslinked structure which forms in the process, and a moulded component will maintain its strength and stiffness at operating temperatures below about 140°C. The laminates can be cut to size in order to fit a particular mould, so that machining after the moulding process may be kept to a minimum. Thus the fabrication is relatively cheap and simple, once the fibres have been manufactured, and this is one of the major advantages of using composite materials. By choice of a suitable fibre with the necessary properties, and a matrix compatible with the fibres, the composite modulus and strength may be varied much more readily than the case of metallic alloys to suit design requirements.

Figure 1.1 shows fibre laminates ("prepregs") and figure 1.2 is an end view of a moulded composite of fibre volume fraction about 60%, showing the distribution of carbon fibres in an epoxy resin matrix. Some static mechanical properties of a carbon fibre composite compared with other engineering materials are shown in table 1. The fibre content in the composite is about 60% by volume (a typical value) and the composite modulus and strength are measured along the fibre direction.

Assuming that when the composite is deformed in the fibre direction both fibres and matrix suffer an equal stain and that both obey Hooke's law to the ultimate strain of the fibres, then a relationship can be formulated for the composite modulus E_c in which:

$$E_c = V_f E_f + (1 - V_f) E_m$$

where V_f = fibre volume fraction

E_f = fibre modulus

E_m = matrix modulus

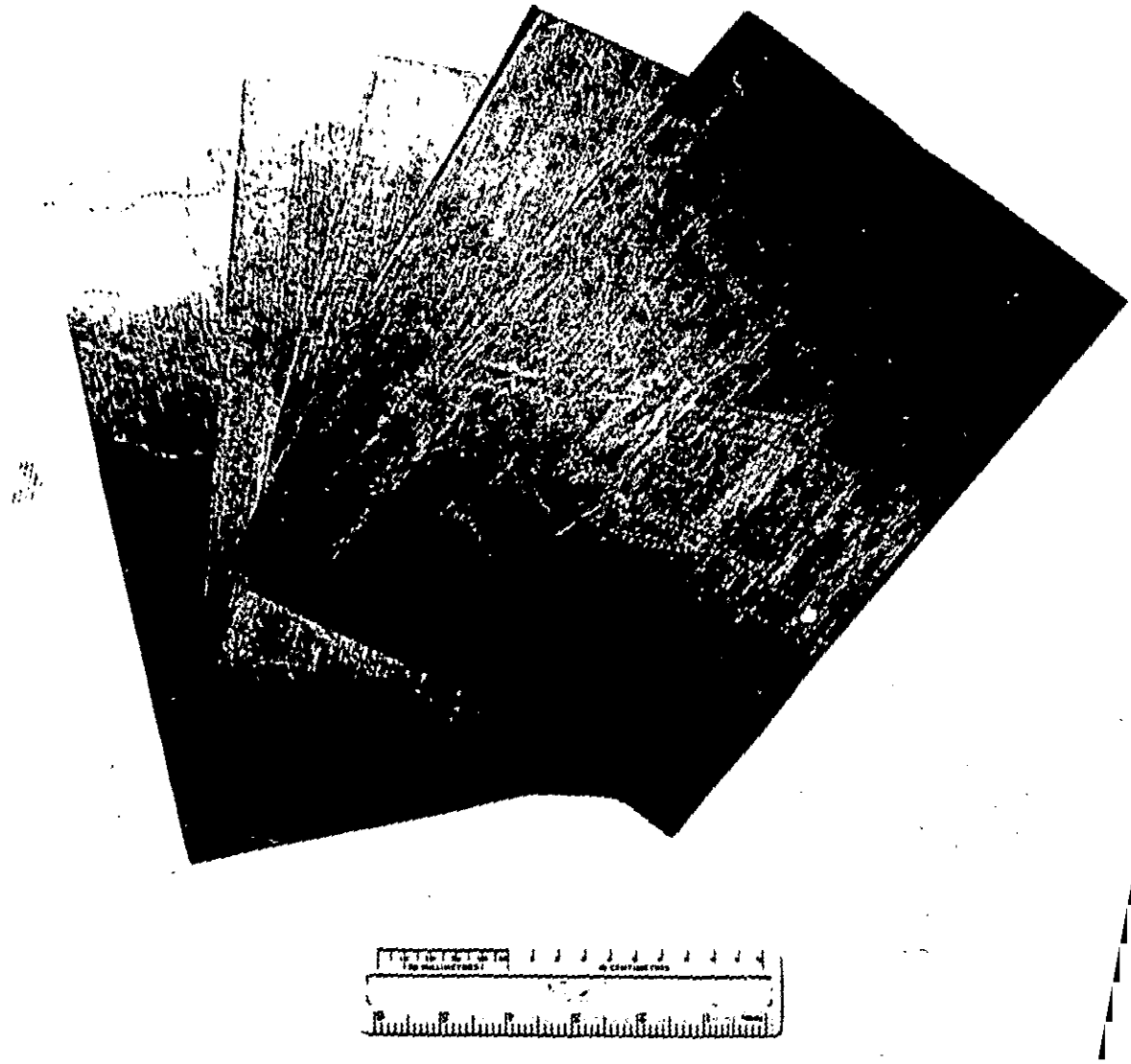

FIG. 1-1

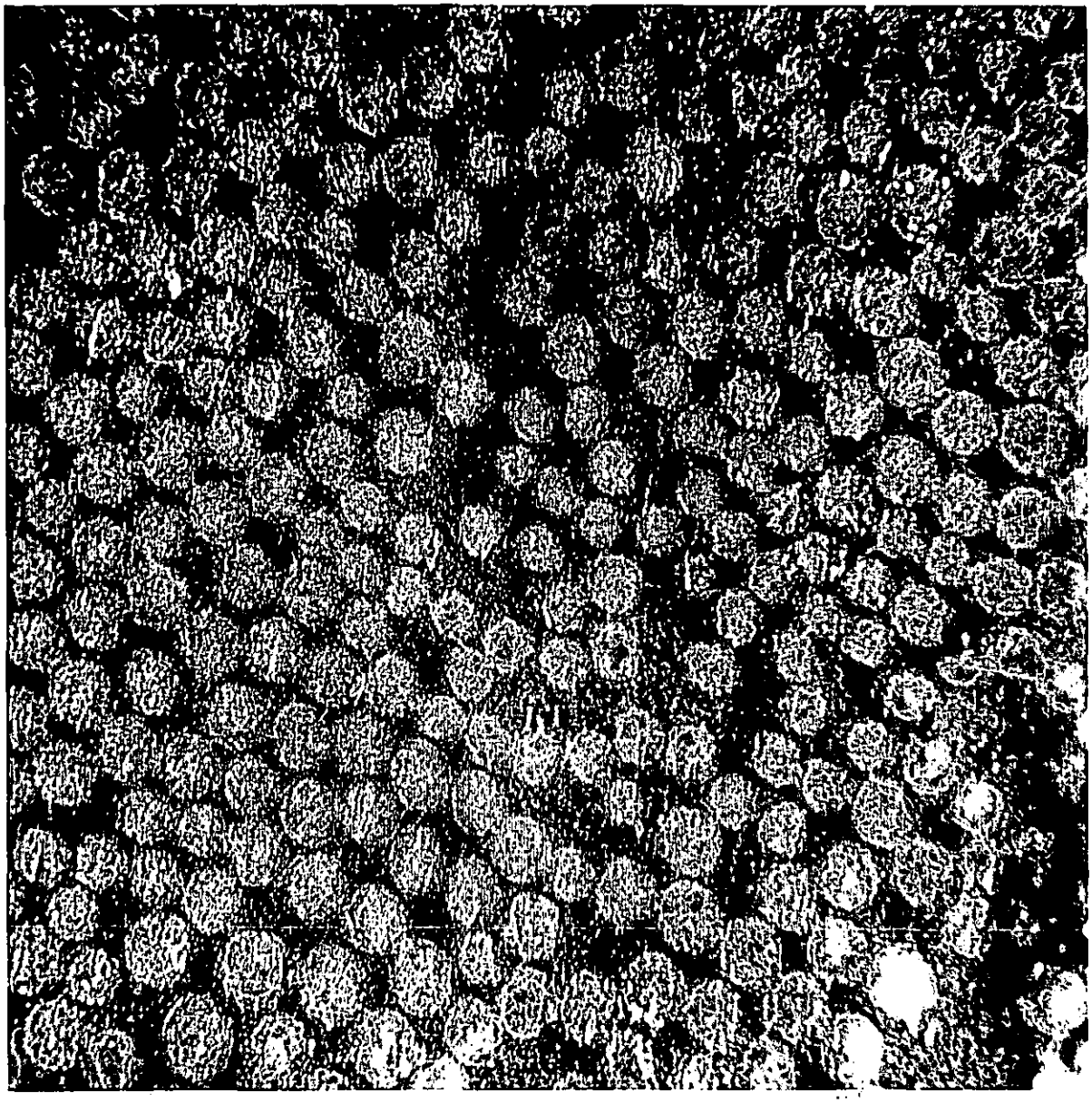

FIG. 1·2 X1050

TABLE 1 Properties of various materials

	Density g/cc	U.T.S. GN/m^2	Modulus GN/m^2	Poisson's ratio
Single fibre	1·8	2·4	180	–
HR4C resin	1·2	0·1	5	0·38
Carbon fibre composite	1·6	1·3	115	0·2 - 0·4
Glass fibre composite	2·0	1·1	48	0·25 - 0·3
Stainless steel	7·8	1·1	215	0·28
Titanium alloy	4·5	1·0	124	0·32
Aluminium alloy	2·7	0·4	69	0·35
Copper	8·9	0·3	130	0·34

This relation is called the law of mixtures, and is found to hold reasonably well over a range of V_f from 10% to 70%; the law of mixtures is the basis for many calculations of static composite behaviour.

The assumption of equal strain in fibres and matrix is not valid for the composite transverse properties. If the applied load is angled at θ to the fibre direction, the composite modulus varies sharply as a function of θ . When $\theta = 90°$, the strength of the composite is related much more closely to the matrix strength. In fact the matrix strength is the upper limit to the composite transverse strength, since the fibres will act as stress concentrators in the matrix. In addition, the shear modulus and shear strength of unidirectional composites are dominated by the matrix behaviour.

In a similar manner, the failure modes of a composite which is loaded in tension will depend on the orientation of the load relative to the fibres. The first mode of failure involves fibre breakage, and is operative over only a small range of angles. The second mode is a shear failure of the matrix or fibre-matrix interface up to about $\theta = 20°$. At all larger angles, a tensile failure of the matrix will occur. The composite modulus thus falls off very rapidly with angle, as shown in figure 1.3.

By crossplying unidirectional laminates, composites can be built up to have good properties in two directions with the penalty of losing some of the unidirectional stiffness. The properties in the third direction are still governed by the relatively weak fibre-matrix bond. Fibre alignment has to be carried out very carefully, and a composite structure should be designed so that the principal stresses are borne by the fibres. Off-axis and transverse stresses, especially tensile stresses even of a subsidiary nature, may well cause failure.

FIG. 1·3 Modulus-v-Angle between fibres & test direction

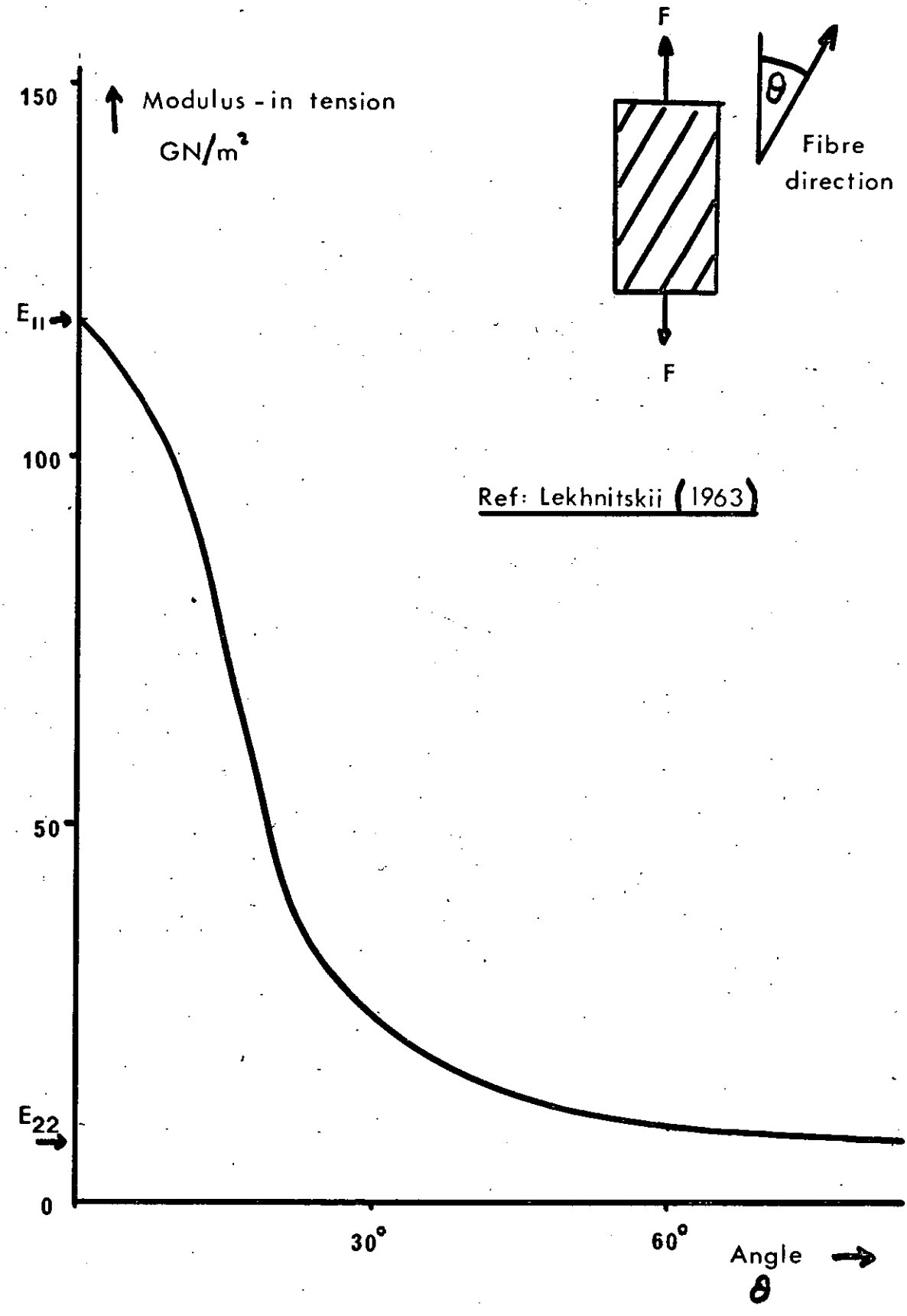

1.2.2 Interfacial properties

The interface between fibre and matrix has a very important part to play in the behaviour of the composite, particularly with regard to the impact strength and crack propagation. Cook and Gordon (1964) have suggested that if a crack in a material approached a weak interface, the interface would break in tension ahead of the crack, due to the stress field in the vicinity of the crack tip. A stress concentration at the tip could be up to 200 times the stress normal to the tip. In a ductile isotropic material, this stress concentration is dealt with by plastic flow, which effectively blunts the crack. For a crack propagating at right angles to the fibre-matrix interface in a composite, a secondary crack would be produced along the interface, and the original crack would run into the interface and be substantially blunted. For this mechanism to apply, the interfacial bond strength has to be less than 0.2 of the cohesive strength of the matrix, otherwise the crack will propagate comparatively unhindered through the material.

A process for improving the bond strength between fibre and matrix has been developed in which the fibre surface is treated with an oxidizing reagent. Bonding is thought to be improved by either polar attraction to the resin material or some form of chemical reaction. Charpy notched impact tests have been carried out on treated and untreated specimens. These tests showed that the weakly bonded untreated fibre specimens had absorbed a considerable amount of energy, and showed a fibrous fracture surface, whereas the well bonded treated fibre specimens showed a clean fracture surface (a brittle failure) and absorbed only a small amount of energy during fracture (Mallinder, 1970). A careful control of bonding is thus needed to balance the requirements of good interlaminar shear strength (i.e. bonding) and good fracture toughness.

A statistical approach to failure prediction has also been used (Scop and Argon, 1969), since a bundle of fibres can be considered to have a statistical distribution of strengths. The Weibull distribution is used to analyse the composite in terms of the extreme strengths; this approach is also called the weakest link theory. When bound in a matrix, the load shed by a broken fibre can be redistributed amongst its neighbours. Depending on the shear strength of the interface, a region along a broken fibre will be ineffective in carrying a load, but at points some distance away from the break, the fibre would be able to sustain some load. Ultimately, as the load on the composite increases, the total accumulation of ineffective lengths will cause the composite to fail.

The practical limit of fibre volume fraction is around 80%, although the theoretical maximum for uniform cylinders packed hexagonally is 91%. Design considerations in using composites need to take account of all composite properties to allow for the anisotropy. The fibre, the matrix and the fibre-matrix bond are all known to have an important function in determining the mechanical behaviour of a reinforced material. (ASTM Conf. 1969).

1.2.3 Impact behaviour

An introduction to the application of using carbon fibre composites in the RB211 fan blade can be found in the paper by Goatham (1970). Some of the problems concerned with characterising the material are dealt with, and in particular the environmental complication of bird impact. This problem is a major hazard to aircraft operation, since potentially severe damage can occur to the engine at the critical points of take off and landing when maximum control of air speed is required. Calculations on simulated bird impact conditions have shown that the kinetic energy at impact will be absorbed by the fan blade in torsion and bending. Before these

bulk structural effects take place, however, the material has to undergo the stress wave loading caused by the impact. The failure modes and the nature of the damage caused by impact tests are somewhat different from fractures produced under static conditions, since complicated stress distributions may arise in the structure due to interference of reflected stress waves. Information regarding stress wave phenomena and dynamic stress - strain characteristics at high rates of loading for carbon fibre composites will be of importance to the development and application of the materials.

CHAPTER 2 REVIEW OF LITERATURE

2.1 STRESS WAVES IN SOLIDS

2.1.1 Theoretical background

The earliest treatment of the propagation of elastic stress waves in solids was developed nearly 100 years ago. A basic assumption was that the material obeyed Hooke's law i.e. the stress was directly proportional to strain, and elastic waves would be present if the applied stress was below the elastic limit. The velocity of propagation depends on the type of material. A fluid is incompressible and cannot support shear stresses, and only one type of wave is propagated at a velocity of $(K/\rho)^{\frac{1}{2}}$ where K is the bulk modulus and ρ is the density. A solid can withstand shear stresses, and two types of wave are propagated in an infinite solid. Distortional waves travel at a velocity of $(\mu/\rho)^{\frac{1}{2}}$ where μ is the shear modulus, and dilatational waves travel at $[(K + 4\mu/3)/\rho]^{\frac{1}{2}}$. Distortional waves involve particle motion at right-angles to the direction of propagation and are transverse waves, whereas dilatational waves involve particle motion parallel to the direction of propagation and are longitudinal waves. At stress levels greater than the elastic limit, propagation takes place at a velocity which may approach or even exceed the elastic velocity. This is due to the bulk modulus increasing with stress intensity, and it is possible for shock stress waves to be set up, in which larger stresses propagate faster than lower stresses. The work of Love (1927) provides a full description of wave phenomena, and there is a more recent review by Kolsky (1953).

When the solid is bounded by a surface, a third type of wave called a Rayleigh surface wave may be present. These waves propagate along the surface, and their amplitude decreases rapidly with depth. Rayleigh waves are of importance in seismic records observed some distance away from an earthquake.

Treatment of the boundary conditions for a practical situation often involves a complex mathematical analysis. An exact solution for an infinite cylindrical bar was given independently by Pochhammer (1876) and Chree (1889).

The Pochhammer-Chree theory considers longitudinal, flexural and torsional vibrations, employing cylindrical polar coordinates (r,θ,Z) to describe the equations of motion. The most usual practical situation is that of longitudinal sinusoidal waves, and the solution here involves Bessel functions of the zero and first order. An important characteristic of the propagation is the phenomenon of dispersion, in which the velocity of a particular vibration depends on its frequency. The frequency dependence is found by satisfying the elasticity equations under the boundary conditions of zero stress at the bar surface. This frequency equation determines the phase velocity as a function of the parameter (a/λ) - radius/wavelength, and has multiple roots such that the dispersion curve consists of an infinite number of branches corresponding to the fundamental and higher modes of vibration.

For sine waves whose wavelength is large compared to the radius of the cylinder, the velocity is that given by the elementary theory i.e. $(E/\rho)^{\frac{1}{2}}$ where E is the Young's modulus. This velocity is the upper limit for large wavelengths in the first mode of vibration, and it is found experimentally that only this fundamental mode is normally excited in bar impact work.

A better approximation is obtained when the bar radius is included in the solution for the frequency equation. Dispersion is then introduced as a result of the lateral motion of the cylinder, and the propagation has to be described in terms of a phase velocity and a group velocity, involving the parameter (a/λ). The limit of both phase and group velocities for small wavelengths is the

Rayleigh surface wave velocity which depends only on material constants.

The description of propagation in finite bars requires approximate solutions, since there will be reflections from the ends of the cylinder. These ends are free from stress and hence there will be discontinuities introduced into the Pochhammer-Chree theory.

The treatment of pulse propagation is complicated by the presence of the Fourier frequency components, and the methods based on Fourier techniques are necessary. (Davies, 1956a).

Using the exact theory and the predicted dispersion curves for infinite sine waves, Davies considered a plane longitudinal pulse which periodically repeated. This pulse can be analysed into a Fourier series, and the velocity of propagation for each term of the series can be found from the dispersion curves for phase velocity. Another approach is to use Kelvin's method of stationary phase, in which an infinitely thin pulse of infinitely large amplitude is considered. This pulse is expressed as a Fourier integral analogous to a superposition of sinusoidal stress waves covering a range of wavelengths, in phase only at the origin. The stress distribution is found from the group velocity dispersion curves, and is a function of transit time along the bar.

As the pulse propagates along the bar, the various waves become out of phase, and destructive interference occurs, so that the main effect is produced by a small group of waves whose phase velocities, periods and wavelengths are nearly equal, and which are in the same phase at a particular position and time.

By these methods Davies showed that a longitudinal pulse whose original length was of the order of the bar radius would become distorted on travelling down the bar, and the main pulse would be followed by a high frequency series of oscillations.

In viscoelastic materials both the phase velocity and the attenuation of sine waves increase with frequency, and consequently when a pulse is propagated through such a solid it both broadens and becomes asymmetrical in shape. Kolsky (1960) has considered pulse propagation for a number of high molecular weight polymers in terms of the linear viscoelastic theory. In general, however, all real solids will behave in some non-elastic manner. When the load producing the stress wave is high enough so that the stress exceeds the Hookean elastic limit, a plastic wave follows the initial elastic wave. For stresses above the elastic limit there is a different relation between stress and strain and on removal of the stress hysteresis is observed. The velocity of plastic waves depends on the stress-strain curve of the material; this velocity is generally lower than the elastic velocity of small stresses in the medium, and the essential property of these waves is that the strain profile develops an elongated front as it passes through the medium.

Metals in the plastic state have a non-linear but time-independent behaviour, whereas polymers and rubbers may have a linear but time-dependent behaviour, and are then known as linear viscoelastic solids.

Viscoelastic materials introduce a further complication into the stress-strain relation, whose form depends on the model representation of the material. A time dependence is now present in the constitutive relation, and Laplace transform methods are normally used to solve the equation of motion (Lee and Morrison, 1956). The emphasis of present day work in wave propagation concerns the problems of boundary conditions and dispersion effects, particularly in viscoelastic bodies. (Hunter, 1959).

2.1.2 Experimental Techniques

The first experiments concerning compressive wave propagation were those conducted by Hopkinson (1914). The accurate measurement of stresses which are subject to rapid time variations is a matter of some difficulty. Hopkinson's experiments consisted in applying the unknown pressure, produced by either an explosion or some other rapid loading mechanism, to one end of a long cylindrical steel bar. The bar was suspended as a ballistic pendulum, and at the far end of the bar was attached a short pellet (the time-piece) of the same diameter and material as the pressure bar. The joint between the two was formed by wringing the shorter piece onto the ground and lapped end face of the pressure bar.

On impact, a longitudinal pressure pulse travelled along the pressure bar, passed unchanged through the joint, and on reaching the free end of the time-piece was reflected as a pulse of tension and travelled back towards the joint. At some stage the net stress at the joint became tensile, so that the time-piece was detached from the pressure bar. The time-piece flew off from the pressure bar, trapping a certain amount of momentum, corresponding to a portion of the pulse which was twice the length of the time-piece. The velocity of the time-piece was measured by means of a ballistic pendulum. Using time-pieces of different lengths, it was possible to partially reconstruct the pressure-v-time profile of the initial impact, caused by the detonation of various explosives.

This method was subject to certain limitations (Davies, 1956b), since it was not possible to determine the exact relation between pressure and time; there were also doubts about the distortion and uniformity of the pulse, and the joint was thought to introduce an unknown variation.

Modern experiments, while using the same principle, employ more sophisticated electronic measuring techniques. Davies (1948) devised a pressure bar in which a continuous record was produced of the longitudinal displacement at the free end of the bar. The displacement was measured by using the bar as the earthed conductor of a parallel-plate condenser. The isolated conductor consisted of a metal plate held in a frame attached close to the free end. When the pressure pulse reached the free end of the bar, the small movement of the earthed side of the condenser caused a change in the capacity of the condenser, and this change was measured on a CRO as a changing potential difference; a photographic record was then taken of the signal. Displacement-v-time records were obtained in this way, and they demonstrated the existence of the so-called Pochhammer-Chree oscillations at the end of the pulse, and showed the effects of dispersion in increasing the pulse length. Davies also used cylindrical condensers, in which an isolated metal tube was held with its axis parallel to the axis of the bar. Measurements of the radial and longitudinal displacements of the bar surface were possible, although these units were only useful for measurements with long pulses.

More recent techniques involve resistance strain gauges mounted on the surface of the pressure bar, so that direct measurements of the strain-time profile may be obtained. Since the pressure bar remains elastic, the relationships for longitudinal elastic stress waves can be used to reconstruct the applied stress loading.

A major use of the Hopkinson pressure bar has been in the dynamic testing of materials. The general principle of the method is to have the specimens in the form of thin discs which are placed between the flat end faces of two cylindrical steel bars (Kolsky, 1949). A transient stress pulse is initiated at one end of the incident

pressure bar, and the pulse propagates along the incident bar, through the specimen and into the transmitter pressure bar. The experiment consists of measuring the dynamic stress-strain characteristic of the specimen material. A more detailed description of the experimental arrangement is given in Chapter 3. Extensions and further applications of Kolsky's original technique have been given by: Krafft, Sullivan and Tipper (1954) and Campbell and Duby (1956) for the yield behaviour of mild steel; Davies and Hunter (1963) for various annealed metals and polymeric materials; Chiddister and Malvern (1963) for aluminium at elevated temperatures; Lindholm (1964) for three annealed face centered cubic metals; Hauser, Simmons and Dorn (1961) for high purity aluminium at temperatures below ambient, and Tennyson, Ewert and Niranjan(1972) for the dynamic viscoelastic response of bone. Various modifications of the technique for tensile testing have been described by Lindholm and Yeakley (1968), for torsion testing by Campbell and Dowling (1970) and for tests on rocks under confining pressure by Christensen, Swanson and Brown (1972). Experimental data are usually analysed by using simplifying assumptions, in particular that the dynamic effects are averaged over the length and cross-section of the specimen. If the specimen length is short enough, the effects of longitudinal inertia may be reduced, and the averaging assumption becomes more acceptable. However, a non-uniform distribution of the stress and strain in the specimen would also result from frictional effects at the boundaries or inertial effects due to radial accelerations.

Davies and Hunter included axial, radial and tangential corrections in their work, and established a criterion for specimen size for all isotropic materials:

$$h = \sqrt{3}\,\nu\, a$$

h = specimen length

a = specimen radius

ν = specimen Poisson's ratio

The requirements for establishing this criterion were short specimens compared to the pulse length so as to ensure a uniform stress in the specimen, and long specimens compared to the bar radius to reduce the friction effects at the specimen/bar interface. These restrictions are not independent, since a long pulse depends partly on bar dispersion and a smoother pulse is associated with a larger bar diameter. The compromise produced a length/radius ratio of about 1. Short specimens and large strains are generally required so that the uniaxial stress theory can be used to obtain a relationship between the principal stress and principal strain present in the specimen.

In Kolsky's work, the specimen geometry was a length/radius ratio of 0.1, and his results for a given strain level in copper gave a dynamic stress which was twice the corresponding static value. Kolsky made several inertial corrections, but Davies and Hunter criticised his results due to the frictional effects arising in his specimens, which would mask the true dynamic behaviour.

There is an abundance of measuring techniques now available for use with the Hopkinson bar. In nearly all cases, however, the stress-strain curves of the materials being studied are determined indirectly, i.e. the specimen stress and strain are inferred from the measurement of some other quantity. The most usual technique is that of strain gauges, positioned on the incident and transmitter bars (figure 2.1) in such a way as to record separately the incident strain wave ε_I, the transmitted strain wave ε_T and the strain wave reflected from the specimen into the incident bar ε_R.

FIG 2·1 STRAIN GAUGE RECORDING SET UP

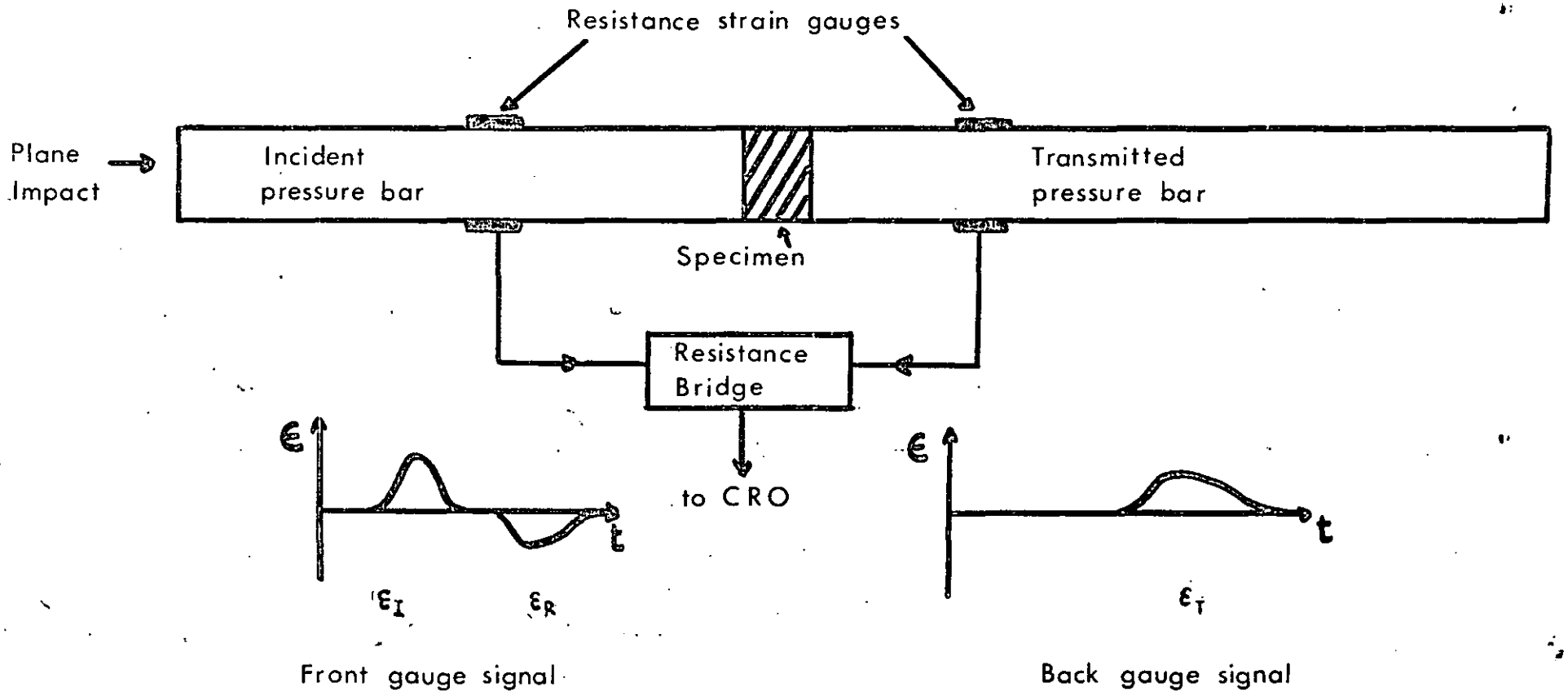

Front gauge signal

Back gauge signal

The one dimensional wave theory shows that the specimen stress σ_s and strain ε_s are given by

$$\sigma_s(t) = E_b \, \varepsilon_T(t)$$

$$\varepsilon_s(t) = -2 \frac{C_b}{\ell} \int_0^t \varepsilon_R \, (t') \, dt'$$

where E_b = elastic modulus of pressure bars

C_b = elastic wave speed in pressure bars

ℓ = specimen length

There is an upper limit to strain rate which can be usefully employed in the Hopkinson bar. Shorter specimens give higher average strain rates for a particular incident loading, but the range is restricted by the elastic limit and the practical lengths of the pressure bars. The maximum strain rates used are in the region 1 000 - 2 000 s^{-1}, and at much higher strain rates, the averaging assumption becomes very critical.

The Hopkinson bar experiment is essentially a plane stress condition, in that the boundaries of the bar produce a non-uniform strain distribution along the bar. An alternative technique is the plate impact experiment for measuring material properties in which an exact state of plane strain can be achieved (Karnes, 1967). The measurements are unaffected by specimen geometry, and very high strain rates can be used. Some disadvantages are that high precision measurements of indirect quantities are required, and only limited times are available for observation. Transforms from one-dimensional stress to one-dimensional strain can be carried out to compare techniques.

Ensminger and Fyfe (1966) have used an exploding wire technique to produce a high amplitude stress wave incident on the inner surface of a hollow cylindrical specimen. This technique requires the measurement of the outer surface displacement and the stress

incident on the inner surface in order to produce a stress-strain relationship.

Measurements of the propagation speed of ultrasonic pulses have been made to determine material properties (Mason, 1958). The pulses are of a few microseconds duration, and the oscillations of which the pulses are composed can have frequencies as high as 100 MHz. The dispersive, attenuative and anisotropic properties of a material can be measured.

Hillier (1949) has used low frequency longitudinal waves in filaments to measure the dynamic elastic behaviour of rubber-like materials and high polymers.

2.1.3 Strain Rate effects

From a fundamental viewpoint a difference between static (or 'quasi-static') and dynamic material behaviour is to be expected, since static loading is essentially an isothermal process whereas dynamic loading is adiabatic.

There has been considerable volume of work reported in the literature on strain rate effects in mechanical behaviour, and only those major aspects of the subject are dealt with in this review. Cristescu (1967) deals with many aspects of the theory of dynamic deformation in plastic bodies; Rakhmatulin and Dem' Yanou (1966) in their book consider material behaviour under transient stress loading. These two books provide a useful survey of the theoretical aspects of stress wave propagation and strain rate effects from an analytical viewpoint. The techniques of solid mechanics have been used extensively in the development of this subject. For example, the method of characteristics is required in the solution of quasi-linear partial differential equations of the second order; this problem arises in the propagation of waves in non-linear elastic and plastic behaviour; the constitutive relations become very

complicated, and it is necessary to use operational calculus and Laplace transform methods to provide solutions for the propagation of waves in these media.

However, physically acceptable explanations for material behaviour of this type are not always satisfactory.

From a molecular viewpoint (i.e. microscopic level) the time scales associated with the changes in strain at a stress wave front are comparable with the time scales of vibrational molecular processes. Hence under conditions of changing strain rate, it is to be expected that there will be changes in these processes. At an elastic wavefront, elastic strain levels are reached very quickly, and the strain rate could be so high that plastic flow processes cannot operate in the times available, whereas at a plastic wavefront, the strain rate could be low enough to allow further plastic flow. Microscopic strain rates may be as high as 10^{12} s^{-1} for elastic waves, and 10^{6} s^{-1} for plastic waves, and these figures would indicate why there is such a wide range of behaviour in metals at differing strain rates and stress levels. Hopkins (1963) has produced an excellent review of mechanical behaviour of metals with reference to these rate effects.

Evidence for the existence of strain rate effects in mild steel is quite conclusive (Campbell and Duby, 1956). The yield and post-yield stresses are increased by a factor of two or three at rates of about 1 000 s^{-1}. Mild steel shows a complex behaviour which is very sensitive to strain rate; this sensitivity appears as soon as there is any departure from quasistatic rates of about 10^{-4} s^{-1}. The evidence for strain rate effects in other metals such as copper and aluminium which have no definite yield point has not been so conclusive. This may be due to the low sensitivity of the behaviour over a wide range of strain rate. A problem then arises over

interpret ing experimental data at high rates when the interpretation cannot be done without a realistic theory of elastic-plastic wave propagation. Such a theory would require assumptions concerning the as yet unknown mechanical behaviour of the material. This problem has been the limiting factor in all analyses of stress wave propagation in solids.

Much detailed work has been carried out using the Hopkinson bar, and the general conclusion is that most materials behave in some strain rate dependent manner which can be expressed in either a power law form or a logarithmic form; Chiddister and Malvern (1963) for annealed aluminium proposed:

$$\sigma = \sigma_0 \dot{\varepsilon}^n \quad \text{OR} \quad \sigma = \sigma_0 + k \log_e \dot{\varepsilon}$$

The theoretical development of longitudinal plastic wave propagation in bars was due to Taylor (1946) and von Karman and Duwez (1950). This work was an elaboration of the elementary Pochhammer-Chree theory from infinitesimal elastic strains to a finite plastic strain. It is important to note the limiting assumptions of the theory, namely that the theory neglects entirely any lateral inertia effects and strain rate sensitivity, and applies only to concave stress-strain curves. Thus the static stress-strain relation $\sigma = f(\varepsilon)$ is used. The velocity of propagation of a given strain level depends on the slope of the stress-strain curve at that strain i.e. $C(\varepsilon) = \left(\frac{\partial f/\partial \varepsilon}{\rho}\right)^{\frac{1}{2}}$.

The existence of elastic and plastic waves is shown, with those higher stresses which cause plastic flow being propagated more slowly than the lower elastic stresses. The theory predicts a plateau of permanent strain extending progressively outwards from the impact end. Later experimental observations showed, however, that there were discrepancies between measured and predicted strain distributions, and these variations were explained as a strain rate

sensitivity in the annealed copper wires used in the experiment. (von Karman and Duwez, 1950).

Malvern (1951) proposed a wave propagation theory based on a more general constitutive equation:

$$E\,\dot{\varepsilon} = \dot{\sigma} + g\,(\sigma,\varepsilon)$$

where g is an arbitrary function expressing the strain rate sensitivity. Taking $\sigma = f(\varepsilon)$ to be the static relation, Malvern used a simple form for g, such that the plastic strain rate $\dot{\varepsilon}_p$ depended on the "dynamic overstress" defined as $(\sigma-f)$, where σ is the dynamic stress and f is the static stress at the same strain;

$$b\,\dot{\varepsilon}_p = \exp\,[(\sigma-f)/a] - 1$$

where a, b are material parameters. On this basis, Malvern developed a strain rate dependent solution, using numerical integration with the equations of motion. One result was the prediction that small incremental strains superimposed on a plastic strain were propagated at the elastic wave speed, but there was no prediction of a permanent strain plateau near the impact end. However, Ripperger and Watson (1968) have produced a computer analysis of the propagation of an intense stress wave along a bar, using a finite difference technique to solve the equations of motion with the constitutive equations expressing various forms of strain rate dependence. Their conclusions were that the constitutive form did influence the wavefront shape, but measurements of shapes or wave speeds were not reliable as indicators of the form of the stress-strain relation, since the same shape was often formed by various combinations of input conditions. Furthermore they showed that there was a constant strain region near the impact end, which would indicate that the strain plateau is not a unique feature of a strain rate independent relation.

Alter and Curtis (1956) produced a step loading in a lead bar by impacting one end with a long steel bar. They found that pulse dispersion occurred which could be predicted from a simple strain rate dependent model similar to Malvern's theory, in preference to a prediction of behaviour from any non-linearity in a time-independent stress-strain relation.

Kolsky and Douch (1962) have obtained dynamic stress-strain curves for annealed metals by firing short specimen bars at a steel pressure bar. These curves were used to obtain predictions about the Taylor-von Karman theory, and a reasonable fit was obtained for the permanent strain and the velocity. The theoretical predictions of strain distribution were less satisfactory, and this could indicate that the Malvern modification was required. Although Kolsky and Douch found a difference between static and dynamic curves, there was little difference between different dynamic loadings.

Sternglass and Stuart (1953) investigated the effects of incremental impact loads superimposed on a static load in copper strips, and showed that the incremental plastic strain propagated at the elastic wave velocity.

A major contribution to free flight impact experimentation has been the work of Bell, which is reviewed comprehensively in Bell (1968). The main feature of Bell's experiments is the impact of two well-aligned identical bars producing a constant velocity boundary condition. The accurate measurement of surface strain is carried out by means of a diffraction grating ruled directly onto the specimen surface (Bell, 1956). The gauge is usually 0.001" long, with about 30,000 lines/inch. The change in diffraction angle due to the deformation of the gauge is measured photoelectrically, and hence the surface strain on the specimen bar can be calculated. Bell claims that this is an accurate measurement which eliminates any

ambiguities in other measuring techniques, and does not require any advance knowledge of the constitutive relation. The time of propagation of the strain pulse between gauge positions is measured, and hence the velocity-strain profile, $C_p(\varepsilon)$, can be calculated. The propagation velocities are found to be constant for each strain increment, which is a prediction of the Taylor-von Karman theory. The specimen stress σ_s is then calculated as a function of strain using the plastic wave speed equation: $C_p(\varepsilon) = (\frac{\partial\sigma/\partial\varepsilon}{\rho})^{\frac{1}{2}}$

$$\text{i.e.} \quad \sigma_s = \int_0^{\varepsilon} (\frac{d\sigma}{d\varepsilon'})\, d\varepsilon' = \int_0^{\varepsilon} \rho\, [C_p(\varepsilon')]^2\, d\varepsilon'$$

Bell's experiments have thus shown strain rate independent stress-strain relations for many crystalline solids, and he summarizes his results in a generalized parabolic stress-strain relation (Bell, 1966), which applies to the non linear plastic deformation in metals:

$$\sigma = \beta\, \varepsilon^{\frac{1}{2}}$$

where β is a temperature dependent, strain rate independent material parameter.

Bell criticises the conventional Hopkinson bar experiment with short specimens because of the assumption of uniaxial conditions which do not include reflection and wave interaction effects, within the elastically-bounded specimen. Conn (1965) made a more detailed analysis of the data published by Hauser, Simmons and Dorn (1961) and showed that their data could be interpreted by a strain rate independent theory. The basis for the analysis was a particular form of the (σ,ε) curve for aluminium, and the nature of the disagreement in interpretation was thought to be caused by the average stress and strain assumption in the specimen.

Conn used the one-dimensional wave propagation theory of Taylor, and included the effects of wave reflections and interactions due to boundaries and interfaces with different materials. The

Lagrangian diagram was used to plot (x,t) characteristics for the stress in the specimen and at the strain gauge recording positions. Conn's analytical $\sigma(t)$ curves were very similar to the experimental curves, but the strain-time curves had very little agreement. The main conclusion reached was that the experimental technique and the subsequent analysis by Hauser et al masked the effects of non-uniform strain in the specimen.

A further point is that dynamic stress-strain curves may not be a measure of material properties in the same sense as the static curves, since the dynamic stress cycle undergone by the specimen is determined by the nature of the experimental method. The conditions of the experiment are uniquely defined for the particular experiment arrangement, and cannot be predetermined as in static experiments.

Bell (1966) showed that the average strain in a Hopkinson bar specimen using the conventional analysis was twice the actual strain measured by a diffraction grating, and in a further experiment with glue and no glue at the specimen interface showed that the average strain was not altered, although the actual strain was changed. He then concluded that the wave reflection and end face effects in short specimens invalidated the analysis used to determine stress and strain.

Another factor, which is hard to assess in longitudinal plastic wave propagation, is the three-dimensional nature of the displacement due to the radial motion caused by Poisson coupling. This radial motion introduces lateral inertia effects as well as transverse shear, and these are not accounted for in the one-dimensional analysis. De Vault (1965) estimated the effect of lateral inertia on the propagation of plastic strain along a bar, and showed that errors in the simple theory could explain the discrepancy between strain rate effects.

There does appear to be the requirement, emphasized by Conn, of being able to distinguish between the mechanical effects of the test and the intrinsic material properties which are to be measured. In any stress wave propagation experiment three features are important: firstly an experimental arrangement which will provide direct and meaningful measurements; secondly measuring techniques which will give unambiguous data and lastly correct interpretation of these measurements in terms of the experiment.

Dillon (1967) reported an investigation of wave effects in long cylindrical specimens. The main purpose of this work was concerned with the effects of having sections of the bar made of different materials, such as annealed (soft) aluminium and hard aluminium. The properties of these dynamic elastic-plastic interfaces indicated that wave reflection phenomena agreed with predictions from the strain rate independent theory. However, other work on aluminium by Karnes and Ripperger (1966) using direct impact experiments with quartz crystal and strain gauge recording techniques, produced results which led them to support the strain rate dependent theory.

Jahsman (1971) has compared the method of characteristics for determining material behaviour with the conventional Kolsky analysis in the Hopkinson pressure bar. This exercise was a check on the features of the experiment such as the specimen geometry criterion and the uniform stress and strain assumptions. Reconstituted stress-strain curves using the one-dimensional theory were found to be in reasonable agreement with the original curves used. These findings would tend to vindicate the Hopkinson bar from several of the criticisms of the technique, since a fundamental criterion for validity is self-consistency.

The work of Duffy, Campbell and Hawley (1971) on torsional wave propagation in a Hopkinson bar arrangement showed that the shapes of the shear strain profiles in various metals could be predicted by a strain rate dependent theory. In torsion, the complicated three-dimensional effects are eliminated, and a pure shear wave is established. The torsion bar thus eliminates any problems due to radial inertia and frictional effects at the specimen interfaces.

It is apparent that most experiments indicate that Malvern's strain rate dependent theory is in agreement with certain results, although this theory may not be realistic for three-dimensional complications such as lateral inertia and shear. Some form of physical theory is required to analyse results of plastic wave propagation in terms of strain rate effects. Hauser, Simmons and Dorn (1961) have emphasized this point, and they indicated that the Malvern theory does not account for crystal structure in determining strain rate effects. A description of strain rate dependence can be obtained using dislocation theory, involving a thermally activated mechanism for the movement of dislocations (Lindholm and Yeakley, 1965). A constitutive equation has been formulated in this way to describe the stress-strain-rate-temperature dependence for several single crystal and polycrystalline materials. Body centered cubic metals appear to be very rate sensitive, even at low rates, whereas face centred cubic metals are only slightly rate sensitive even at the extremes of loading rates. The explanation for these observations was that the strain rate effects depend on the dislocation movement in the metal, since b.c.c. crystals have more dislocation locking mechanisms and fewer slip modes and hence more obstruction to dislocation movement than f.c.c. crystals. Macroscopic creep, quasi-static stress-strain and impact tests can be interpreted with a

strain rate relation based on a microscopic dislocation theory. Further work indicated that the addition of impurities in aluminium crystals led to a reduction in rate sensitivity.

In summary, the assumed one dimensional stress situation of the pressure bar test is really quite complex, since the interpretation of experimental data requires a wave propagation theory, the validity of which is inevitably linked to the physical limitations of the theory and the material properties under consideration. The results of Bell's experiments, for instance, have indicated that there are many difficulties associated with producing satisfactory explanations for all the phenomena of dynamic behaviour. In particular, Bell has criticised the short specimen experiment because the non-linear plastic deformation is often ignored in the calculations for average stress and strain in the specimen. (see also Huffington, 1965).

2.2 FIBRE COMPOSITES

2.2.1 Theoretical stress wave behaviour

The fundamental analysis of the mechanical response of a composite material may involve analytical investigations using two methods of approach. These are treatments on a micromechanical and macromechanical level. In the former, the two component nature of the composite is recognised, and the analysis involves the study of a hetereogeneous material consisting of fibres embedded in a matrix. Various assumptions are required for continuity conditions, such as a perfect interfacial bond, and the effect of a fibre on a propagating discontinuity such as a stress wave can be estimated from some mathematical analysis.

Ting and Lee (1969) have analysed the propagation of a plane pressure pulse through a linear elastic composite medium. Wave theory similar to geometrical optics was used to predict the influence of the fibres on the shapeof the wavefront, due to reflection and refraction effects, considering the fibres to be cylindrical inclusions in a uniform matrix material. It was shown that for the case of elastic waves, the stress amplitude at the initial wavefront was given by geometrical optics-type laws associated with the motion of dilatational waves.

Constitutive equations for the composite as a bulk form may be obtained using the macroscopic stress and strain components, and including geometrical factors in the material description. Thus a laminate structure may be treated as being homogeneous but anisotropic on a macromechanical level, and the governing equations may be found from the characteristics of the individual laminates. Achenbach and Herrmann (1968) proposed a set of displacement equations of motion, derived by using representative elastic moduli for the matrix and elastic and geometric properties of the reinforcing

elements, combined into " effective stiffnesses". In a further paper, (Sun, Achenbach and Herrmann, 1968) they considered a continuum theory for a representative laminated medium. In deriving displacement equations for laminate motion, any interaction of the fibre-matrix interface was allowed only through displacement of the fibre and matrix layers - considered as alternate layers of reinforcing and reinforced material. Dynamic interactions due to the applied stress wave were included using continuity relations. By means of a smoothing operation, averaging over all the fibres, particular kinetic and strain energy densities were obtained, and application of Hamilton's principle gave six displacement equations of motion. This set of equations was used to study the propagation of plane harmonic waves parallel to and normal to the fibre direction. Dispersion curves were calculated, and these indicated the extent to which a fibre or layered composite would influence stress wave propagation by means of geometrical dispersion. A layered composite was represented as a kind of waveguide system, although non-perfect interface properties would have to be considered in a real composite. An inadequacy of this continuum theory was the prediction that torsional waves could propagate in the fibre layer, without any interaction with the surrounding matrix. This result arose from the restricted continuity conditions imposed on the fibre-matrix interaction.

Peck and Gurtman (1969) also considered a pulse loading which was propagated parallel to the interfaces of a laminated composite. The theory of wave propagation in rods was used as a general mathematical guide, and the problem was taken to be two-dimensional. Fourier transforms were required to express a set of ordinary differential equations in terms of the propagation of infinite sinusoidal wave trains. The result was that for waves generated by

a uniform stress loading on a plane perpendicular to the laminates, the peak disturbance at long times after impact was given by a simple expression called the "head of the pulse" approximation. This approximation depended on the low frequency behaviour of the first sinusoidal wave mode, which was analogous to the bar velocity $(E/\rho)^{\frac{1}{2}}$ in rods. A characteristic dispersion time could be defined for the composite structure; this time was shown to depend algebraically on the material properties and layer spacing, and also on the propagation distance. The use of this characteristic dispersion time simplified the determination of parametric variations in the dispersivity of the composite. Some representative dispersion curves were presented for boron-epoxy and glass-epoxy laminates, and these showed a significant dispersion in phase velocity above 5 MHz for the boron and 75 MHz for the glass fibre reinforcement.

The head of the pulse approximation was also used by Voelker and Achenbach (1969) in their paper, which considered stress wave propagation in a laminated medium, with the forces being applied normal to the layering. A marked dispersive behaviour was predicted using the continuum theories for a laminated medium.

Chou and Wang (1970) have studied the propagation of an elastic disturbance in a composite material using the mathematical device of a control volume to surround the wavefront. Several authors have used this device to describe shock wave propagation in laminated and composite materials, which require the additional complication of boundary conditions between laminates or between fibres and matrix. Torvik (1970) calculated the pressure, density and particle velocities behind a plane shock, and considered the composite to be either alternate layers of two dissimilar materials, or parallel fibres embedded in a matrix. In developing the description

of shock propagation, steady one-dimensional flow along the layering or fibres was assumed. Conservation of mass showed that the effect of area change was significant, since a small area change was equivalent to a density change of the same order, and density changes corresponded to large pressure changes. One feature was that modified forms of the Hugoniot jump conditions were required, so as to account for the transverse strains in each component. Calculated values of the Hugoniot shock parameters were given for a hypothetical aluminium/polymethyl - methracrylate composite, and it was shown that shock speeds in the composite which were lower than the sonic velocity of one of the constituents were possible. This treatment was applicable only to the hydrodynamic portion of a deformation. A real composite material would also have an elastic response, which may be important since elastic waves may travel almost as fast as the shock waves, due to the hetereogeneous nature of the material. In the complex multi-dimensional flow field around a bird impact, the condition that the material behind the steady shock was free to acquire any particle velocity necessary for the shock to exist would not be valid. For this situation, the particle velocities are dependent on the specific properties of the impact loading.

Further theoretical work by L.M. Barker (1971) on shock propagation perpendicular to the planes of the laminates in a composite structure also indicated geometrical dispersion. These dispersive effects were described by a simple viscoelastic model, and the theory predicted stress wave shapes and the attenuation of short stress pulses.

Other shock propagation problems have been investigated by Tsou and Chou (1969 and 1970). These authors considered a shock travelling along the fibres in a unidirectional fibre composite,

using a control volume which surrounded the shock front. Conservation of mass, momentum and energy were applied to the material before and after the control volume, and a set of equations describing the material behaviour were produced. The local discontinuity at the shock wave front was thus ignored. For a steady shock, the speed must be the same in both fibre and matrix, since there could be no pressure change across the interface. The presence of the interfacial bonding produced shear forces which tended to impede the progress of the wavefront in the fibre and push forward the wavefront in the matrix. Thus there was a varying shock velocity across each layer to ensure continuity of the shock wave-front. Calculations were presented for shock velocity, particle velocity and shock pressure in a beryllium fibre-polyethylene matrix composite, together with results for the interface shear and heat transfer across the fibre-matrix interface.

All these mathematical models have been used with some success in analysing composite behaviour. Depending on the model, predictions are possible for the effects of the boundary conditions, interfacial compatibility, intrinsic material properties and dynamic characteristics in stress wave propagation.

The most used characterisation of fibre composites is that of transverse isotropy. This is the simplest form of elastic symmetry which would apply to unidirectionally aligned composites of continuous fibres. Such a medium has five independent elastic properties, and is circularly symmetrical about the normal to the basal plane i.e. the fibre axis. If there is no symmetry about this plane, a lower order of symmetry would be required, such as a tetragonal system of six elastic constants which is not isotropic in the basal plane. The next simplest system would be the orthorhombic system with nine elastic constants, and this has been used to describe

the elastic constants of wood.

The five elastic constants of transverse isotropy can be thought of as two "Young's moduli" for loading along and across the fibre direction, and three "Poisson's ratios" describing the coupling between mutually perpendicular displacements when loads are applied in various directions. Theoretical predictions and experimental observations of stress waves in fibre composites will involve consideration of these elastic material constants, together with possible extrapolation to viscous behaviour.

Knaus (1968) has considered one-dimensional wave propagation in a viscoelastic material, which was intended to simulate the features of the matrix material of a composite, and the viscoelastic nature of the material was characterised by a complex, frequency dependent modulus.

Macroscopic viscoelastic properties of a fibre reinforced material were considered by Hashin (1966). Here the fibres were assumed to be elastic, and the matrix linearly viscoelastic, but the analysis was limited to an extent in that some of the calculations were expressed in terms of a spring-dashpot viscous model, which is not necessarily realistic. Analytical expressions for effective relaxation and creep functions were given, on the basis of the composite cylinder assemblage model which had been proposed by Hashin and Rosen (1964) as an idealized representation of a random array of parallel fibres embedded in a matrix.

2.2.2 Experimental investigations in composites

Published work on experiments concerning the dynamic properties of fibre reinforced composites appears to be rather limited. Back and Campbell (1957) were the first to use the Hopkinson pressure bar to investigate the properties of a material consisting of a phenol formaldehyde resin reinforced with asbestos fibres ("durestos"). A dropped weight impact device was used, together with strain gauges mounted on the transmitter pressure bar. A calibrating shot with no specimen present had to be carried out each time in order to measure the incident strain pulse. The one-dimensional wave theory was used to calculate the specimen stress and strain. Corrections were made to the original strain records to allow for the finite specimen length and the finite length of the strain gauges. The derived stress-strain curves lay much above those obtained at slow loading rates, the stress and strain at fracture being doubled in the dynamic tests. The resin appeared to fracture in a brittle manner under the high loading rates of this experiment, indicating that the material had become much harder. The failure mode observed was that of fibre-matrix interface failure, and the results indicated that the increase in strength of the composite was due to a change in resin properties rather than a change in fibre properties.

Tardiff and Marquis (1963) used a similar dropped weight assembly to determine the dynamic properties of a range of plastics, including composites made from steel wool and glass-fibre wool reinforced araldite resins. This type of reinforcement caused an increase in the elastic modulus and the strength of the resin, and in the specimens with glass fibre wool, a high degree of brittleness was induced in the composite. The reduction in ductility of the araldite resin when reinforced was such that the fracture strength

decreased with higher strain rates. Tardiff and Marquis suggested that deformation mechanisms in plastics could originate from the uncoiling of long chain molecules and other flow processes caused by the presence of these molecules, and that at the high rates of strain present in dynamic tests the response times of these various flow mechanisms were exceeded. An increase in the elastic response would then occur.

Sierakowski, Nevill, Ross and Jones (1970) investigated the properties of a steel wire reinforced epoxy resin composite. Several parametric variations were employed, such as wire diameter, volume fraction of wire reinforcement and strain rate. Dynamic loads were applied in a Hopkinson bar experiment and quasi-static loads in a hydraulic testing machine. It was seen that higher strength and modulus properties were obtained with smaller wire diameters for a particular volume fraction, and that increasing the volume fraction also led to higher strength values. Up to 100% increase in material strength was obtained in dynamic tests at a strain rate of about 1 000 s^{-1} compared with quasi-static tests at strain rates of about 10^{-4} s^{-1}. The stress increase for a given strain in a dynamic test on smaller wire diameters was thought to be due to the greater surface bonding area between fibre and matrix.

In further tests on glass-fibre reinforced resins a similar stress-strain behaviour was reported, together with brittle failure modes. Aluminium-nickel alloy composites in which the reinforcement is grown in situ by directional solidification were also tested. A whisker or plate-like reinforcement is produced by this process, depending on the particular substructure present in the alloy system. Dynamic stress-strain curves for these composites again showed considerable increases in strength over quasi-static behaviour.

Billington and Brissenden (1971a) used glass-fibre reinforced plastics with various forms of matrix material and fabrication. The Hopkinson bar apparatus which they employed incorporated a gas driven projectile for the impact loading, and by varying the velocity of impact, the amplitude of the incident stress pulse could be varied over a wide range. Using strain gauges on the pressure bars, the stress-strain behaviour showed that all the curves compounded together over the initial portion for all values of impact velocity, and hence for all the strain rates used. The main conclusion was that the material behaviour was strain rate independent and that the form of the stress-strain curve consisted of two distinct regions. An empirical functional representation of these two regions indicated a logarithmic relation between stress and strain up to a critical strain value, and then a straight line relation for larger values of strain. The transition from one region to the other was identified with the phenomenon of thixotropy as seen in various forms of non-Newtonian flow. This could arise from the coiling and uncoiling of the long chain molecular structure of the plastic matrix, in some time dependent manner.

In other work on polymers, such as perspex, polycarbonate etc., (Billington and Brissenden, 1971b) and on annealed forms of polycrystalline copper, zinc and aluminium (Billington and Tate, 1972) this two region representation has been extended to include a description of isotropic material behaviour. The main feature was the strain rate independence over the range of strain rates used. However, there was a difference between the dynamic behaviour in the impact experiment (lasting about 120 μs) and the quasi-static behaviour whereas the annealed metals underwent permanent strain, although for both types of material the loading portion of the dynamic cycle could be described by similar non linear stress-strain relations.

Various moduli and other material constants were identified with certain parts of the dynamic characteristic response. In particular, the Young's modulus was used in the dynamic description even though the analysis covered the transition from elastic to plastic response for the metallic specimens.

Damage was seen to appear in composite specimens at stresses and strains significantly greater than those in pure matrix specimens. Load bearing under these high strain rates was thus increased by reinforcement. Billington's work is a significant advance in the knowledge of the dynamic properties of composites and metals. However, no satisfactory physical explanation has been proposed to account for the response of fibre composites at high rates of loading.

Other work on composites has involved the plate impact or plane strain experiment. Whittier and Peck (1969) used composites manufactured from alternate layers of high and low modulus material in a phenolic resin. The reinforcement consisted of high modulus graphite fibres and boron fibres. A flat plate of this material was subjected to a uniform step pressure induced by a gaseous shock wave and the resulting backface velocity-time signal was recorded by a capacitance gauge. The central portion of the specimen behaved as if laterally unbounded, and the effects of geometric dispersion due to the material properties were evident in the records. Comparison with theoretical predictions calculated by Peck and Gurtman (1969) showed that the "head of the pulse" approximation was valid for long times after impact. This experimental technique suppressed the micromechanical detail and gave representative data of the average response over a finite gauge area.

Reed and Munsen (1972) reported similar experiments with phenolic coated/quartz cloth laminated plates using direct impact of a plate of the same material. The experimental results showed appreciable dispersion of the step loading together with a large stress attenuation. These results compared favourably with calculations of plane strain conditions based on a rate dependent model using a Maxwell representation of the viscous behaviour. However, the two material features of the viscoelastic nature of the phenolic matrix and the geometric dispersion due to the fibrous layered structure could not be separated.

Markham (1973) has developed an ultrasonic method of determining the elastic constants of materials in which the propagation speed of ultrasonic pulses of about 5 MHz is measured. In unidirectional composites with carbon and silica fibres, the five elastic constants of transverse isotropy can be found by orienting the fibre direction in the specimen at various angles to the direction of the pulses. Transverse (shear) waves and longitudinal waves were initiated in the specimen under certain conditions, with the specimen and ultrasonic probes immersed in a bath of water. Wave refraction theory similar to Snell's law in optics was used to calculate wave speeds from which the appropriate elastic constant could be found using the general relation:

$$\rho v^2 = C_{ij}$$

where v = wave speed in a particular direction and mode

C_{ij} = the equivalent elastic constant

ρ = density of composite

These ultrasonic experiments have not given any indication of the viscoelastic nature of a composite. Tauchert and Moon (1970) described a method of measuring the damping coefficient of a composite beam when subjected to low frequency vibrations up to a

maximum of 10 KHz. Glass fibre-epoxy and boron fibre-epoxy composites were used in this study. The damping was found from the bandwidth of the resonance curve at each mode of resonance, with calculations based on the elastic beam theory. A linear viscoelastic approach was then used to represent the material behaviour, and a phase velocity and attenuation coefficient were defined as functions of frequency. A stress pulse propagating along a bar of the material would then undergo dispersion and attenuation. Kolsky (1960) had developed Fourier integral expressions for the propagation of a pulse in bars of polymeric material, and this approach for composite bars was very similar. Experimental observations of pulse propagation were then compared with the predictions of the theory for the fibre reinforced composites, and it was shown that the materials behaved in a linear viscoelastic manner.

Schuster and Reed (1969) have investigated the dynamic fracture of boron fibre reinforced aluminium composites by means of plate impact experiments. The shock wave loading caused spall type fracture and filament damage in the composites, at different impact velocity levels depending on the bonding fabrication process of the fibre reinforcement; the peak stress amplitude was reduced by geometric dispersion of the loading pulse. In a later paper (Reed and Schuster, 1970), they showed that the impact velocity necessary to produce a substantial reduction in tensile strength in the composite was much higher than that required in an unreinforced aluminium alloy.

2.3 CONCLUSIONS FROM THE REVIEW

The shortcomings of the usual methods employed to obtain dynamic stress-strain data are recognised, and the difficulties inherent in the Hopkinson pressure bar can be reconciled using appropriate limiting assumptions. The roles of strain rate and viscoelasticity in material behaviour are not fully understood, particularly in the case of composite materials. Various mathematical complexities may be a limiting factor on theoretical studies of this nature. In spite of many years work in the subject, there are few definitive experimental results which can be linked with a satisfactory physical interpretation. The features of dynamic tests on composites, such as the increased strength and fracture behaviour compared with quasi-static tests, make this work of great interest to both engineering design studies and to studies of the macroscopic physics of fibre reinforced materials.

The Hopkinson pressure bar is considered to be the best available technique for measuring dynamic properties of materials; the behaviour of carbon fibre composites at high rates of loading can then be determined using the assumptions of average stress and strain in the specimen.

CHAPTER 3 THE HOPKINSON PRESSURE BAR

3.1 GENERAL DESCRIPTION OF APPARATUS

The two main features of the Hopkinson pressure bar are the loading mechanism and the method of recording the dynamic response of a specimen material. The basis of the recording technique used here was to measure the particle displacement of the endfaces of the specimen in the split bar arrangement during the time it was subjected to a stress pulse. Thus the method differed from the more usual strain gauge recording technique (fig. 2.1) and some of the difficulties of analysing the strain pulses in the pressure bars, as outlined by Bell, can be eliminated, although other difficulties arise in this method. With a short specimen, the stress and strain are considered uniform over the length, and lateral inertia can be ignored, provided that the Davies and Hunter criterion is obeyed. All specimens had a nominal diameter of 0.5" (12.7 mm) and lengths of 0.5" and 0.25" were used.

The general arrangement of the apparatus is shown in fig. 3.1. The impact is produced by firing a standard 0.22" bullet at the free end of a steel input transducer bar, causing a stress pulse of peak amplitude about 2 K bar (2×10^8 N/m^2) and of duration 35-40 μs to propagate along the bar. The specimen is sandwiched between the input transducer bar and the output transducer bar, each face of the specimen being in intimate contact with the faces of the steel bars. When the pulse reaches the specimen, the specimen undergoes the dynamic loading, part of the incident compressive pulse being reflected into the input bar as a pulse of tension, while the remainder of the incident pulse passes into the output bar as a transmitted compression. Many reflections occur within the specimen at this time, and it is assumed that these average out over the specimen length to provide a uniform one-dimensional state of strain along the length.

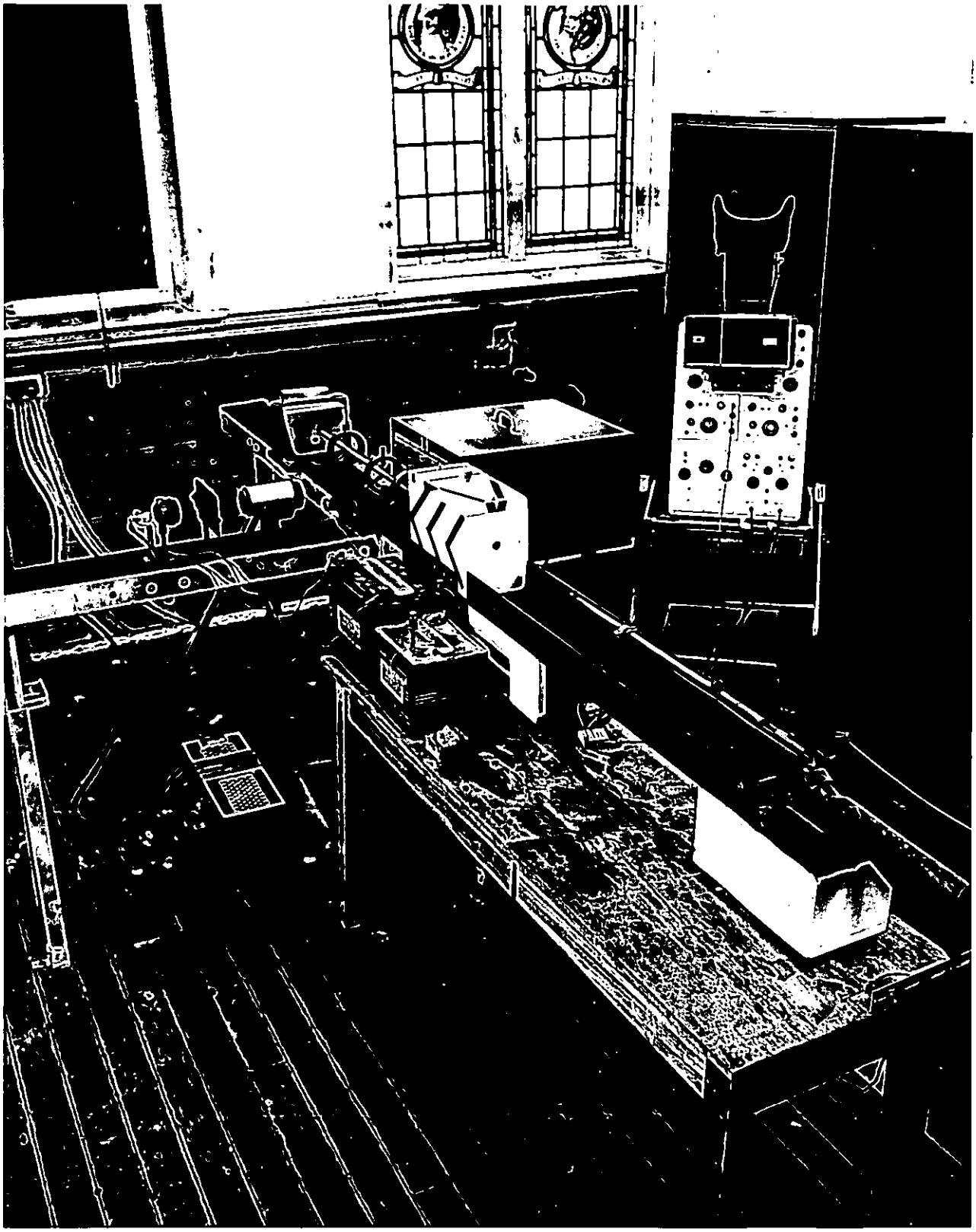

FIG. 3·1

During the transmission through the pressure bars, the pulse may suffer considerable dispersion, governed by the geometric and elastic properties of the bar. The bar material was stainless steel, which has a tensile strength of about 10^9 N/m^2 and can be expected to remain elastic during the propagation of pulses of the amplitude used. In a pulse duration of 40μs , the dominant frequency is 25 kHz, which corresponds to a wavelength of about 200 mm (taking the wavespeed in the steel to be $(E/\rho)^{\frac{1}{2}} \sim 5$ km/s). Hence in a bar of diameter 12.7 mm, the ratio (a/Λ) is only of the order of 0.06 and the dispersive character of these long wavelengths can be ignored. Higher frequency components in the pulse may undergo a larger dispersion, but these effects will produce only a small contribution to the overall pulse shape. The stress pulse on arrival at the specimen can be considered to be plane longitudinal, since Davies (1948) showed that at distances eight times the bar diameter from the impacted end, the pulse becomes uniform over the cross-section of the bar.

To investigate the nature of the impact loading, photographs were taken of the bullet impacting an anvil placed at the end of the input pressure bar, using an "Imacon" image converting camera. This device produces a series of images of a high speed event on a phosphorescent screen, and a polaroid camera is used to photograph these images. The area around the anvil was illuminated by an ordinary commercial flash gun, which produced a uniform field of illumination for a period of 2-3 ms. The flash gun was triggered to fire by the bullet bursting through a piece of paper rigidly held in its path separating two strips of aluminium foil, the bullet shorting these strips together. The Imacon was itself triggered so as to start the recording sweep by a photocell which detected the flash output. The general arrangement is shown in figure 3.2.

FIG.3-2 Arrangement for photographing bullet in flight

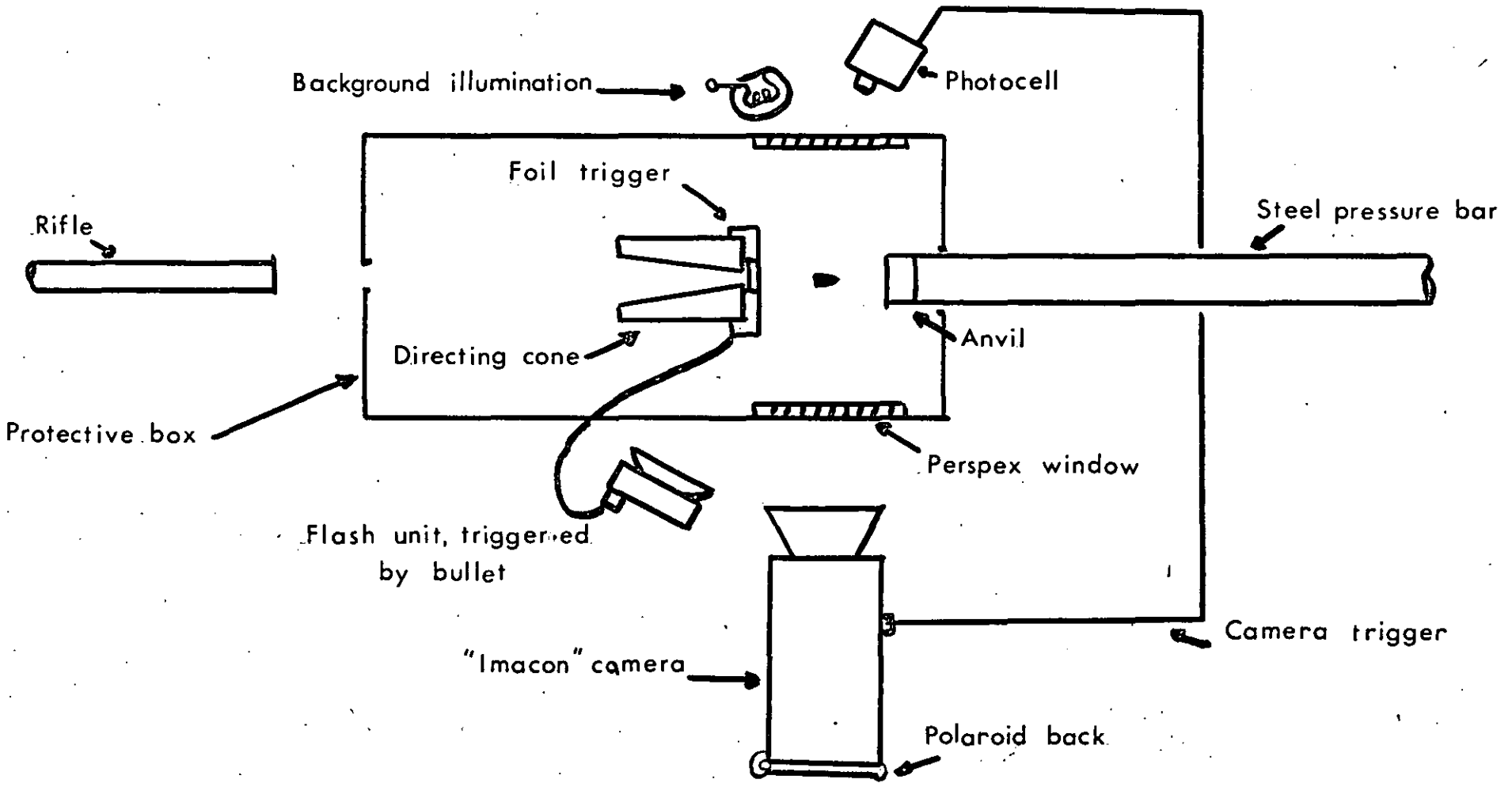

The Imacon was provided with the facility of producing between 8 and 16 separate images on its viewing screen; the writing speed was 10^5 frames/sec, which corresponded to 8 μs between each exposure and a 2 μs exposure time. Ten frames were found to be adequate to give a good coverage of the impact event, which was readily observed in the time of 100 μs. Three polaroid prints obtained by photographing the viewing screen with this set up are shown in figure 3.3. The sequence of reading the series of frames should be noted. Records were taken of the standard bullets (Eley "long rifle") on impact, and also high velocity bullet impact, both of which were used in dynamic experiments. The quoted muzzle velocities of these two bullets are 335 m/s and 419 m/s, and both bullets are 11.7 mm in length. Estimates of the bullet velocity from the high speed photographs indicated that these velocities were approximately correct, although an accurate determination was not possible by these measurements.

A simple calculation shows that the force F produced by the bullet on striking the impact area, assuming all the bullet momentum to be used up, is:

$$F = \frac{mv^2}{L} = \rho v^2 A$$

where m = mass, v = impact velocity, L = Length, ρ = density, A = area) of the bullet.

hence $F \sim 3.7 \times 10^3$ N for the standard bullet. This force corresponds to a pressure in the steel transducer bar of about 2.9×10^8 N/m^2, and the pressure produced by the high velocity bullet is about 1.5 times that with the standard bullet.

From the photographs it is seen that the momentum of the bullet is effectively destroyed during the impact. Some of its kinetic energy is dissipated in disintegrating the bullet so that the pressure pulse which passes into the bar is not as large as that calculated

FIG.3·3 BULLET STRIKING ANVIL 10μs between frames

(a) Standard bullet

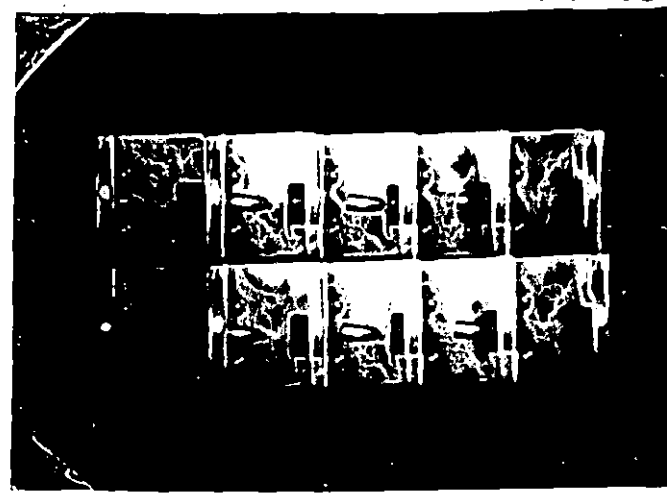

(b) Standard

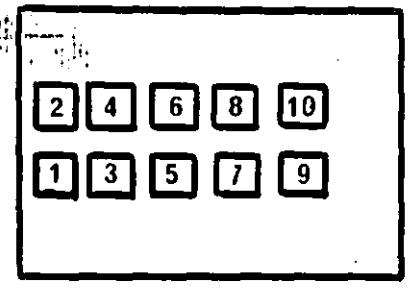

Sequence of frames

(c) High Velocity

above, and measurements have shown that the peak amplitude is about 2.2×10^8 N/m^2. It is thought that the bullet melts on impact, although the lead debris is in a molten state for only a very short time before being ejected in a solid angle of almost 2π radians. This debris is then surrounded by the atmospheric pressure wave surface associated with the bullet and makes no contribution to the propagation of the elastic disturbance in the bar. The duration of the stress pulse in the steel bar is dictated by the time during which the bullet is in contact with the face of the anvil, which in turn depends on the length and velocity of the bullet on impact. A pulse duration of about 40 μs is produced by the standard bullet.

The alignment of the rifle and bullet trajectory with the axis of the pressure bar is quite critical, since an off-axis impact could induce torsional and flexural waves in the bar. These waves may then interfere with the recording of the purely longitudinal wave required. To assist alignment, a directing cone was positioned between the rifle and the anvil so that any deviation from a purely axial impact was kept to a minimum. The bars were supported on roller bearings with only a small frictional drag, and alignment could also be carried out by adjustment of the horizontal level of the bars at these supports.

Replaceable anvils were used in order to protect the endface of the input steel bar from damage at impact. Normally an anvil required replacement after 8 or 10 shots.

3.2 Recording technique

Experimental measurements were made of the displacement-v-time profile of each end of the short specimen. This motion was determined by following photoelectrically the movement of a small metal shutter attached to each of the pressure bars, and positioned immediately adjacent to the specimen/bar interface.

A rectangular beam of light of uniform intensity is focussed onto each shutter, and the shutter moves across this focal plane due to the passage of the stress pulse. The uninterrupted light falls onto the cathode of a photomultiplier. Thus the motion of the shutter changes the intensity of the light received in the photomultiplier by covering or uncovering part of the beam, and hence there is a change in the potential developed across the photomultiplier load resistor. The output signal from the photomultiplier is first amplified and then displayed on a Tektronix 555 oscilloscope. This photoelectric method of determining dynamic material behaviour was first suggested for the Hopkinson bar experiment by Wright and Lyon (1957). Earlier work by Manjoine and Nadai (1940) also incorporated an optical displacement measuring technique using an elastic force bar in high speed tension tests at elevated temperatures.

The general arrangement of the recording system is shown in figure 3.4 and the optical system arrangement is shown in figure 3.5.

The light source is a tungsten filament car headlamp, 12V D.C., contained in a spherical plane glass bulb. Lens A (figure 3.5) produces a circular image of uniform intensity in a plane containing two rectangular apertures whose size is adjustable. These apertures act as sources for lenses B, which produce the required rectangular images of the two apertures in the plane of the bar axis. The metal shutters are located in this plane and the positions of lenses B are adjusted to produce focussed images on the shutters.

FIG 3·4 Hopkinson bar apparatus.

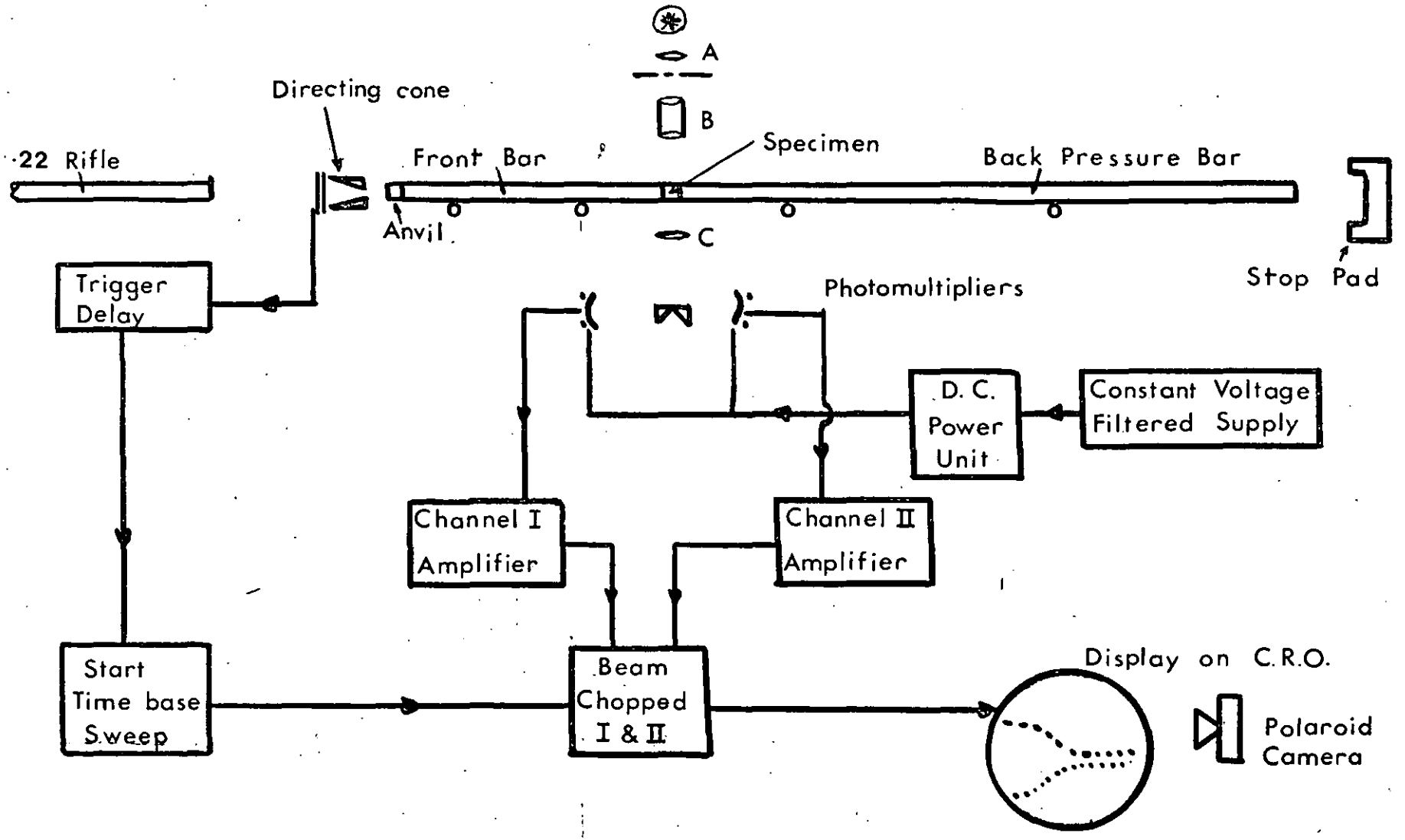

FIG. 3·5

OPTICAL ARRANGEMENT

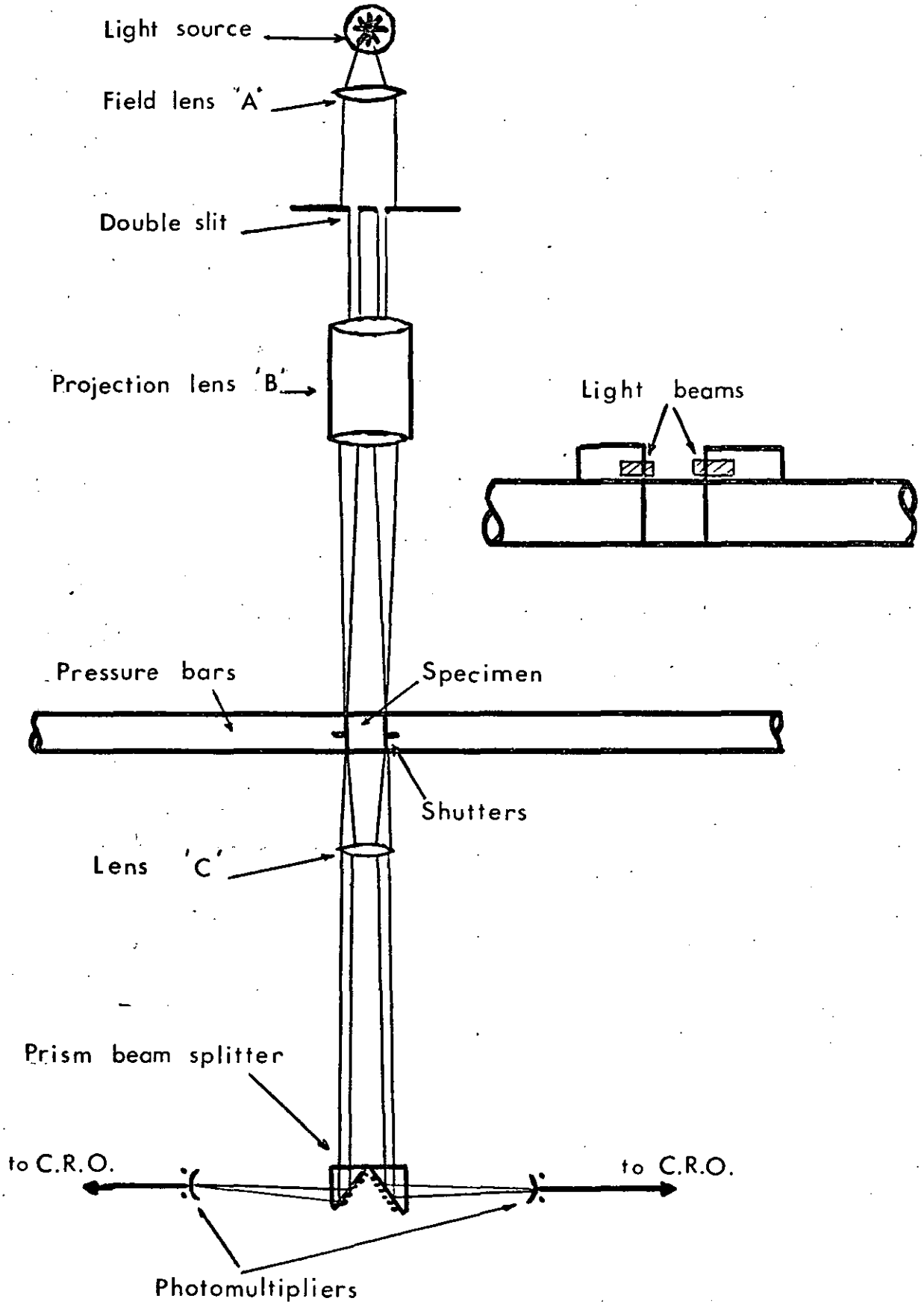

Lens C then focusses the uninterrupted part of each beam onto the photomultiplier cathode. The prism beam splitter simply allows a convenient physical arrangement of the photomultiplier tubes. To avoid errors resulting from any variation of sensitivity on the cathode surface, the images formed at the cathode are those of the tungsten filament. As the shutters move across their associated rectangular beams, only the intensity of the filament image on the cathode changes, and a constant area of illumination is preserved.

Wright and Lyon showed that the transient voltages, as recorded by the photomultipliers, were proportional to the particle displacements at each end of the specimen. This displacement pulse shape is defined by the Rayleigh equation and can be expressed analytically in terms of the Airy function.

It was necessary to accurately calibrate the voltage displacement of the oscilloscope trace as a function of the shutter movement after each shot to ensure accuracy in the subsequent calculations of stress and strain. This was done by chopping the light beam mechanically by means of a castellated disc driven by a small electric motor to produce a square wave voltage signal (see figure 3.6(a)), and then the shutters were moved through the beam, with the change in amplitude of the square wave signal being measured on the oscilloscope. The chopping frequency was about 100 Hz and the shutter movement was measured using a fixed dial gauge in spring-loaded pressure contact with the other end of the bar.

A movement of only 0.010" to 0.015" was normally required to cover the range of the beam involved in an experimental recording, and over this range the calibration was accurately linear. A signal sensitivity of between 50 and 100 μm/Volt was obtained with the apparatus, although this value could vary considerably if the image was not on the most sensitive part of the cathode surface or if the

optics were disturbed in any way. Signals of maximum amplitude 2 - 4 volts were usually obtained during a shot.

Photographs of the transient signals received from the photomultipliers on the oscilloscope screen were taken using a polaroid camera with a high speed film for subsequent analysis. A typical shutter displacement record is shown in figure 3.6(b) for the duration of the initial loading, together with a longer time-base record in figure 3.6(c).

The sensitivity of the photomultiplier arrangement depended on the operating voltage. It can be shown that the signal/noise ratio S can be expressed in terms of certain electrical parameters:

$$S \sim \sqrt{\frac{Ia}{V.W}}$$

where Ia = anode current

V = voltage/stage

W = bandwidth of circuitry

S can be increased by decreasing W or decreasing V while keeping Ia constant. To decrease W would adversely affect the transient response of the system, and Ia cannot be increased because of the need for linearity and stability in the tube rating. Hence V must be decreased to improve S, and the photomultipliers were run unsaturated at low applied voltage levels. The range 600 - 700 V D.C. was used, compared with the usual operating maximum of 1,100 V D.C. A constant voltage linear supply transformer with harmonic filtering of the mains A.C. voltage was used to provide the photomultiplier D.C. level, and a powerful light source also improved the signal content by increasing the initial photocurrent. The noise content of the recorded signals was thus reduced to negligible proportions for most photographs taken.

FIG. 3·6

(a) Square wave calibration

SWEEP RATE 5 ms/cm

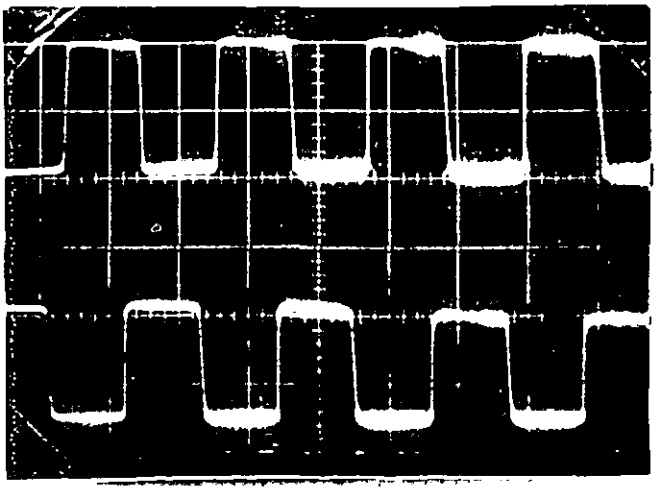

(b) Optical-shutter record

FRONT SHUTTER →

GAIN 10 V/cm

SWEEP 10 μs/cm

BACK SHUTTER →

GAIN 5 V/cm

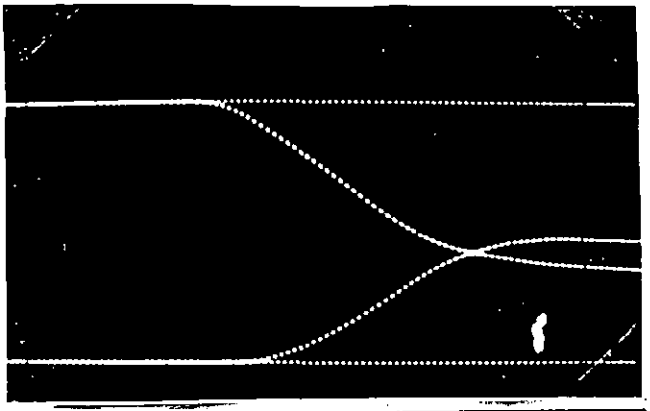

(c) Long time base

100 μs/cm

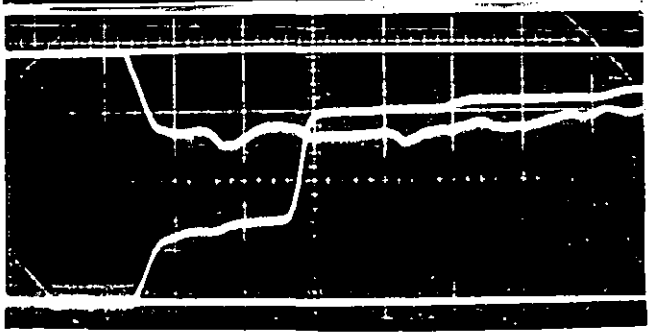

(d) Beams set up as in Fig. 3·8

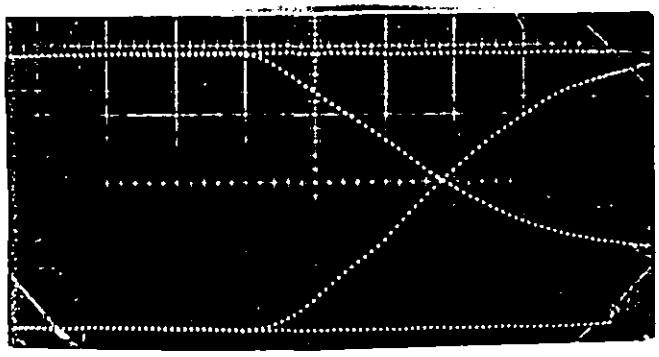

Triggering of the oscilloscope was achieved by the bursting foil method. As the bullet passed a position on the directing cone a trigger pulse was produced by the shorting of the foil, which completed a simple circuit. The trigger pulse was fed into the Tektronix oscilloscope 555, which contained a variable delay facility. This variable delay was set so that a single sweep of one time-base could be fired a given time after the initiating pulse had been fed into the other time-base. This delay, which was typically 400 μs duration, was necessary to allow the bullet to travel from the foil trigger position to the anvil, and for the stress pulse to commence its propagation in the input bar. During the sweep of about 100 μs duration, provided by the second oscilloscope time-base, the two transient signals of the particle displacement as the pulse passed through the specimen were recorded on polaroid film.

3.3 Tests on Shutter reliability

Preliminary experiments were carried out to demonstrate the validity of the shutter displacement measuring tec hnique.

Davies (1948) investigated the theory of pulse propagation down cylindrical bars and showed under what conditions the distortions become too severe for the Hopkinson pressure bar to be used satisfactorily. In particular, Davies showed that the error in using the one-dimensional stress wave propagation theory for calculation of the stress in the bar from the particle velocity at that cross-section was largest for those pulses with a short rise time compared with the pulse duration. The bullet pulse used in these experiments had a rise time of about 15 μs and a duration of 40-50 μs, so that the application of the simple propagation theory was assumed to be valid.

In order to check that the shutter accurately followed the motion of the cross-section of the input pressure bar, two beams were set up as shown in figure 3.7, so that simultaneous signals could be recorded from the shutter crossi ng one light beam and the end of the bar crossing the other beam.

Withthe upper light beam positioned at the base of the shutter, close to the top of the bar, both records started at the same time and had the same period and similar shapes. Other records with the upper beam shifted to a position higher up the shutter showed a delay between the start of the two signals. This delay was as much as 6μs, and corresponded to the time required for a plate or edge wave to propagate in the steel shutter. The velocity of this wave was of the order of 1 mm/μs for a beam centred 6 mm up the shutter from the top surface of the bar. Allowing for this delay, comparisons of the displacement records showed no difference between the shutter record

FIG. 3-7 EXPERIMENT on the ENDFACE-SHUTTER DISPLACEMENT

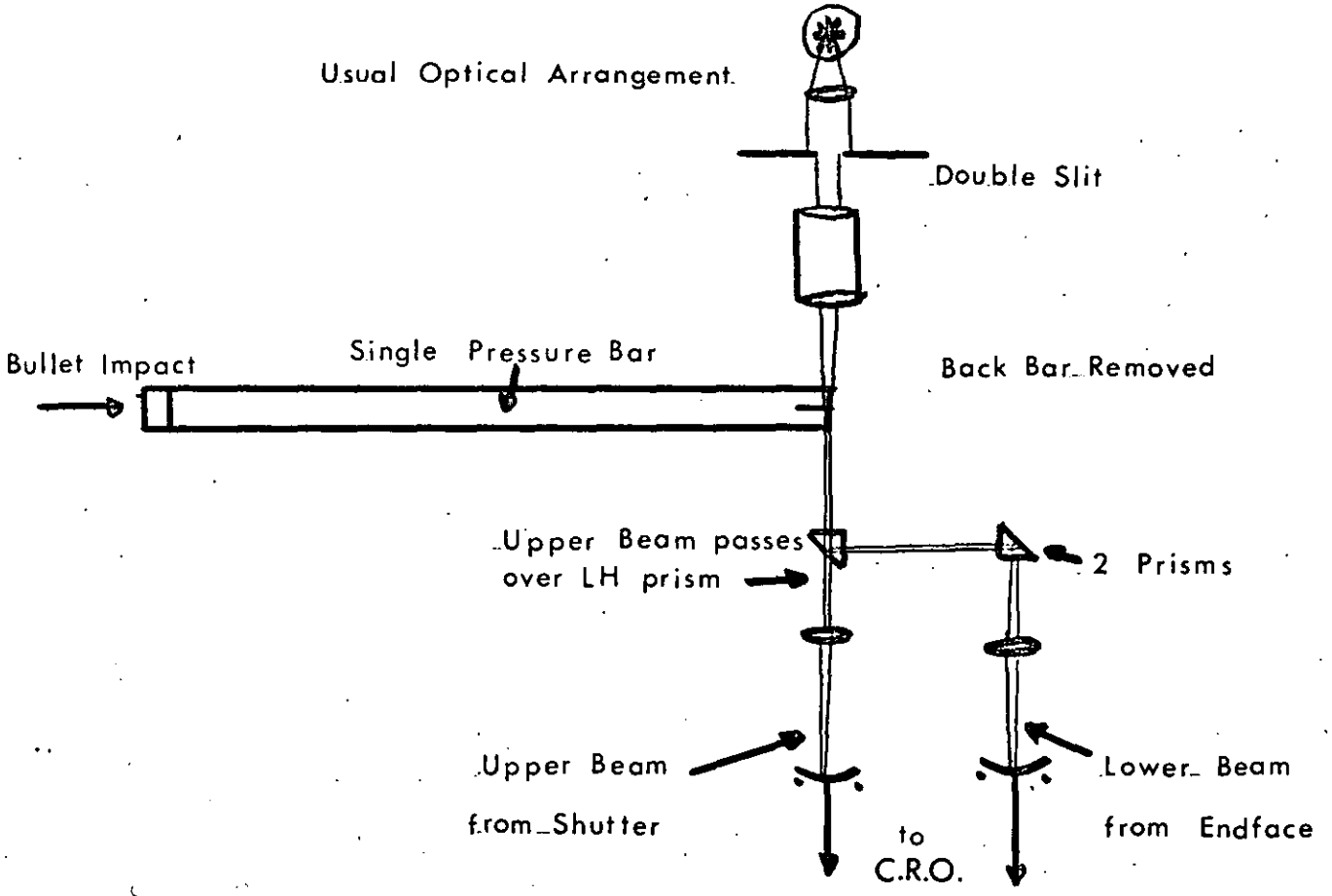

Plan View

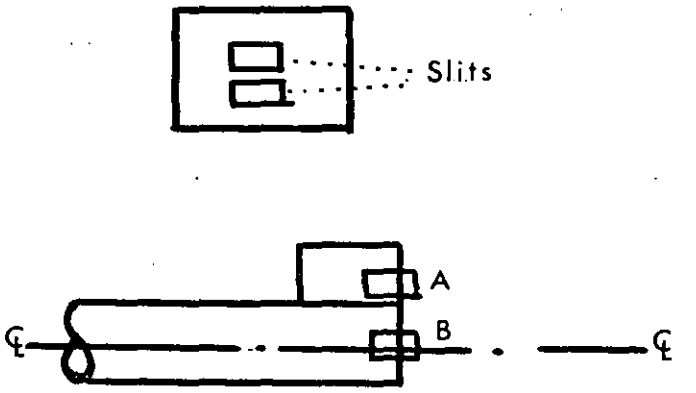

A – Upper Beam; Width 4 mm

B – Lower Beam; Width 4 mm

Bar Diameter 12·7 mm

Front View

and the endface record. Intermediate positions of the shutter beam showed a correspondingly smaller delay between the start of the records.

A further test was to use a light beam on each shutter, (with no specimen) the bars rung together, and positioned so that a record of each shutter displacement could be obtained (figure 3.8). With the bars accurately aligned and the endfaces polished to a ringing finish, there was no apparent delay or difference in shapes of the two records, as shown in figure 3.6(d).

From these experiments it was concluded that the joint was not producing any measurable delay or change in displacement signal, and that the two shutters were accurately following the motion of the cross-section of the bar, provided that the shutter light beam was positioned close to the bottom of the shutter.

The shutters and bars were made of stainless steel, and the shutters were normally brazed into position in a narrow slit on the bar surface. A rigid joint was thus obtained and no indication of a loosening of this joint was ever noticed. A thin layer of lubricating oil was always placed on the endfaces of the bars in order to ensure a friction free interface between the specimen and the pressure bars.

FIG. 3·8 LIGHT BEAMS POSITIONED ABOVE & BELOW JOINT

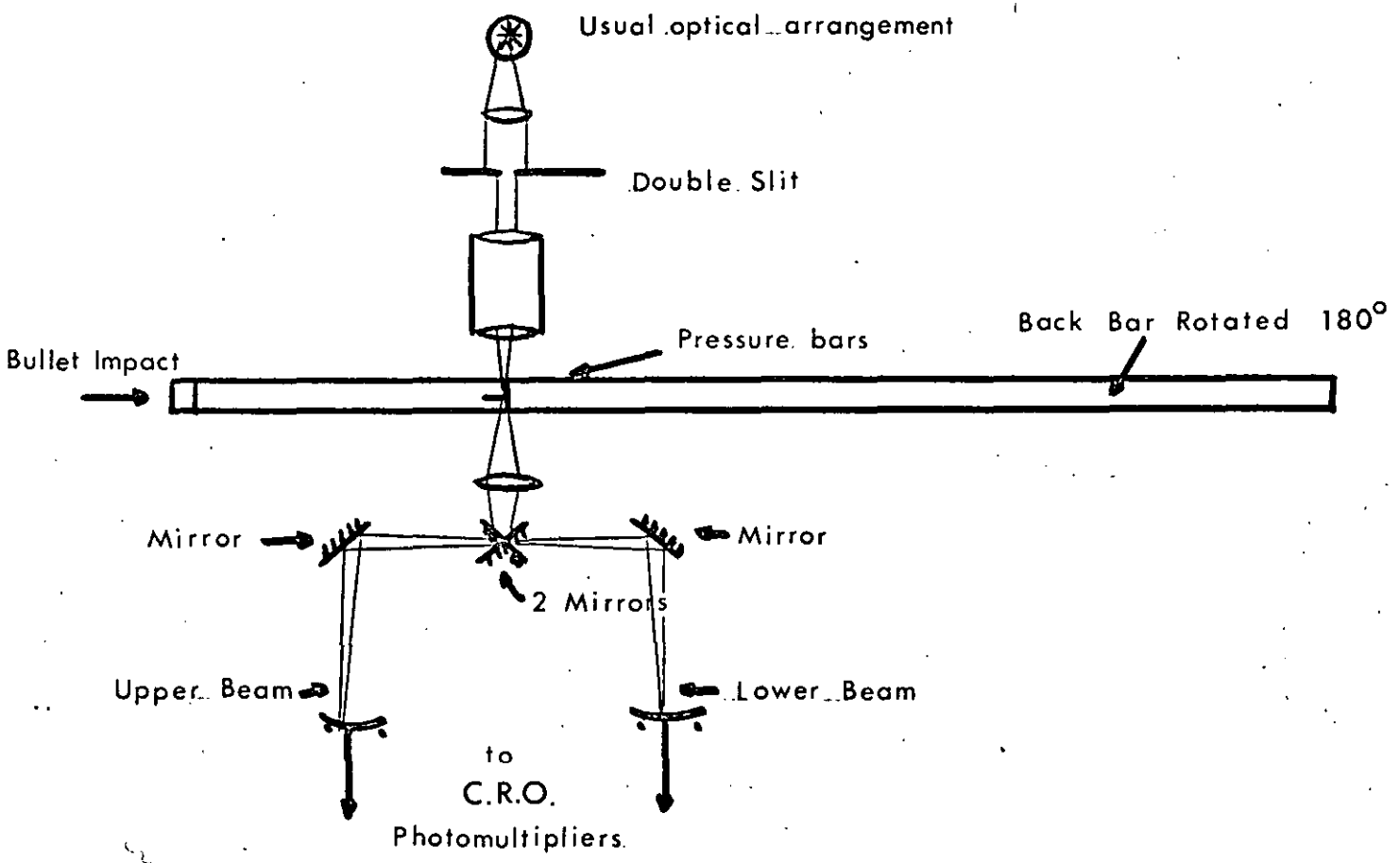

Plan View

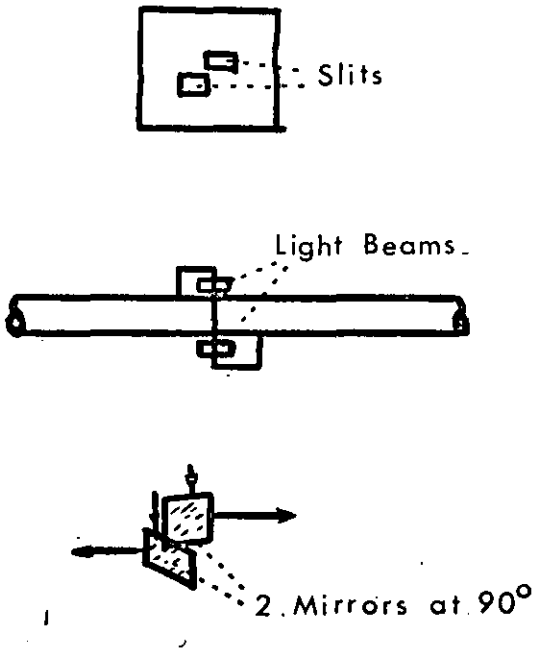

Front View

3.4 Other recording techniques

Strain gauges and quartz crystal gauges have been used extensively in pulse propagation measurements, and so these two techniques were also employed to determine their usefulness and to demonstrate certain features of the experiment.

Etched foil strain gauges were positioned on the surface of the input pressure bar in such a way as to record separately the incident and reflected strain pulses (figure 2.1). Two gauges were used, placed in series on opposite sides of the bar in order to cancel out any bending strains. A constant current supply to the gauges was required to ensure that the voltage change measured on the oscilloscope was proportional to change in gauge resistance due to the strain. A typical record is shown in figure 3.9(a) in which the incident compressive pulse is recorded first, closely followed by the reflected tensile pulse. Random electrical noise variations are present, together with certain large fluctuations in the signal, particularly after the initial rise. These fluctuations are thought to occur due to the dynamic viscoelastic nature of the straingauge cement used to bond the gauges to the bar. This cement may yield and flow non-uniformly during passage of the pulse, and hence adversely affect the transmission of strain to the gauge.

Analysis of the strain gauge records ε_I, ε_T and ε_R requires certain assumptions of equilibrium of loading conditions in the specimen and the use of time translations of the records to allow for propagation in the steel bars. The calculation of specimen stress and strain then proceeds using the equations given in section 2.1.2. Difficulties may arise in the analysis, particularly with noisy signals, and in view of Bell's objections to this measuring technique it was decided not to use strain gauges on the steel bars for measurements of dynamic specimen behaviour.

FIG. 3-9

(a) Strain gauge signal : free bar

SWEEP 10 μs/cm

GAIN ·002 V/cm

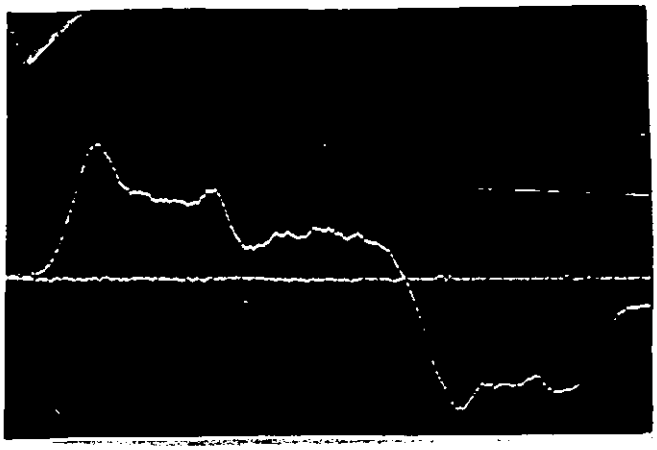

(b) Quartz Crystal on steel bar

GAIN 1 V c/m

SWEEP 10 μs/cm

Shutter beam 4-7 mm above bar

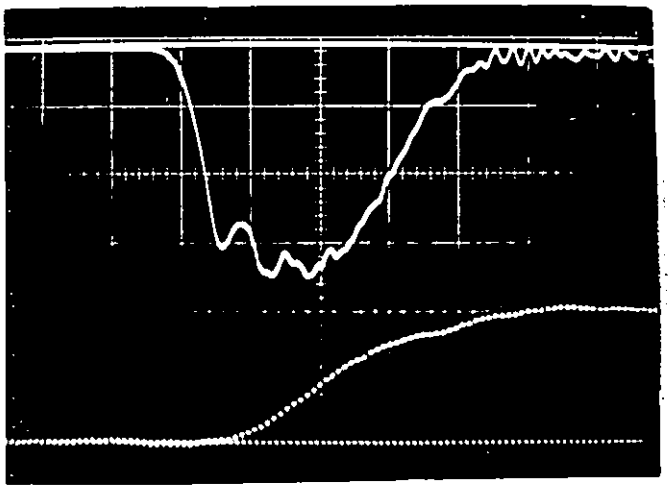

(c) & (d) Crystal in centre of input bar SWEEP 10 μs/cm

(d) GAIN 2 V/cm

SWEEP 20 μs/cm

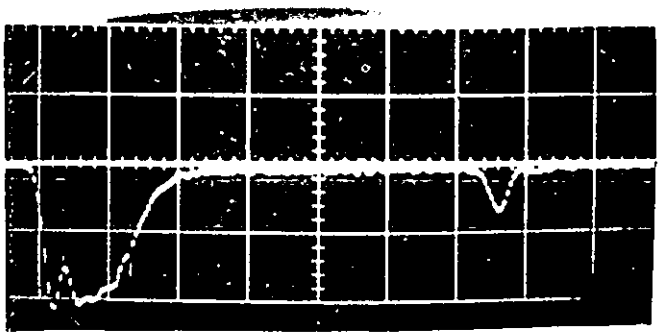

FIG. 3·9 Cont

SWEEP RATE 20 μs/cm

(e) & (f) Shutters repositioned on bars.

Crystal stress

GAIN 2 V/cm

Front shutter

Axial 60% fibres

Back shutter

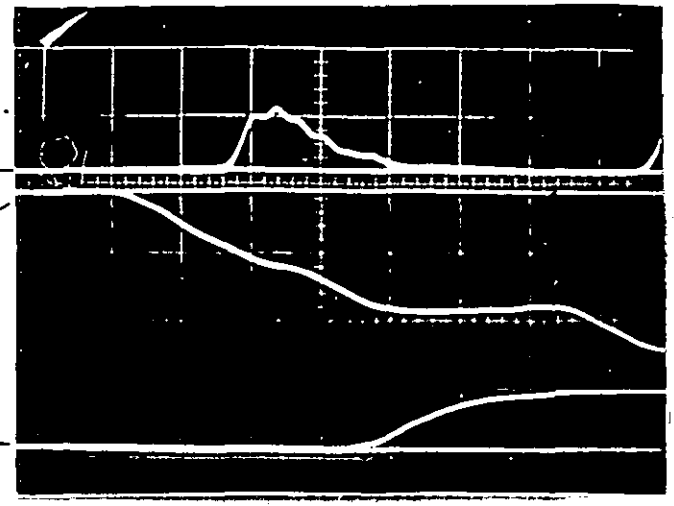

(f) Chordal 60%

SHUTTER GAINS 5 V/cm

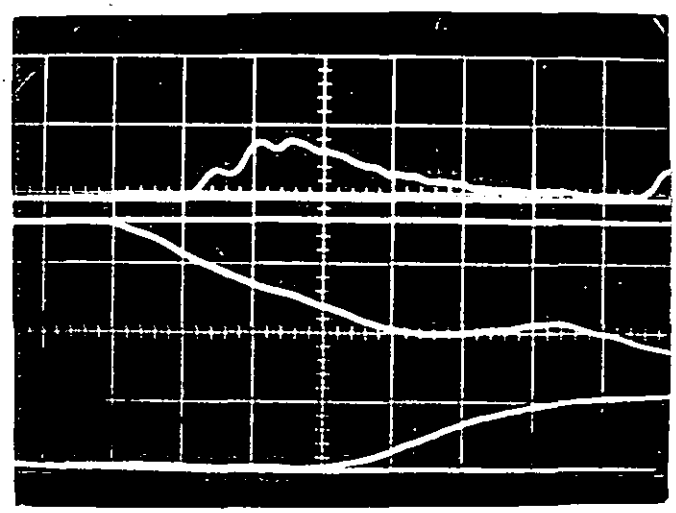

(g) Front strain gauge

GAIN 5 mV/cm

Back gauge

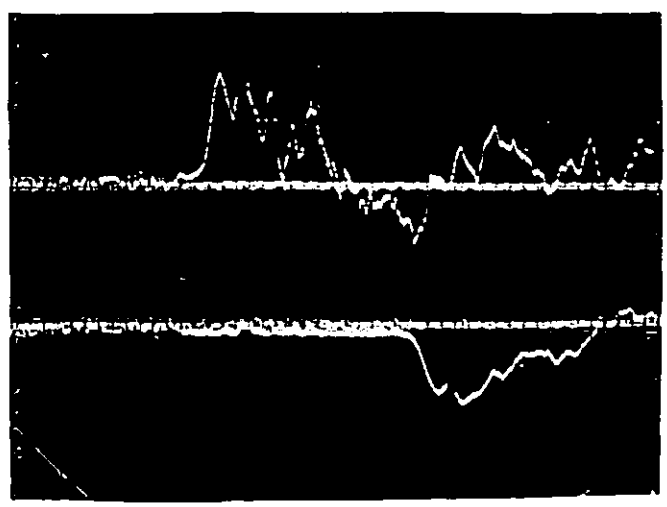

The noise content in figure 3.9(a) on a signal of 4-5mV obtained for a strain of 0.1% in the steel bar can be compared with the noise in figure 3.6(b) for a signal of 2V from the shutter displacement record.

Figure 3.9(g) shows the strain signals from the gauge placed on each of the steel pressure bars, with a specimen sandwiched in between the bars. The gauges were positioned 15 cm away from the specimen so that the gauge on the front bar would record the reflected strain signal at the same time as the back gauge was recording the transmitted strain signal. It can be seen that the signals are very noisy, and it is difficult to identify the reflected strain pulse. The bullet pulse in the steel bars produced a very small strain, so that the etched foil gauges provided a small signal on the oscilloscope.

Figures 3.9(e) and (f) show the particle displacement signals from shutters placed on the pressure bars 15 cm away from the specimen. The front shutter produces a record of the incident and reflected particle displacements, while the back shutter produces a record of the transmitted particle displacement. This arrangement was set up initially to provide a measure of the stress pulse for the circumstances in which the specimen was enclosed in a furnace during elevated temperature experiments. However , it was found that the shutter displacement signal amplitudes were rather too small for accurate measurement; in addition, since a sweep time of 20 μs/cm was required to fit all the signals in one sweep, the errors associated with identifying start times and propagation times were quite large, so this measuring technique was not used for any stress-strain determinations.

As an alternative measuring technique, thin discs of piezoelectric quartz crystal were used to measure the stress at a particular cross-section in the bar arrangement.

These crystals produce a charge output when a pressure is applied across them; this charge was collected by a small capacitor of 0.015μf, which transmitted a voltage to the oscilloscope. A direct relationship exists between the voltage across the capacitor and the pressure in the 0.5" diameter bar, such that a pressure of about 2×10^8 N/m^2 produces a voltage signal of about 4V. In this arrangement there were no problems of signal/noise ratio as the noise content was very small in comparison with 4V.

The time constant or RC value of the recording circuit was chosen to be considerably longer than the required recording time for the signal. With a 1 MΩ input impedance to the oscilloscope, the RC value was 15 ms, much longer than the 100 μs recording time.

The crystals were X-cut quartz, in the form of thin discs, 0.5" diameter, and either 1 mm or 0.5 mm thick. When the discs were attached to the pressure bars, a good electrical contact was required and silver loaded araldite which had the necessary conductance properties was used to bond the discs to the bars.

A comparison was made between the stress response of the quartz crystal and the record produced by the shutter and optical system, on a bar with a crystal and shutter both positioned at the end of the bar (figure 3.9(b)). From the crystal record it was possible to identify radial oscillations in the bar, and these appear superimposed on the longitudinal stress pulse. Similar behaviour was reported by Karnes and Ripperger (1966) in their quartz crystal records. When both sides of the thin crystal disc were rigidly held, then the radial oscillations were not so apparent (figure 3.9(c) and (d)). These records show the incident compressive pulse measured at a position

12.5 cm from the free end of an input bar. The start of the reflected tensile pulse reached the crystal as the tail of the incident compressive pulse had just passed the crystal, and the tensile pulse caused the cement bond to break since the tensile strength of the cement was much less than the reflected tensile loading. Thus there was no record of the reflected pulse, and this bond failure prevented the use of crystals in positions similar to strain gauges in figure 2.1.

However, it was possible to use the crystals at the interfaces between the specimen and the pressure bars, such that one side of the crystal was bonded to the steel bar, and the side next to the specimen was free. The two crystals recorded the stress at the interface, and figure 3.10(a) shows a photograph of these stress signals and the signals from two shutters placed immediately adjacent to the crystals on the pressure bars. This particular shot with a 0.25" long copper specimen, together with the shot in figure 3.9(b) of a free bar with no specimen, showed an important feature of the shutter displacement records compared with the crystal stress records.

The crystal at the backface of the specimen is seen to respond almost instantaneously after the response of the frontface crystal. A short time lag is present due to the propagation time across the specimen, which is only 1-2 μs. The shutter displacement records, at the same position as the crystal stress records, have a rather low amplitude in the initial portion, and there appears to be a delay time between any discernible start of the back shutter signal compared with the front shutter signal. This apparent delay is due to the nature of the signal, i.e. a displacement, rather than any systematic defect of the shutter response time, since the initial portion of the displacement would be of low amplitude until the pressure built up sufficiently to cause the shutter to move more rapidly. Thus identification of the start of each shutter record is a little difficult

FIG. 3·10

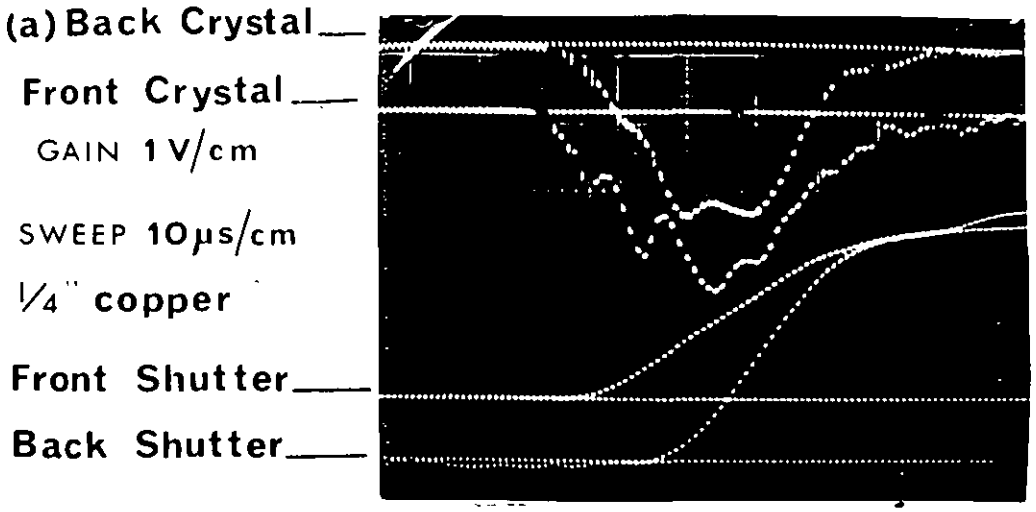
(a) Back Crystal
Front Crystal
GAIN 1 V/cm
SWEEP 10 μs/cm
¼" copper
Front Shutter
Back Shutter

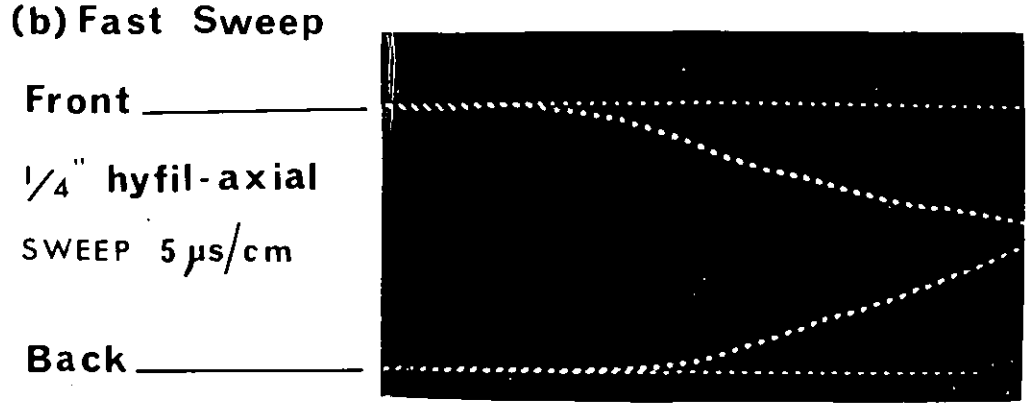
(b) Fast Sweep
Front
¼" hyfil-axial
SWEEP 5 μs/cm
Back

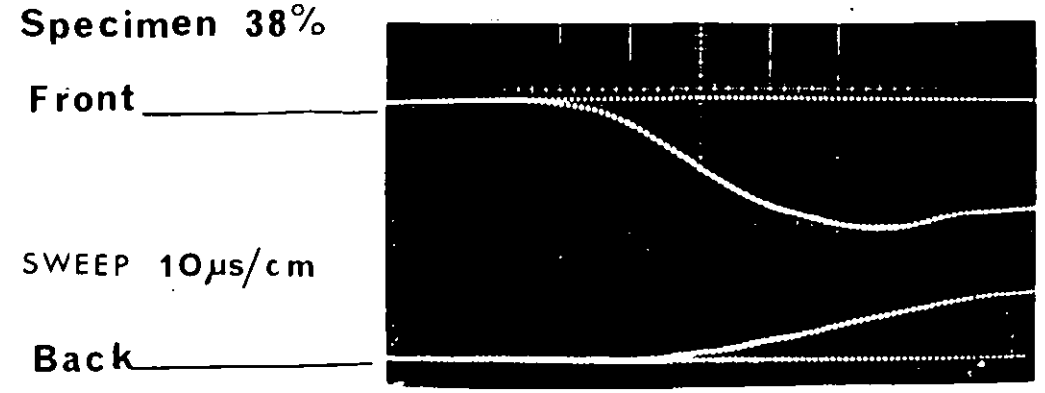
(c) Chordal 0·5"
Specimen 38%
Front
SWEEP 10 μs/cm
Back

FIG. 3·10 cont. SWEEP 10 μs/cm

(d) & (e) Axial 30% Large back shutter gain

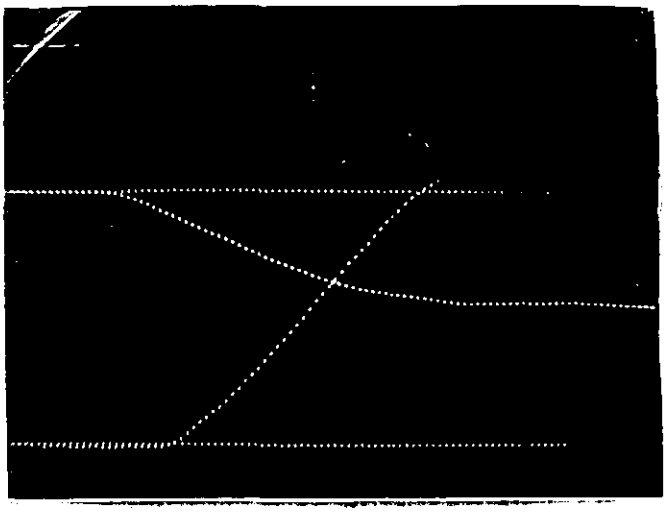

(e) Small back shutter gain showing large apparent delay

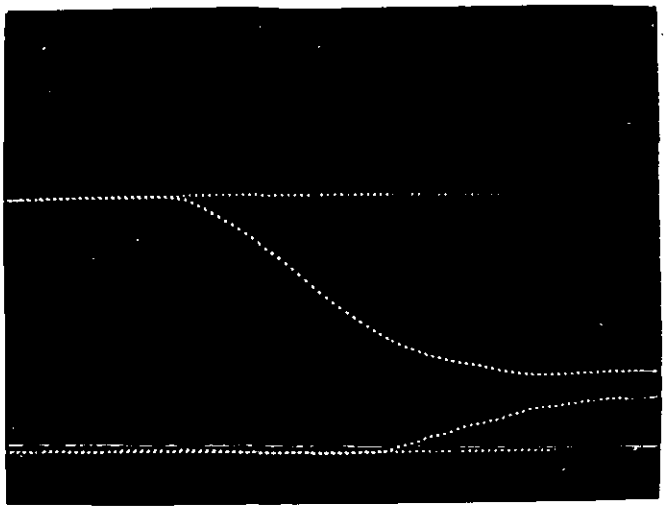

(f) Front & Back shutter displacements; (Axial fibres) 'O' unit used as Differentiator

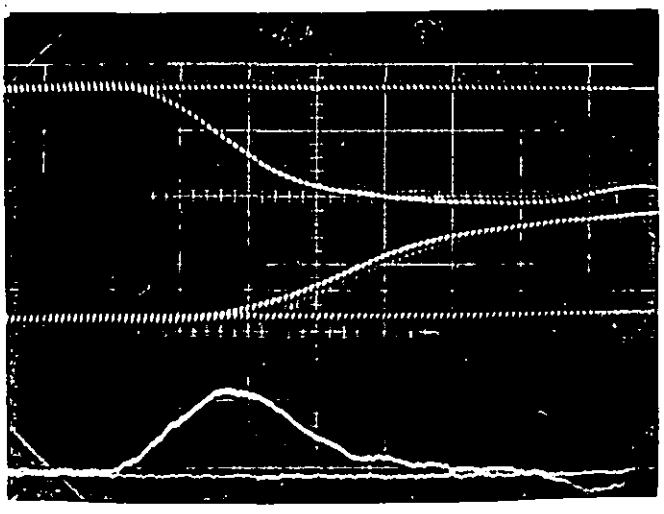

and corrections have to be made in the subsequent analysis.

Figure 3.10(b) shows a record of the front and back shutters with a 0.25" fibre composite specimen, photographed with a faster sweep speed than normally used. Close examination of the initial portion shows that the back shutter record starts to rise at around 2-3 μs after the front shutter record has started. This would imply a propagation speed across the specimen of about 3 mm/μs, much less than the expected value of about 8 mm/μs, taking the speed to be given by $(E/\rho)^{\frac{1}{2}}$. A greater amplification of the signals shows that this apparent delay is only of the order of 1-2 μs, although at large amplifications the noise content of both signals is quite appreciable and accurate displacement measurements would not be possible.

Figure 3.10(c) is a record of the two-shutter signals for a specimen in which a longer transit time would be expected, in addition to a lower amplitude at the back shutter. These features arise because of the specimen material properties, and are to be compared with the two signals in figure 3.6(b) where the transit time is short, and the back shutter amplitude is only a little lower than that of the front shutter. Figure 3.6(b) refers to a composite specimen with a high acoustic impedance, comparable with that of the steel pressure bar, with the result that there is a small reflected pulse in the incident pressure bar, and a relatively large transmitted pulse. Figure 3.10(c), however, refers to a composite specimen with a low acoustic impedance, resulting in a large reflected pulse and a small transmitted pulse. It can be seen that the properties of the specimen determine the ease with which the signals can be measured, and hence the apparent transit time across the specimen.

Figure 3.10(d) and (e) show records obtained for two identical specimens, the only difference between the shots being the signal amplification at the oscilloscope. The back shutter signal in figure 3.10(d) has about 5 times the gain of the back shutter signal in figure 3.10 (e) and identification of the start of this signal is difficult due to the low gain factor. There is an apparent delay of about 28 μs in this case, whereas figure 3.10 (d) indicates a delay of 6-7μs between the starts of front and back signals. Thus it was necessary to obtain displacement signals of sufficient amplitude for the subsequent analysis so that these systematic effects could be eliminated.

3.5 Analysis of displacement records

Displacement signals were recorded using a 1 MHz beam chopping facility on the oscilloscope so that the actual form of the signals consisted of a series of dots separated in time by 1 μs. This temporal division allowed a convenient co-ordinate marker. The vertical deflection of each dot from the horizontal zero line was measured with a two-directional travelling microscope accurate to ± 0.01 mm. Within the limitations of the instrument and its operator, the position of the centre of each dot was measured and noted as the appropriate point. The front and back shutter displacement measurements were then transferred to punched card form for computer analysis.

The net displacement at the front interface $y_1(t)$ is the sum of the incident compressive pulse (termed +ve) and the reflected tensile pulse (-ve) which is travelling in the opposite direction to the incident pulse, but contributes positively to the front displacement:

hence: $$y_1(t) = U_I(t) + U_R(t)$$

where U_I = incident pulse displacement

U_R = reflected pulse displacement

At the interface between the back pressure bar and the specimen, the pulse which passes into the back bar is that which is recorded by the back shutter as the displacement $y_2(t)$. There are many reflections within the specimen caused by the impedance mismatch between the steel bars and the specimen, but what is recorded only depends on the transmitted compression pulse.

hence: $$y_2(t) = U_T(t)$$

where U_T = transmitted pulse displacement.

Application of the one-dimensional elastic wave propagation theory shows that the stress at the front interface is given by:

$$\sigma_f(t) = (\rho c).(\dot{U}_I(t) - \dot{U}_R(t))$$

and at the back interface by:

$$\sigma b(t) = (\rho c).(\dot{U}_T(t))$$

where (ρc) is the acoustic impedance of the steel pressure bars.

The reflected wave at the front interface is a tensile stress, and thus subtracts from the net stress at that position.

The stress $\sigma(t)$ in the specimen is assumed to be the average of the stressesat each interface, and the strain $\varepsilon(t)$ in the specimen is given by the difference in displacements at each interface.

viz. $$\sigma(t) = \frac{\sigma_f + \sigma_b}{2} = \frac{(\rho c)}{2} . (\dot{U}_I + \dot{U}_T - \dot{U}_R)$$

$$\varepsilon(t) = \frac{y_1 - y_2}{\ell} = \frac{U_I + U_R - U_T}{\ell}$$

where ℓ = specimen length

An approximation can be made in which the net stress at the front interface is assumed to be equal to the stress at the back interface.

i.e. $$\dot{U}_I - \dot{U}_R = \dot{U}_T$$

Hence the shutter displacement-v-time records and the specimen stress and strain can be related in this way:

$$\sigma(t) = (\rho c)\, \dot{y}_2 \ (t); \quad \varepsilon(t) = \frac{y_1(t) - y_2(t)}{\ell}$$

An operational amplifier was first used to provide a differentiated signal of the back shutter displacement. This required the use of a Tektronix plug-in unit with resistive feedback and a capacitance in series with the amplifier. The RC value of the differentiating circuit was set at 10^{-4} s with C = 10^{-4} μf and R = 1 MΩ.

A large gain was required to present a reasonable signal, and a 50 pf noise suppressing capacitor was placed across the resistive feedback to limit the high frequency response caused by differentiation. Figure 3.10 (f) shows a record with the two displacement signals and a differentiated signal. A large noise content was present on the differentiated pulse, and this made measuring the co-ordinates of the signal waveform quite difficult.

A further systematic defect was that the RC value can only be truly adequate for a range of frequency components of the signal, and this was taken to be around 10^4 Hz. Other frequency components in the pulse were not differentiated properly, and the resulting waveform was thus in error.

Graphical differentiation as an alternative method was thought to be prone to quite serious errors, so a computer based mathematical analysis was used for all the records taken.

The back shutter displacement was considered to be adequately represented as a fifth order polynomial, and an ICL subroutine was used to fit an orthogonal polynomial to the data points by the method of least squares. The coefficients of the polynomial a_i $(i = 0 \to 5)$ were generated by the subroutine, together with the residuals at each point and the RMS error of the particular fitted form. Differentiation of the polynomial is readily done and the backface stress is then given by:

$$\sigma_b(t) = (\rho c).(5a_5t^4 + 4a_4t^3 + 3a_3t^2 + 2a_2t + a_1)$$

with the appropriate calibration factor to convert volts on the oscilloscope to displacement of the shutter.

Figure 3.11 is a graph comparing the actual data points of a back shutter displacement and the fitted fifth order polynomial points, and figure 3.12 is a comparison of this analytically differentiated back stress and that obtained by the operational amplifier method.

Thus the stress and strain in the specimen are obtained, and elimination of time between the two gives the dynamic stress-strain characteristic. Corrections have to be made for the initial part of the displacement record so that this averaging process is valid for the actual specimen stress and strain. The correction is a time translation of the back shutter stress record so that this record starts at the same time as the strain record to allow for the propagation time in the specimen

FIG. 3·11 BACK SHUTTER DISPLACEMENT SIGNAL

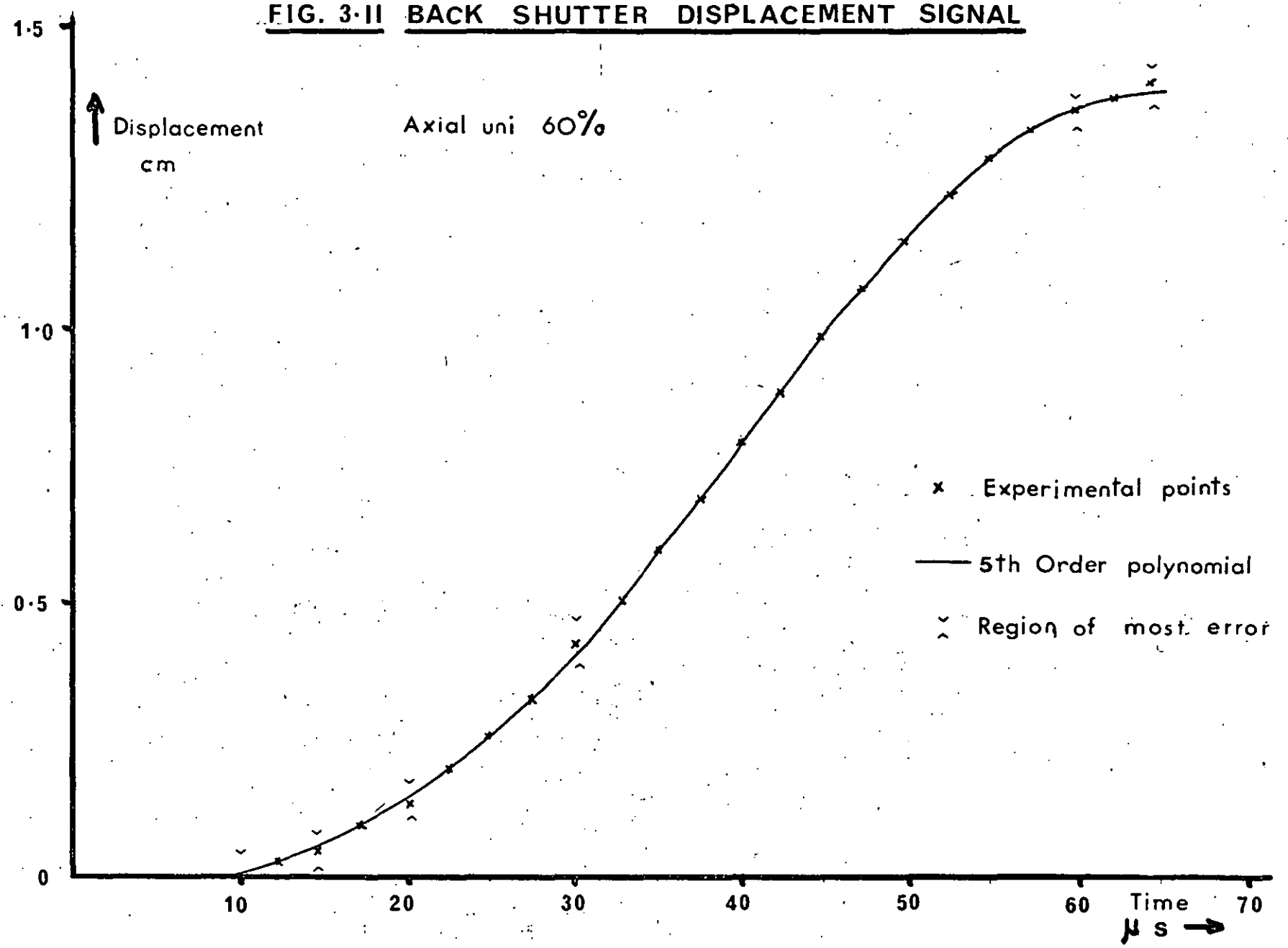

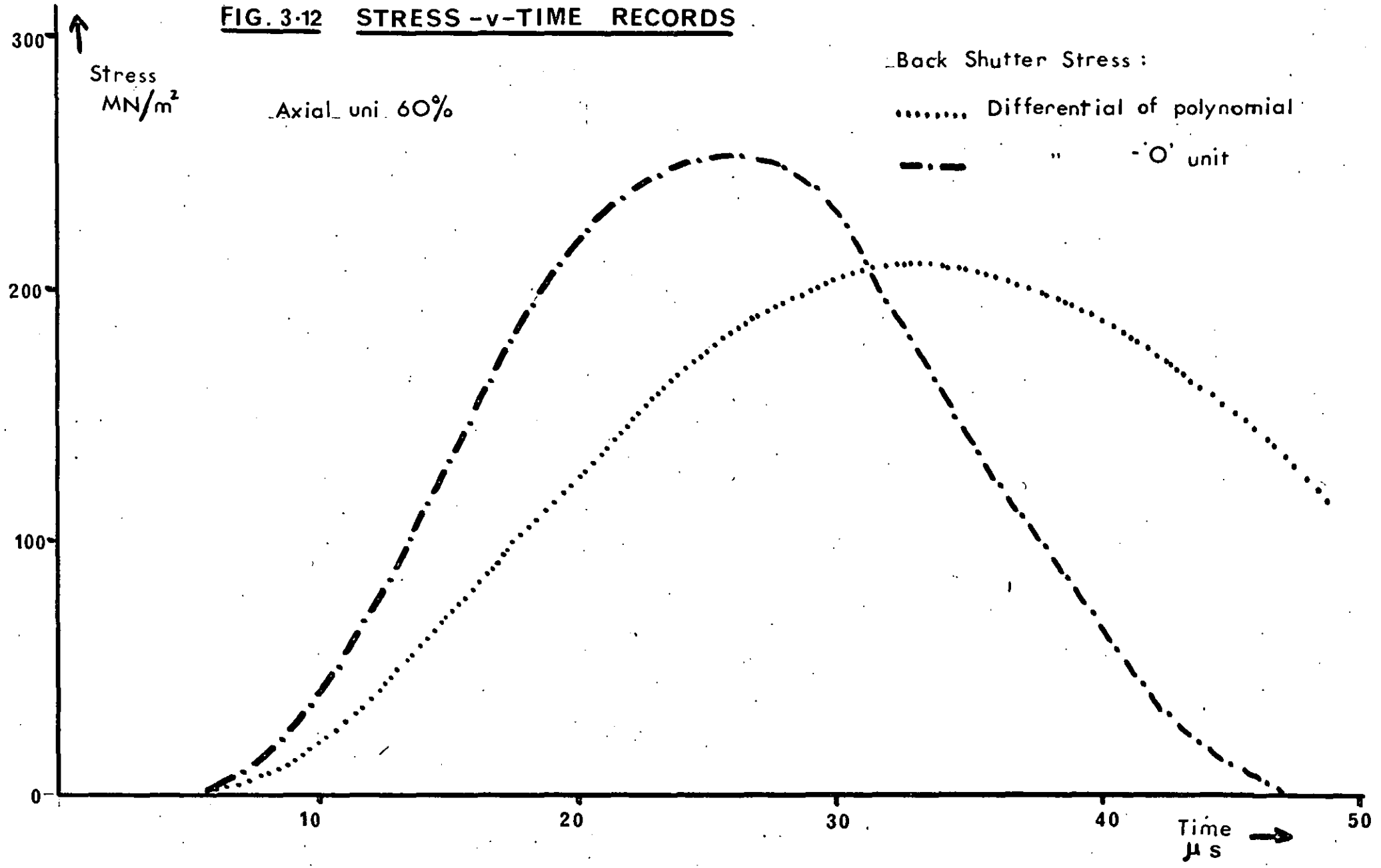
FIG. 3·12 STRESS -v- TIME RECORDS
Stress MN/m²
Axial uni 60%
Back Shutter Stress :
Differential of polynomial
" 'O' unit
300
200
100
0
10
20
30
40
50
Time μs

(1-2 μs) and the time during which no measurable deflection is seen in the back shutter displacement record. The total correction time was usually between 4 μs and 8 μs.

The time translation for the back shutter stress can be further justified because of the experimental requirement that there are sufficient reflections in the specimen before a stress-strain measurement is made so that the stress gradients existing between the interfaces at front and back of the specimen are minimized. Thus the material has to be in a state of combined uniform stress and uniform strain throughout the whole of the specimen in order that the stress-strain measurements are representative of the true specimen behaviour. This condition may be obtained for an isotropic material, in which there are only two elastic constants. For a carbon fibre composite, however, the anisotropic nature of the material construction may give rise to non-uniform stress and strain distributions within the short specimen of the Hopkinson pressure bar.

It should be noted that the stress-strain cycle undergone by a specimen in the Hopkinson bar depends almost entirely on the specimen material properties, since the stress which is transmitted through the specimen depends on its acoustic impedance and the acoustic impedance of the steel pressure bar. For a large mismatch between these values, a large reflected wave and a small transmitted wave will be produced, together with a correspondingly small specimen strain. Thus the reaction of the front shutter is determined solely by the acoustic mismatch, initially at the front interface but then later by the reflected waves in the specimen itself. The reaction of the back shutter is also determined by the properties under investigation, that is how much strain the specimen undergoes, which is a function of the dynamic characteristic. For a given incident stress amplitude the resulting stress-strain curve cannot be predicted in advance without

knowing the (ρc) values for the steel and the specimen and also details of the specimen dynamic characteristics, and so it is not possible to subject the specimen to a particular dynamic stress-strain curve.

Chiu and Neubert (1967) presented a finite difference method of calculating the net stresses in the front and back pressure bars for a given incident loading. A Maxwell-type viscoelastic response for the specimen was assumed, and the theoretical stress-v-time profiles were compared with an experimental situation. The values of Young's modulus and the viscosity coefficient in the model were varied in order to fit the experimental results and so produce viscoelastic parameters for the model. The major limitation of this analysis was the requirement for a smooth input pulse with a narrow frequency band, since the simple Maxwell model had only a single frequency response. Moreover its use would be limited in the present application since the pulse produced in the bullet impact is quite broad in frequency content, and the behaviour of fibre composites could not be uniquely described by such a simple viscoelastic model.

The acoustic impedance at a viscoelastic material boundary is dependent on frequency, and so the stress reflections and transmissions for an incident bullet pulse would be very complicated for the case of a general viscoelastic specimen.

3.6 Comparison with other work.

In order to check the validity of the optical shutter method for obtaining dynamic stress-strain characteristics, several isotropic materials were tested and the results compared with other published work.

Polycrystalline aluminium and copper alloy specimens and also perspex specimens were prepared, and at least four shots taken with each material. Figures 3.13, 3.14 and 3.15 show the average stress-strain curves obtained for aluminium, copper and perspex. Results for these materials have been well documented in the literature, and curves extracted from Billington and Tate (1972) and Davies and Hunter (1963) for both aluminium and copper are shown. Percy and Meikle (1969) have presented results for perspex over a large range of strain rates as a summary of the results of several different investigations, and representative curves from the literature are also shown on the perspex graph.

The 0.25" long aluminium and copper specimens used for these experiments were annealed for one hour at 500°C in normal atmospheric conditions. It is seen from the graphs that the permanent strain measured after the experiment agrees quite well with that shown by the stress-strain curves for these metals, and that the other published results indicate reasonable agreement with these curves. The stress-strain curves for copper and aluminium obtained by Billington and Tate showed a plastic strain after the experiment which depended on the amplitude of the stress loading. Their minimum plastic strains were 5% for aluminium and 5.5% for copper. The stress-strain curves from the literature are not shown completely on the figures 3.13, 3.14 and 3.15. No definite conclusions can be drawn on a comparison here, since the behaviour may differ in detail due to the various alloy compositions and annealing conditions used, but there is no reason to

FIG. 3-13 ALUMINIUM - Polycrystalline, annealed

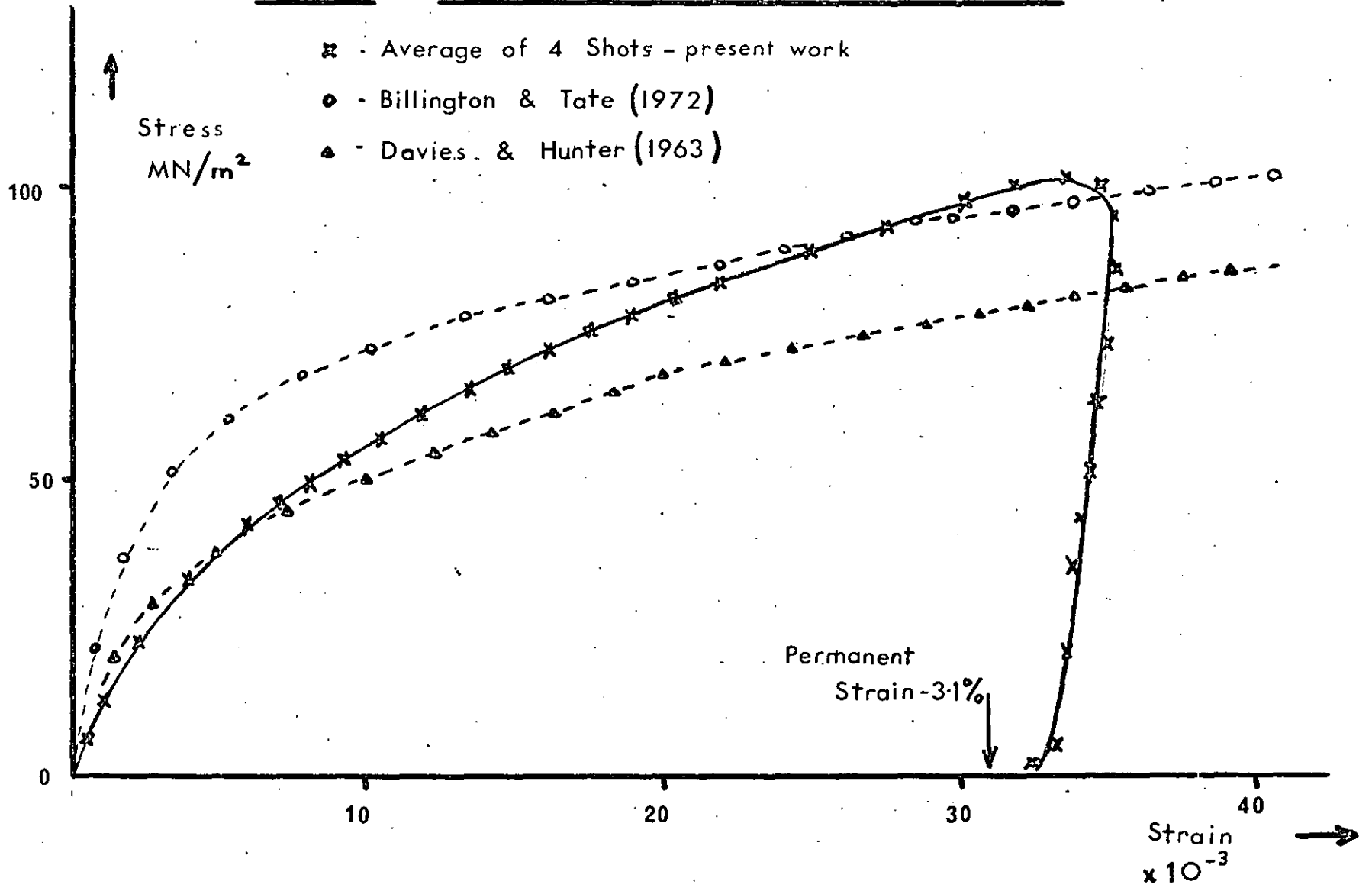

FIG 3·14 COPPER - Annealed, polycrystal

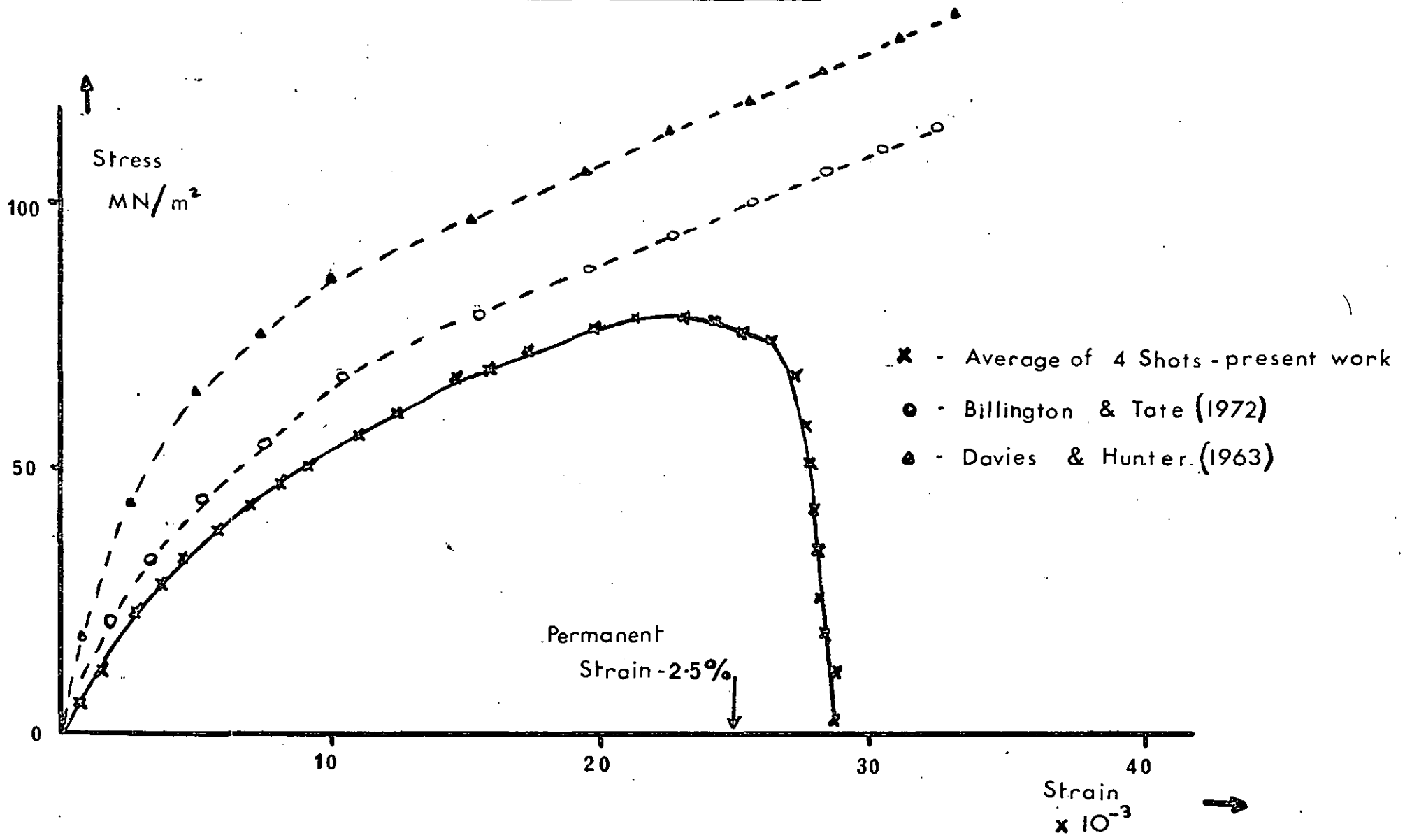

FIG. 3·15 PERSPEX - commercial quality

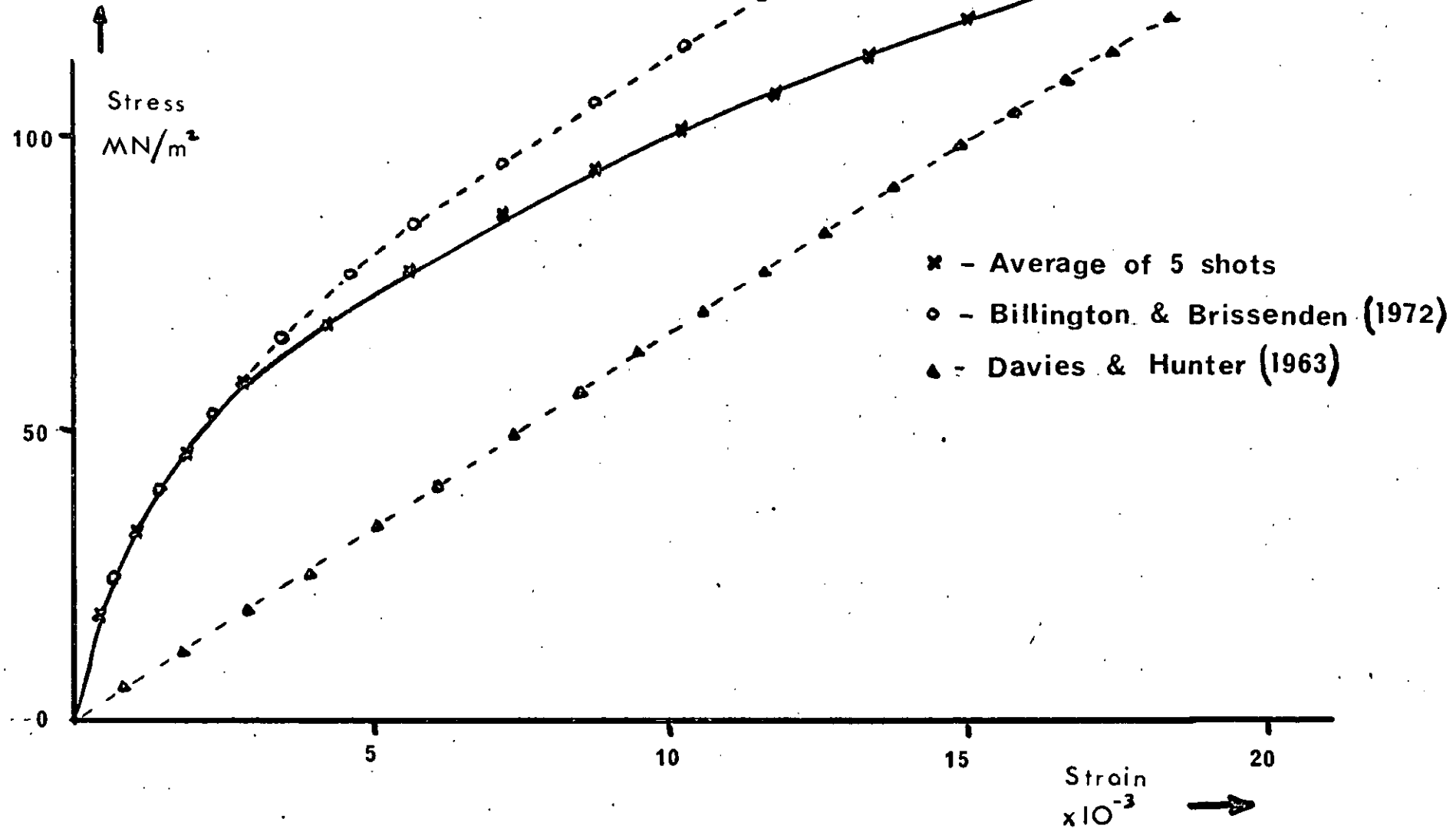

suspect that the optical/shutter method is incorrect in providing dynamic characteristics. In the case of perspex results, Percy and Meikle suggested that several factors could account for any unsatisfactory comparison. The mechanical properties of perspex may vary considerably, depending on manufacturing processes, humidity conditions and temperature conditions. In addition, the strain rate quoted was generally not a single value, but was variable throughout the test, so that a wide variation in the characteristics could be expected.

It should also be noted that the dynamic stress-strain curves for aluminium and copper presented by Bell (1966) differ considerably from those curves which are used in figures 3.13 and 3.14. It is on the interpretation of such dissimilar curves that the current controversy over strain rate effects in dynamic plasticity has evolved.

CHAPTER 4 EXPERIMENTS WITH FIBRE COMPOSITES

4.1 GENERAL

Experimental investigations of dynamic mechanical properties may be divided into four distinct classes:

(i) direct observation of stress-strain curves

(ii) wave propagation methods

(iii) resonance methods

(iv) free vibrations.

The method of approach has largely depended on the period and amplitude of the deformation, the nature of the material and its anticipated properties and on the shape and size of specimen which was readily available.

The split Hopkinson pressure bar was used to determine the dynamic stress-strain behaviour of a variety of carbon fibre composites, and the results are described in this chapter. Wave propagation and resonance methods are described in Chapter 5. A number of additional observations and experiments are contained in Chapters 6 and 7; Chapter 8 provides a summary and a fuller description of the results. The methods of free vibration were not considered in this investigation; as will be shown, the internal friction of fibre composites is relatively low at the frequencies used, and errors in the free vibration measurements become large when the internal friction is low.

Internal friction is the collective term for the various mechanisms by which some of the elastic energy present in vibration is converted into heat; these viscoelastic effects are considered in Chapter 8 for the composite materials of present interest.

4.2 PREPARATION OF SPECIMENS

4.2.1 Moulding procedure

Carbon fibre laminates are manufactured by Rolls-Royce on a mass production basis in a continuous form, pre-impregnated with the matrix material. The matrix is an epoxy resin, designated HR4C, containing boron trifluoride as a catalytic crosslinking agent and a second phase dispersionof a polysulphone. It is thought that the polysulphone surrounds regions of the epoxy and so extends the fracture toughness by crack blunting and also increases the viscosity of the basic resin system.

The "pre-preg" laminates take the form of sheets 15" long and 10" wide, either 0.010" or 0.005" thick (figure 1.1). The quantity of resin introduced onto the fibre surface is such that when the laminates are made up into a composite specimen, the fibre volume fraction is between 60% and 65%. The trade name of these sheets is "hyfil".

Moulded composites were produced with unidirectional fibres and with 0/90 crossply fibres at this volume fraction. The crossplied composites were made by laying up alternate layers of fibres at 90° to each other. In order to manufacture composite specimens with a lower volume fraction of fibres, these standard laminates were taken as a base, and a simple manufacturing technique was devised:

(1) Cut a standard HR4C prepreg fibre sheet (thickness 0.005") into the shape required - for the mould used here, this was 8.5 " x 4".

(2) Cut n sheets of HR4C epoxy resin film adhesive (thickness 0.001") into the shape required.

(3) Lay up the n sheets of resin onto the fibre sheet (to produce the"preform")

(4) Mould composite block with the necessary number of preforms to make up the moulded thickness.

The n sheets of resin material added to each fibre sheet determined the fibre volume fraction of the composite according to the formula:

$$V_f = \frac{5 \times 60}{5 + n} \% \quad (\pm 3\%)$$

since there were 5 parts of 60% fibre volume fraction, and n parts of 0% fibre volume fraction to each preform. 1, 3 and 5 sheets of HR4C were added to fibre sheets and made into specimens, resulting in fibre volume fractions of about 50%, 38% and 30%.

The moulding procedure was as follows:

(1) Pack the preforms into the 8.5" x 4" moulding box, and precure the stack of preforms in a constant temperature oven at 125° C for 20 minutes. This allowed the resin to flow throughout the stack of layers and produce a more homogenous and consistent block.

(2) Mould the block in the moulding box under constant temperature and pressure (165°C, 0.5 tsi) with fixed stops on the press to determine the moulded thickness. After the block was inserted, 10 minutes were allowed for the temperature to regain 165°C, and then moulding was continued for 60 minutes.

(3) The composite block was finally postcured for over 2 hours at 180°C to evaporate off all solvents and to allow final cross-linking of the resin to occur.

The volume fractions produced were accurate only within $\pm$ 3%, because the moulding process was quite likely to produce slight irregularities within the block, and a certain degree of inhomogeneity resulted.

Blocks were moulded to a design thickness of 0.600" in order that specimens of maximum dimension 0.500" could be machined for the Hopkinson bar apparatus.

Unidirectional fibre blocks of all these volume fractions were prepared, in addition to a 0/90 crossply block of volume fraction about 30%. From all the fabricated blocks there were two types of specimen which could be prepared; from the four unidirectional fibre blocks, cylindrical specimens of diameter 0.5" were machined with the fibres running along the axis (designated "axial" specimens) and with the fibres running across the circular cross-section (designated "chordal"). The 0/90 crossply blocks also provided specimens with alternate layers of fibres running along the axis and across the cross-section (designated "axial/chordal") and with alternate layers of fibres running across the cross-section at 90° to each other (designated "chordal/chordal"). Twelve types of specimen were thus prepared, covering a range of volume fraction, fibre direction and fibre lay-up.

4.2.2 Polishing

In order to perform the experiment correctly, it was necessary to prepare a close fitting bond between the two end surfaces of the cylindrical specimen and the end surfaces of the pressure bars. The specimens were hand polished to produce a satisfactory surface finish on the end faces, using a "Struers" wet pregrinder. Four grinding paper grades were available, with grain sizes of 70, 50, 35 and 20 μm. Water lubricated polishing was carried out on each face using successively finer grain sizes. For the experimental measurements to be realistic, the specimen end faces should be parallel to $\pm$ 15 μm and perpendicular to the axis of the cylinder to within $\pm$ 15 μm. These criteria were checked on the specimens using a surface plate and dial gauge. Further polishing was carried out on some specimens held in a centre lathe, with a buffing material held in the tool post.

These preparations were sufficient to use the surface tension of a thin layer of oil to attach the specimen in between the pressure bars; moreover, lubrication was necessary at the interface to minimise any frictional boundary restraint. Similar polishing was carried out on the steel pressure bars, a special jig being used to hold the bars perpendicular to the polishing plane. Care was taken to ensure that the shutter at the end of each bar was also polished and aligned with its edge parallel to the bar endface.

Specimen dimensions were measured before and after the experiment using a micrometer, accurate to $\pm$ 5 μm. The machined specimen sizes were of diameter 12.60 to 12.70 mm, and the two lengths used were in the ranges 6.15 to 6.30 mm and 12.60 to 12.75 mm.

4.3 STRESS-STRAIN RESULTS FROM HOPKINSON BAR

Dynamic stress-strain characteristics were obtained for several different types of carbon fibre composite, covering a range of material parameters. At least four separate shots were taken of each type, and the averages of the resulting stress-strain curves were calculated. These curves are presented in figures 4.1 to 4.8 so that the variations in material parameters can be compared.

Figures 4.1 and 4.2 show respectively results for the axial and chordal unidirectional fibre specimens at volume fractions of 60, 50 38 and 30%. Axial specimens undergo a much larger stress loading and are compressed to a smaller strain than the chordal specimens. The volume fraction of fibres in an axial specimen determines the stress-strain relation, whereas the behaviour of chordal specimens is not so dependent on the fibre content.

The graphs are plotted using the 'engineering'stress and strain, in which the stress is measured over the original area of the specimen, and the strain is measured over the original length. This procedure is acceptable for the small values of strain involved in these experiments, whereas if there had been a larger strain, the 'true' stress-strain behaviour would be required. Representative error bars are shown on the graphs at several points. The errors were calculated from the means and deviations of the stress-strain response using four or five experimental determinations of each stress-strain curve.

A correction for the radial inertia of the specimens, using the Davies and Hunter (1963) criterion, may be applied to these stress-strain curves. The correction becomes important in regions of the response where the strain rate is changing rapidly. The stress correction Δ is given by:

$$\Delta = \rho\left(\frac{1}{6}h^2 - \frac{1}{2}\nu_s^2 a^2\right), \ddot{\varepsilon}\ (t)$$

where ρ = specimen density $\doteq 1.6 \times 10^3$ kgm/m^3

h = specimen length $\doteq 1.2 \times 10^{-2}$m

ν_s = specimen Poisson's ratio $\doteq 0.2 - 0.5$

a = specimen radius $\doteq 0.6 \times 10^{-2}$ m

The rate of change of strain rate ($\dddot{\varepsilon}$) has a maximum value of about $- 120 \times 10^6$ s^{-2} at a strain of 4×10^{-3} (i.e. at the peak strain, 20 μs after the start of the pulse), and the stress correction for the axial unidirectional specimens is about $- 5$ MN/m^2.

The stress correction for the chordal unidirectional specimens is of the same order ($\sim - 4$ MN/m^2 at a strain of 10×10^{-3}) although the correction is particularly sensitive to Poisson's ratio, which is quite different for the two cases. ($\nu_s \sim 0.2$ for the axial specimens and between 0.2 and 0.4 for the chordal specimens). The size of the correction is within the experimental error of the stress-strain curves, so that the correction is not included on the graphs 4.1 or 4.2.

A more complete discussion of all the dynamic stress-strain characteristics, together with comparisons of quasi-static behaviour is given in Chapter 8.

Figure 4.3 shows the curves for the 0/90 crossply specimens - axial/chordal and chordal/chordal - at two volume fractions of 60 and 30%. The crossplied materials show a response similar to the axial unidirectional and chordal unidirectional responses at these fibre volume fractions, with the chordal/chordal material undergoing a larger strain and having a smaller initial modulus than the axial /chordal.

Figures 4.4 and 4.5 show the effect on the stress-strain curve of using specimens of length 0.5" and 0.25" for both axial and chordal specimens. Little change is seen in the case of axial specimens,

FIG. 4·1

AXIAL UNIDIRECTIONAL FIBRES

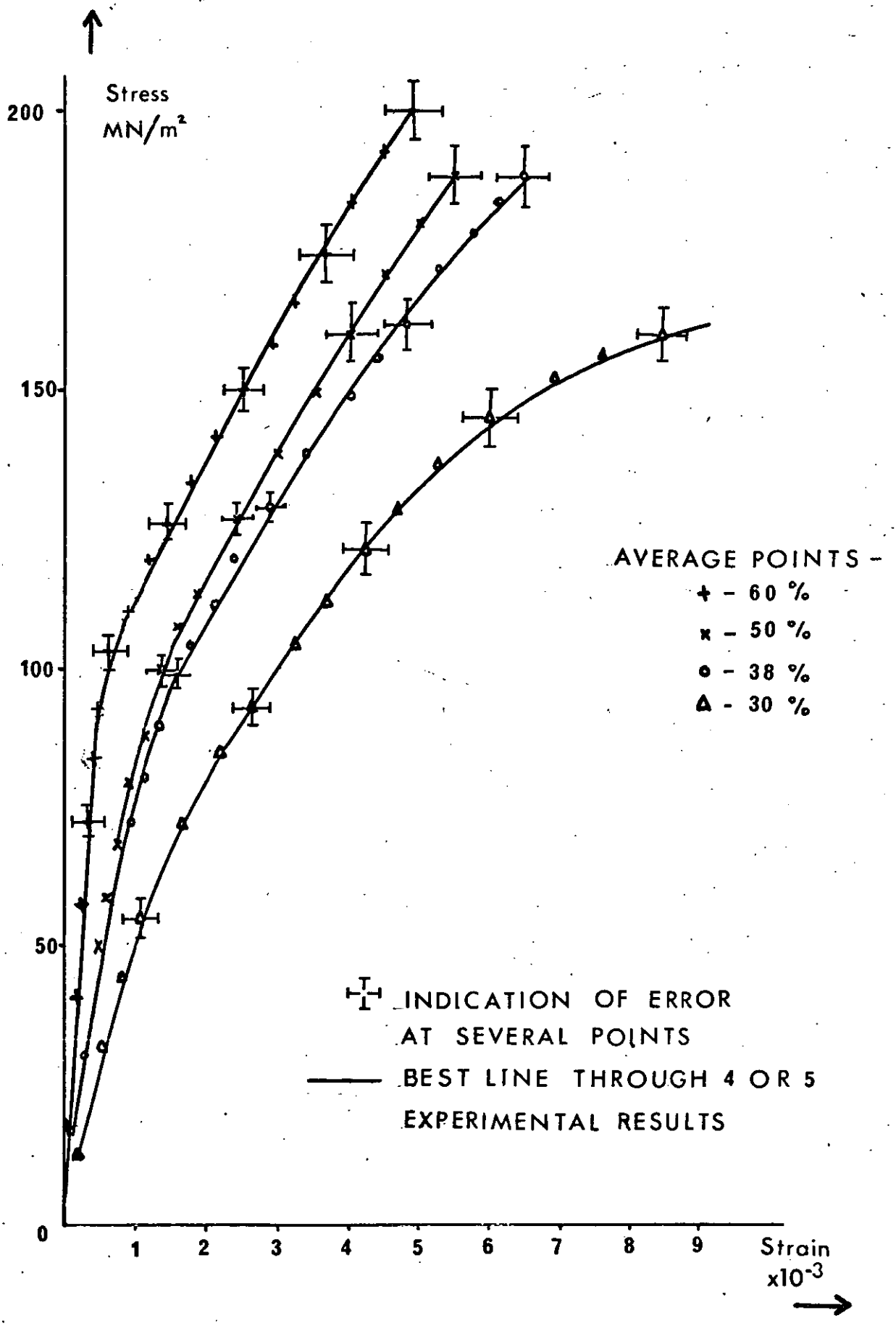

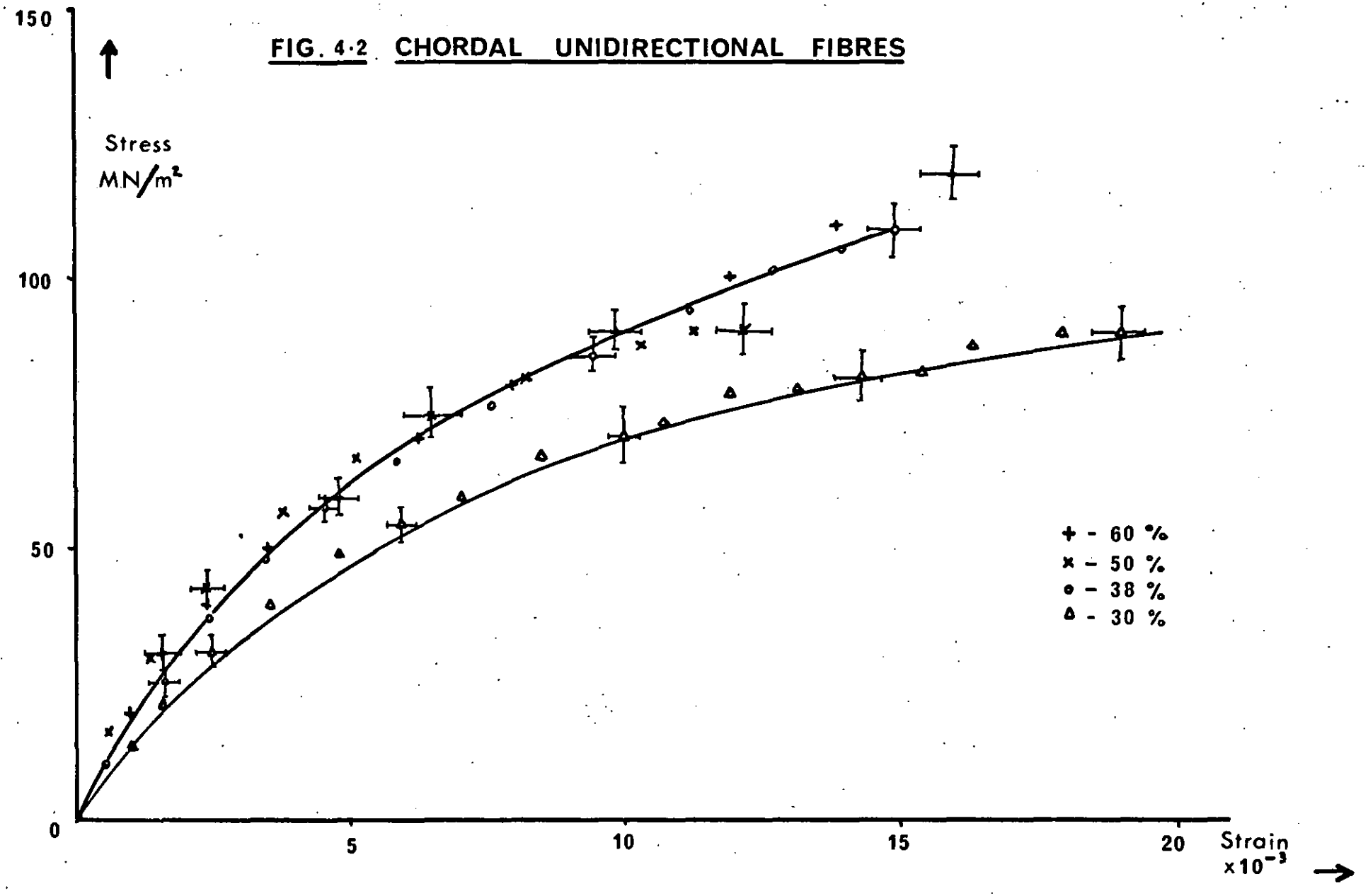
FIG. 4·2 CHORDAL UNIDIRECTIONAL FIBRES
Stress
MN/m²
150
100
50
0
5
10
15
20
Strain
x10⁻³
+ - 60 %
× - 50 %
o - 38 %
Δ - 30 %

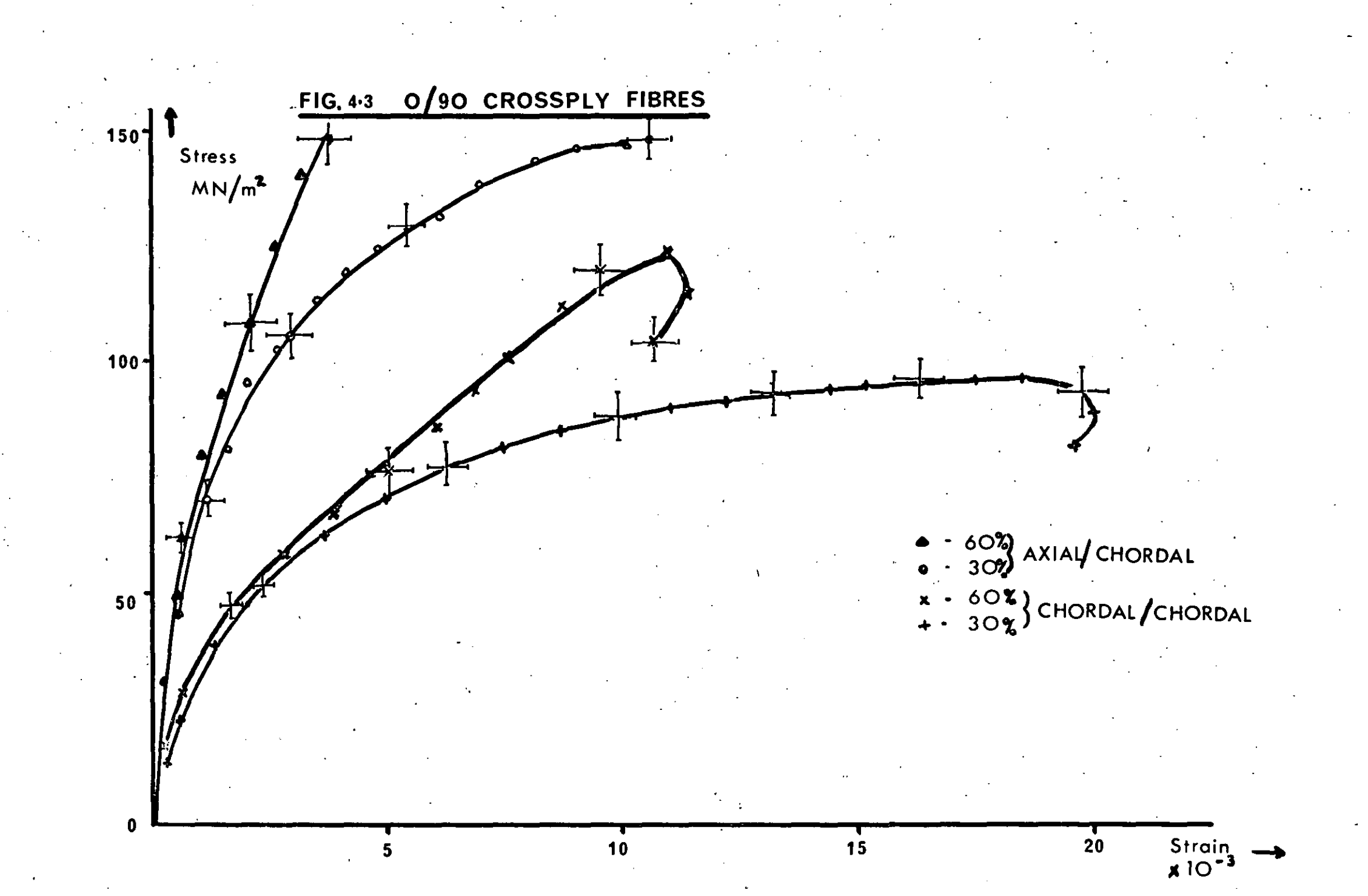
FIG. 4·3 O/90 CROSSPLY FIBRES
Stress
MN/m²
150
100
50
0
5
10
15
20
Strain
x 10⁻³
▲ - 60%
● - 30%
AXIAL/CHORDAL
× - 60%
+ - 30%
CHORDAL/CHORDAL

FIG. 4·4

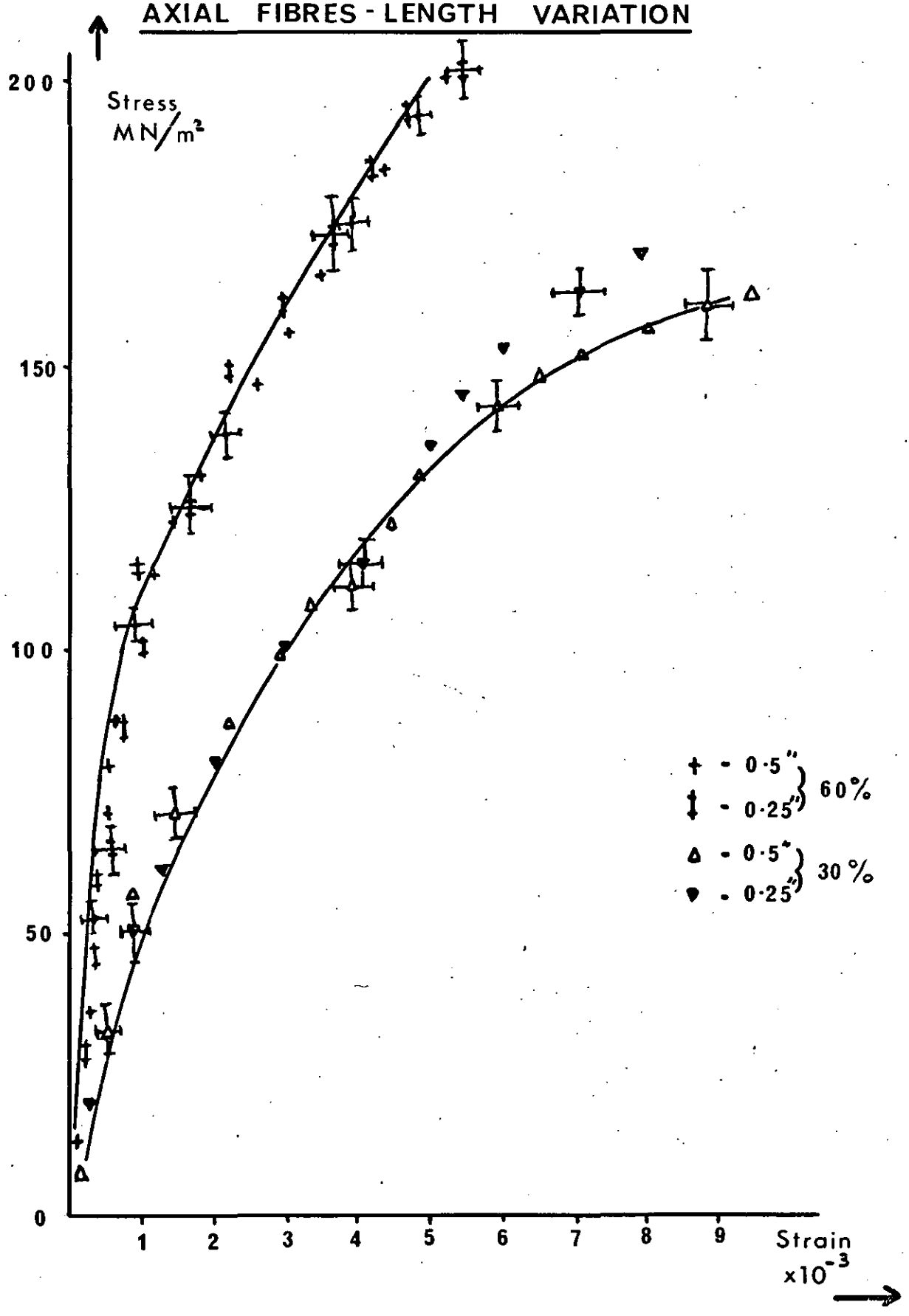
AXIAL FIBRES - LENGTH VARIATION
Stress MN/m²
200
150
100
50
0
1
2
3
4
5
6
7
8
9
Strain x10⁻³
+ - 0·5"
‡ - 0·25"
60%
Δ - 0·5"
▼ - 0·25"
30%

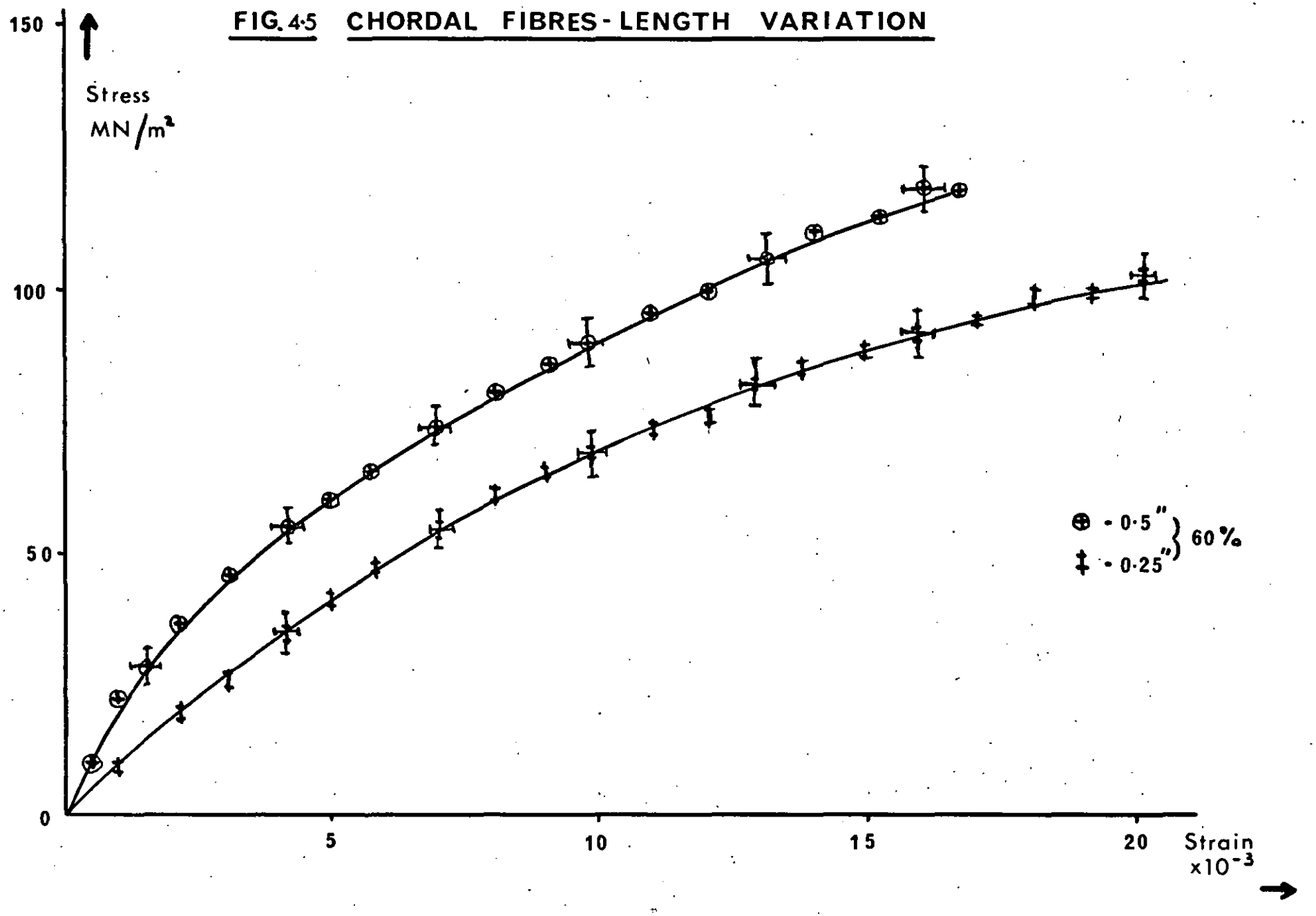
FIG. 4·5 CHORDAL FIBRES - LENGTH VARIATION
150
100
50
0
Stress
MN/m²
5
10
15
20
Strain
×10⁻³
⊕ - 0·5"
‡ - 0·25"
60 %

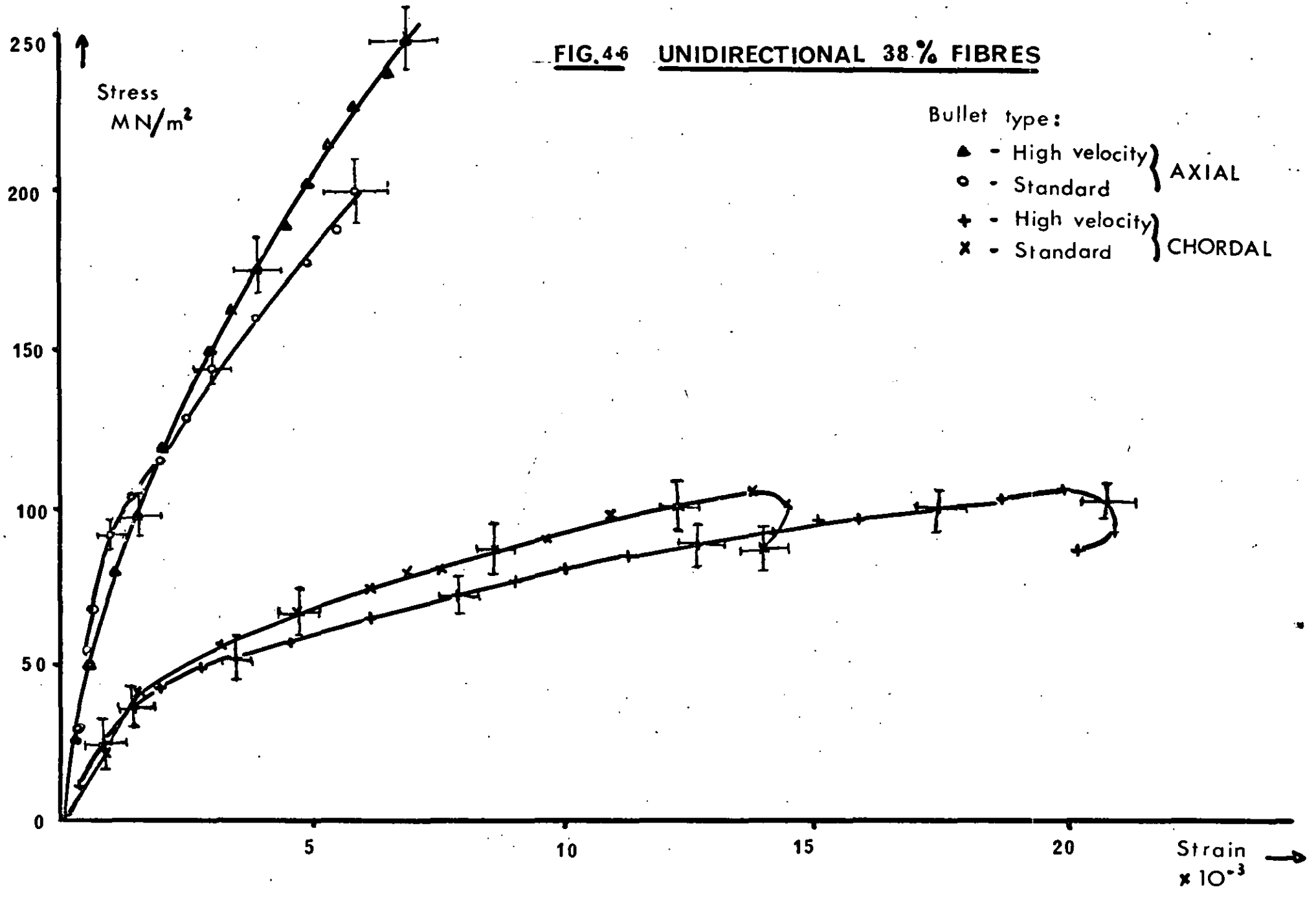
FIG. 4·6 UNIDIRECTIONAL 38 % FIBRES
Stress
MN/m²
250
200
150
100
50
0
5
10
15
20
Strain
× 10⁻³
Bullet type:
▲ - High velocity
○ - Standard
AXIAL
+ - High velocity
× - Standard
CHORDAL

FIG. 4·7

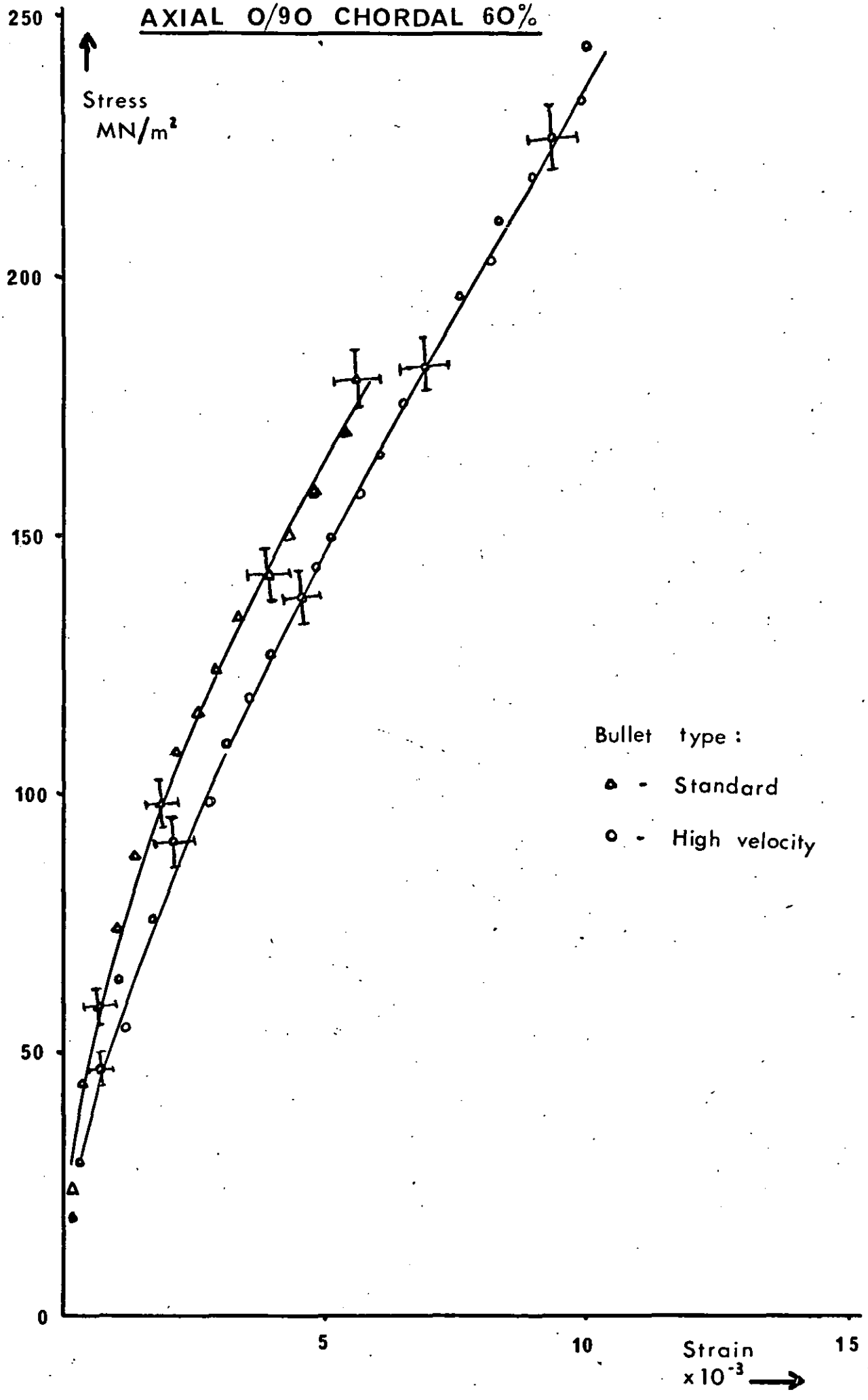
AXIAL O/90 CHORDAL 60%
Stress
MN/m²
250
200
150
100
50
0
5
10
15
Strain
x10⁻³
Bullet type :
- Standard
- High velocity

FIG. 4·8

AXIAL FIBRES 52% Used in long bar experiments

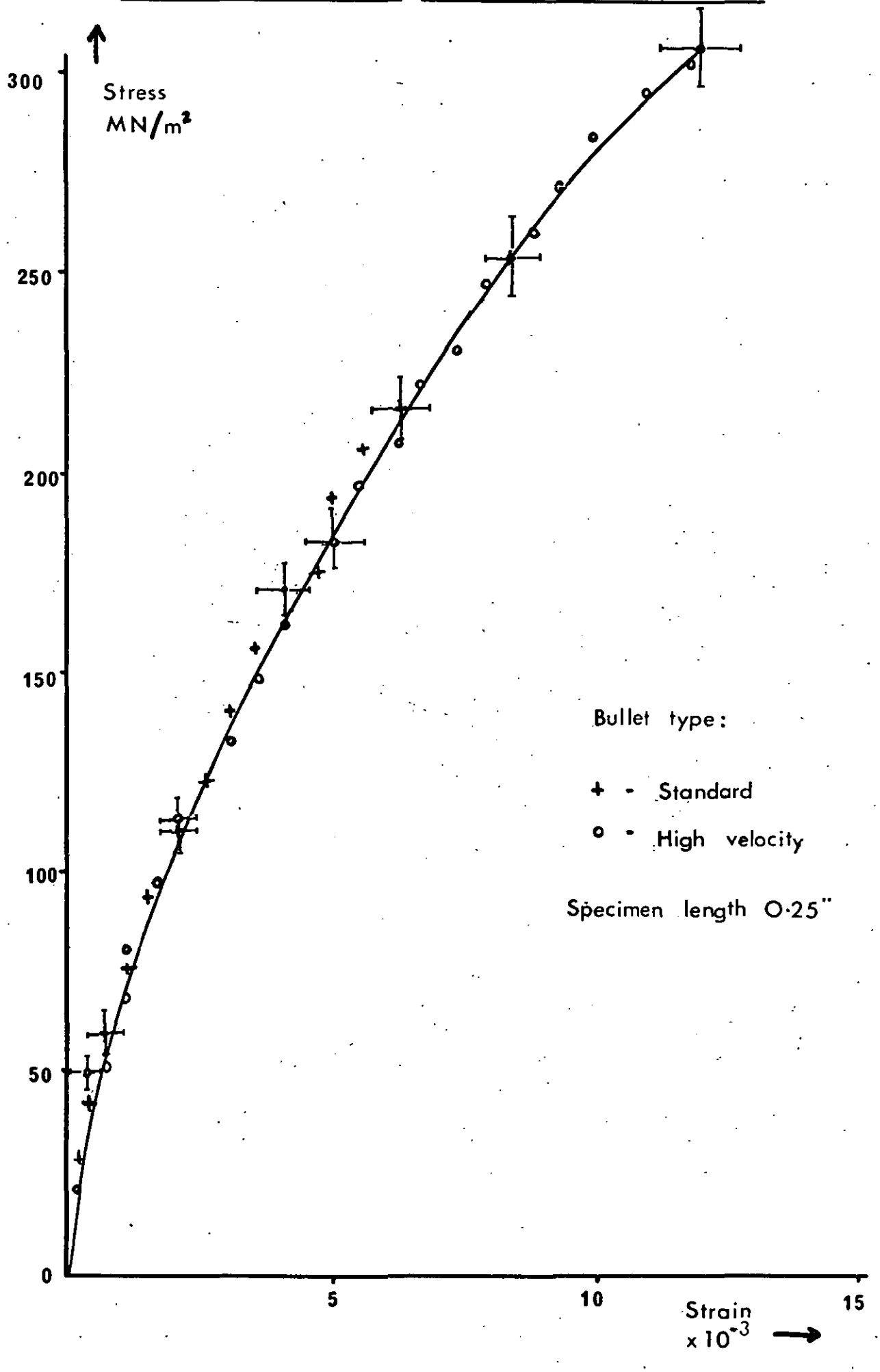

where the material is transversely isotropic on the macroscopic scale of this experiment. The Davies and Hunter criterion for specimen length/diameter, as calculated above, showed that the lengths 0.5" and 0.25" were within the limits of this criterion for the 0.5" diameter bars. Thus the axial specimen behaviour was independent of specimen geometry. The chordal fibre specimens are transversely anisotropic, and the Davies and Hunter criterion cannot be readily applied to these materials because the conditions for radial displacements are non-uniform around the circumference of the specimen. The response of these specimens is thus seen to depend on the specimen size.

In chordal unidirectional fibre specimens, there are two "Poisson's ratios" which couple the compression along the axis of the cylinder to the radial displacement perpendicular to and parallel to the fibre direction. In general, these two values differ significantly, since the elastic properties of fibre and matrix are so different. Thus the inertial stress correction given by Davies and Hunter becomes much more complicated, and the expression $h = \sqrt{3}\nu a$, where h, a are the specimen length and radius, with a Poisson's ratio ν, is replaced by:

$$h^2 = 3\left[(\nu_1^2 + \nu_2^2)\frac{3}{4} + \frac{\nu_1\nu_2}{2}\right]a^2$$

where ν_1 and ν_2 are the coupling factors for the chordal specimen. In the case of $\nu_1 = 0.2$ and $\nu_2 = 0.4$, $h^2 \sim 0.57a^2 \rightarrow h \sim 0.75\ a$ This geometry is more nearly satisfied by the chordal specimens of length 0.25".

Figure 4.6 shows the stress-strain graphs obtained with the standard 0.22" bullet and the high velocity bullet for 38% unidirectional specimens in the axial and chordal directions. The high velocity bullet produces a higher stress amplitude in the specimen, but the stress-strain curve follows that given by the standard bullet pulse.

A greater specimen strain is also produced by the high velocity bullet. Fig. 4.7 shows the effects of the standard and high velocity bullets on the 0/90 axial/chordal 60% specimens, and a similar behaviour is seen.

Fig. 4.8 shows the results for axial unidirectional 52% specimens with high velocity and standard bullets and a specimen length of 0.25". These specimens were made from the same batch of material which was used in the pulse propagation experiments described in Chapter 5, and the graphs provided a useful indication of the dynamic stress-strain curve which could be compared with the propagation results in long bars of this material.

Figures 4.9 and 4.10 show respectively the stress-time and strain-time variations for an axial/chordal 60% fibre specimen. The stress pulse which loads the specimen is increased by about 50% to about 240 MN/m^2 and rises to this maximum in about 25 μs for the high velocity bullet, whereas the standard bullet requires 30 μs to reach its maximum.

The strain rate in the axial fibre specimens is a function of fibre volume fraction, since larger strains are produced in longer times for low volume fraction specimens; figure 4.11 shows a graph of the maximum strain rate-v-volume fraction for all the unidirectional specimens.

The strain rates in the specimen for the standard and high velocity bullets differ by a factor of 1.5 or 2, and so it can be expected that the stress-strain characteristics appear very similar for shots with these two pulses; the only differences arising in the curves were the maximum stress amplitude and the corresponding maximum strain.

FIG. 4·9 Stress pulse shape – AXIAL 0/90 CHORDAL 60%

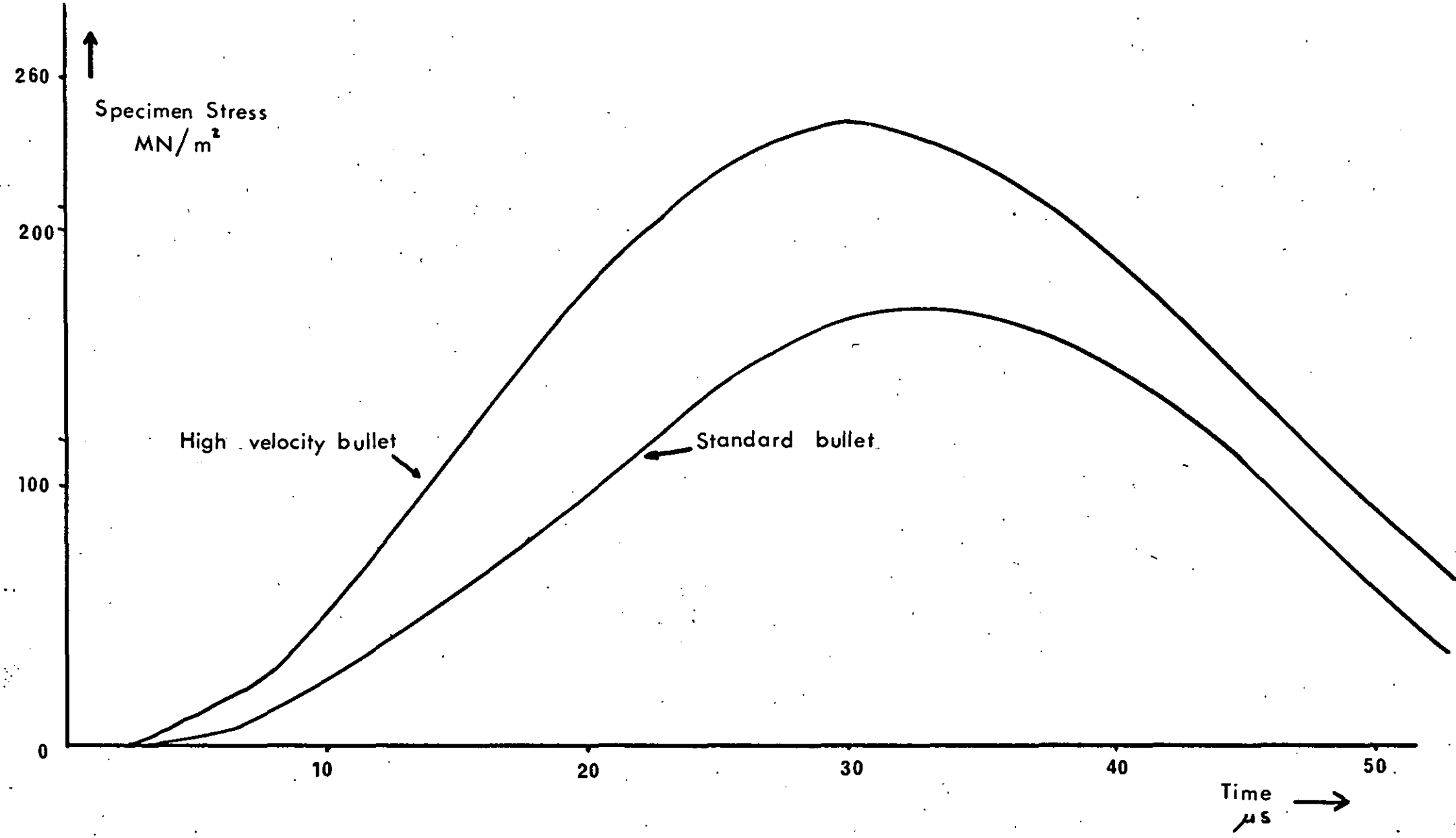

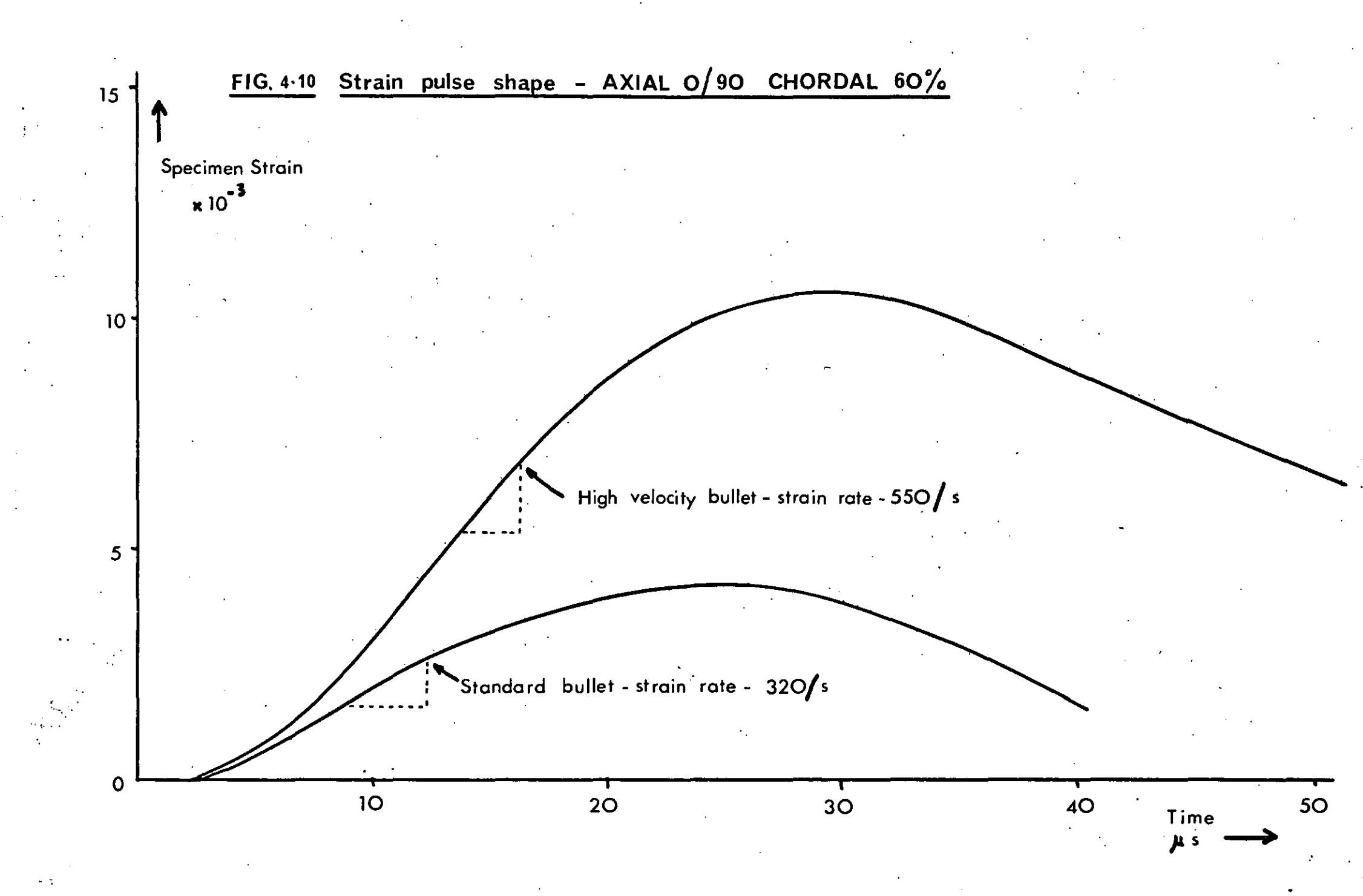
FIG. 4·10 Strain pulse shape - AXIAL O/90 CHORDAL 60%
15
10
5
0
Specimen Strain
x 10⁻³
High velocity bullet - strain rate - 550/s
Standard bullet - strain rate - 320/s
10
20
30
40
50
Time
μs

FIG. 4·11 STRAIN RATES - v - FIBRE VOLUME

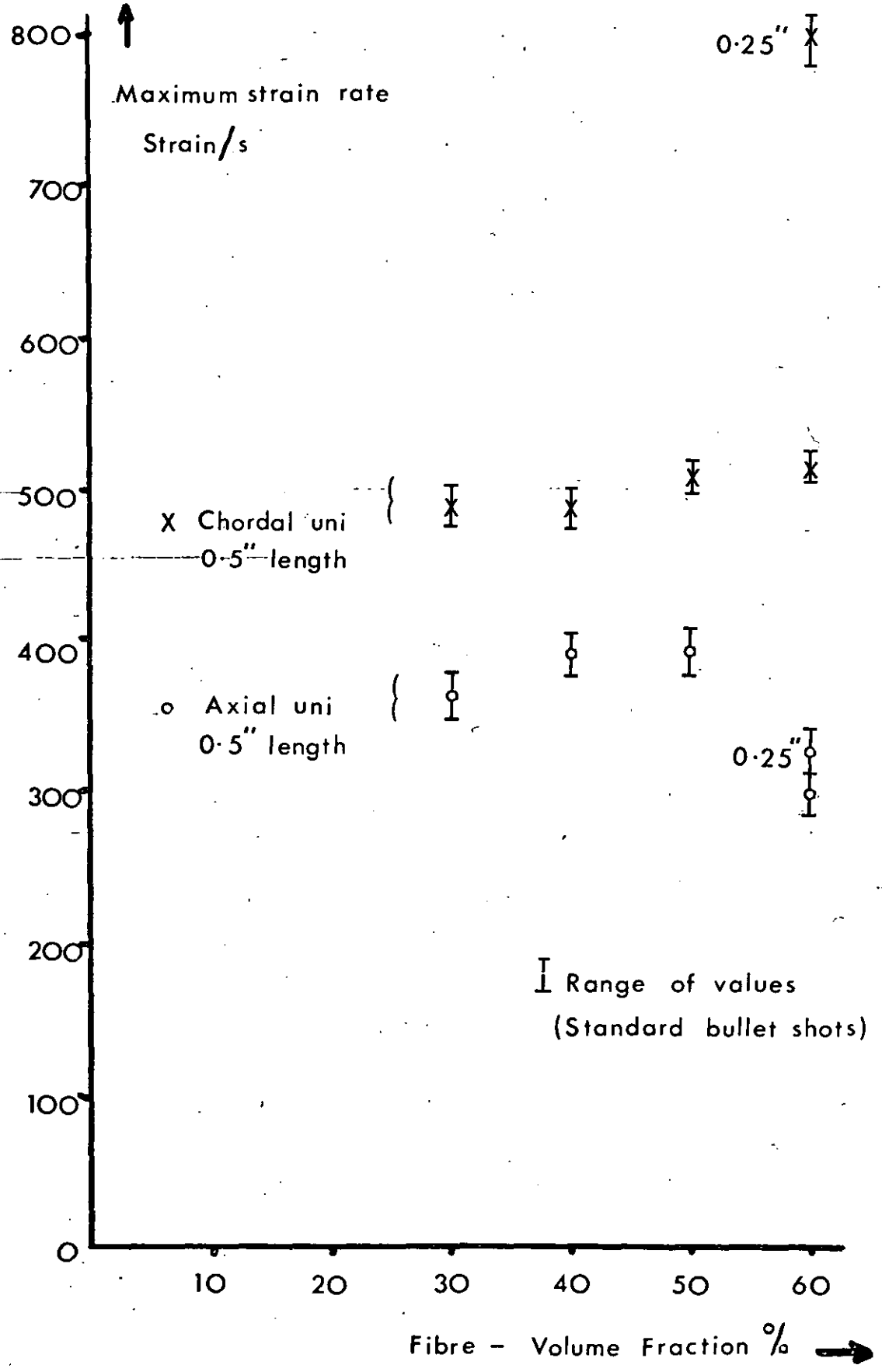

4.4 ERRORS IN STRESS-STRAIN GRAPHS

A representative signal for the displacement of each shutter can be obtained with an accuracy which depends on several contributory experimental factors. These factors can be broadly classified as mechanical and electrical. In addition, analytical factors will determine the accuracy of the calculations for the specimen stress, and the resulting stress-strain characteristic.

Sharpe and Hoge (1972) compared strain-time curves from Hopkinson pressure bar experiments using the average strain calculation of the usual strain gauge technique with the surface strain measurements of Bell. The lack of lubrication in Bell's experiments was thought to be the main cause of the discrepancy between the surface strain and the strain gauge techniques, and the validity of the method for calculating stress and strain was examined. From an analysis of the uncertainty associated with identifying the start of the incident, reflected and transmitted strain pulses, they concluded that the strain gauge technique was in great error (up to 25%) for the small strain in the initial stages. The surface strain measurements approached the one dimensional stress state for large strains, typically above 1.5% strain, and for the plastic region of strain in annealed aluminium specimens.

The shutter displacement technique provides the average specimen strain directly, without any reference to the one dimensional propagation theory and any errors associated with the strain gauge technique are eliminated. Systematic errors may occur, however, in the use of the back shutter displacement for the average specimen stress. These errors were considerably reduced by a time translation of the stress calculated by differentiating this displacement. The start of the average stressrecord was made to coincide with the start of the average strain, so that an average stress-strain curve was produced.

4.4.1 Mechanical errors

The tests on the shutters which were described earlier showed that the shutter displacement recorded with the light beam at the bottom of the shutter was identical with the displacement recorded across the end of the bar; also the joint between the two steel bars was shown to have little effect on the pulse propagation. A non-uniform loading in the experimental rig would be caused by misaligned pressure bars and specimen or by the bullet impact off-centre. Large discrepancies would produce oscillations in the displacement records, and for cases in which poor quality records were obtained, that particular shot was rejected as unsatisfactory. The hand polishing process sometimes gave rise to a shallow chamfer around the edge of the specimen endface, and errors were possible here. This small degree of non-parallelism was not readily visible when the specimen was set up in the split pressure bar, and could result in a non-uniform loading of the endface. The poor alignment would then cause a discrepancy between the displacement of the front shutter and the displacement of the back shutter which was not dependent on the material properties alone, and hence the specimen strain would not be directly related to the specimen stress obtained by differentiating the back displacement.

Billington and Tate (1972) estimated that a misalignment of one degree between the normal to the circular faces of the bars and the longitudinal axis of the specimen gave rise to a 2% difference between the maximum stress loading and the stress obtained from their strain gauge records. For the shutter recording method, an exaggerated case is shown schematically in figure 4.12, where the edge of the specimen has a maximum chamfer of 0.035 mm. The front displacement pulse causes the front pressure bar to move to the right, reducing the gap until the whole cross-section of the specimen is loaded. This

FIG. 4·12 ERROR IN POLISHED SPECIMEN DUE TO CHAMFERS

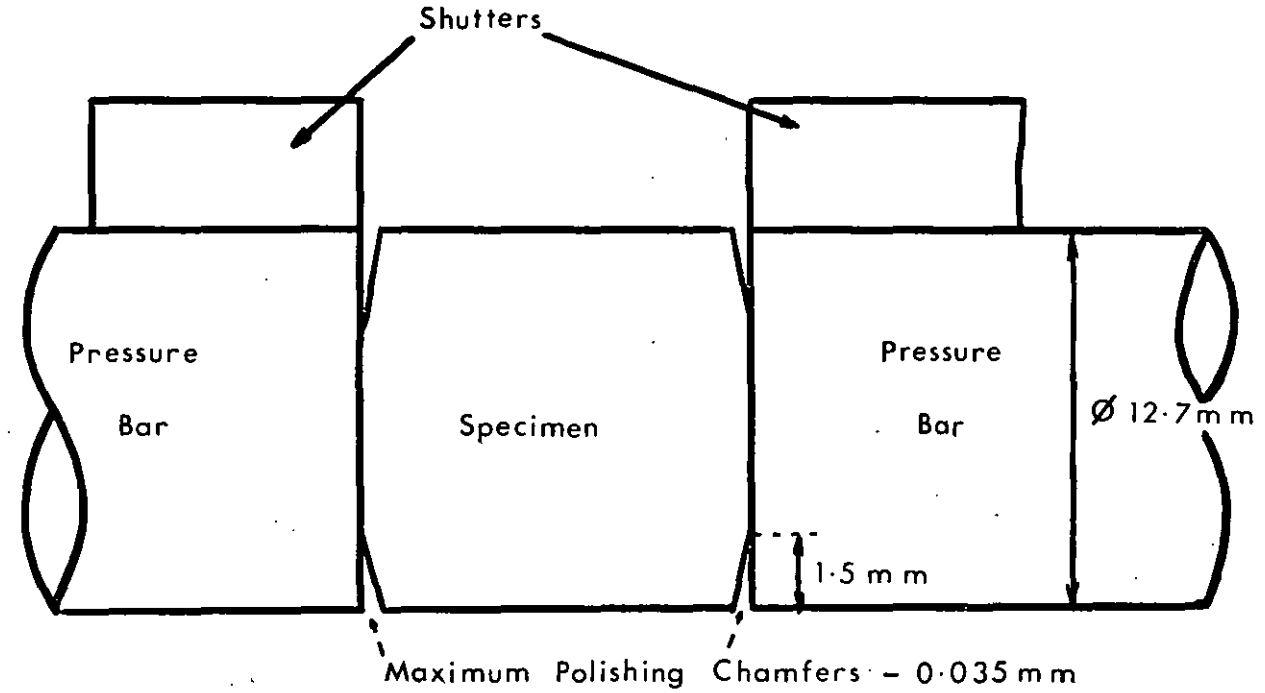

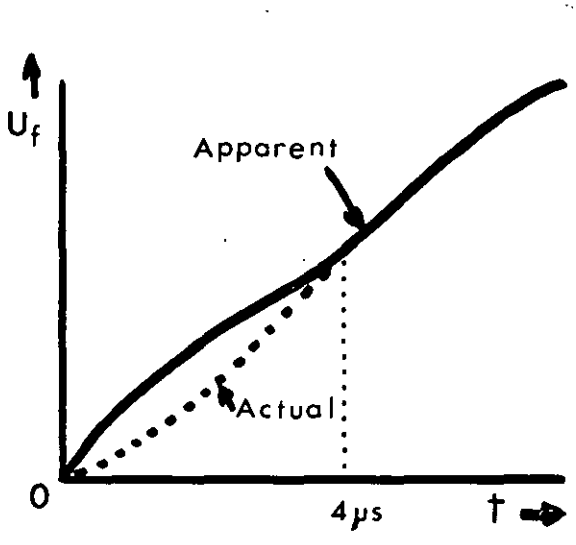

Front Shutter Displacement

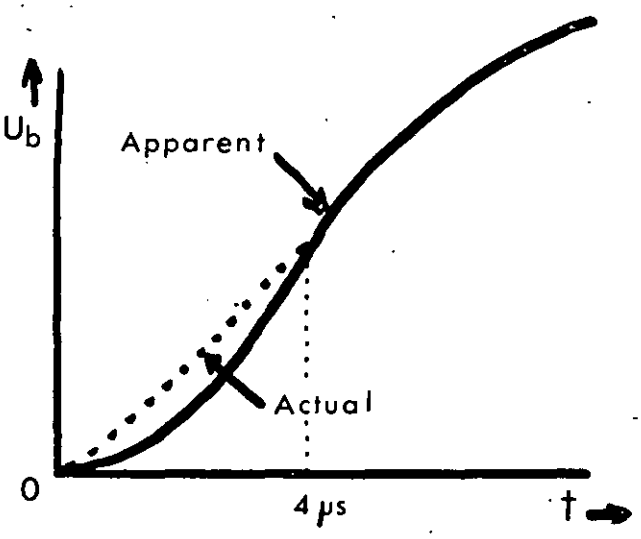

Back Shutter Displacement

THE ERROR IS SHOWN EXAGGERATED FOR CLARITY

would occur in a time of about 4-5 μs. Thus the recorded movement is in excess of the real movement for this initial period since the force in the pulse is applied over a smaller area than the real cross-section of the bar, and the apparent stress is increased. The reverse situation occurs at the back interface, since the back pressure bar receives a force over a larger area than the specimen area, and so a reduced signal for displacement movement is recorded. For the rest of the displacement pulse, the movement is unaffected, so any corrections required are necessary only for the initial 4 μs of the pulse. The calculated strain for this initial period is greater than the actual strain; the difference may be + 25% at 1 μs after the start reducing to no difference at 5 μs. The stress calculation is also in error, but the time translation of the stress pulse used in the analysis allows for an adjustment to be made for any initial discrepancy where there would appear to be no stress in the specimen for an initial strain.

The overall error in stress was estimated at $\pm$ 6%, and in strain at $\pm$ 8%. These values were estimated from measurement errors in specimen size and from the errors associated with measurements on the photographic record.

4.4.2 Electrical errors

Care was taken to ensure a uniform light beam so that the photomultiplier response was constant for the duration of the experiment. Noise in the electronic recording system was seen to be negligible, since, as described, the photomultiplier was not run at saturation and it was blanked off from ambient light. The oscilloscope gain was mid-range (at about 1V/cm vertical amplification) and there was little oscilloscope noise.

More serious errors may arise from the direct calibration experiment which accompanied each shot. Calibration was carried out by moving the shutter through the beam and observing the change in amplitude of the square wave produced by mechanically chopping the light beam. The resolution limit for a change in square wave signal on the oscilloscope screen was a factor here, and it was essential to ensure that the region of beam used in the experiment was covered in the calibration. An additional check was to produce a calibration curve for both shutters while opening and closing the beam, i.e. while increasing and decreasing the image intensity on the photomultiplier surface. The calculated stress-strain curves were very dependent on the accuracy of the calibration values; however, no independent check on the stress-strain curves for fibre composites was possible since there was no measurable permanent deformation after the experiment.

4.4.3 Analytical errors

The calculation of specimen stress and strain depends also on the analytical means used once the photographic recording of the shutter displacements are obtained. Reading errors may arise during operation of the travelling microscope. The centres of the dots for each trace were used in the measurement of vertical deflection, subject to the limitations of the grain size on the polaroid print surface, and the intensity of the dot. A 1:1 relation was assumed for the screen image on the photograph and the actual screen size on the oscilloscope.

Errors in the parameters used for the fifth order polynomial fitting program to calculate the specimen stress could be reduced by using higher orders. However, the data points have errors associated with them, and a goodness of fit criterion was applied, to prove the

validity of the fifth order polynomial. From the use of the travelling microscope, a reading error of $\pm$ 0.003 cm was estimated, and assigned as the error for each data point.

Polynomials up to the 8th order were fitted to a set of data points for one shot using the least squares method, and the residuals at each point were calculated for all the polynomial expressions. The goodness of fit was indicated by the "χ^2 test" where

$$\chi^2 = \sum_i \frac{r_i^2}{\sigma_i^2} \qquad \text{for all i points}$$

r_i = residual at each point

σ_i = standard deviation at each point

χ^2 should be approximately equal to the number of degrees of freedom M for the polynomial fit, with M = N - (n + 1)

where N = number of experimental points

n = degree of polynomial

For this particular shot, N = 67, hence M $\sim$ 65 - 58. Figure 4.13 shows a plot of χ^2 as a function of n, and it can be seen that a polynomial of the fifth order satisfies the criterion for $\chi^2 \simeq$ M.

It was assumed that the general shape of the displacement signal was very similar for all the specimens used, allowing for differences in amplitude and duration, so that the fifth order could be used in all cases.

In view of the limitations of the polishing and specimen preparation it was necessary to obtain several recordings for each specimen type in order that sufficient data were available. Statistical differences in the specimen material properties could also be averaged in this way, and the stress-strain graphs shown in the figures are the average curves for at least four shots for each specimen type. It was possible then to have an indication of the

FIG. 4·13 GOODNESS OF FIT

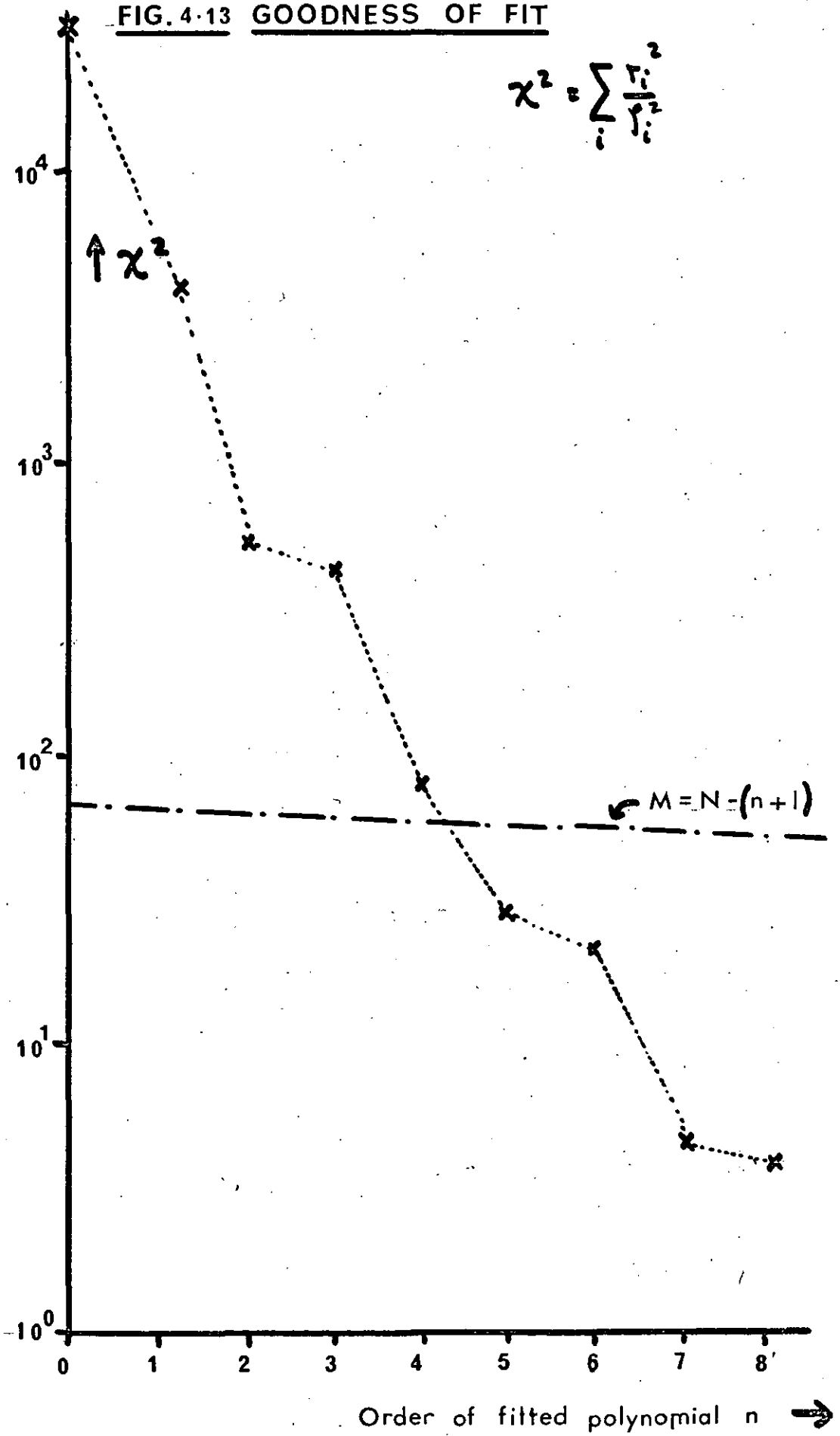

repeatability of the experimental results for all the specimens used.

Several independent shots also provided a check on the calibration values used in the analysis, since a calibrated experiment was performed after every shot. It should also be noted that each specimen used in the experimental apparatus, and for which a stress-strain curve has been presented in the figures, had been previously untested.

All the fibre laminate material which was used in the specimen manufacture had been obtained from the same batch of hyfil product. It was thought, then, that statistical differences in the material properties would be minimised, and that useful comparisons could be made between the results for the volume fractions, fibre directions and lay-up, as indicated on the graphs shown in figures 4.1 to 4.8.

4.4.4 Shutter displacement curves

A further indication of the reliability of the shutter displacement records can be given by comparing the records for several independent shots under identical conditions. Three records were obtained for the front shutter displacement signal with the back pressure bar and specimen removed, and these records are shown in figure 4.14. It can be seen that the maximum deviation between these signals is about 10%, and this figure is an upper limit to the overall error for the shutter displacement curves.

Examination of the front and back displacement signals for the fibre composite specimens showed that the maximum deviation may be as much as 10 - 12% at times greater than 45 μs after the arrival of the pulse. Nevertheless it was felt that, by using the results for at least four separate shots, an average stress-strain curve could be produced which was a true representation of the short specimen material behaviour.

FIG. 4-14 SHUTTER DISPLACEMENT RECORDS

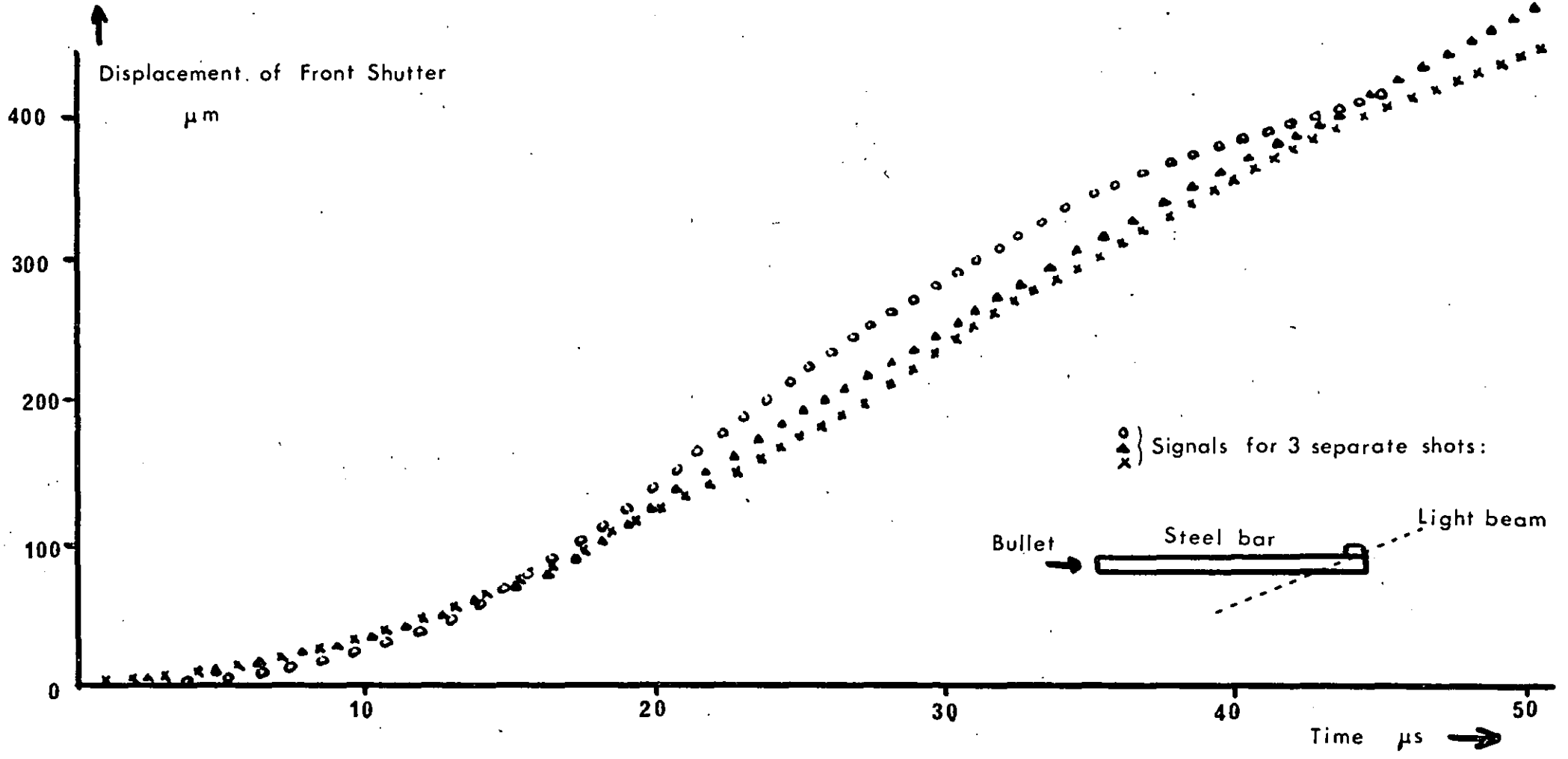

CHAPTER 5 PULSE PROPAGATION MEASUREMENTS

5.1 GENERAL

A number of additional experiments were carried out to determine features of the pulse propagation behaviour using composite specimens in the form of long bars. In particular, the propagation of a stress pulse down a long bar of the material enabled measurements of the propagation velocity to be made. Any change in pulse shape due to dispersion could also be observed. Several long bars of composite material were prepared with the fibres running along the axis and a fibre volume fraction of about 52%, and the propagation speeds of elastic disturbances in these bars were measured using three different techniques. A complete series of tests covering a range of volume fraction was not possible because of the large quantity of material which would be required, and because of practical difficulties in fabricating these bars in suitable moulding boxes.

5.2 BULLET PULSE PROPAGATION

5.2.1 Stress measuring technique

Quartz crystals were used to provide measurements of the stress-time functions at various positions in the bar system. A direct relation exists between the stress applied (σ_j) at a quartz crystal and the polarisation (P_i) induced at the crystal by the piezo-electric effect:

$$P_i = d_{ij}\sigma_j \quad (j = 1 \ldots 6;\ i = 1 \ldots 3)$$

where d_{ij} is the nontensorial piezoelectric modulus. For X-cut quartz, a thin disc is cut perpendicular to the x-axis, and for a uniaxial stress σ_1 in the x-direction, $d_{ij} \equiv d_{11} = 2.3 \times 10^{-12}$ Coulombs/Newton.

A charge Q generated by polarisation in the x-direction over the disc of area A is then:

$$Q = d_{11}\,\sigma_1\,A$$

Let C be the total capacitance charged and E_1 the voltage generated such that $Q = CE_1$, then:

$$\sigma_1 = \frac{C\,E_1}{d_{11}A}$$

Using C = 0.015μf and a 0.5" diameter bar, the calibration factor for the relation between voltage on the capacitor and stress at the crystal was 51.5 M N/m^2/Volt.

Cunningham and Goldsmith (1958) showed that surface strain gauges and quartz crystals gave very similar results for stress impulse loading of long steel bars. More recently, Dragnich and Calder (1973) have also confirmed the validity of quartz crystals for measurement of internal dynamic stresses.

5.2.2 Experimental arrangement

A long bar of the fibre composite was prepared by joining together two 8" long bars with a 1 mm thick quartz crystal bonded in at the joint. Silver loaded commercial araldite was used to secure the joint and rigidly hold the crystal in place.

The acoustic match between quartz and the 52% axial fibre composite was good, and the quartz disc was thin compared to the pulse wavelength, so that there was only a small reflected pulse at the crystal/bar joint.

All the endfaces of the bars were carefully machined perpendicular to the bar axis and polished to ensure a close fitting bond. During the cure process of the araldite, carried out in an oven at 120° - 140° C, the two sections of bar were set up and rigidly held in a jig so that the resulting long bar (either steel or fibre composite) was accurately aligned.

The built-in calibrator on the Tektronix 555 oscilloscope was used to calibrate the vertical amplification of the signal traces, and the calibration factor of section 5.2.1 was utilized in the analysis of the photographic record, as was the case for all subsequent experiments which employed crystal measurements.

The experimental arrangement is shown in figure 5.1 in which the short specimen and back pressure bar of the usual Hopkinson split bar experiment are replaced by the composite bar. The shunting capacitors placed across each crystal acted as voltage dividers to reduce the generated voltages to desired values for display on the oscilloscope.

The standard 0.22" bullets were used to produce a stress pulse which propagated along the bar system; the crystal in the steel pressure bar provided a measurement of the incident compressive pulse, and the crystal in the composite bar provided a measure of the transmitted compressive pulse. This latter pulse had travelled

FIG. 5·1 CRYSTAL MEASUREMENT of PRESSURE PULSE

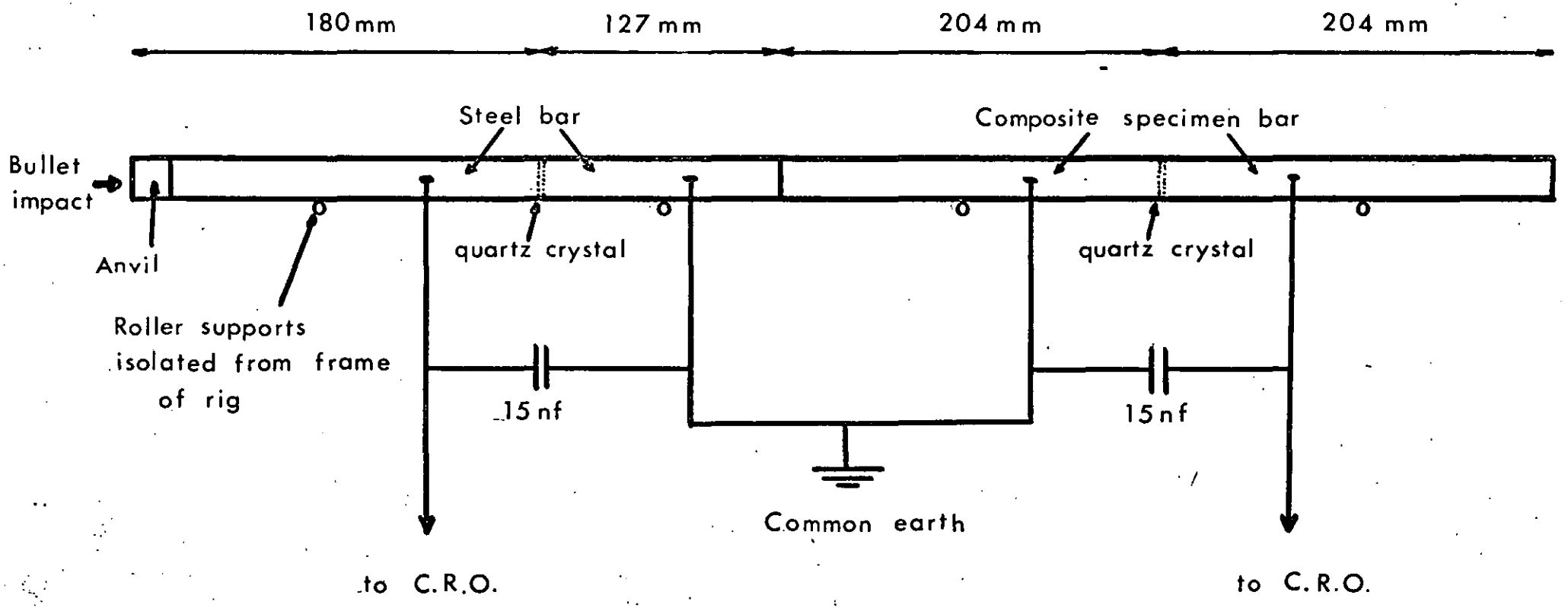

elastically through a section of steel bar, and then through a section of fibre composite bar. A comparison of the shapes of the two pulses would give an indication of any viscoelastic properties of the fibre composite; Norris (1967) has reported experimental work on the propagation of stress pulses in a viscoelastic rod using a similar arrangement.

At the single interface between the front steel bar and the specimen, a portion of the incident pulse σ_I was reflected as a pulse of tension σ_R back into the steel. The amplitude of this reflection depended on the acoustic impedances at each side of the interface. Hence σ_R is given by:

$$\sigma_R = \sigma_I \cdot \left(\frac{Z_2 - Z_1}{Z_2 + Z_1}\right)$$

where Z_1 = acoustic impedance of steel

Z_2 = acoustic impedance of composite

Using accepted values of the density and Young's modulus for the stainless steel, and taking the density and modulus for the composite bar from the static law of mixtures relation, then the acoustic impedances have the values:

$$Z_1 = (\rho E)^{\frac{1}{2}} \doteq 4.1 \times 10^7 \text{ k gm/s/m}^2$$

and $$Z_2 \doteq 1.3 \times 10^7 \text{ k gm/s/m}^2$$

thus $$Z_1 \doteq 3 Z_2 \quad \therefore |\sigma_R| \sim \frac{\sigma_I}{2}$$

Figure 5.2(a) shows a polaroid record of the stress pulses recorded by the crystals at the two positions. It can be seen that the transmitted pulse in the bar of composite has an amplitude about half that of the incident pulse in the steel bar. Thus only half the incident pulse was transmitted into the composite bar. This condition is the same as that for the front interface in the split pressure bar, and an axial composite specimen of this fibre content would be subjected to about half the incident stress loading.

FIG. 5·2 LONG SPECIMEN BARS

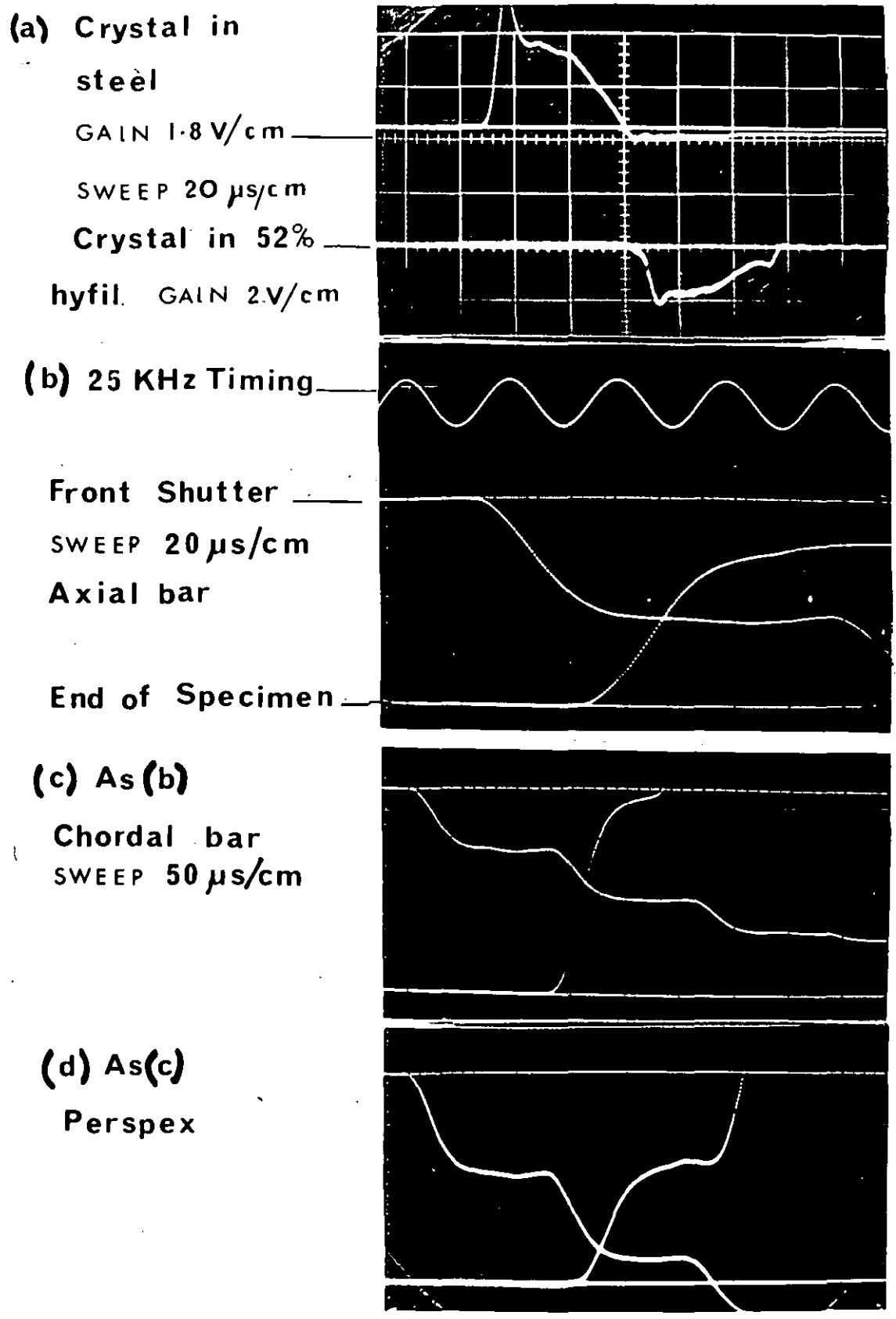

For chordal composites, the acoustic impedance is about 0.1 Z_1 due to the low transverse modulus, and a larger reflected pulse would be produced with the specimen undergoing a small stress loading. No recording at the reflected pulse in the steel is seen in the photograph, nor any signal of the pulse reflected from the far end of the composite bar. These pulses were tensile in nature, and of sufficient magnitude to break the araldite bond. Both crystals were broken by shear failure due to these reflected pulses, although the bars themselves were not damaged.

The time difference between the start of each stress pulse corresponded to the time required for the pulse to travel along the steel bar (12.5 cm long) and along the composite bar (20.4 cm long). A value for the bar velocity in steel, $(E/\rho)^{\frac{1}{2}}$, was assumed to be 5.2 km/s, and the propagation speed in the composite bar was then calculated. Table 2 shows the bar wave speeds from this pulse propagation experiment for several axial unidirectional specimens, of fibre content about 52%.

Very little change in shape of the stress pulse was apparent. The large fluctuation in stress after the initial rise was transmitted faithfully through the two materials and the joint. This fluctuation was thought to be caused by radial oscillations in the crystal due to lateral movements of the bars. No significant spreading out of the pulse was seen, which would be a characteristic of dispersion. Such dispersion could arise from either the geometrical restraints of the bar diameter, from the internal geometrical configuration of fibres embedded in a matrix material or from the viscoelastic nature of the composite due to the matrix properties. These effects may not be additive, and indeed some cancellation of one with another may have occurred. Considering

TABLE 2 Wave Speeds in Composite Bars

Bar type	Fibre Volume %	Bullet Pulse: Speed – Km/s	Vibrating Rods Resonance		Ultrasonic Pulse Speed Km/s	Law of Mixtures Speed Km/s
			Frequency	Speed – Km/s		
Axial 1	55	8·5 ± ·2	21·53 KHz	8·75 ± ·05	9·10 ± ·02	8·6
2	54	8·5 ± ·2	21·44	8·65 ± ·05	9·24 ± ·02	8·6
3	55	8·6 ± ·2	21·71	8·80 ± ·05	9·19 ± ·03	8·6
4	53	8·6 ± ·2	21·69	8·80 ± ·05	9·18 ± ·04	8·6
Small Ø Axial 5	59	–	13·34	8·75 ±·05	9·11 ± ·03	8·7
Chordal	59	–	8·28	2·61 ± ·02	2·97 ± ·01	–

the rather complex mathematical analysis involved and the limited experimental data available, no quantitative assessment of dispersive effects was made.

A further experiment involved similar long bars of about 60% fibre composite, with measurements made of the particle displacements at two positions. The displacement at the interface between the steel bar and the composite was indicated by a shutter on the steel bar, and the displacement at the free end of the composite bar was measured using the end of the bar as the "shutter" This free end moved across a light beam as the pulse reached and was reflected at the end face. The movement here was twice that of the transmitted pulse alone, since with a phase change of 180° on reflection the reflected pulse displacement added to the initial displacement. Figures 5.2(b), (c) and (d) show polaroid records of the two displacements for an axial fibre bar, a chordal fibre bar and a perspex bar respectively. Successive reflections in the steel and specimen bar were recorded, since there was no crystal bond vulnerable to failure.

The time difference between the displacement records again gave a measure of the propagation time over the length of the composite bar, although the difficulties in assessing the start of the trace deflection were present as before. These results and the corresponding wave velocities for a number of shots with the 60% fibre bars are given in table 3. For purposes of comparison, bars of perspex were also used in this experiment; the value for perspex wavespeed of 2.24 $\pm$ 0.04 km/s is in good agreement with the value of 2.25 km/s derived by Davies and Hunter (1963) from the initial slope of their stress-strain curve for perspex. Tennyson, Zimcik and Tulk (1972) gave a value of 2.26 km/s for the

TABLE 3.

BULLET PULSE PROPAGATION SPEEDS

- Measured using two shutters

Shot Number	Fibre Volume %	Bar Length cm	Transit Time μs	Wave Speed Km/s
LB 1-3			41 ± 2	8·04
LB 1-5	59	32·95	38 ± 1	8·66
LB 1-6			37 ± 1	8·90
LB 2-1			37 ± 1	8·85
LB 2-2	61	32·75	40 ± 1	8·19
LB 2-3			40 ± 1	8·19
LB 2-4			38 ± 1	8·62
LB 4-1			36 ± 2	9·04
LB 4-2	61	32·55	37 ± 1	8·79
LB 4-3			37 ± 1	8·79
LB 4-4			39 ± 1	8·35
	Axial Fibres Mean Value 8·63 ± ·25 Km/s			
101-1		33·12	125 ± 2	2·65
102-1	59	17·97	70 ± 2	2·57
103-1		15·72	60 ± 3	2·62
	Chordal Fibres Mean Value 2·61 ± ·03 Km/s			
PERSPEX	–	33·11	148 ± 2	2·24 ± ·04

phase velocity of perspex at frequencies up to 50 kHz; these measurements were made with a pulse produced by detonating an explosive charge.

For the axial fibre long bars, the mean velocity obtained was within experimental error of the longitudinal bar velocity using the static law of mixtures. There was little apparent change in the shape of the displacement pulse. For the chordal fibre long bars the measured propagation velocity was less than that for axial fibres by a factor of 3. The matrix alone would have a wavespeed of about 1.5km/s and the fibre material alone would have a wavespeed along the fibres of about 11.2 km/s. However, in the chordal fibre specimens, the fibres do not carry any load, and only contribute to the composite stiffness by some transverse modulus. Thus the chordal fibre specimen pulse velocity appears to be composed of a contribution from the matrix together with a small contribution from the transverse fibre properties.

All three chordal long bars used in this experiment were seen to fracture during the pulse propagation in the first shot fired at them. No breaks were seen in the axial fibre bars, although the bar LB1 had several cracks in the loading end when testing was discontinued after ten impacts.

Figure 5.3 shows the relative position of the broken piece on one of the three bars tested. It should be noted that on each bar a crack also appeared near the loading end of the bar, a similar distance from the front end as the break was from the free end. These breaks in the chordal specimens were all of a similar nature; a short piece at the far end of the bar broke off in a manner of a Hopkinson fracture. This type of fracture is caused by the net stress loading reaching a value at a particular

FIG. 5·3

position along the bar where the reflected tensile stress is greater than the incident compressive stress, and of sufficient magnitude to break the fibre-matrix bond in tension. A further discussion of fracture is given in Chapter 6.

5.3 ULTRASONIC PULSE PROPAGATION

The velocity of propagation of an ultrasonic pulse, whose frequency was around 5 MHz and which had a very low stress amplitude, was determined by measuring the transit time of the pulse along a composite bar. A transmitting and a receiving probe were placed at opposite ends of the bar and in contact with the flat polished ends. Good contact was required in this case in order to pass as much energy as possible into and out of the bar, and a thin layer of transformer oil was used to ensure adequate contact. The form of the pulses available from the ultrasonic generator was a rapid succession of wave packets, up to a repetition rate of 1 kHz, with the central frequency around 5 MHz. This value was much greater than the main frequency components of the pulse produced by the bullet impact in the steel pressure bar. The apparatus was arranged so that it was possible to pass part of the transmitted pulse along a delay line and to compare the transit time through the specimen bar with the transit time along the delay line. The delay was adjusted so that there was temporal coincidence between the pulse transmitted through the specimen and the pulse being delayed. Both these pulses were displayed on the ultrasonoscope screen. The delay line was directly calibrated in microseconds, accurate to $\pm$ 0.1 μs, and hence the propagation time of one transit in the specimen was readily measured. The arrangement of the experimental apparatus is shown in figure 5.4.

The shape of the ultrasonic pulse transmitted from the contact probe is thought to be a relatively narrow beam which does not diverge significantly during this one transit through the bar. For a distance $D^2/4\lambda$, where D is the probe diameter (12.7 mm) and λ the wavelength of the disturbance, the beam is known to converge in

FIG.5·4 ULTRASONIC EXPERIMENT - Pulse propagation

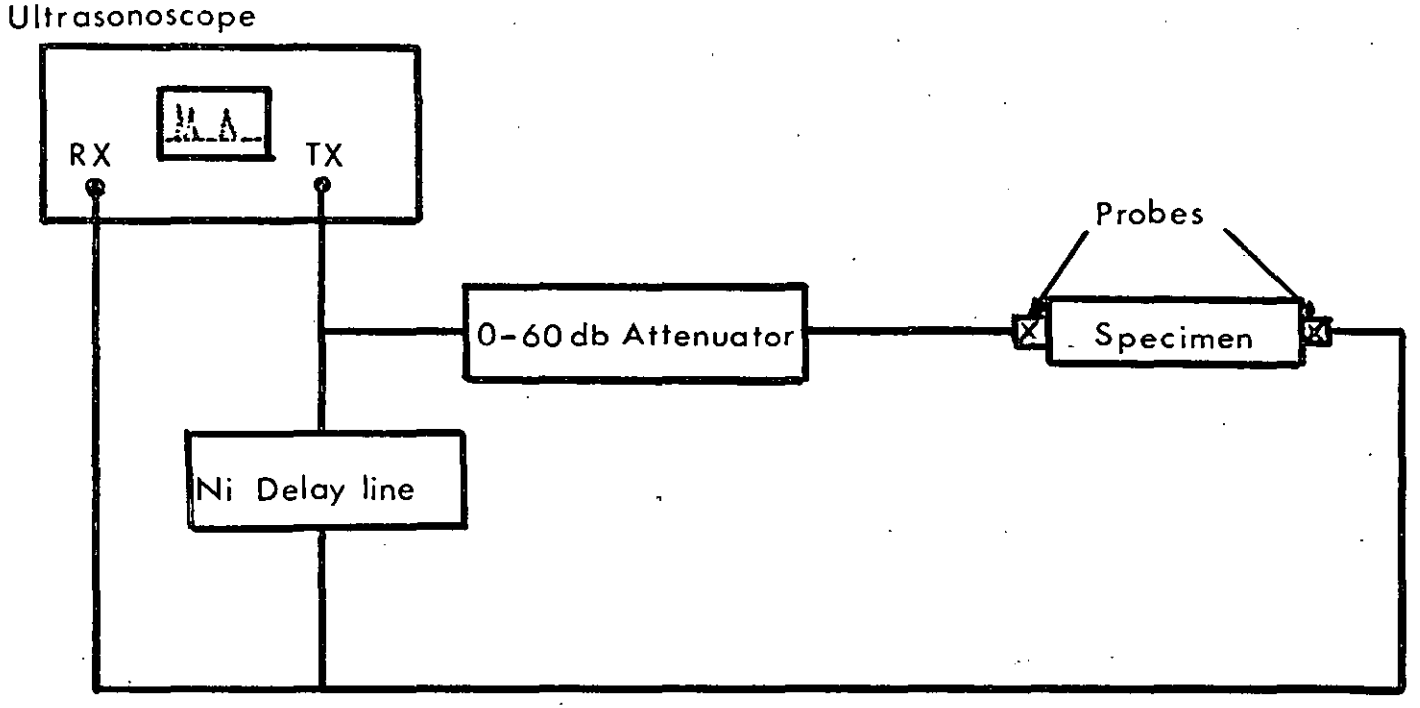

a near or Fresnel zone, and then to diverge at an angle λ/D in the far or Fraunhofer zone (Aldridge and Lidington, 1969). The bars used here were normally 6" - 8" long (152 or 203 mm).

The near zone for 5 MHz pulses was approximately 23 mm, and the beam reached the edges of the 12.7 mm diameter bar at about 92 mm from the transmitting probe. At the receiving probe, the initial signal present was always that which had passed along the centre of the bar at the infinite medium speed, and later signals were those produced by reflections from the bar surfaces.

The wavespeed measured was essentially the infinite medium speed, which was the fastest velocity of propagation of elastic pulses. Nevertheless, there may have been end effects in this particular experiment which introduced boundary conditions on the form of the pulse, and the assumption of an infinite medium may have been in error. All results of wave speed calculations are shown in table 2.

A 2" cube of unidirectional fibre composite was also manufactured in order for the ultrasonic wave speed to be measured; with this size of specimen, there were no boundaries which interfered with the wave propagation and so an infinite medium was assumed. The propagation of 5 MHz pulses along the fibres was observed, and a wave speed of 8.92 km/s for this 43% fibre content block was obtained. This value should be compared with the value 9.20 km/s for the 52% fibre content bars.

No measurements could be made for the propagation velocity across the fibres in the cube of composite, since the signal transmitted was very low amplitude. It was assumed that the attenuation of the pulse by the geometrical and mechanical properties of the material had reduced the signal amplitude.

Wave speed determinations at ultrasonic pulse frequencies of about 2.5 MHz and 10 MHz were also carried out on the fibre composite cube. The propagation times obtained were found to be identical with that for 5 MHz pulses, so that any frequency dispersion of the ultrasonic propagation velocity was not present over this frequency range for longitudinal wave propagation in the fibre direction.

Measurements of the amplitudes of successive pulse transits along the bars would give an indication of the attenuation present in the composite, but this was not undertaken due to the noise content of the signals, and the additional difficulties of assessing losses in the clamps and in the joints between the bar and the contact probes.

5.4 VIBRATING ROD TECHNIQUE

The longitudinal bar velocity $(E/\rho)^{\frac{1}{2}}$ was also found by a vibrating rod technique which utilised the resonant frequency of an oscillating specimen bar. The bar was lightly clamped at its centre and an excitation was induced at one end of the bar by means of an electromagnetic transducer. This transducer was made to oscillate at various frequencies so that it acted magnetically on a small disc of mu-metal which was bonded to the end of the bar. There was a small gap of about 1 mm between the disc and the transducer, so that the bar was excited without physical contact with the transducer and the bar ends were free of stress. The vibration of the bar was detected by a similar transducer at the other end of the bar. Standing waves were set up in the bar, and resonance occurred when both ends of the bar were vibrating in phase. The resonance was displayed on an oscilloscope, and occurred when the standing wave had a wavelength λ where:

$$\ell = \text{bar length} = \frac{n\lambda}{2} \qquad n = 1, 2, 3 \ldots$$

and the resonances had a frequency:

$$f = \frac{n}{2\ell} \left(\frac{E}{\rho}\right)^{\frac{1}{2}}$$

Thus, by observing the resonant frequency for a given length of bar, the wavespeed can be determined.

The experimental arrangement is shown in figure 5.5.

The resonant frequency for the first mode of excitation (n = 1) was found for several axial fibre unidirectional 52% composite bars, and the longitudinal wave velocities calculated from these results are shown in table 2. In addition, it was possible to measure the resonant frequency for a chordal fibre 60% bar, and this result is also shown.

FIG. 5·5 VIBRATING RODS EXPERIMENT

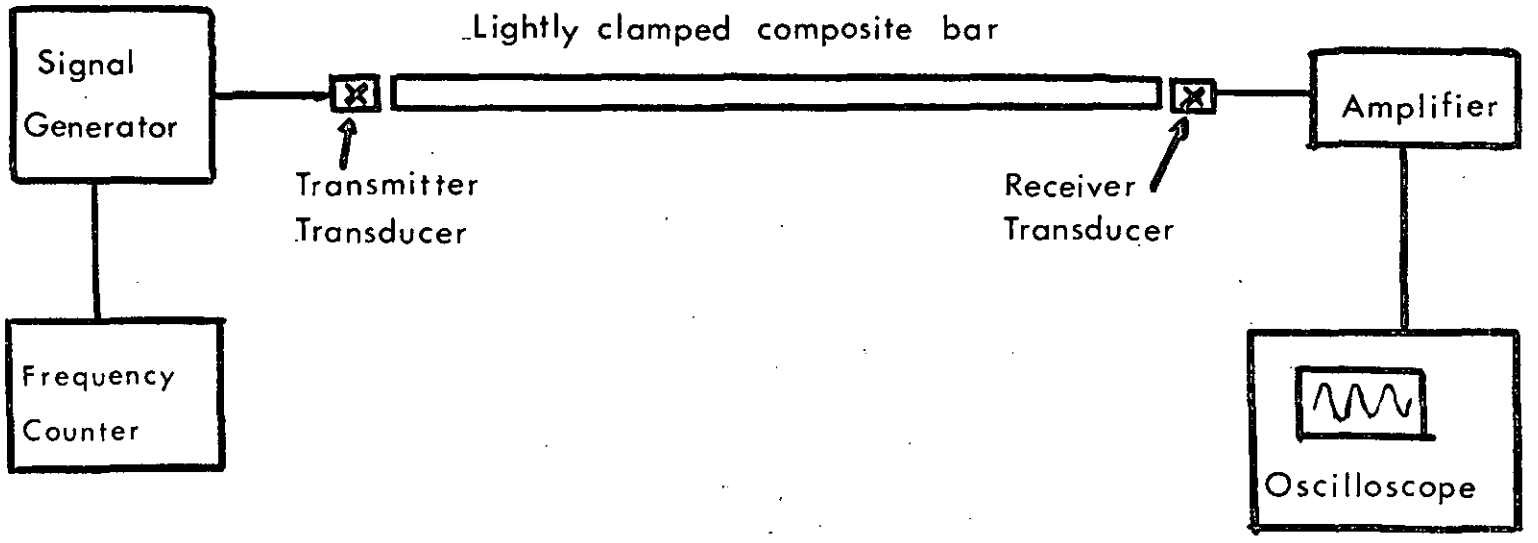

5.5 VISCOELASTIC PROPERTIES

5.5.1 Theoretical considerations

Real solids are never perfectly elastic, so that when a disturbance is propagated through them, some mechanical energy is always converted into heat by several mechanisms which are collectively called internal friction. Material behaviour may be termed viscoelastic by including a viscous as well as an elastic element in the response. Viscoelasticity gives rise to attenuation and dispersion of the stress wave. A model representation for such a material is considered in Chapter 8.

A linear viscoelastic material may be characterised by a complex modulus E*, which is frequency dependent:

i.e. $E^*(w) = E_1(w) + iE_2(w)$

Consider a sinusoidal strain $\varepsilon = \varepsilon_o e^{iwt}$ imposed on a viscoelastic material; the corresponding stress will oscillate at the same frequency, but out of phase by some amount δ:

$$\sigma = \sigma_o e^{i(wt + \delta)}$$

and $$\sigma = (E_1 + iE_2)\varepsilon_o e^{iwt}; \quad \tan\delta = \frac{E_2}{E_1}$$

A measure of the value for tan δ can be found by determining the shape of the resonance peak in a vibrating rod and observing the bandwidth Δf of the resonance curve at the half power point ($\frac{1}{\sqrt{2}}$ x voltage max.).

The shapes of the resonance curves for axial fibre and chordal fibre bars were found by measuring the relative amplitude of the resonant signal on the oscilloscope as a function of frequency. A timer counter was used to measure the frequency of the driving oscillator; measurements were accurate to $\pm$ 2 Hz. The resonance curves are shown in figure 5.6. From these curves, the axial bar ($V_f \doteq 60\%$) shows a damping coefficient of about 10^{-3}, whereas the chordal fibre bar has a damping of about 10^{-2} at the resonant frequencies shown for the particular bar lengths. These damping

FIG. 5·6 VIBRATING ROD RESONANCE CURVES

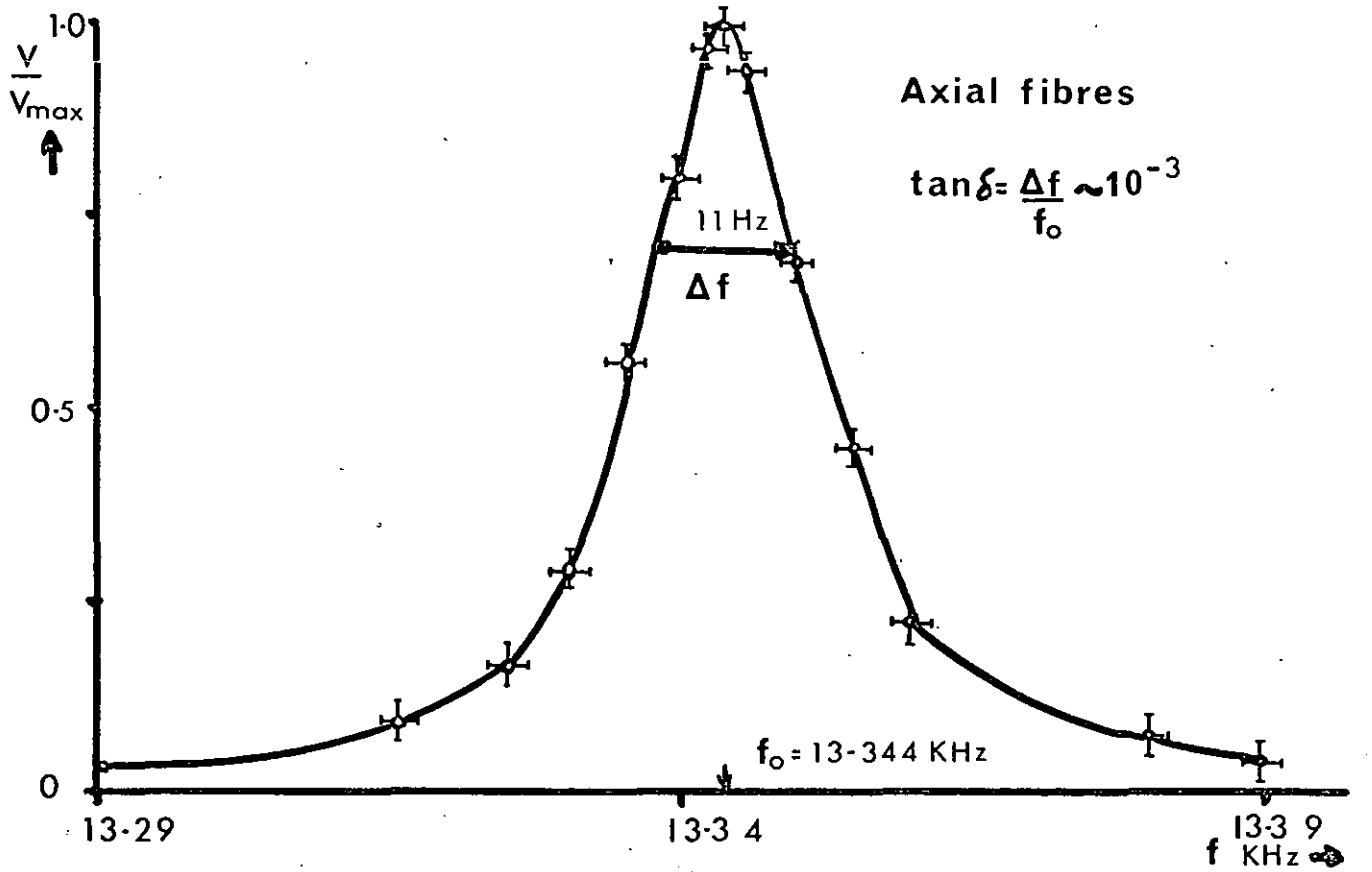

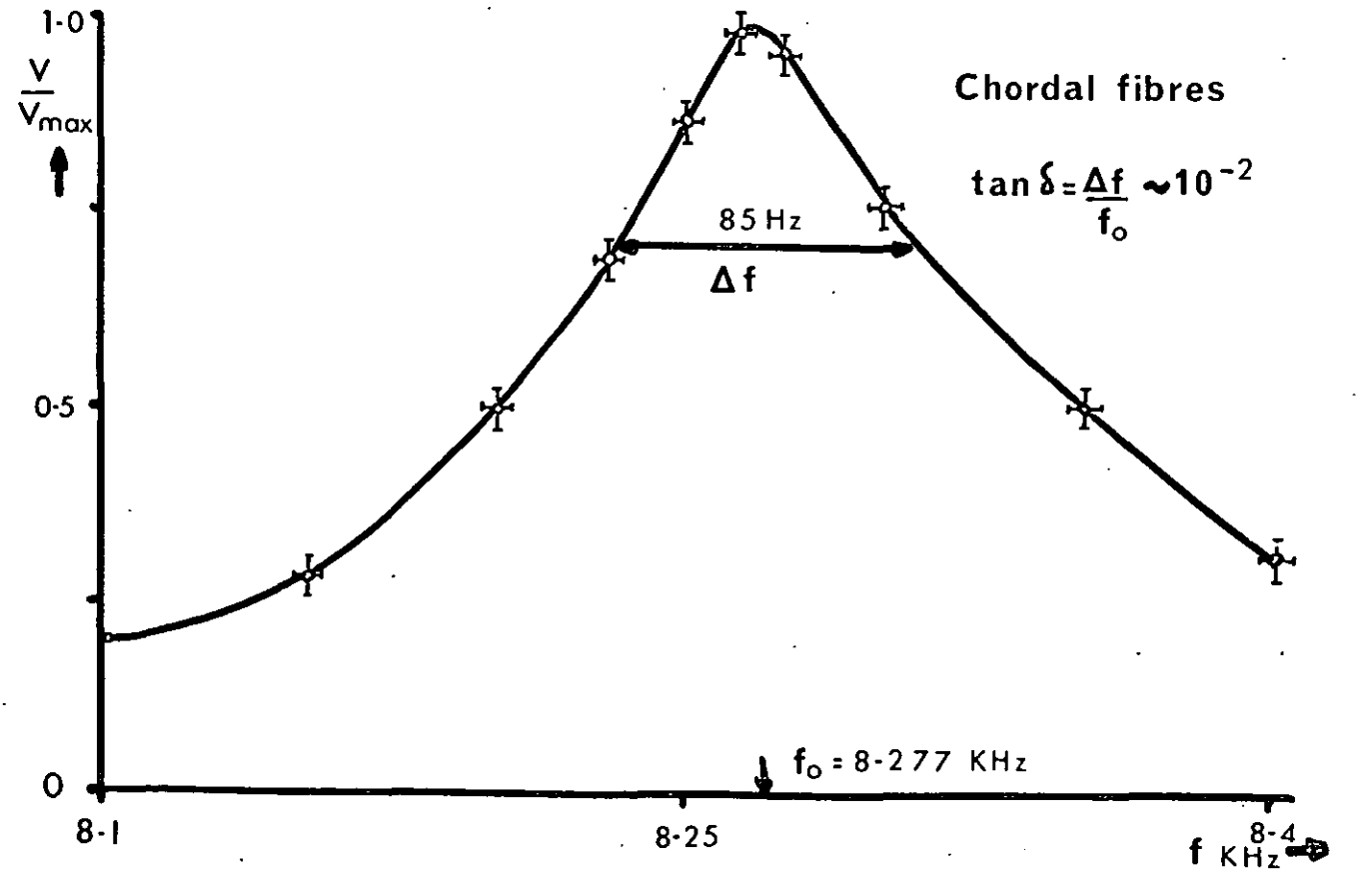

factors are of the same order as those reported by Tauchert and Moon (1970) for axial fibre boron-epoxy beams around 4 kHz.

The larger damping in the chordal fibre case is indicative of the larger viscoelastic content in the properties of this fibre direction.

Using the linear viscoelastic characterisation, it can be shown that a stress pulse, which is propagated in a material with these properties, will have the features of attenuation ($e^{-\alpha x}$) and dispersion such that (Kolsky, 1960);

$$\alpha = \frac{w}{c} \tan \frac{\delta}{2} \quad ; \quad c = \left(\frac{|E^*|}{\rho}\right)^{1/2} \sec \delta/2$$

where α = attenuation, c = wave speed. Both c and α are frequency dependent since both E^* and δ are functions of frequency.

5.5.2 Experimental arrangement

An indication of the extent of the attenuation and dispersion of the bullet pulse was observed by bonding a semiconductor strain gauge onto the surface of a long axial fibre bar; the gauge was positioned in the centre of the bar so that successive reflections of compressive and tensile pulses could be recorded over a long time. A semiconductor gauge was used, with a gauge factor of about 125, so that the strain response of the axial fibres could be recorded without a high noise content. The principle of operation is the piezoresistive effect, which is defined as the change in electrical resistivity with applied stress. The number of carriers and their average mobility are dependent on the stress, and a large effect can be produced in certain semiconductors so that a large gauge factor is introduced into the gauge response. A constant current supply was provided for the gauge, and the signal was recorded on an oscilloscope. A commercial strain gauge cement was used to secure the gauge to the surface of the bar.

Typical records are shown in figure 5.7; a range of sweep times and vertical amplifications are used, and it can be seen that there is very little attenuation or dispersion of the pulse. It should be noted that the gauge factor in tension (shown as a negative signal on the photographs) is about -115 at these strain levels. The propagation speed for all parts of the pulse (i.e. all frequency components) is effectively constant, at 8.75 $\pm$ 0.03 km/s, calculated from the times at which successive pulses pass the gauge position (in the centre of a bar 32.5 cm long). This value of wave speed compares favourably with the values given in tables 2 and 3 for axial fibre 60% bars.

An indication of the amplitude of the attenuation coefficient α for axial fibre and chordal fibre bars can be found by using the relation $\alpha = \frac{w}{c} \tan \delta/2$ and the damping coefficients measured in the vibrating rod experiment. Thus for the axial fibre bar, $\alpha \doteq 2 \times 10^{-3}$ m^{-1} and for the chordal fibre bar $\alpha \doteq 8 \times 10^{-2}$ m^{-1}. These values indicate the small attenuation present for stress pulses in these fibre composites, at the frequencies used in the vibrating rod experiments.

FIG. 5·7 STRAIN GAUGE ON AXIAL BAR

(a) Semiconductor gauge

GAIN 0·05 V/cm

SWEEP 20 μs/cm

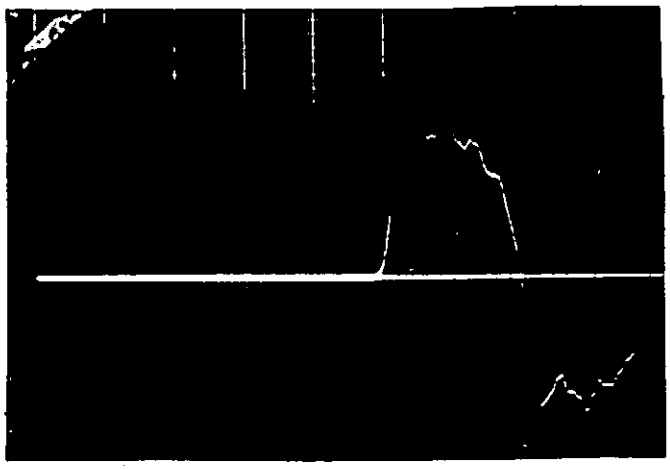

(b) GAIN 0·1 V/cm

SWEEP 20 μs/cm

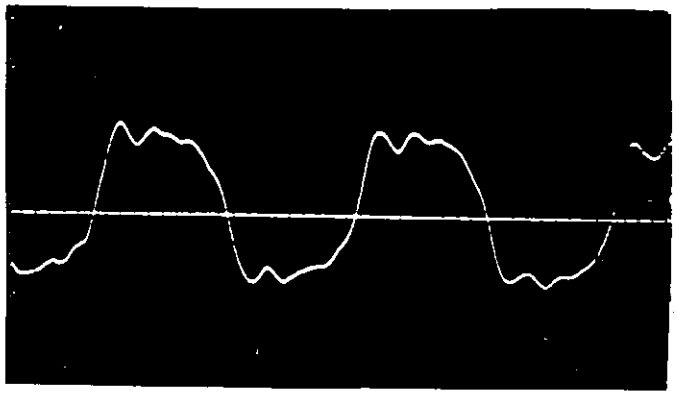

(c) GAIN 0·1 V/cm

SWEEP 50 μs/cm

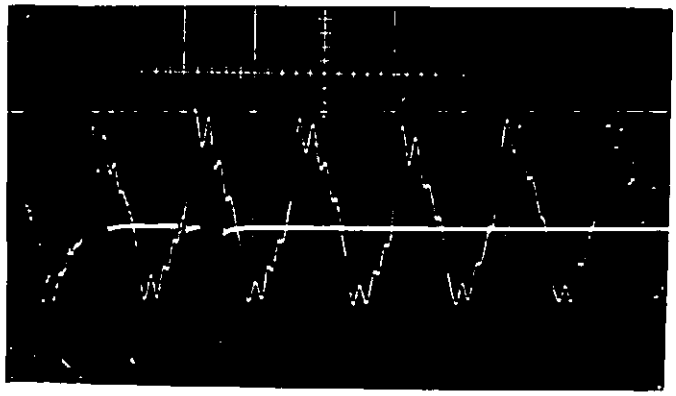

(d) GAIN 0·2 V/cm

SWEEP 100 μs/cm

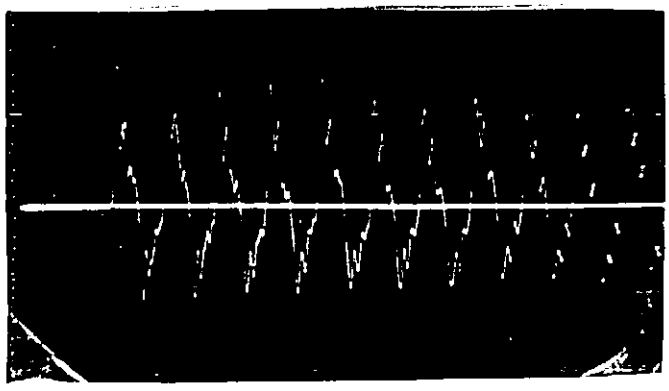

5.6 DISCUSSION OF RESULTS

In an isotropic material, described by only two elastic constants, the longitudinal infinite medium velocity c_l is given by:

$$c_l^2 = \left(\frac{E}{\rho}\right) \frac{(1 - \nu)}{(1 + \nu)(1 - 2\nu)}$$

where E = Young's modulus

ν = Poisson's ratio

ρ = density

The bar velocity c_o given from the simple bar propagation theory which ignores dispersive effects is given by $c_o^2 = \left(\frac{E}{\rho}\right)$.

If the assumption of an infinite medium was correct for the ultrasonic pulse propagation experiments, then c_l should be measured from these results, whereas the vibrating rod experiments should both give the bar velocity c_o.

The ratio of these two velocities is a measure of the Poisson's ratio for the material;

since $$\frac{c_l^2}{c_o^2} = \frac{(1 - \nu)}{(1 + \nu)(1 - 2\nu)}$$

Hence for the axial unidirectional fibre composite bars, a Poisson's ratio can be calculated from the results. This ratio expresses the coupling between compressions of the composite in the fibre direction and extensions in the transverse or radial direction, and assumes there is transverse isotropy i.e. no directionality of properties in a plane perpendicular to the fibre axis. Thus from the results, $\frac{c_l^2}{c_o^2} \doteq 1.12$ for axial fibre 52% bars and the positive solution for $\nu \doteq 0.22$.

From the results shown in table 2, it can be seen that the vibrating rod experiments gave results close to the bar velocity c_o calculated from the conventional static law of mixtures:

$$\text{i.e. } c_o = \left(\frac{E_f V_f + E_m(1 - V_f)}{\rho_f V_f + \rho_m(1 - V_f)}\right)^{\frac{1}{2}} \sim \left(\frac{E_f V_f}{\rho_f V_f + \rho_m(1 - V_f)}\right)^{\frac{1}{2}}$$

with the values:

E_m = matrix modulus = 4 GN/m^2

E_f = fibre modulus = 190 GN/m^2

ρ_f = fibre density = 1.78×10^3 kgm/m^3

ρ_m = matrix density = 1.24×10^3 kgm/m^3

and V_f was approximately 52% fibre volume fraction.

Thus the law of mixtures appears to be a valid expression for calculating average dynamic properties in the fibre direction. In the case of the 43% fibre content block, a similar calculation using the value of c_1 from the ultrasonic pulse experiment and a value for c_o from the law of mixtures gave a "Poisson's ratio" of 0.21.

These approximate expressions cannot be used for the properties across the fibres (as in a chordal fibre bar) because the condition of transverse isotropy is incorrect, and no simple expression analogous to the law of mixtures is available. Moreover there are two transverse "Poisson's ratio" coupling factors in the case of chordal fibre bars.

The values of wave velocity obtained by measuring wave propagation transit times with the quartz crystals are about 2% lower than the expected values from the law of mixtures and the similar experiment using the displacements of a shutter and the endface of the composite bar. This discrepancy could be accounted for by the systematic error of identifying the start of each displacement signal, as these signals had an initial portion of lower amplitude than the crystal stress signals. A large error in measuring the transit time for propagation in the axial fibre bars was thus assumed in the case of the displacement experiment, and so less reliability could be placed on these results. For the chordal fibre and perspex bars,

the proportional error was much smaller, since the propagation time was longer for these materials. It is possible, however, that the law of mixtures assumption is not valid for the high stress levels which were propagated in the experiment with crystal recording. The vibrating rod and ultrasonic pulse experiments both involved very low stress levels so that any amplitude dispersion of the stress pulse would not be evident in these experiments.

The short specimen dynamic stress-strain curve for the axial 52% fibre bars was shown in figure 4.8. There is a continuous change in the slope of this curve over the stress and strain range, so that no definite wave speed could be identified from the curve. The long bar experiment indicated, however, that the wave speed should be equivalent to the law of mixtures modulus (100 GN/m^2 for the 52% fibre bars). Further consideration of the validity of the short specimen results is given in Chapter 7.

Other work on pulse propagation includes Tauchert and Guzelsu (1972), who have used the ultrasonic technique to investigate the dispersive behaviour of plane waves in a boron-epoxy composite. Longitudinal waves showed dispersion above 5 MHz, at which the wave length in the epoxy matrix was of the order of the fibre diameter. The dispersion was caused by the hetereogeneous structure of the composite, and tetragonal symmetry was assumed. Nine independent elastic constants could then be determined.

Nevill, Sierakowski, Ross and Jones (1972) have reported experiments on wave propagation in steel wire epoxy composites, where the wave was initiated in a long bar of the material by impact with a steel striker. The wave speeds were found to be accurately predicted from a law of mixtures relation using the properties of the separate components, and lower stress amplitudes were found to propagate at higher speeds.

CHAPTER 6 EXAMINATION OF FRACTURE SURFACES

6.1 MACROSCOPIC BEHAVIOUR

Fractures and specimen failure have occurred in several of the specimen types tested in the split bar arrangement. The first sign of fracture was always given by a crack which appeared on the flat endfaces of the specimen. This crack would appear at the second or third shot with a chordal fibre specimen, and after two or three more shots it would extend around the specimen, eventually causing the specimen to break into two almost equal parts. Figure 6.1 shows a crack on the curved surface of a chordal fibre specimen.

There are several distinct failure modes present in the broken specimens, and these modes can be seen with a visual inspection of the fracture surface. Figure 6.2 is a schematic representation of possible crack sites in relation to the specimen lay-up and the direction of the impact loading. For the axial 0/90 chordal specimens, with half the fibres running parallel to the loading direction and half perpendicular to the loading direction, there are two independent failure types. At sites labelled A, cracks can be initiated between the unidirectional layers of a 0.010" layer, this layer being made up of two laminates 0.005" thick. This mode of failure initiation is independent of the fibre lay-up of the rest of the specimens, and also occurs in the unidirectional chordal specimens. At sites B, cracks can start between alternate 0/90 layers. This mode appears to be dominant in the 0/90 specimen fractures, although there is some evidence of a mixed mode failure in which a crack has run along a 0/90 interface and at some stage crossed between layers to run along a unidirectional interface. Figure 6.3 shows this particular crack, which had to break fibres within the unidirectional layer in order to cross between the interfaces. A further mode of failure

FIG. 6·1 x10

FIG. 6·2

CRACK SITES RELATIVE TO LAY-UP

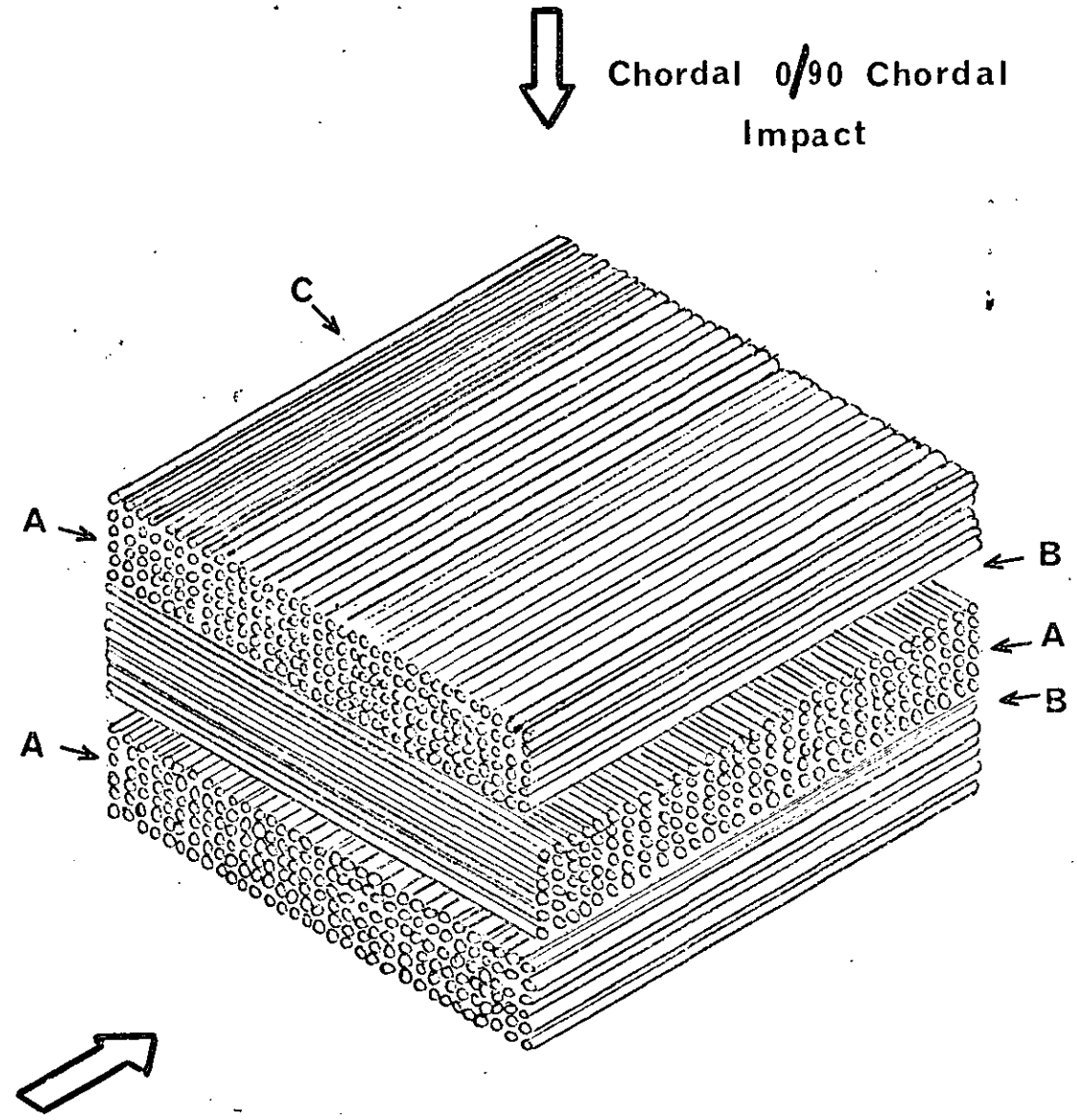

Schematic Representation Only.

FIG. 6·3

CRACK IN Axial 0/90 Chordal Specimen

Appearance at shot 6.

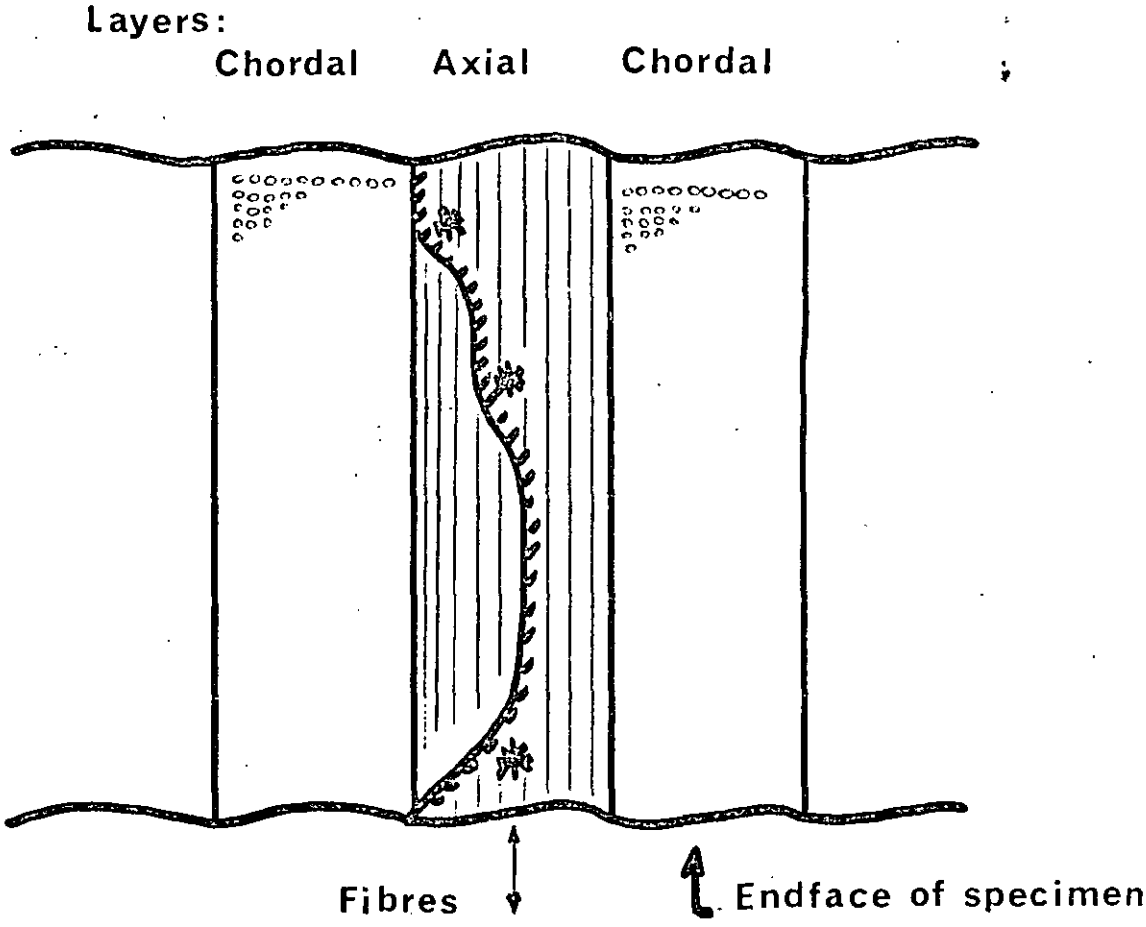

in the composite, at sites C in figure 6.2, is the possibility of breaking fibres at certain points in the structure. This crack would then propagate across the layers of fibres causing the composite to fail. This mode does not appear to be a primary cause of failure, since broken fibres have been seen in only a few cases. The superior strength of the fibres compared with the matrix strength seemed to ensure that primary failure of the composite occurred due to matrix or fibre-matrix interface failure.

Kolsky (1953) has identified fracture mechanisms in Hopkinson bar specimens caused by the compressive pulse being reflected in tension. In more recent experiments, Berg and Rinsky (1971) have shown by high speed photography of crack propagation initiated from known sites in composite sheets that the propagation along fibre layers was due to wave reflections of a form similar to the mechanism proposed by Kolsky. These reflections caused crack initiation and propagation in preference to initiation of further cracks by crack branching at the original crack.

The fractures of the Hopkinson bar fibre composites had the appearance of tensile failures caused by radial forces coupled to the longitudinal compressive stress in the specimens during passage of the stress pulse. The axial unidirectional and chordal 0/90 chordal specimens were not seen to fail since these types were more uniformly isotropic around the curved surface of the cylinder. The axial fibre specimens were transversely isotropic, and the chordal 0/90 chordal specimens had some measure of uniformity around the circumference which apparently was sufficient to maintain an integral specimen structure. Both axial 0/90 chordal specimens and chordal unidirectional specimens were seen to fail after a number of successive impact loadings. This observation indicated that the large strain response in the dynamic stress-strain response

of chordal specimens was virtually all matrix strain. The fibres stay essentially the same shape under the impact loading, but the matrix between the fibres is caused to strain, and thus chordal specimens will fail in the matrix.

Assuming an infinite modulus for the fibres across the fibre diameter, compared with the matrix modulus, and ignoring any transverse effect due to Poisson's ratio coupling, then there is a strain magnification k for the matrix, since the matrix must undergo an additional strain corresponding to the holes occupied by the fibres.

Thus k is given by:

$$k = \frac{a}{a - 2r} = \frac{d + 2r}{d} = 1 + \frac{2r}{d}$$

where r = fibre radius ($\doteq$ 6 μm)

d = distance between fibres

a = separation of fibre centres = $d + 2r$

For a hexagonal fibre arrangement in a volume fraction of 60% $r/d \doteq 2$, hence $k \doteq 5$. This strain magnification causes a much increased strain in the matrix; at weakly bonded points, or where there are voids in the structure caused by the composite moulding process, cracks could propagate along the highly strained and weakened plane. The fracture behaviour of the composite is then determined by the matrix material properties alone.

For the axial fibre specimens, in which the stress loading is along the fibres and there is transverse isotropy around the circumference of the specimen, no failures were obtained. Repeated impact testing was carried out on an axial 60% specimen, up to the level of fourteen impacts. Even at this high aggregate stress loading, no visible damage was seen on the specimen. Repeated testing on a chordal 0/90 chordal 60% specimen showed a similar resistance to fracture, although after nine impacts, a small piece of a laminate at the end face had chipped off. The specimen was

still an integral structure, however, and presumably would have maintained this condition for a large number of successive loadings. The stress-strain curves for both these specimen types had the feature of a small longitudinal strain for this dynamic loading, and hence a small transverse strain coupled to this longitudinal strain. Thus there would be less strain energy available for any fracture processes than for the cases where a larger strain is produced, as in the chordal unidirectional specimens. The ultimate compressive strength of these specimen types could well be much higher than the stress amplitudes which were produced by the bullet impact stress loading used in these experiments.

Under static conditions of loading it has been found that the chordal 0/90 chordal lay-up shows the largest compressive strength, with failure occurring by inter-laminar shear. Short beam shear tests have been widely used for empirical studies of the fracture characteristics in laminated fibre composites under static compressive loading conditions.

The three energy absorbing processes in a composite structure are plastic deformation of the matrix, fibre breakage coupled with fibre deformation, and fibre pull-out. The Cook-Gordon (1964) mechanism of crack stopping by failure of a weak interface ahead of the crack may also be operative in laminated composites. The matrix material is generally thought to be more susceptible to failure processes than the fibres, and previous work in this subject has been directed to improvement of the matrix properties. In particular , the use of crosslinked epoxy resins together with a second phase dispersion to improve impact toughness have been of importance.

6.2 MICROSCOPIC BEHAVIOUR

A group of photographs, figures 6.4 to 6.7 are presented to demonstrate various microscopic failure characteristics. These photographs were taken using a scanning electron microscope (Cambridge "Stereoscan") and are direct views of the failed surfaces of several specimens. The irregular topography of the fracture surfaces made it impossible to use optical or electron microscopy techniques, and so it was necessary to use a scanning electron microscope to examine the specimens. The advantages of this method over the conventional techniques were the large depth of field and high resolution obtained, and the facility to observe the surfaces without the inconvenience of making a replica. A thin coating of a conductive material, such as a gold-palladium alloy, was evaporated onto the fracture surface to assist in the conduction of primary, absorbed electrons from the surface. This layer was about 40 nm thick, and was produced by vacuum deposition.

All the specimens which had failed broke into two similar pieces, with the fracture surface lying along the axis of the cylinder. The fracture surface photographs showed that failure had occurred at (or indistinguishably near) the fibre-matrix interface. This type of failure was characterised by a fracture surface which exhibited (i) large areas of exposed fibre material with little or no bonded matrix material, (ii) thin cracks between the fibre and matrix parallel to the line of the fibres and the fracture surface, (iii) clear "mould" marks in the epoxy resin where the fibres have been removed. These marks reproduced the fibre surface, and did not have the usual features of cohesive failure in a polymer.

Figure 6.4(a) and (b) show general views of the surfaces for 60% axial 0/90 chordal and unidirectional chordal specimens. Clean fibres, lumps of resin debris and some short lengths of broken fibres are visible.

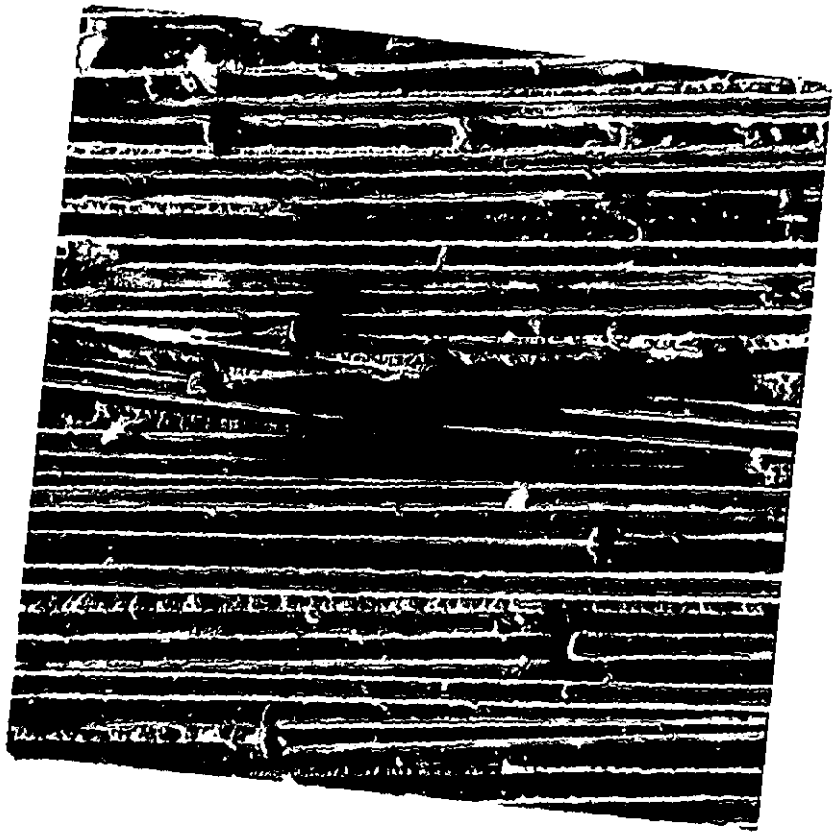

FIG. 6·4 (a) x 350

FIG. 6·4 (b) x 425

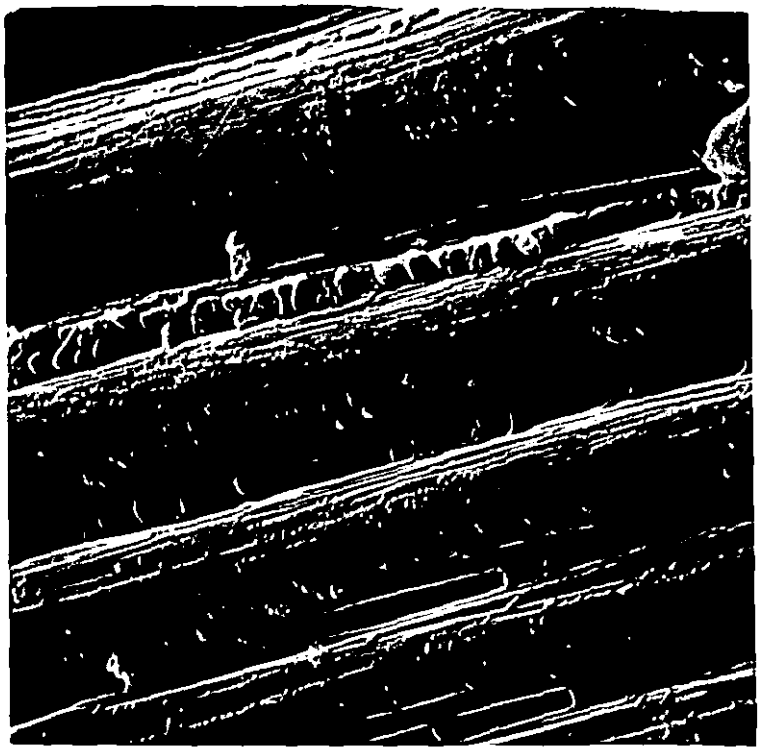

FIG. 6·5 (a) x 2200

FIG. 6·5(b) x 2000

FIG. 6·6(a) x 900

FIG. 6·6(b) x 1400

FIG.6·7(a) x910

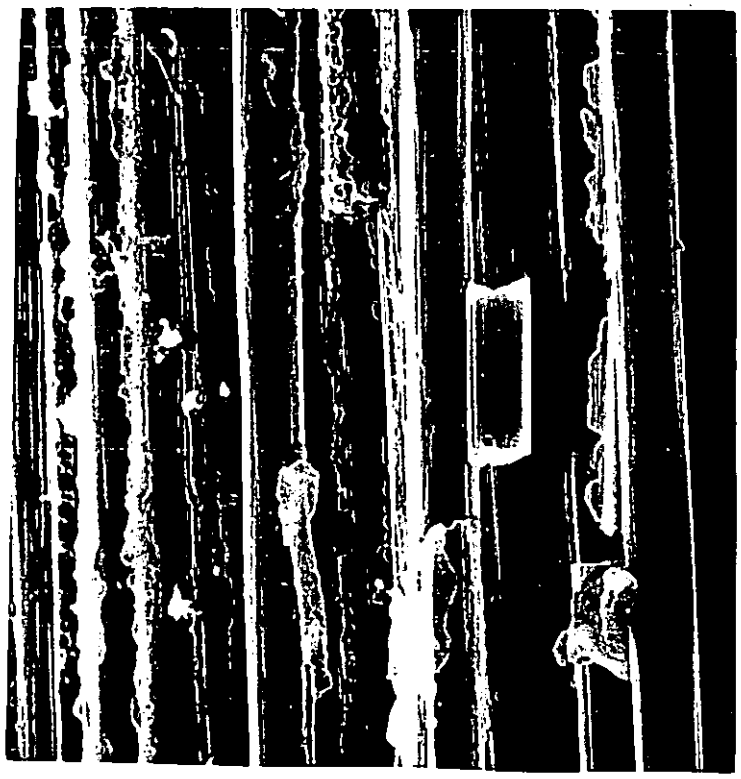

FIG.6·7(b) x900

Figure 6.5(a) and (b) are closer views of the axial/chordal specimen showing the resin debris between the fibres. Striations on the fibre surface are evident, caused by uneven flow in the extrusion process. The fibre-matrix interface has been the region of failure, and the fibres have been almost cleaned of matrix material. A similar picture has been seen on the other surface of the broken specimen, so that the matrix material seems to have disappeared completely.

Figure 6.6(a) shows a region of an axial/chordal specimen in which part of the upper layer has been torn away to expose a perpendicular layer below. The 0/90 interlaminate failure has left little resin material on the lower area of fibres, but in between these fibres there are lumps of resin which may be bonding the fibres together. The failure in the upper layer between unidirectional fibres has again been caused by a fibre-matrix failure. The mould marks of several fibres can be seen in the matrix remains on the upper layer.

Figure 6.6(b) shows a larger region of resin debris and an area of torn resin. The exposed fibres have been cleaned of resin as before.

Figure 6.7(a) and (b) show the surface of a chordal 50% fibre specimen, and the fibres are seen to be less rigidly held. This lower volume fraction specimen contains large regions where the matrix has disappeared, allowing the fibres to move a little out of alignment after the failure occurred, perhaps during handling before photography. Some broken fibres are visible, and this indicates that a considerable radial loading has taken place, both along and across the fibre direction. The torn line of resin to the right in figure 6.7(b) is evidence of a crack in the resin itself.

The fracture surface of one of the chordal fibre long bars which broke into two pieces, as described in Chapter 5, was also

examined with the Stereoscan. This fracture was a tensile break caused by the stress wave reflected from the free end of the bar which produced a tensile loading greater than the tensile strength of the material. The break was seen to be very similar to those chordal fracture surfaces in figure 6.7 (a) and (b) for the Hopkinson bar specimens; that is few broken fibres and several lumps of matrix material left as debris. This appearance was assumed to be that of a fibre-matrix interface failure in tension.

6.3 GENERAL CONSIDERATIONS

The complex stress situation caused by successive reflections within the specimen will lead to different regions of the specimen being subject to compressive and/or tensile stresses at varying times during the passage of the pulse. The radial inertia loading will also complicate the behaviour of those specimens with transverse anisotropy. It is possible that some parts of the specimen will start to fail or crack due to a compressive loading and then fail subsequently due to a tensile loading. With repeated impact loading, further cracks will be caused within the specimen, and there may be the situation of many bonds being broken at each loading, and at some aggregate level of stress loading, sufficient fibre-matrix bonds are broken to ensure that the specimen fails completely.

The stress-strain cycle undergone by a chordal specimen indicates that some strain energy in the incident compression pulse may be absorbed by the specimen, although no plastic strain is observed. This strain energy may be dissipated as a temperature rise in localised regions which would affect the material bonding, or it may contribute directly to the crack propagation. The strain energy released in this way is balanced by the surface energy of the newly created fracture surfaces on each side of the crack. (Griffith, 1920). Fractures in a brittle material such as the epoxy resin used in the fibre composites are usually caused by stress concentration at the tip of an advancing crack, assuming that a microcrack or some other defect is present to initiate the process. When the applied tensile stress is greater than a static fracture stress, the crack will grow at the crack tip velocity (up to 1km/s). At a larger applied stress level, more microcracks become susceptible to failure and all cracks are accelerated by the greater force on the crack tip,

provided that it is energetically favourable to do so. Thermal fatigue centres produced during the moulding and curing cycles by unequal heating and cooling of the fibre and matrix could induce stress considerations which contribute to crack initiation when a stress is applied.

Under high rates of compressive loading, even isotropic elastic and ductile materials suffer inhomogeneous flow because some micro-areas flow more easily than others. The HR4C matrix material used in these composites consists of two phases, the epoxy resin base and also a dispersed phase of polysulphone. It is the resin lumps which are seen on the fibre surface in many of the fracture photographs, while the polysulphone has been separated and apparently has disappeared. In other areas, a network of holes similar to a honeycomb structure shows where these lumps have been pulled away, to leave the polysulphone intact. Any cracks propagating in the two phase matrix are thought to branch around the dispersed lumps which reduce the stress concentration at the crack tip.

In the case of the low fibre content specimens, in which there are large regions of matrix, as the stress becomes tensile there will be stress concentrations in the resin and fracture could occur before the total strain in transverse tension has reached the value required to produce failure in a static tensile test; combined with strain magnification due to the presence of the fibres in chordal specimens, then failure becomes a likely process.

No failures of axial unidirectional nor chordal 0/90 chordal specimens were obtained. The chordal/chordal specimen can be considered as a "strong" laminate structure for the one dimensional stress loading across the fibres. The RB211 fan blade would have been fabricated using 0/90 layers of fibre composite, the fibre

laminates running alternately along and across the blade.

The strength involved in this construction would inhibit any failure occurring due to this component. The longitudinal impact component acts on the axial 0/90 chordal type of lay up, which would react with a different failure mechanism. The familiar "delamination" fan blade failure observed in the simulated impact tests can be directly related to this type of failure seen in the photographs of axial 0/90 chordal specimens.

A.J. Barker (1971) investigated the Charpy notched impact strength of carbon fibre composites over a range of temperatures above and below the glass transition temperature (Tg) of the epoxy resin matrix. Stereoscan observations of the fracture surfaces, together with the Charpy impact data, gave information about the mechanisms controlling material failure. Below the resin Tg, the energy absorbed in fracture was dependent on whether the material failed predominantly in compression or tension. Long fibre pull-out was associated with a fibre-matrix interface failure in tension, whereas a non-fibrous fracture surface was associated with the buckling failure of fibres in compression at the fibre-matrix interface.

CHAPTER 7 ADDITIONAL EXPERIMENTS

7.1 STRAIN GAUGE AND QUARTZ CRYSTAL COMBINED

7.1.1 Experimental arrangement

The anisotropic nature of the carbon fibre specimens indicated that a complex strain distribution might exist in these specimens during the dynamic loading. A fuller instrumentation of the specimen was therefore carried out in an attempt to obtain more precise details of the dynamic response. The method was to bond a strain gauge to the outer surface of a specimen close to the front interface, in order to measure the strain response of the material, and to bond a quartz crystal on the steel bar immediately adjacent to the specimen to measure the stress applied to the material. The stress and strain were measured independently by these electrical means, in contrast with the mechanical shutter technique.

Figure 7.1 indicates the position of the strain gauge on a specimen. The strain recorded by this gauge was the surface strain, which was assumed to be equivalent to the axial specimen strain. The gauges used were Philips etched foil type, temperature compensated for a stainless steel surface, with a guaranteed linearity of $\pm$ 1% up to a strain of 1%. The gauges were glued to each specimen surface with Philips PR9246 strain gauge cement, a two component polyester mixture, which required a curing time of one hour at 20°C with an applied pressure of 1 kgm/cm^2, followed by a hardening time of about 24 hours at 20°C. This preparation was recommended for measurements of strain under dynamic conditions. The quartz crystals were in the form of discs, 0.5 mm or 1 mm thick, bonded onto the end of the front steel pressure bar using the CIBA cement X83/483 (a one-phase conductive epoxy adhesive, requiring a cure of 2-3 hours at 140°C). All the surfaces which were used in a bonding process were prepared by cleaning with a universal solvent.

FIG. 7·1 STRAIN GAUGE on the SPECIMEN

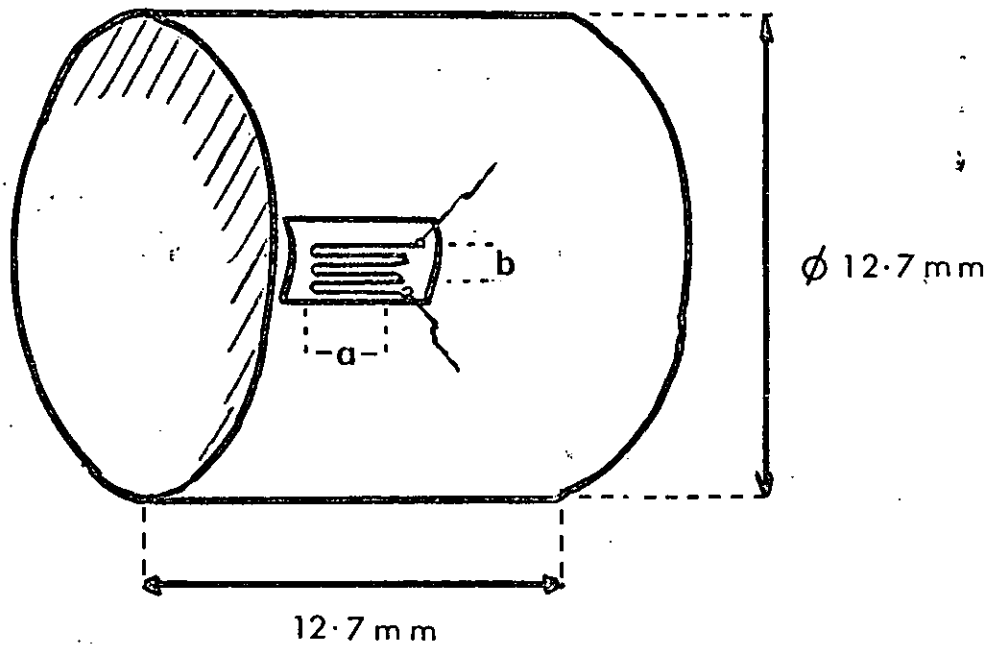

a = gauge length, 2·5 m m

b = " width, 1·5 m m

Recording circuit:

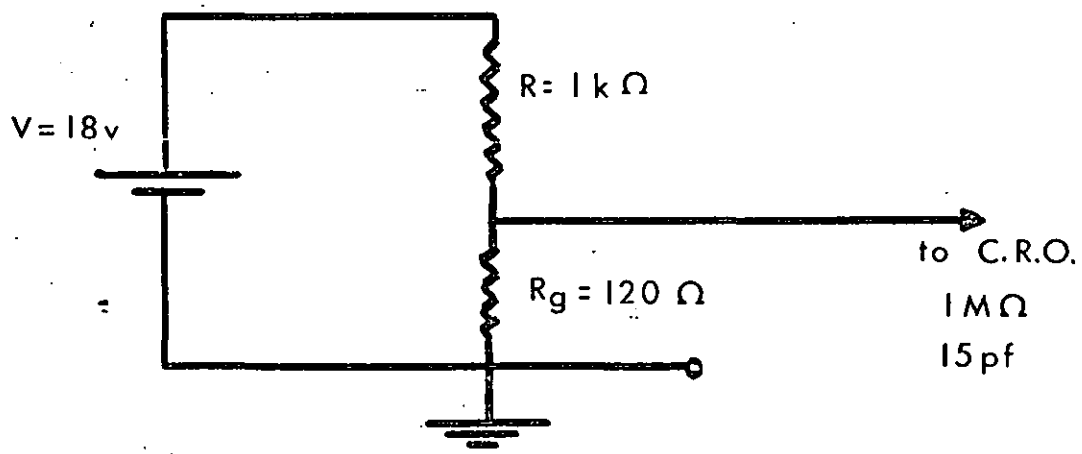

The stress recording circuit is shown in figure 5.1, and figure 7.1 shows the constant current supply for the strain gauge. Satisfactory records free from pick up were obtained only after taking earthing precautions involving an electrical earth to the pressure bars and surrounding the specimen with a wire mesh screen. Without these precautions, the current output from the crystal transducer adversely affected the strain gauge records causing noise and random oscillations.

The gauge signals were between 3 and 20 mV, and the maximum amplification range of the oscilloscope was required to suitably display these voltages. It was also important that the usual setting up procedures for aligning the specimen/bar interfaces were observed.

Watson (1970) used a similar combined measuring technique in experiments on iron alloys; Wasley, Hoge and Cast (1969) used crystals next to the specimen at each interface together with strain gauges positioned on the front and back pressure bars.

7.1.2 Unidirectional axial specimens

For all the axial fibre specimens examined, the crystal transducer stress records were satisfactory, but it was not possible to make measurements from the etched foil gauge records. These strain signals were rather noisy and had spurious oscillations which could not be reduced by improving the electrical circuit. In some cases there appeared to be a tensile strain, which would indicate a peculiar gauge behaviour. For axial fibre specimens, only a very small strain was expected, (about 0.1%) corresponding to a 3 - 4 mV signal, and any electrical noise present would contribute quite significantly in this range. However, the noise content should not completely mask the strain signal, and it was thought that the surface conditions of these

specimens were not suitable for transmitting the strain response to the strain gauge. Any non-uniformity in the specimen surface due to its fibrous nature would cause misleading signals to appear in the gauge record, and this appeared to be the case for these axial fibre specimens. From these records it was not possible to estimate any stress-strain behaviour for the axial specimens.

7.1.3 Unidirectional and crossplied chordal specimens

More success was obtained with the chordal fibre specimens; it was possible to identify the stress and strain responses for a few specimen types. A typical polaroid record is shown in figure 7.2(a) for a chordal 0/90 chordal 60% specimen.

The records of stress and strain both have various oscillations superimposed on the usual pulse shape. If these oscillations represent the real behaviour, then this technique appears to provide more detail of the material response, in contrast with the shutter technique which could average out the response only over the specimen length. The gauge was positioned so that it covered an area of the crossply layers over both the ends and sides of the chordal fibres in this specimen lay-up.

The first peak in stress at 10 μs does not correspond with the first peak in strain (at 14 μs). However, the strain appears to start about 5 μs after the stress, which suggests that the strain is delayed with respect to the stress due to the distance of 5 mm between the strain gauge and the quartz crystal. This indicates that the stress pulse propagates at about 1 mm/μs in the material, and reaches the gauge 5 μs after passing the quartz crystal. This propagation speed is a little lower than the $(E/\rho)^{\frac{1}{2}}$ value for the resin material (about 1.4 mm/μs), but no definite conclusions could be made regarding the form of the chordal fibre wave speed.

FIG. 7·2 QUARTZ CRYSTAL & ETCHED FOIL STRAIN GAUGE

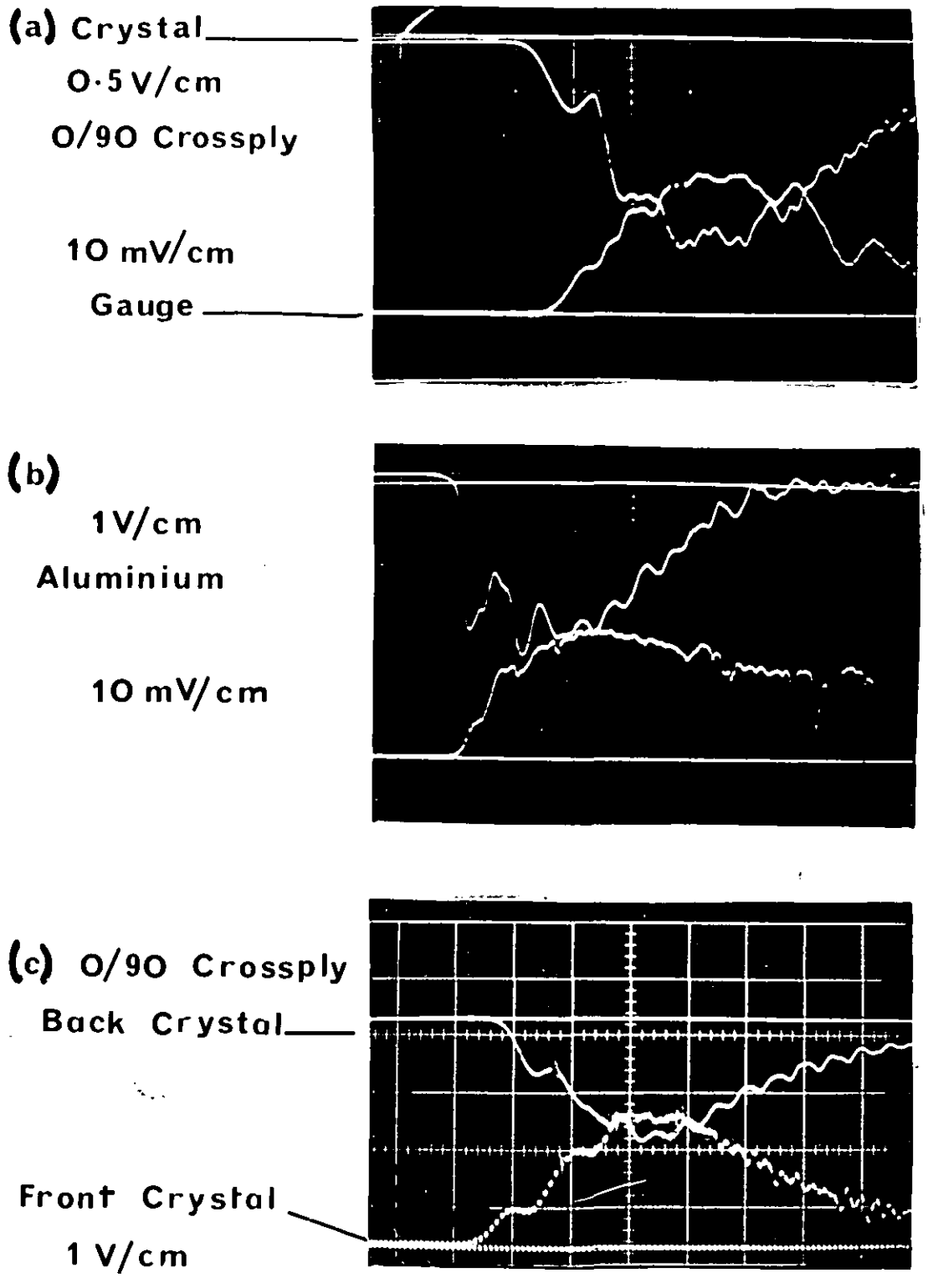

SWEEP RATE 10 μs/cm

After a time of about 15 μs the reflections from the back interface return to the strain gauge position, and these reflections tend to distort the initial shapes of the stress and strain records. However, by averaging out the smaller oscillations in both stress and strain records, and shifting the strain record by 5 μs so that it coincided with the start of the stress record, a stress-strain diagram can be drawn for the chordal/chordal specimen. The first part of the response up to 30 μs is shown in figure 7.3, together with the stress-strain curve calculated using the shutter displacement technique.

The shutter method averaged the strain over the whole specimen length of 12.7 mm, whereas the strain gauge recorded over about 2.5 mm; in this way the strain gauge reproduced more exactly the actual specimen strain in that small region. The strain calculated from the shutter method had apparently underestimated the actual strain in the specimen by up to 10% at 10 μs after the pulse start. A comparison of the stress obtained from crystal measurements at front and back interfaces with the record obtained from the shutter displacement is shown in figure 7.4. The initial stress calculated from the back shutter displacement is greater than the average crystal stress for this axial unidirectional 60% specimen, whereas the peak shutter stress is less than the crystal stress. Thus the initial stress-strain curve obtained from the combined crystal stress and strain gauge records lies below the curve calculated from the shutter technique. Because of the difficulties involved with identifying the nature of the many oscillations of the combined recordings in terms of successive reflections within the specimen, measurements using the combined technique were not attempted for all the specimen types.

FIG. 7·3 COMPARISON of METHODS

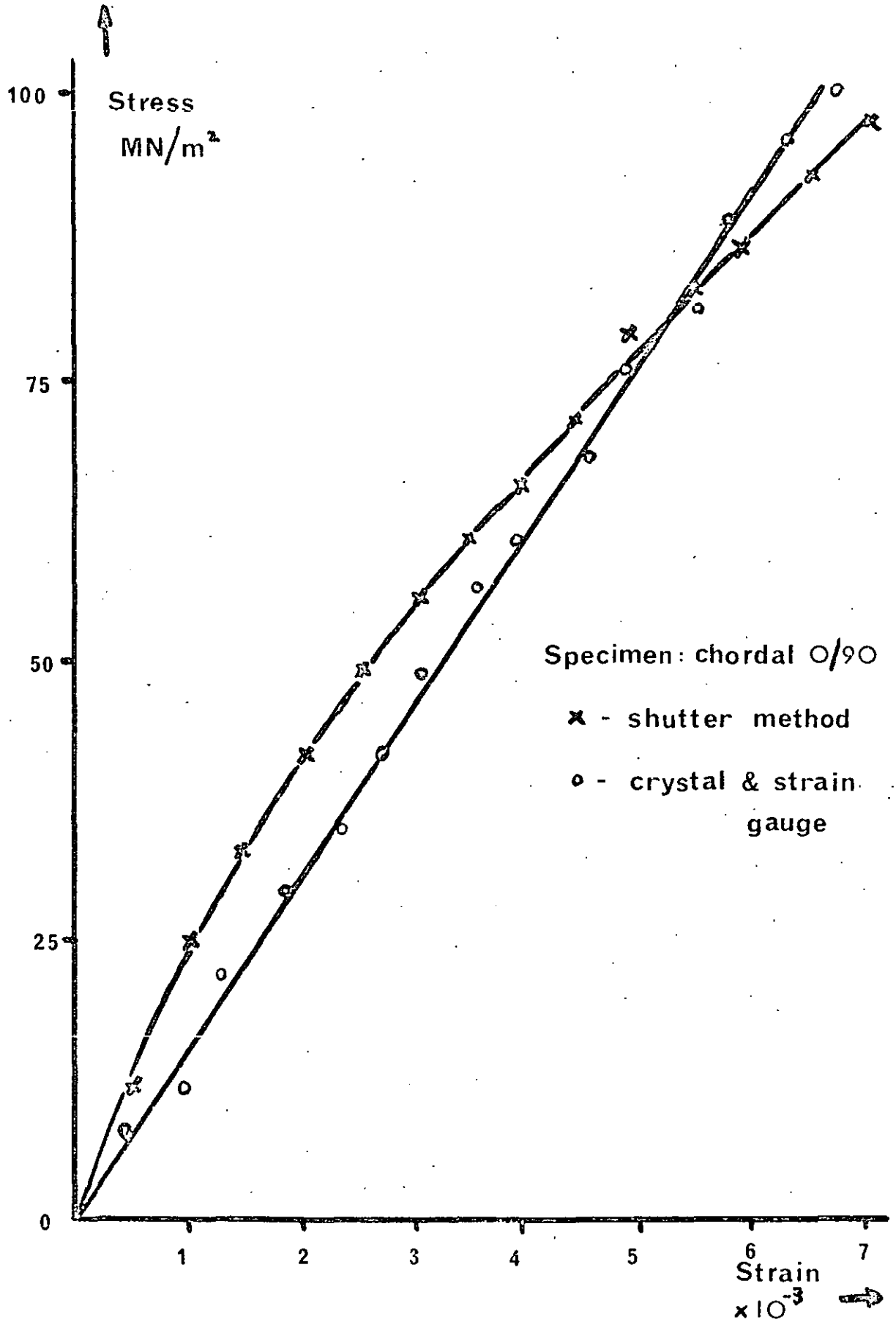

FIG. 7·4 Comparison of crystal & shutter stress records

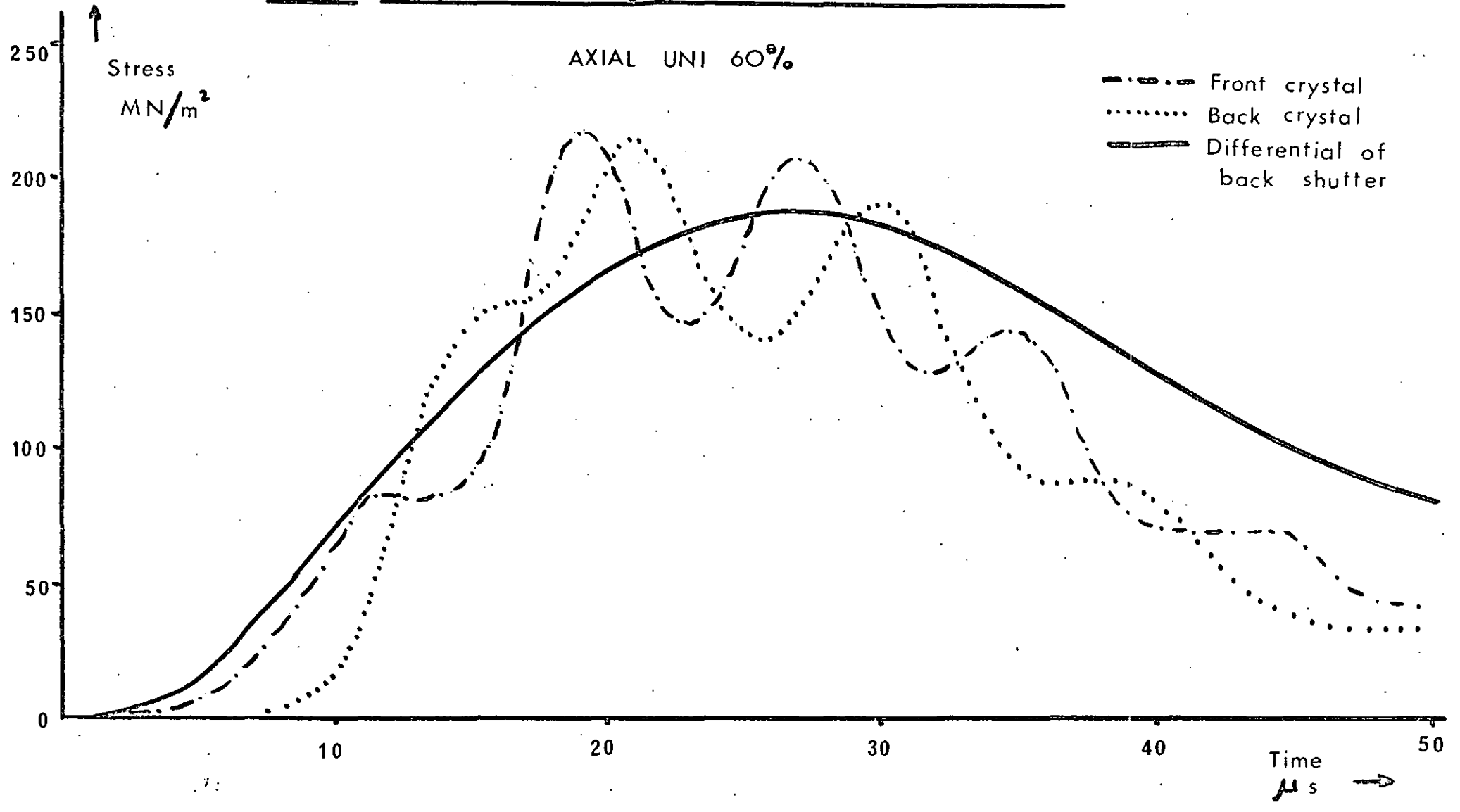

Figure 7.2(b) shows the rather noisy signals for an annealed aluminium polycrystalline specimen. Even this isotropic material produced rapid fluctuations in both stress and strain records, together with a short delay of about 3 μs between the start of each record. The maximum (or permanent) strain was about 0.48%, which compared favourably with the observed 0.5% plastic deformation of the specimen after the shot. A complex stress situation at the front interface was again indicated by the crystal record.

The detailed stress and strain behaviour shown in this combined method appeared to be somewhat different from the behaviour observed in the shutter displacement method. The response of the strain gauge cement in adequately transmitting the surface strain to the strain gauge is a critical factor in these experiments. If the cement behaved non-linearly for any part of the dynamic loading, then the gauge signal would be in error; for example if the cement flowed in a viscous manner during transmission of the pulse then any increased strain shown by the gauge may not be a local material effect but a feature of the dynamic behaviour of the cement. Bell (1966) has made this comment about strain gauge work, and his experiments indicated that the actual local strain (measured by a diffraction grating over 0.001") was less than the average specimen strain calculated from strain gauges at positions as in figure 2.1.

Thus it was felt that the shutter method provided a better average measure of the specimen stress and strain because any rapid oscillations were smoothed out by the shutter motion and the average strain response over the whole 0.5" specimen length could be measured. This was especially so for the axial fibre specimens which were transversely isotropic and had a more uniform strain distribution within the specimen length than the chordal fibre specimens.

7.2 CRYSTALS AT FRONT AND BACK INTERFACES

Several experiments were carried out using a quartz crystal situated at both front and back interfaces in order to determine the stress-time response at these positions during the dynamic loading. The crystals were bonded onto the incident and transmitter pressure bars, as described in section 7.1.1, and the stress-time signal was recorded for a number of experimental conditions. Typical records for the front and back crystals are shown in figures 7.2(c) and 7.10.

The front crystal provided the history of the net stress pulse incident on the specimen, and hence can be expressed as:

$$\vec{\sigma}_{front} = \vec{\sigma}_I + \overleftarrow{\sigma}_R = \vec{\sigma}_I - \vec{\sigma}_R$$

where $\vec{\sigma}_I$ = incident compressive stress (+ve)

$\overleftarrow{\sigma}_R$ = reflected tensile stress (-ve) = $-\vec{\sigma}_R$

At the back interface, the crystal provided the history of the stress pulse transmitted through the specimen:

$$\vec{\sigma}_{back} = \vec{\sigma}_T .$$

where $\vec{\sigma}_T$ = transmitted compressive stress (+ve).

When the stresses on both faces of the specimen are approximately equivalent, $\sigma_{front} \sim \sigma_{back}$

hence $\vec{\sigma}_I - \vec{\sigma}_R \sim \vec{\sigma}_T$

From the records shown in figure 7.10(a), the stresses are approximately equal, allowing for a short propagation time across the specimen. This stress equivalence can be seen more clearly in figure 7.5 in which the front and back crystal records for an axial and a chordal unidirectional 60% specimen of length 0.25" are plotted.

It was not possible for the crystal records to provide a direct measure of the strain in the specimen since this would require a particle displacement referred to a laboratory coordinate system.

FIG. 7·5 CRYSTAL STRESS - Unidirectional, 60% fibres 0·25" length

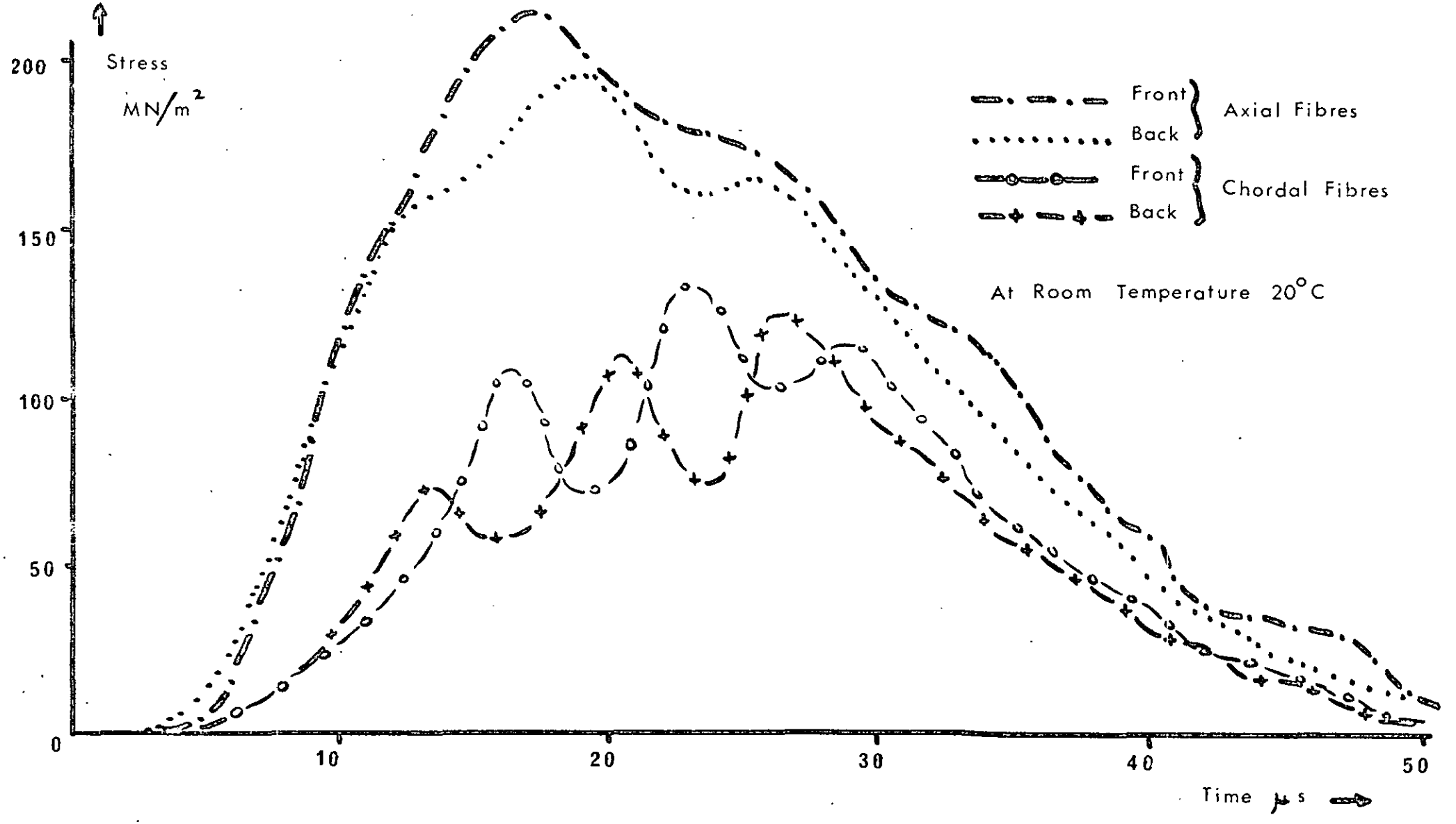

This condition is not the case for the front crystal stress record, since the reflected stress subtracts from the incident stress, and the time integral of the net front stress is not then equivalent to the actual particle displacement at the front interface. The shutter displacement Ufront is a true representation of the particle displacement at the interface, since

$$U_{front} = \vec{U}_I + \vec{U}_R$$

$$\therefore \quad U_{front} = \frac{1}{(\rho c)} \int_0^t (\vec{\sigma}_I + \vec{\sigma}_R)\, dt'$$

The light beam for the optical-shutter displacement measurement is an absolute reference coordinate, independent of the motion at the specimen/pressure bar interface.

These crystal stress records were used for comparisons with records obtained at 150°C, as outlined in the next section.

7.3 DYNAMIC STRESS RESPONSE AT 150°C

7.3.1 Experimental arrangement

Under operating conditions, such as in an aero engine, a composite material may be required to withstand a temperature of over 100°C. It is known that there are significant changes in resin behaviour at the glass transition temperature (Tg); for example, the surface hardness of HR4C resin falls abruptly at this temperature (135°C). For cured polymer systems, a temperature increase may be equivalent to a wider range of viscous relaxation times.

A series of tests was carried out in which the specimen and adjacent bars were surrounded by a small furnace, which provided a uniform temperature of about 150°C. A copper/constantan thermocouple was used to measure this temperature at the specimen. The furnace blocked the path of the light beam, so the alternative method of two quartz crystals placed between the specimens and the front and back pressure bars was used to record the stress. The recording circuits were identical with those used in the previous crystal experiments, but no measure of strain was made as the behaviour of the strain gauge cement at 150°C was unknown.

Crystal records of the stress at the front and back interfaces are shown in figure 7.10(a) and (b) for the specimen at room temperature (20°C) and at 150°C. Figure 7.6 shows the crystal stress-v-time records at the two temperatures for axial unidirectional 60% fibre specimens. Similar graphs for chordal unidirectional 60% specimens are shown in figure 7.7; for axial unidirectional 30% specimens in figure 7.8, and for chordal 0/90 chordal 60% specimens in figure 7.9.

FIG. 7·6 CRYSTAL STRESS - Axial uni 60%

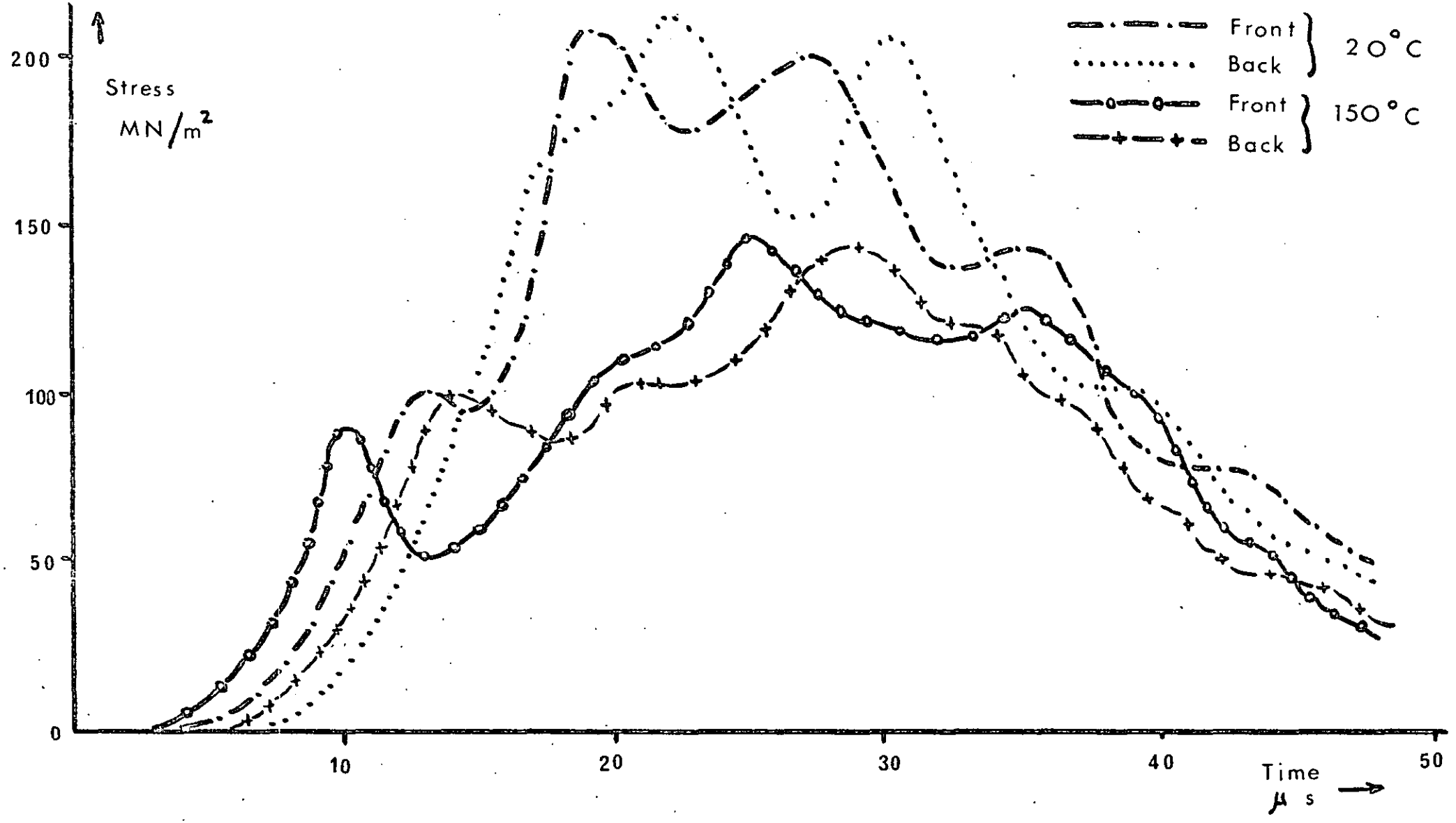

FIG. 7-7 CRYSTAL STRESS - CHORDAL uni 60%

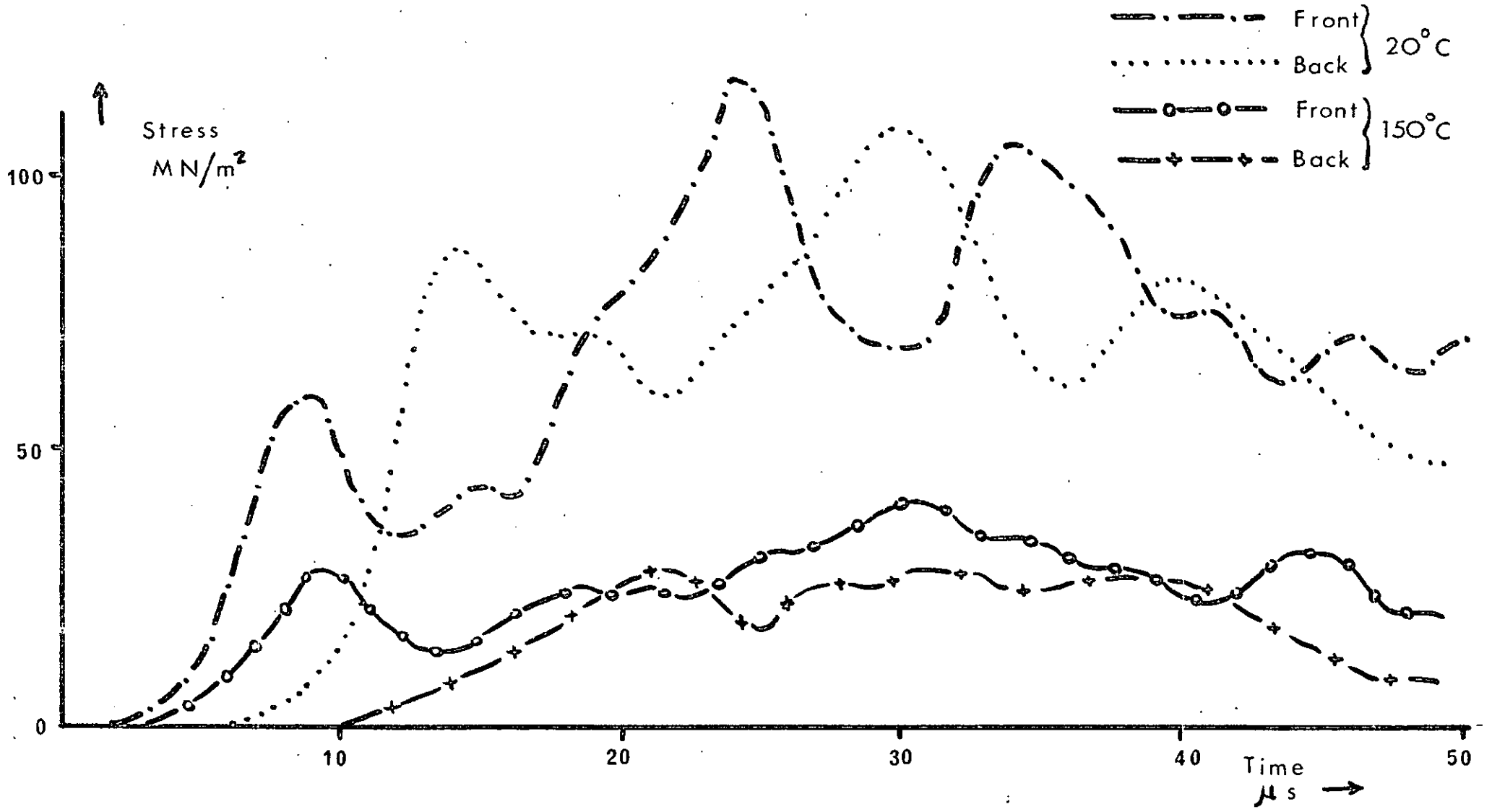

FIG. 7·8 CRYSTAL STRESS - Axial uni 30%

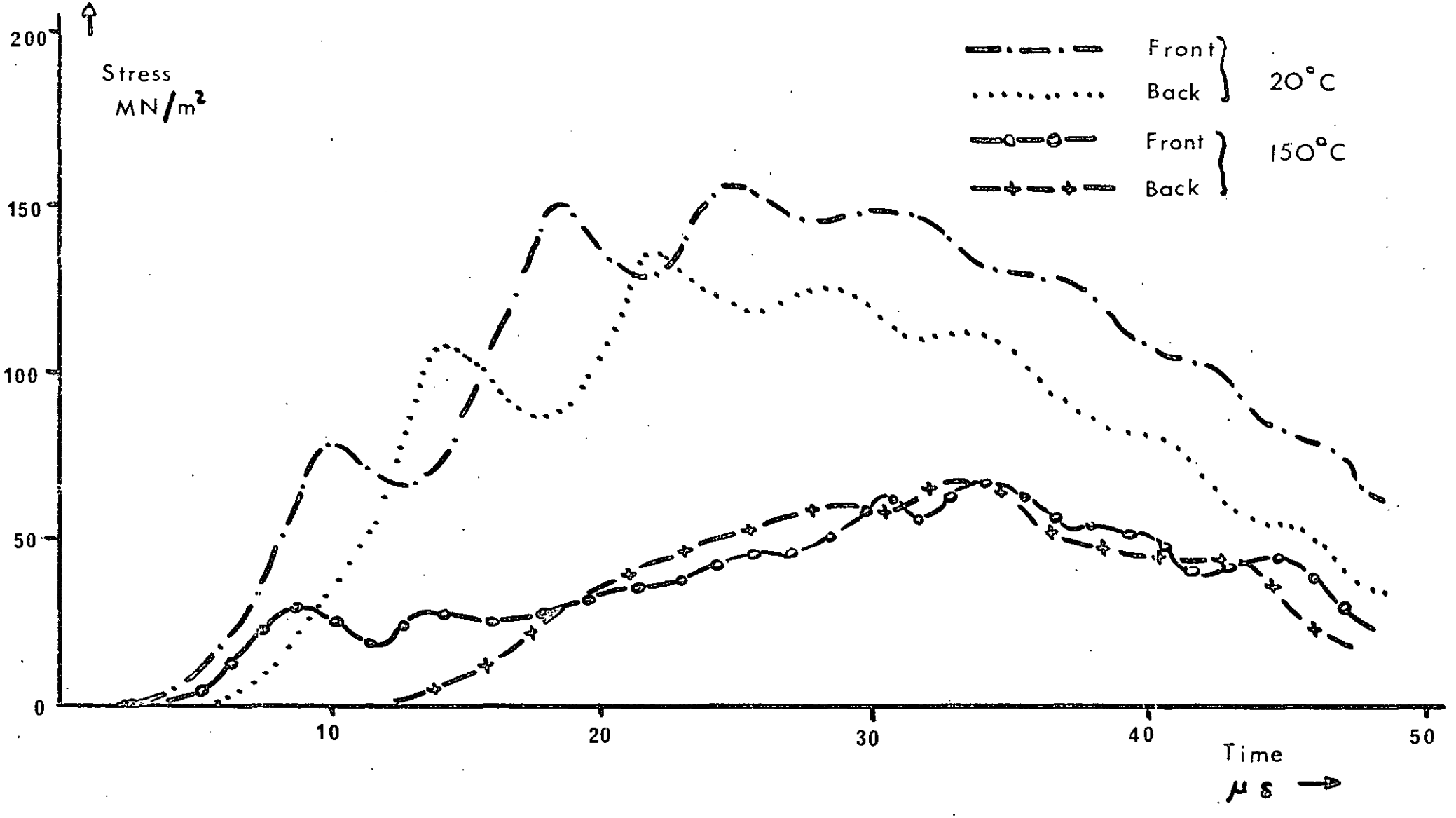

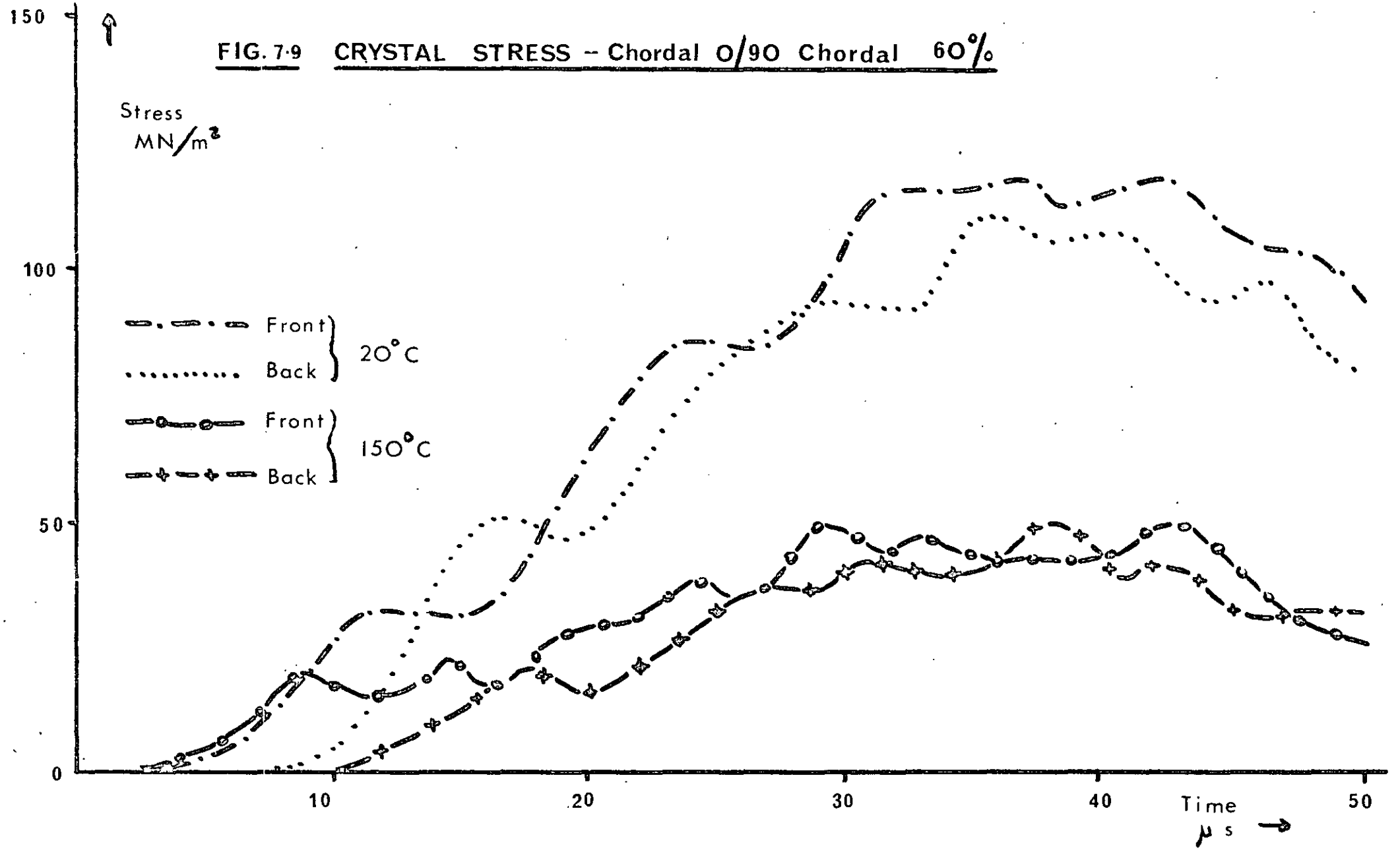
FIG. 7·9 CRYSTAL STRESS – Chordal 0/90 Chordal 60%
Stress MN/m²
150
100
50
0
Front
Back
20°C
Front
Back
150°C
10
20
30
40
50
Time μs

FIG. 7·10 CRYSTAL STRESS RECORDING

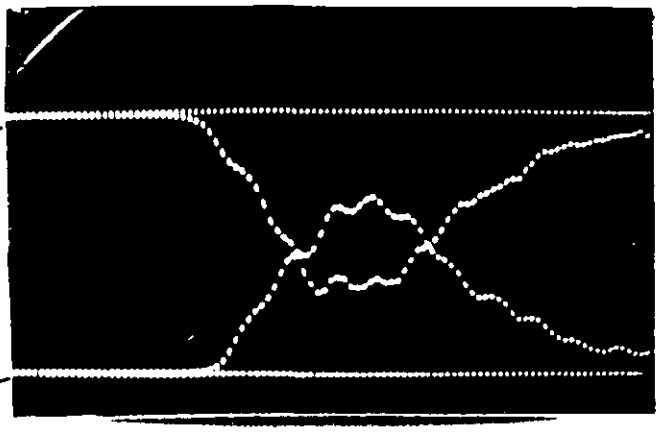

SWEEP RATE 10μs/cm

(a) Front Crystal

Axial Uni 60%

20°C

GAINS 1V/cm

Back Crystal

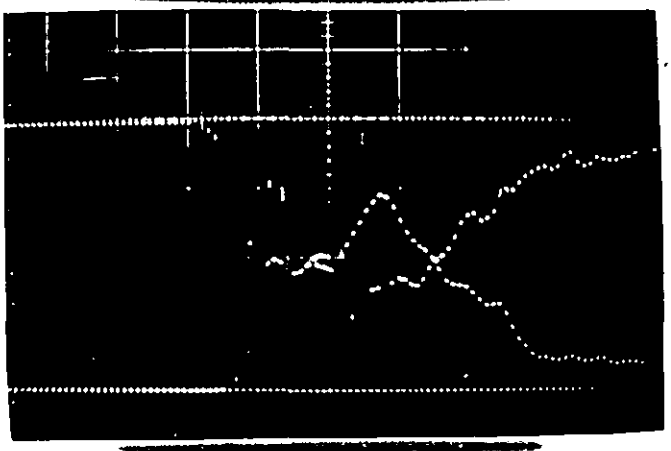

(b) As (a) 150°C

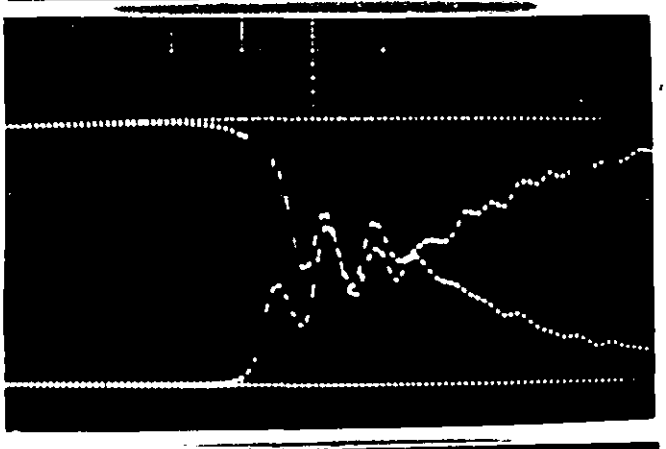

(c)

Chordal Uni 60%

20°C

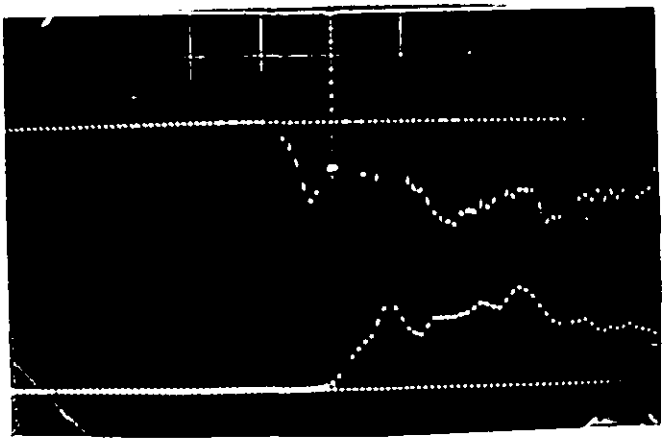

(d) As (c) 150°C

GAINS 0·6 V/cm

7.3.2 Discussion of crystal stress results

The time difference between the start of the front and back stress records gave an indication of the propagation time across the 0.5" length of the specimen. This time difference at 150°C can be compared with that seen at room temperature, as in table 4. At least two useful records were obtained for each of six specimen types and it is seen that in every case the propagation time has been increased by increasing the specimen temperature from 20°C to 150°C. This effect can be attributed to the viscoelastic characteristic of the resin material.

At a high temperature, the resin binding influence on the fibres by maintaining dimensional stability is reduced since the resin viscosity has decreased. Thus the composite tends to act as a bundle of fibres which is less rigidly held together than at room temperature. To describe the physical behaviour of the composite in viscoelastic terms is a very complicated problem; the interaction of the fibres, assumed to behave elastically, with the viscoelastic resin has not yet been treated analytically.

The increased propagation time is thought to arise because the effective dynamic modulus of the composite is reduced, and hence the propagation speed for stress waves is also reduced. As the volume fraction of fibre is reduced, then the propagation time increases, due to the increased contribution to the effective modulus from the viscous resin. The "most viscoelastic" case is for 30% fibres with the fibres in the chordal direction - in which the fibres contribute least to the composite stiffness. This case does show the largest change in propagation time. The "least viscoelastic" case is that of 60% axial fibre specimens, and these show the least propagation times, and also the smallest change in propagation time as the temperature is increased.

TABLE 4 2-Crystal propagation times

Specimen type	Time μs	
	20°C	150°C
Axial uni 60%	4	5-6
Chordal uni 60%	5-6	10-11
Axial uni 30%	4-5	9-10
Chordal uni 30%	8-9	14
Axial/chordal 60%	5-6	6-7
Chordal/chordal 60%	5	8

It was also possible to compare the stress pulse shapes for both front and back crystals at the two temperatures. All the stress records obtained from the quartz crystals were subject to oscillations of periods varying from 3 - 10 μs, superimposed onto the pulse shape.

One cause of these oscillations may have been the change in crystal size as the pulse passed due to geometrical dispersion in the bar system. Any small misalignment of the crystal/specimen interface would also cause spurious oscillations in the stress record due to waves passing across the crystal. An estimate of the dominant frequency of Pochhammer-Chree oscillations, using Kelvin's method of stationary phase as outlined by Davies (1948), showed that oscillations of period 8 μs would occur. These oscillations would have a small amplitude, however, and would be expected towards the end of the pulse.

In general, for all six specimen types examined, the higher temperature caused the stress pulse to be elongated, and the maximum stresses reached were reduced. This would imply that the acoustic impedance of the specimen was reduced at the higher temperature, since there would then be a larger pulse reflected at the front interface, and the specimen would undergo a reduced stress loading. The net stress at the front interface was the difference between the incident stress and the reflected stress, and this net stress corresponded to the transmitted stress in the specimen. The net stress at the back interface also corresponded to the stress in the specimen which was transmitted into the back pressure bar. For large impedance mismatches, as with the chordal specimens, a small net stress was recorded at each interface. The changes in stress loading can be seen in the figures 7.6 to 7.9.

The features of the stress records at 150°C indicated that the oscillations were smoothed out, and in some cases a very small stress amplitude was transmitted into the specimen. No evidence of any fracture behaviour was seen in the elevated temperature experiments, and insufficient results were obtained to investigate any fracture behaviour with repeated impacts.

The increased propagation times at 150°C indicate that the effective composite moduli have been significantly reduced. For example in the case of chordal unidirectional 30% specimens, the wave speed falls by a factor of 1.6, so that the modulus at 150°C is less than that at 20°C by a factor of 2.5. This implies that a considerable change has occurred in the nature of the response, in such a way that the material properties become more dependent on the matrix properties rather than the fibre properties.

7.4 LONG BAR EXPERIMENT WITH STRAIN GAUGE RECORDING

7.4.1 Experimental observations

The effects of a pulse propagating in a long axial fibre bar were investigated by modifying the arrangement which was described in section 5.2 to include a measurement of the surface strain near the joint between the two fibre bars. A semiconductor strain gauge was used for this purpose, because the signal sensitivity available with these gauges was in the region of 300 Volts/strain with an allowable noise content at 10 με of 1,200 ppm, whereas the etched foil strain gauges which were used earlier had a sensitivity of 120 Volts/strain and a noise content at 10 με of 40 ppm. It was possible to obtain good signals for the surface strain in the axial bars by using the semiconductor gauges, and the only disadvantages with these gauges were the high cost and the additional care required when bonding the gauges to the bar surface.

Several recordings were made of the surface strain together with the crystal stress at the joint between the bars. The gauges were positioned with their centres approximately 6 - 8 mm from the bar joint, and all the gauges used were of length 8 mm. Commercial strain gauge cement was used to bond the gauges, together with the CIBA conductive epoxy adhesive to bond the crystals in the joint between the two bars. As in the previous work, the crystal joint was broken when the reflected tensile wave in the second bar reached the joint position. High velocity bullets were used in these experiments so that a large stress amplitude was available.

Typical records are shown in figure 7.11(a) and (b). The axial fibre bar (figure 7.11(a)) produced a peak crystal stress of 220 MN/m^2, and a peak strain of 1.1×10^{-3} at about 10 μs

FIG. 7·11

SEMICONDUCTOR GAUGE & QUARTZ CRYSTAL

SWEEP RATES 20μs/cm

(a) Joint Axial Bar

STRESS 2·2V/cm

STRAIN 0·1V/cm

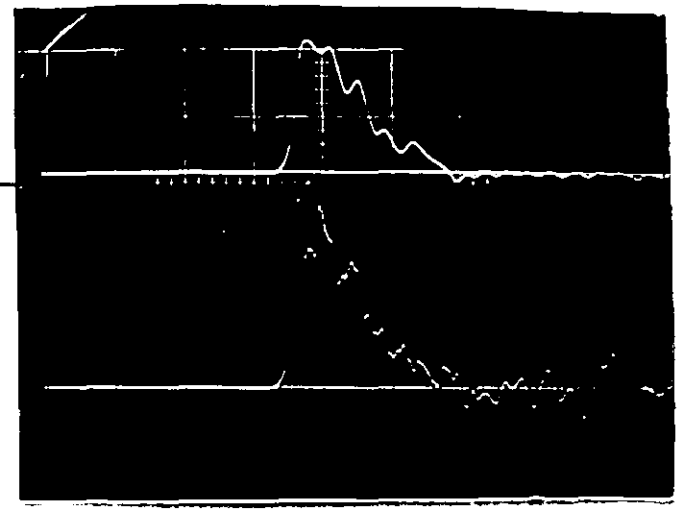

(b) Chordal Bar

STRESS 1V/cm

STRAIN 0·02V/cm

(Etched foil gauge)

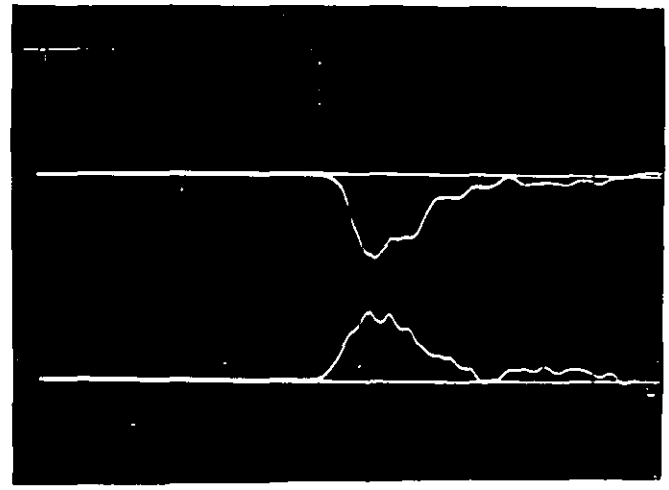

(c) Short Specimen cut from Axial Bar

STRESS 1·8V/cm

STRAIN 0·2V/cm

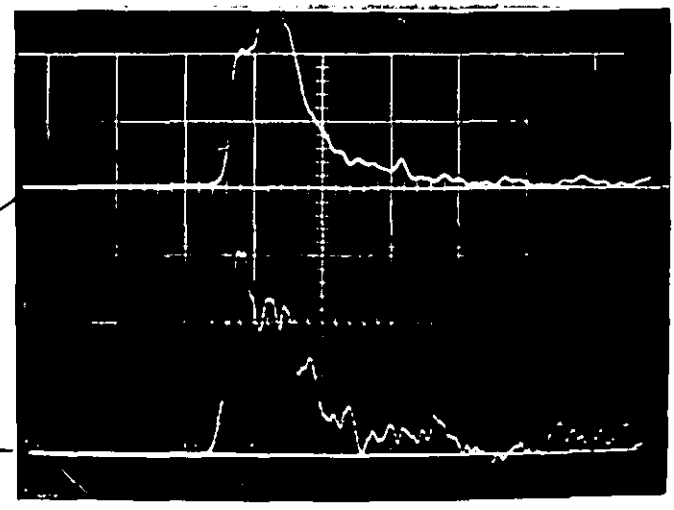

after the pulse start. The chordal fibre bar underwent a much smaller stress loading, about 60 MN/m^2 at the peak, with a corresponding peak strain of 5×10^{-3} at about 18 μs after the pulse start. The differences in maximum stress loading were caused by the different acoustic impedances between the fibre composite bars and the input steel pressure bar. A larger reflected wave in the steel bar was produced in the case of a chordal fibre specimen bar, which was then loaded by a smaller transmitted wave than the axial fibre bar. In both cases the pulse duration was about 40μs, after which time the tensile wave reflected from the far end of the fibre specimen bar arrived at the crystal joint and no further signal was obtained, as the crystal was broken up.

The two jointed sections of the chordal fibre bar also broke up into several short pieces during the reflected tensile loading, in the manner of a Hopkinson fracture described earlier in section 5.2.

The strain gauge signals obtained from the semiconductor gauges were in the region 0.1 to 0.3 volts, and , as can be seen from the photographs, these signals were relatively noise free compared with the signals from etched foil gauges. Nevertheless, some large amplitude oscillations were present, and it was thought that these were caused by the gauge responding to torsional and flexural modes in the pulse. The gauge was enclosed by the cement bond, and hence acted effectively as a short beam "floating" in the cement. Any non-uniform distribution of stress in the cement would cause bending of the gauge during the passage of the longitudinal pulse.

7.4.2 Strain response in short specimens

The longitudinal stress and strain pulses were recorded at essentially the same gauge position in these long bar experiments, so that it was possible to construct stress-strain diagrams for the axial fibre material (V_f = 55%) and for the chordal fibre material (V_f = 60%). The strain-time record was shifted by 1 μs (axial bar) or 4 μs (chordal bar) to allow for the short distance between the gauge position and the crystal. It was found that the maximum strain measured in this experiment for the axial fibre bars was only about 40% of the strain obtained from the shutter displacement technique with short 0.5" and 0.25" specimens, whereas the stress levels were approximately the same.

A further experiment was carried out therefore, in which the end portion of an axial fibre bar was machined off into a short specimen of length 0.6" (15.19 mm), care being taken not to damage the semiconductor strain gauge attached to this portion. The ends of this specimen were carefully polished and prepared as for the previous short specimen experiments; a high velocity bullet pulse was then used to load the specimen in a split pressure bar arrangement. Crystal stress and semiconductor strain gauge measurements of the specimen behaviour were then possible, with a typical record shown in figure 7.11(c). The maximum strain reached was nearly 2.3 times the strain recorded in the long bar pulse propagation experiment with the identical material and strain gauge. The two strain pulses are directly compared in figure 7.12. The crystal stress signals were of the same order, with maximum stresses in the region 210 to 230 MN/m^2.

A comparison of the strain pulses obtained from the chordal fibre long bar experiment, and from an etched foil strain gauge on a short chordal specimen ($V_f \sim 60\%$) is shown in figure 7.13.

FIG. 7·12 STRAIN-v-TIME by Semiconductor gauge - AXIAL uni 55 %

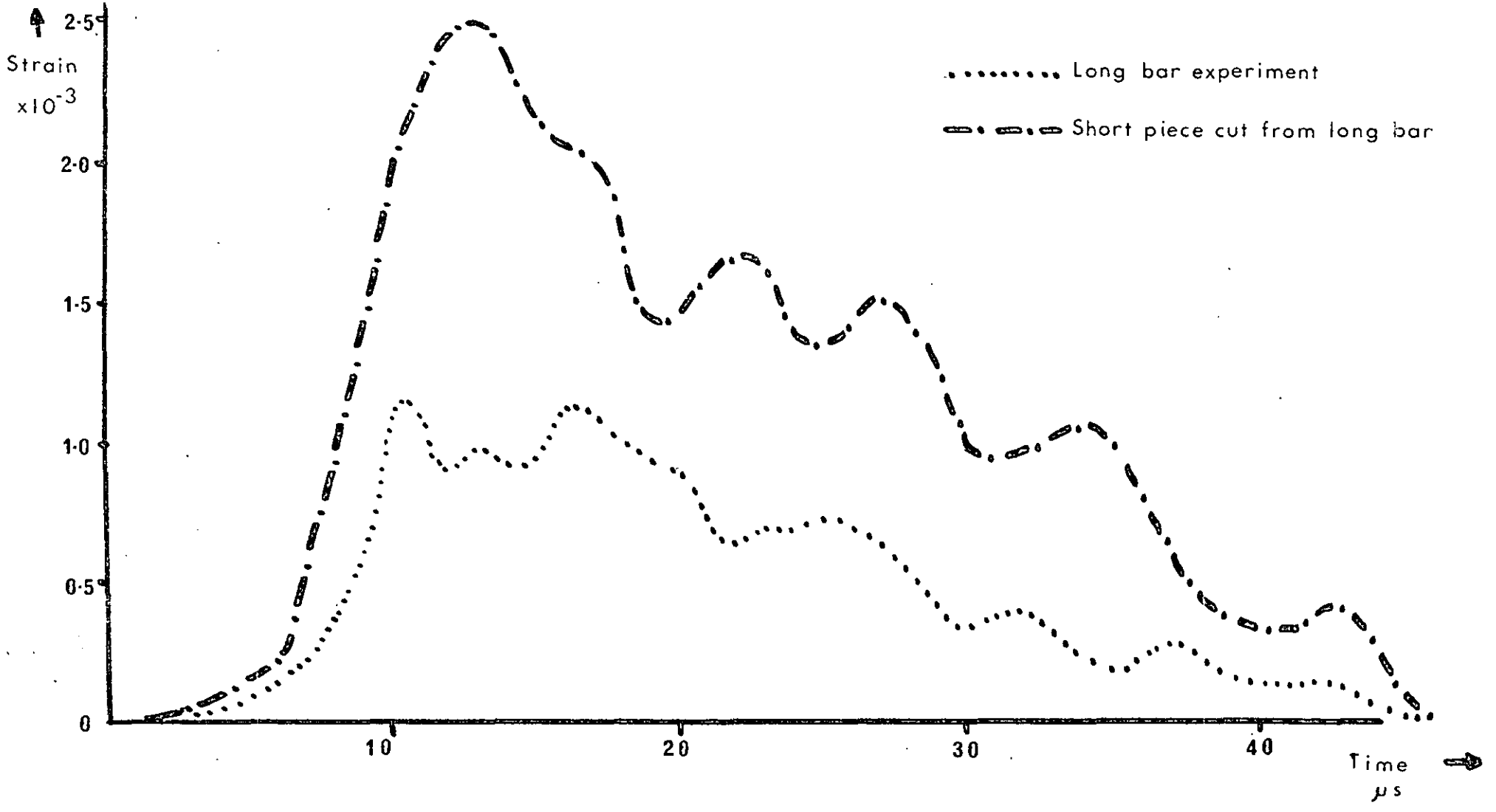

FIG. 7·13 STRAIN-v-TIME by Semiconductor gauge - Chordal uni 60%

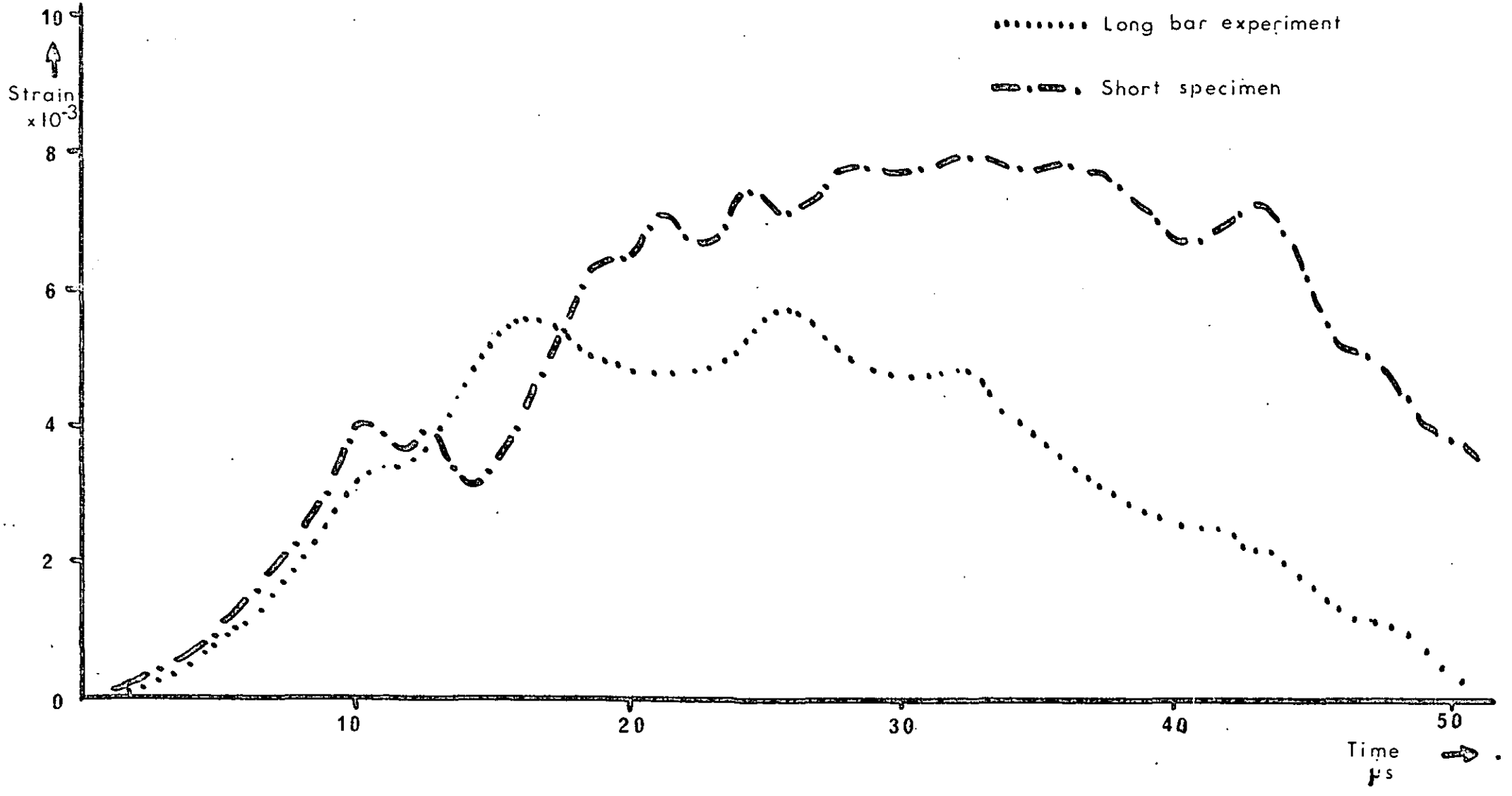

Initially the strain were quite similar, and the long bar strain maximum was over 5×10^{-3} , compared with a maximum strain of about 8×10^{-3} in the short specimen experiment.

It is evident that there is a significant difference in the stress-strain behaviour of an axial fibre composite in the experimental configurations of long bars and short specimens, whereas the behaviour is not so different for chordal fibre composites. Figures 7.14 and 7.15 show respectively the stress-strain curves for axial fibre and chordal fibre specimens using the long bar stress and strain results, and the short specimen stress and strain results with crystal and strain gauge instrumentation compared with the short specimen (0.5" length) average results using the earlier work on shutter displacements.

The stress-strain behaviour of the axial fibre long bar is seen to be a single relation over this region of the response, with an initial modulus of 190 GN/m^2, whereas the short sandwich axial fibre specimens show a two part behaviour, which initially follows the large modulus of the long bar response. Above a stress level of 100 MN/m^2 the behaviour of both the shutter displacement measurements and the crystal and strain gauge measurements on short specimens follows a different relation with a lower modulus of 25 GN/m^2. As the maximum stresses reached in long bar and short specimen experiments were about the same, it appears that the strain response of the short axial fibre specimens was much greater than that of a short region in a long bar of material.

7.4.3 Lateral motion

This behaviour is consistent with a local fibre buckling or lateral movement phenomenon in the short specimen experiment, which is not present in the behaviour of a short unbounded region of a long axial fibre bar. The fibres in this short region are

FIG. 7·14 STRESS - v - STRAIN Axial uni 55°/o

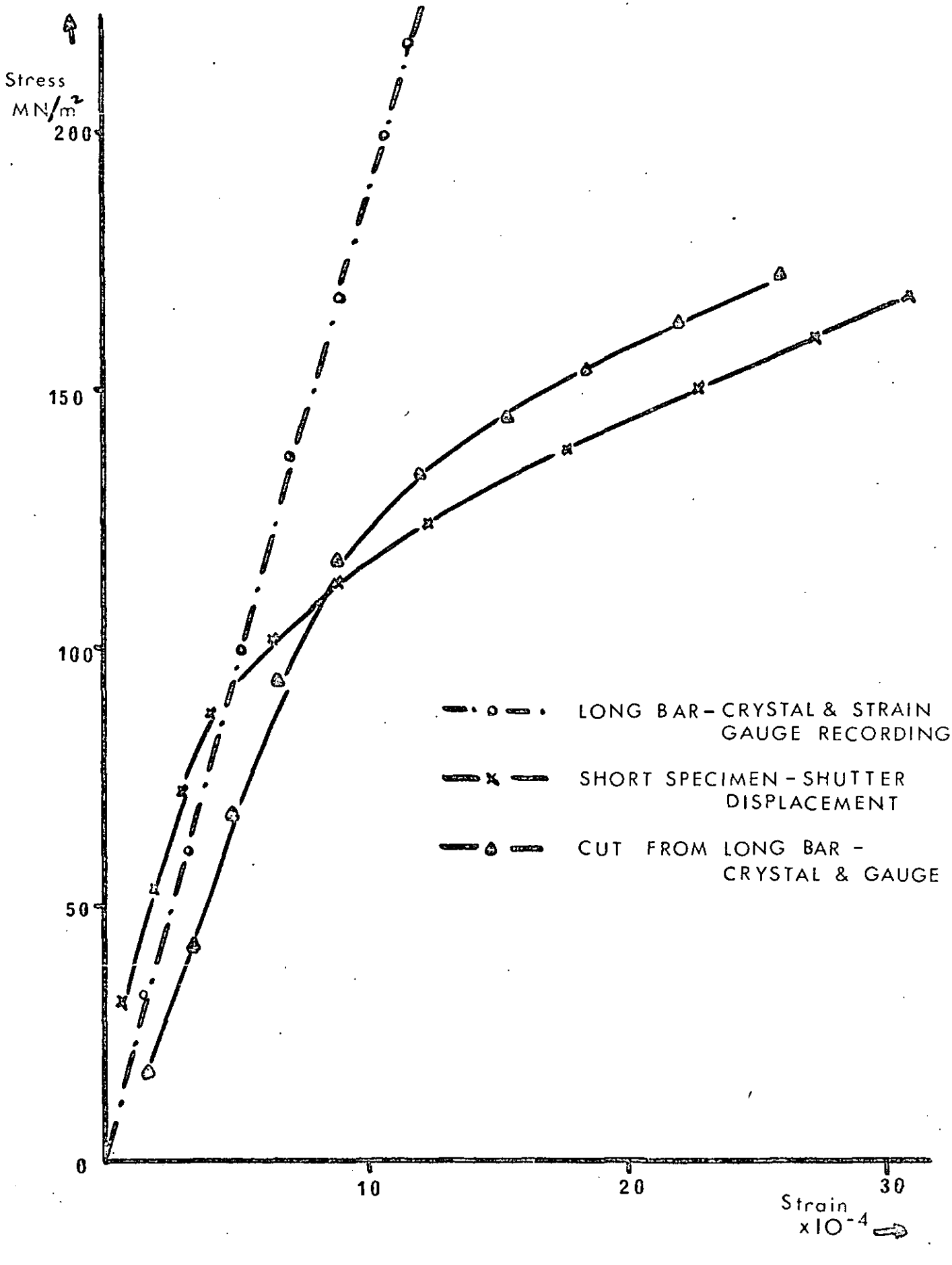

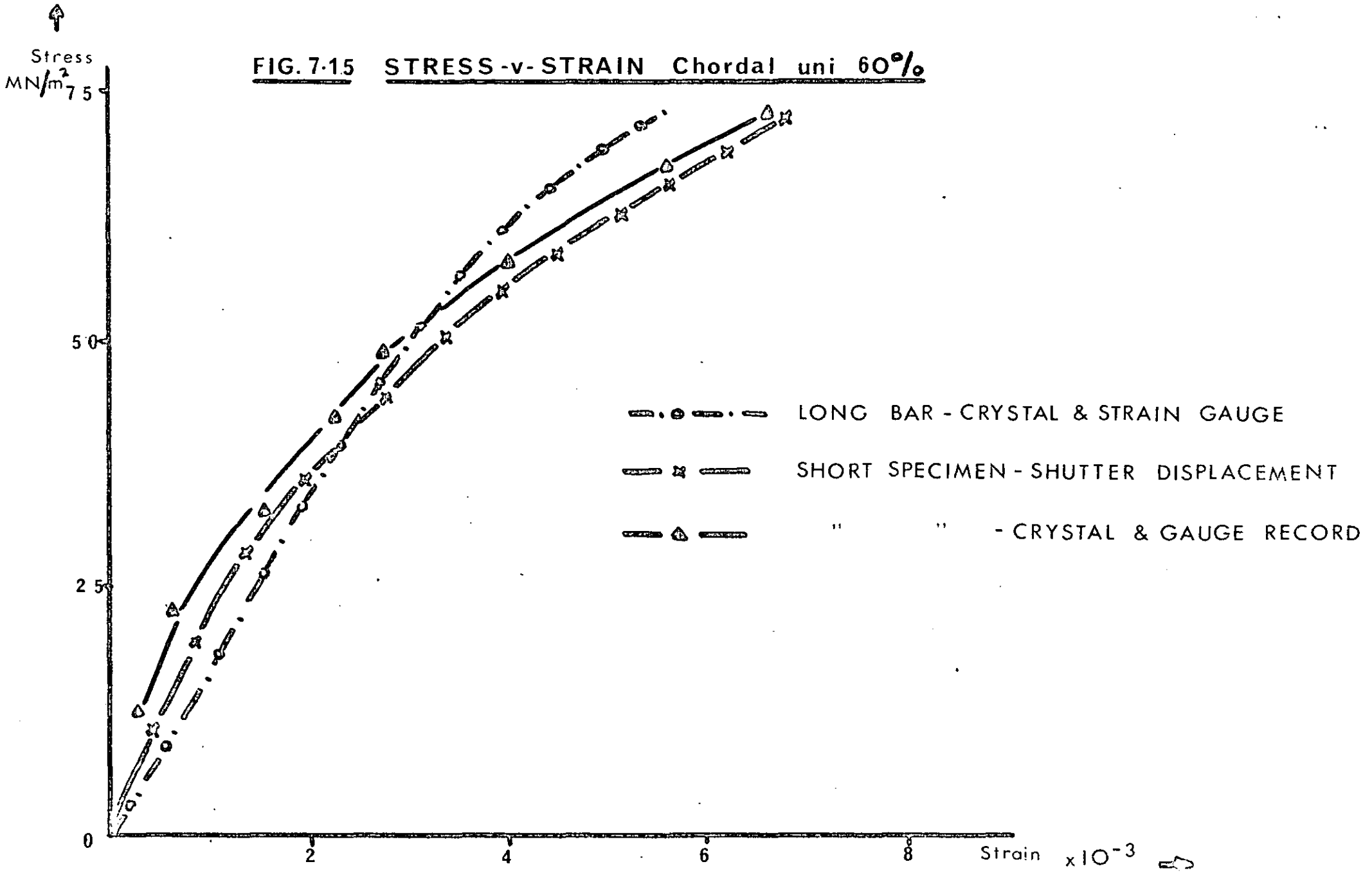

FIG. 7·15 STRESS-v-STRAIN Chordal uni 60%

quite rigidly held by the remainder of the continuous lengths of fibre on each side, whereas the fibres in the short specimen are not restrained at the endfaces of the specimen.

If the fibres move laterally as a result of resin flow within the short specimen during the stress loading, the longitudinal compression will be increased and an apparently greater strain response will be recorded by the shutter technique or the strain gauge on the specimen surface. Thus for the initial small strain, the fibres sustain most of the load until the relaxation effect of the viscous resin appears and the composite undergoes a larger strain. The specimen maintains its original shape, however, and no permanent flow of the resin occurs.

The lateral motion is significant after a number of reflections have traversed the specimen, that is after a particular strain level has been reached. A non-uniform three dimensional state of stress and strain may have arisen in the specimen. Usually, for isotropic materials, these three dimensional effects may be minimized by choosing the specimen geometry to allow for lateral inertia through a term involving Poisson's ratio. For fibre composites, however, it appears that the short specimen behaviour is not representative of the true one-dimensional behaviour. The region of the dynamic stress-strain relation showing a reduced modulus must be regarded as a misleading effect caused by the lateral flow or buckling in axial fibre specimens.

The problem of fibre buckling has always been of importance in compression testing of fibre composites. Under static conditions, the problem is reduced by using short specimens with a large cross-sectional area. End effects are then eliminated by measuring the stress-strain curve for a range of specimen lengths, and extrapolating the behaviour for zero end restraint. In a dynamic

test, this is not possible because of the very nature of the measurement involving inertial considerations and because of the complications introduced by successive reflections in the specimen.

Rosen (1964) has considered the fibre buckling effects under compressive loads in terms of an analytical model of a column on an elastic foundation. The buckling wavelength was found to be proportional to the fibre diameter.

No fibre buckling would be expected in the chordal fibre specimens, so that the behaviour of a short specimen should be identical with that of a long bar of material. Figure 7.15 shows this to be the case. A larger strain is recorded here for the short specimens because of the successive reflections within the specimen, and there is a correspondingly larger stress in the specimen. These reflections cause a build up of the stain loading in the specimen to a level greater than that undergone by the long bar of material, where no reflections are present during the stress-strain recording. In the long bar experiment, for both fibre direction types, the response is the material behaviour for a dynamic stress pulse and is not complicated by any reflections. No assumptions concerning elastic wave propagation are required, since the stress and strain are measured by direct electrical phenomena and the experimental results can be used directly to produce a dynamic stress-strain characteristic. Watson (1970) found that experiments on short and long specimens of Armco iron using strain gauges on the specimens and quartz crystal stress recording gave identical results which could be used in a strain rate dependent wave propagation treatment.

The short axial fibre specimens of lengths 0.5" and 0.25" at 60% V_f both gave similar stress-strain graphs. It was not possible to obtain measurements with axial fibre specimens of

a shorter length (say 0.125") because of difficulties encountered in machining and polishing such thin wafer-like specimens. An additional difficulty was that these thin axial fibre discs tended to break apart very easily during handling.

An optimum specimen length, somewhat less than 0.25", may provide a specimen response which is not distorted by a fibre buckling effect. However, consideration would have to be given to the lateral inertia of the specimen using the Davies and Hunter criterion, as well as any interface friction between the specimen and pressure bars.

CHAPTER 8 DISCUSSION OF RESULTS

8.1 GENERAL REMARKS

The dynamic behaviour of carbon fibre composites may be described in terms of the properties of each constituent or in terms of the bulk material response. It is the latter approach which is followed in this chapter.

In the pulse propagation experiments with axial fibre long bars, the wave speed was given by the static law of mixtures relation, whereas the stress-strain response over a small region of a long bar showed a behaviour which was rather different from the static material properties. On the other hand, the Hopkinson bar involved a three-dimensional situation with the fibre buckling or lateral motion producing a complex strain distribution within the short axial fibre specimen. A non-uniform strain distribution also occurred in the chordal fibre specimens due to the transverse anisotropy of this lay-up. Some care is necessary, then, in the interpretation of results from the split pressure bar.

The loading mechanism in the fibre direction under static conditions is for the fibres to carry the load while the matrix ensures equal distribution of the load throughout the material. During pulse propagation, however, the matrix may not have sufficient time to distribute the load. At the loading end of a bar of material the fibres will initially carry the load and the stress wave will start to travel along the fibres. There is then a fibre motion perpendicular to the loading direction at the matrix interface due to the Poisson's ratio coupling. Thus the matrix influences the pulse as the pulse proceeds along the fibre, and the net result of this coupling will be a retardation of the pulse group velocity due to the fibre properties along, because energy is being radiated from the fibres into the surrounding matrix. There can be no discontinuity in stress or particle velocity at the fibre-matrix interface, so that

wave becomes uniform over the composite cross-section in times corresponding to the propagation times across the fibre and matrix layers. A shear stress is produced at the interface during pulse propagation, and the size of this shear stress will depend on the nature of the bonding between the two constituents. The pulse speed is that speed appropriate to the average fibre content and the bulk response cannot be distinguished in terms of the separate components.

If there is an imperfect mechanical bond between the fibres and matrix, as is likely in a practical situation, then the interface coupling will be reduced and the fibres may act more independently of the surrounding matrix. In the extreme case of complete debond between fibre and matrix, in which there is no dimensional stability of the composite, the response would be separated into waves travelling along the fibres and matrix with no interaction. This situation may be approached at the temperature of 150°C, where the matrix influence will be reduced since its viscosity decreases, and the fibres will act more independently due to the reduced binding.

8.2 VOLUME FRACTION INFLUENCE ON RESPONSE

We now examine whether the axial fibre dynamic characteristics show a volume fraction dependence for the composite modulus.

In this analysis, the initial slope of the short specimen dynamic response was measured. These values are plotted in figure 8.1, which also shows the strains at which the response changed to a lower modulus. For all the axial unidirectional fibre specimens, this lower modulus was in the region 21-25 GN/m^2. The values given were obtained from at least four or five experiments with each specimen type, for which the stress-strain curves obtained from shutter displacement measurements were given in figure 4.1. The errors associated with the values were calculated from the experimental errors of the several observations.

For the two sets of parameters shown in figure 8.1 an empirical relation can be formed to express the initial modulus E_I and the strain ε_c at the change in modulus in terms of the fibre volume fraction V_f:

$$\left.\begin{aligned} E_I &= E_f\,(2V_f - 1/4) \\ \varepsilon_c &= 1.45(1 - V_f)\,\% \end{aligned}\right\} \text{over the range of } V_f \text{ used}$$

thus when $V_f \to 12.5\%$, $E_I \to 0$, which implies a critical fibre volume fraction under these dynamic conditions. These relations express the best straight lines through the respective points on the graph. No significant volume fraction dependence was seen for the secondary modulus and the stress at the change of modulus.

The empirical relations above indicate that the composite behaves with a much increased stiffness over the quasi-static behaviour. This increased response is characteristic of the rate dependence of the properties of a viscoelastic material. The fibres are generally considered to be elastic, however, so that an apparent viscoelastic effect may be caused by the geometric configuration

FIG. 8·1 Volume Fraction dependence of Axial uni dynamic response

VOLUME FRACTION	INITIAL MODULUS-GN/m²	SECONDARY MODULUS	AT CHANGE OF MODULUS STRESS MN/m²	STRAIN x 10^{-4}
60 %	182 ± 14	25 ± 5	98 ± 5	5·9 ± ·3
50 %	126 ± 11	24 ± 4	75 ± 15	7·5 ± ·4
38 %	103 ± 9	22 ± 5	91 ± 12	8·7 ± ·3
30 %	63 ± 4	21 ± 6	63 ± 6	10·4 ± ·4

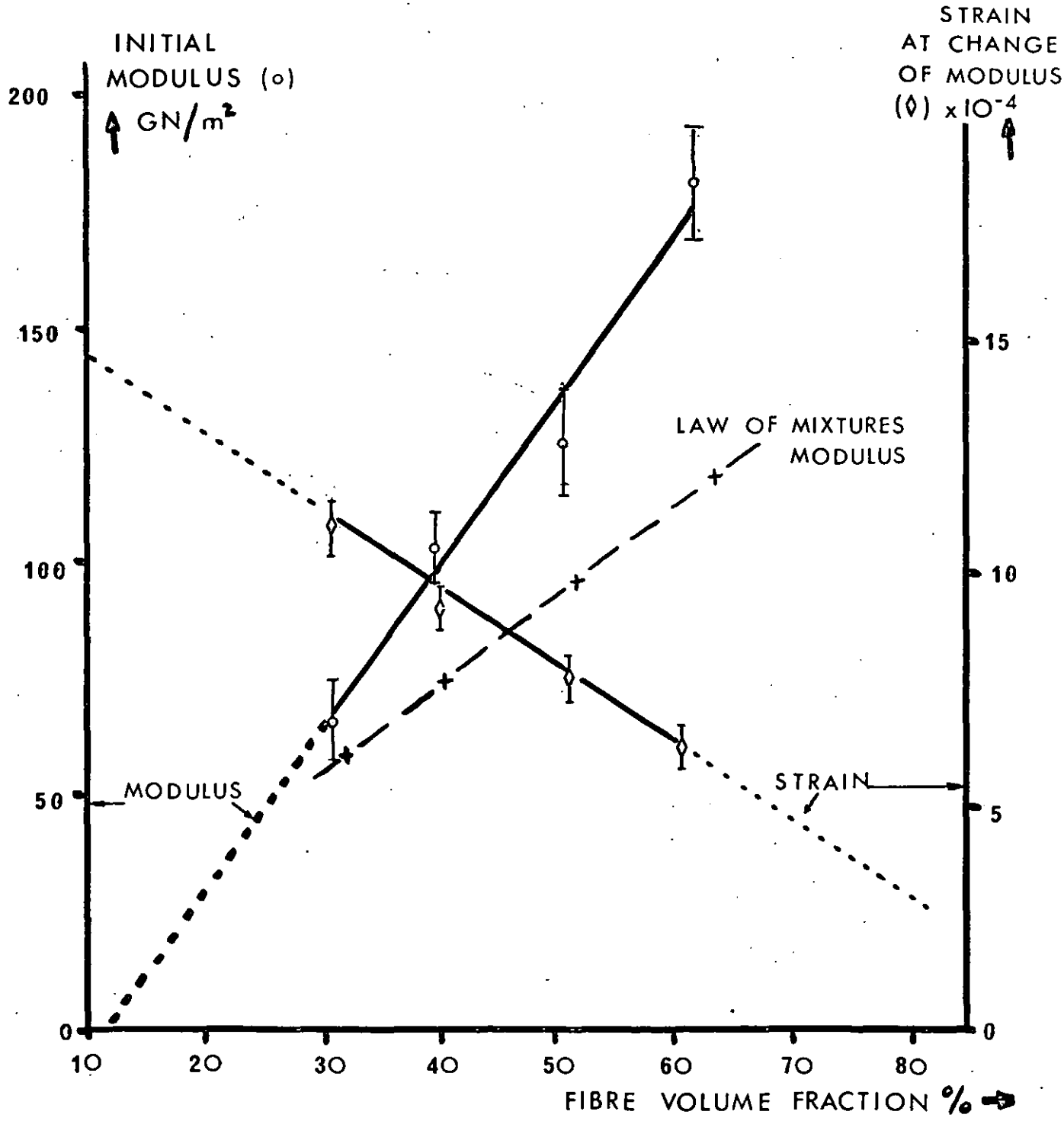

of fibres embedded in a matrix, or by the matrix properties themselves.

The static law of mixtures is derived by assuming equal longitudinal strains in the fibres and matrix under a condition of plane stress parallel to the fibres, and neglecting any interaction between the constituents. This relation is independent of fibre geometry and the fibre distribution. In the short specimens used for the split pressure bar, the experimental assumption was that the plane stress situation in the loading bar also produced a plane strain situation within the specimen. Thus an average stress-strain response may be determined for the duration of rapid stress loading. However, the lateral motion phenomenon in the axial fibre composites appears to invalidate this assumption because the material response is not then equivalent to a one-dimensional state of strain for later times in the loading duration.

8.3 VISCOELASTIC RESPONSE OF THE RESIN

It is well known that polymer systems in general show a viscoelastic behaviour - that is a time dependence is required in the constitutive relation for these materials. Both thermosetting and thermoplastic materials demonstrate viscoelastic behaviour under load, accompanied by internal friction losses especially when subjected to high frequency dynamic loading. The response may be characterised as linear for a limited frequency or time domain, but the major deficiency in the use of dynamic data over a short time such as in the Hopkinson bar arises because of the lack of an appropriate mechanical model. If a model were available which adequately described dynamic viscoelastic behaviour, the complex modulus could be determined in terms of the model parameters and thus the data from such tests as the Hopkinson bar could be used to demonstrate the validity of the model.

The HR4C matrix material used in the composites of present interest was a crosslinked epoxy resin. However, it was not possible to obtain any of this material in bulk form because of the difficulties involved in casting a void free test-piece and the difficulties of handling and curing in bulk a material which was designed to cure on a fibre surface as a relatively thin layer. The viscous and chemical properties of this thermosetting resin in bulk form thus precluded any attempt at producing specimens for use in the Hopkinson bar.

As an alternative epoxy resin system, an "araldite" commercial resin -CT200 - was used to provide some information on the behaviour of epoxies at high rates of loading. CT200 is a crosslinked, single phase, curing resin often used for photoelastic work, and readily available in bulk form. This material was considered to be reasonably similar in its macroscopic properties to the HR4C epoxy resin, so that

a comparison of the CT200 dynamic behaviour in the Hopkinson bar would indicate how epoxy resins behaved in general under high rates of loading. The term crosslinked as applied to these materials means that during the curing process, the long chain molecules of the epoxy have coupled into three dimensional networks through reactive sites (such as the epoxide group) to form the desired thermoset. This chemical coupling provides a mechanism for holding the long chain molecules together in the polymer.

Figure 8.2 shows the dynamic stress-strain results obtained for CT200, as well as an indication of the quasi-static behaviour. The static modulus at small strains was quoted as 3.5 GN/m^2. This value was confirmed by measuring the ultrasonic infinite medium velocity in a large cube of the material. These measurements were made at 5 MHz, as described in Chapter 5.

It is apparent from figure 8.2 that a considerable change in the mechanical behaviour has occurred between the quasistatic response and the dynamic response. The shutter displacement method was used for this experiment (specimen length 0.5") and no permanent deformation was observed. Ogorkiewicz (1973) has reported measurements on a cast Araldite-type epoxy resin which showed that short term loading (up to 15 mins.) produced a linear elastic deformation in compression and in tension. This response was shown to apply in the region of small strains, at least up to 10×10^{-3} strain.

FIG. 8·2 Stress-v-Strain Behaviour -CT 200 Epoxy resin

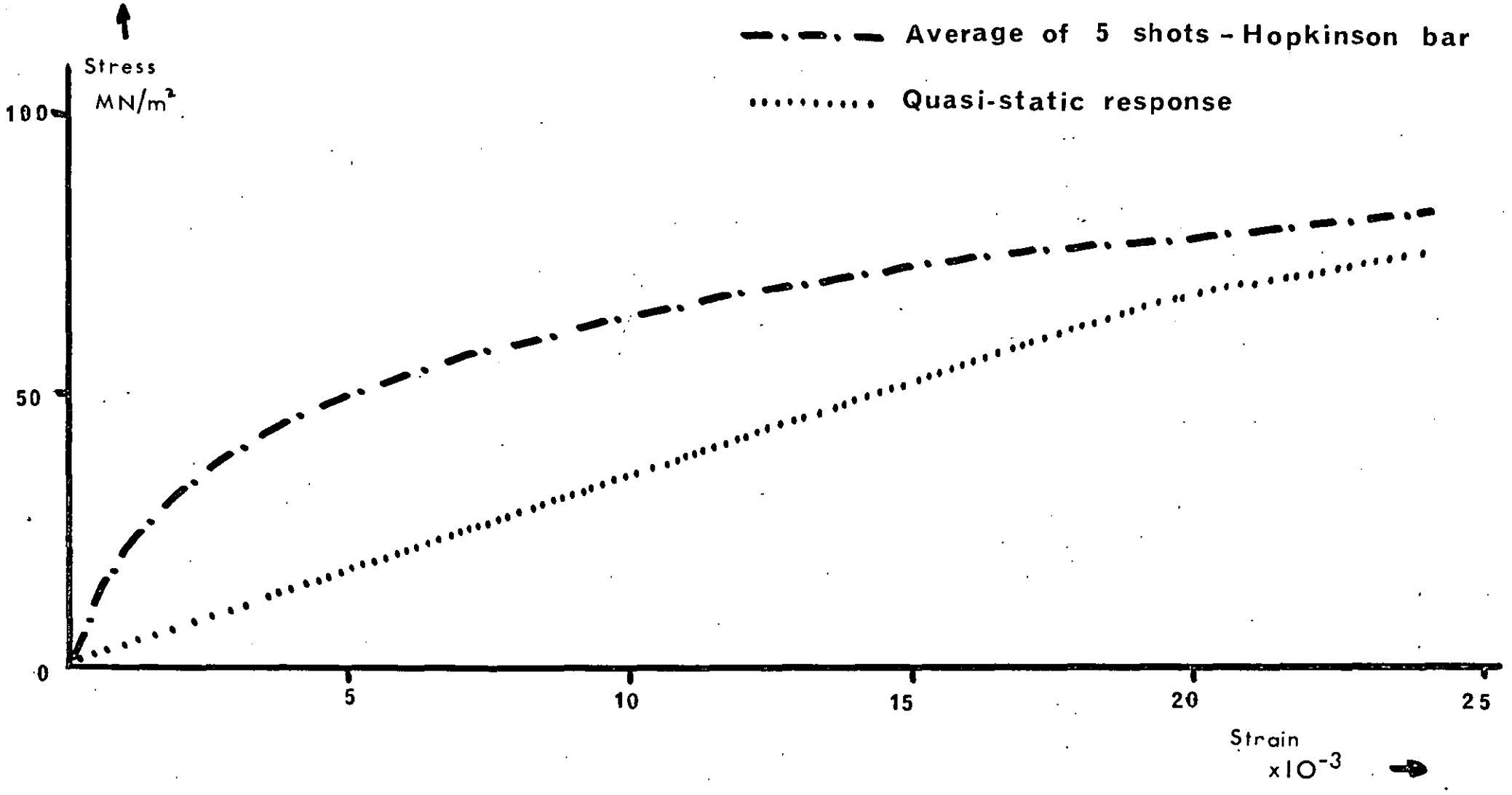

8.4 CROSSPLIED FIBRE SPECIMENS

The dynamic behaviour of the 0/90 crossplied specimens showed certain of the characteristics of both axial and chordal unidirectional types. The axial/chordal material (at 60% and 30% V_f) behaved in a similar manner to the axial unidirectional material, although little fibre buckling would have been possible in the 0/90 material since the axial layers were rigidly bounded by an adjacent chordal layer. The presence of a less marked 'secondary' modulus in the axial/chordal response tended to confirm this more rigid binding. The maximum stress levels reached in these specimens were a little lower than those in the unidirectional material. This arose because the acoustic impedances of the 0/90 specimens were less than the unidirectional material so that a large reflected pulse and a small transmitted pulse were produced in the experiment.

The chordal/chordal material response, however, involved a larger acoustic impedance than the unidirectional chordal material since a larger specimen stress was sustained, together with a slightly reduced maximum strain. Under static loading the chordal/chordal lay-up has been found to have a high compressive strength due to the stiffening effect of layers of material at right angles to the loading direction. For the chordal unidirectional material static loading has shown a relatively low compressive strength.

The 'initial' slope of the crossplied material response from the graphs shown in figure 4.3 indicated that both 60% and 30% axial/chordal types had an initial modulus of 70 GN/m^2 and both chordal/chordal types had an initial modulus of about 34 GN/m^2. Thus the volume fraction of fibres was not significant in the initial stages of the material behaviour, whereas at later times in the loading the 'secondary' moduli were rather different:

axial/chordal	60%	22 GN/m^2
axial/chordal	30%	15 "
chordal/chordal	60%	10 "
chordal/chordal	30%	4 "

The high velocity bullet loading pulse produced a stress-strain response in the axial/chordal material which was similar to the standard bullet loading.

Sayers and Harris (1973) have measured the interlaminar shear strength (ILS) of carbon fibre composites under impact conditions by recording the transient load in a drop-weight striker machine. The impact ILS strengths were about 70% of the static values for both unidirectional and crossplied material loaded across the fibres (i.e. in the "chordal" direction). There was a steady decrease in strength as the loading rate was increased. This result is contrary to the conventional rate dependence of strength in a viscoelastic material which would lead to higher strengths at greater rates. Sayers and Harris thought that non-uniform stresses on the initial cracking plane produced edge stresses which caused a premature failure. The plane loading condition used in the Hopkinson bar would not introduce these edge effects, so that the compressive dynamic behaviour of the present materials should provide a better measure of the rate dependence in these fibre composites.

8.5 MODEL REPRESENTATION

8.5.1 Memory function

Kolsky (1949) interpreted his results for various plastic and rubber specimens in terms of the Boltzmann Superposition Principle, in which the viscoelastic material behaviour was considered a function of the entire loading history. Thus when a specimen had undergone a number of deformations, the effect of each deformation was independent of the others, so that the behaviour could be calculated by adding the effects which would occur when the deformations took place singly.

Taylor (1946) had developed Boltzmann's original work by considering the small changes in strain which had occurred in the past history and summed the residual elements of stress produced by them. Between the times τ and $\tau + \delta\tau$, the strain changes from ε to $\varepsilon + \delta\varepsilon$, resulting in a change in stress $\delta\sigma$ which will relax in time. If the final value of stress at complete relaxation is $F(\delta\varepsilon)$, then at time t the residual stress is:

$$\delta\sigma = F(\delta\varepsilon) + f(t - \tau)\delta\varepsilon$$

where f is a memory function which $\to 0$ as $t \to \infty$.

The resultant stress is then:

$$\sigma = F(\varepsilon) + \int_{-\infty}^{t} f(t - \tau)\frac{\delta\varepsilon}{\delta\tau}\,.d\tau$$

No permanent strain remains, but there is a delayed recovery in the material.

Kolsky used a form $A \exp[-(t - \tau)/\alpha]$ for the function f; this supposed that the behaviour was equivalent to a three element system of two springs in series with a dashpot connected across one of the springs. (the "standard linear solid"). The springs obey Hooke's law and the dashpot obeys Newton's law of viscosity. The function $F(\varepsilon)$ can be reduced to the simple elastic form $E\varepsilon$, so that E is then the effective modulus of the two springs in series and

is the static modulus for strains which have taken place very slowly. Calculation of A and α for a particular experimental situation would indicate the viscoelastic nature of the response; (E + A) is the modulus for the spring which has no dashpot across it.

8.5.2 Static behaviour

A Mayers universal testing machine was used to measure the quasistatic response of the fibre composites. Specimens were machined to the size 1" x 0.5" x 0.5", with the fibres running along the largest dimension, and the samples were placed between the two flat steel plattens on this machine, which was operated by an electrohydraulic servo system. The axial and chordal fibre directions of the dynamic experiment were simulated by loading the static samples along and across the fibre direction.

A ramp compressive load was applied in a time of 60 - 90s; the maximum stress used was about 0.3 GN/m^2 at a strain rate of about $3 \times 10^{-3}\ s^{-1}$. The load was measured by a strain gauge load cell on the machine, with a read-out possible on an X-Y chart recorder. The cross head displacement, equivalent to specimen compression, was used as a feedback control and directly compared with the load command signal. The compression was measured by a linear voltage displacement transducer. In this way, a static load-displacement curve was obtained, and the static stress-strain response could be calculated. Measurements were taken for the axial 55% and chordal 60% composites up to specimen failure and these results are included in figures 8.3 and 8.4. The law of mixtures prediction for the axial direction is also shown in figure 8.3.

The problem of fibre buckling may have arisen in the axial fibre specimens because the sides of these specimens were unsupported in this experiment. Thus the experimental stress-strain curve lies somewhat below the law of mixtures prediction. It was important in

FIG. 8·3 Stress-v-Strain - Memory function

Axial uni 55%

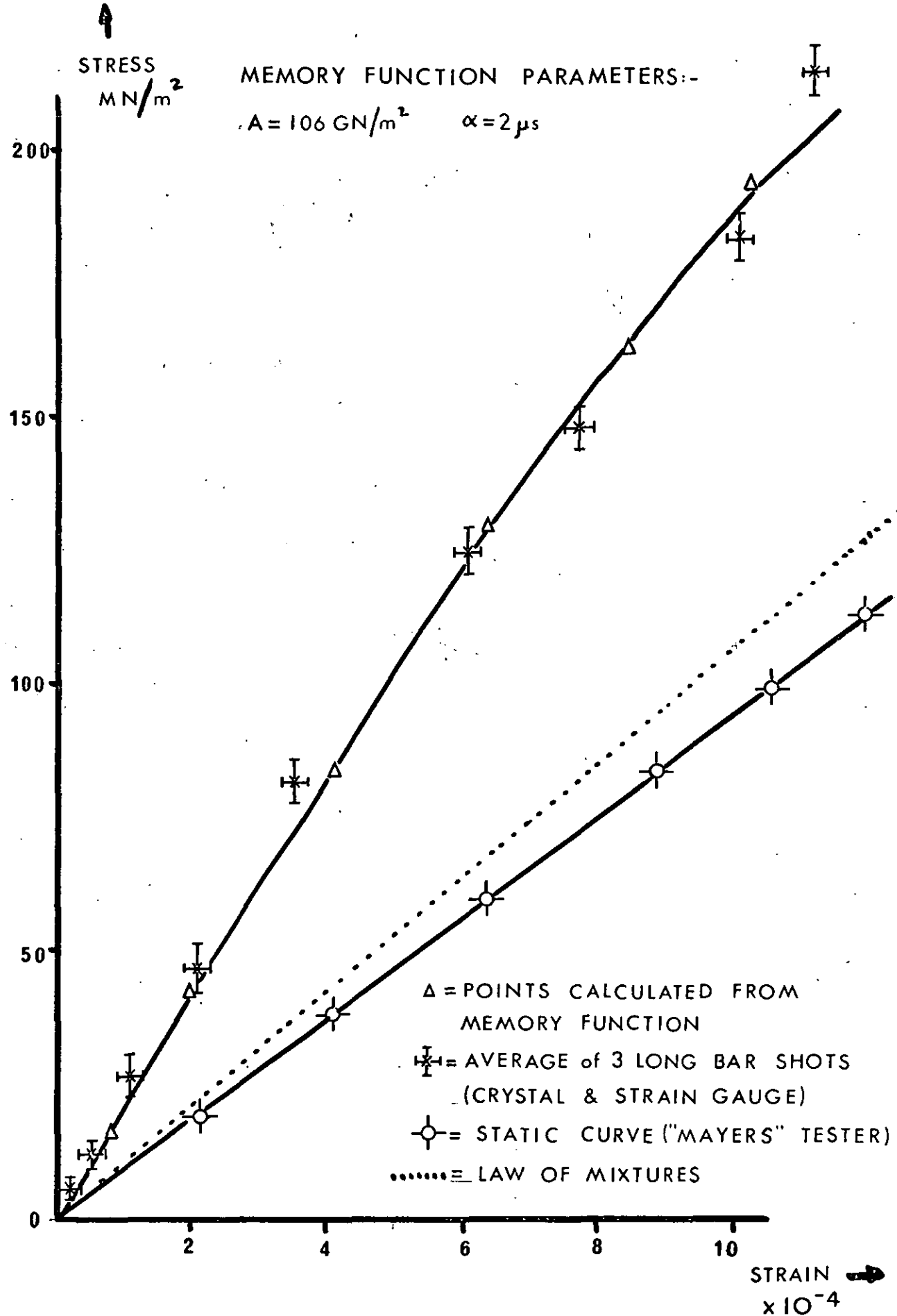

FIG. 8·4 Stress-v-Strain - Memory function

Chordal uni 60 %

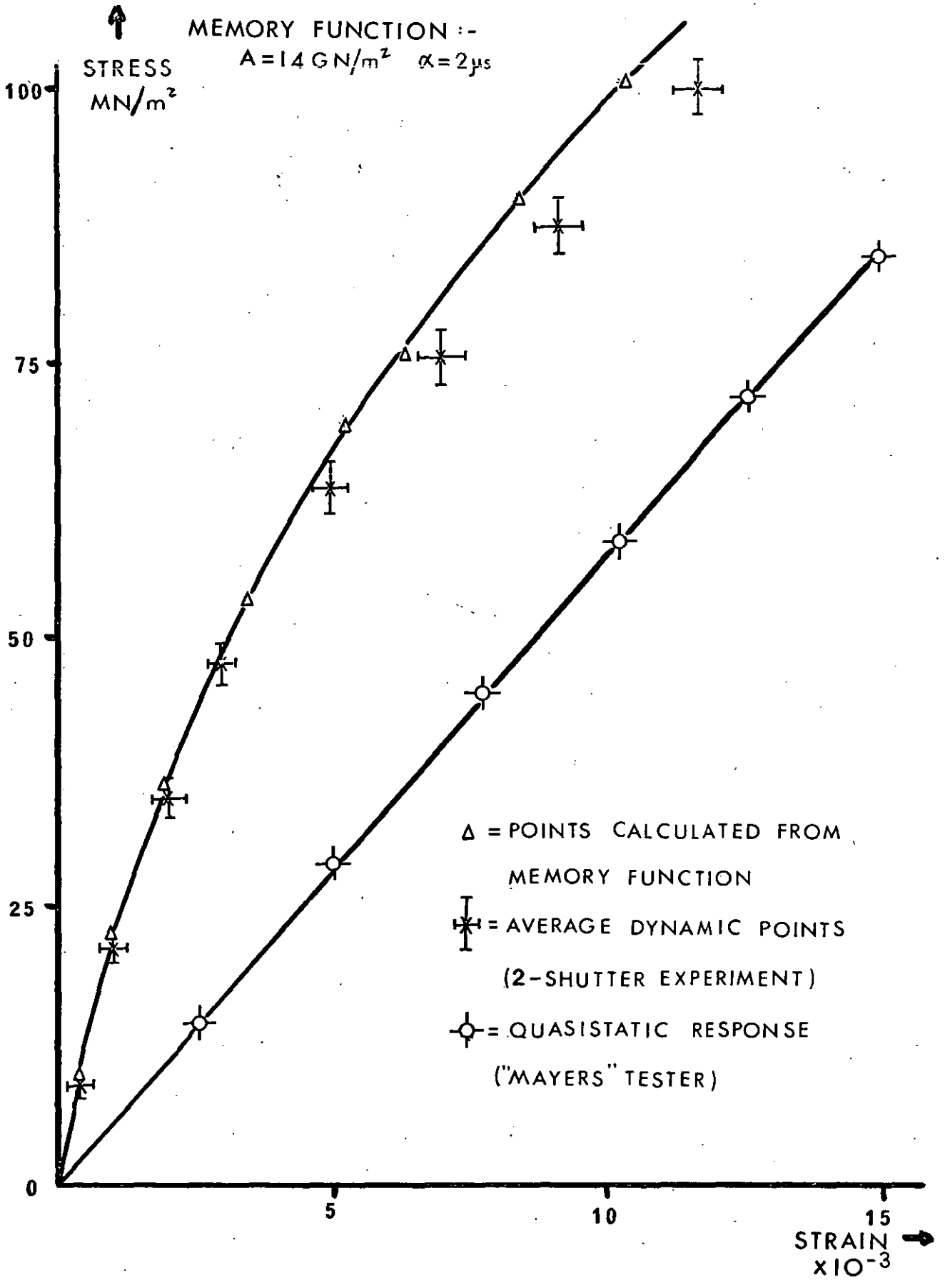

these experiments to ensure that the endfaces and loading surfaces were flat and parallel so that any non-uniform stress distribution was minimized.

8.5.3 Use of memory function

The memory function proposed by Kolsky was used as an empirical fit to the dynamic response of these fibre composites, and the results are shown in figures 8.3 and 8.4.

The form of the memory function is:

$$\sigma(t) = E\varepsilon(t) + A\left(\frac{d\varepsilon}{dt}\right)_k . \alpha . (1 - e^{-t/\alpha})$$

where the values of strain rate $(d\varepsilon/dt)_k$ are taken at the appropriate times from $\varepsilon(t)$ and the solution for $t < 0$ is neglected since it does not enter into the physical situation. When $t >> \alpha$, (the characteristic relaxation time) the stress-strain relation approximates to a linear form.

The procedure for calculating the memory function was to use the dynamic data for $\varepsilon(t)$ and $\sigma(t)$ to find the values of $(\sigma - E\varepsilon)$ and $(d\varepsilon/dt)_k$ at certain times t after the start of the loading. The maximum value of $A.\alpha.(d\varepsilon/dt)_k$ at long times was found from the (σ,ε) curve, and an estimated value of α was then used to calculate the exponential term in the memory function for all earlier times. The best fit obtained gave value of $\alpha = 2\mu s$ and $A = 106$ GN/m^2 for the axial 55% composite, and $\alpha = 6\mu s$ and $A = 14$ GN/m^2 for the chordal 60% composite. The axial fibre long bar dynamic stress-strain result was used for the axial composite, with the static modulus $E = 110$ GN/m^2. The chordal fibre composite static modulus was taken to be 6 GN/m^2.

From figures 8.3 and 8.4 it can be seen that the memory function does provide a reasonable fit to the experimental results. The two parameters A and α are important for this particular loading duration only, and the value of α was of the order of 10% of the

loading duration. This result was also obtained by Kolsky, who noted that although a single relaxation time gave some agreement with the experimental results, the complicated molecular structure of a polymer would involve a large number of different relaxation phenomena. Thus a more complicated memory function would be required to cover the whole spectrum of dynamic behaviour.

Kolsky (1953) describes the variation in propagation velocity with frequency for the standard linear solid. For these results it can be shown that at the frequency of 20 kHZ in the pressure pulse and for the axial fibre composite (α = 2μs), the wave speed is identical with $C_o = (E/\rho)^{\frac{1}{2}}$. Thus there is no dispersion under these conditions, and the wave speed may be predicted using the static law of mixtures modulus.

The standard linear solid model is shown in figure 8.5, together with the stress-strain relation for this model. The memory function and the relaxation time spectrum describe the mechanical behaviour of a linear system, in a very approximate and rather empirical manner. Physically, one could suppose that the instantaneous stress-strain response is time dependent, with contributions from the previous deformations adding to the current behaviour. These contributions decay with time, so that a short time after the dynamic loading the material has completely relaxed. The longitudinal wave speed then becomes an average value over all elements in the viscous response, and it is not possible to calculate the speed from the instantaneous slope of the dynamic stress-strain curve for these materials.

A single relaxation time will give good agreement over a limited time scale since any molecular processes associated with long times will not influence the mechanical behaviour, while processes with short relaxation times will appear as part of the instantaneous

FIG. 8·5 STANDARD LINEAR SOLID

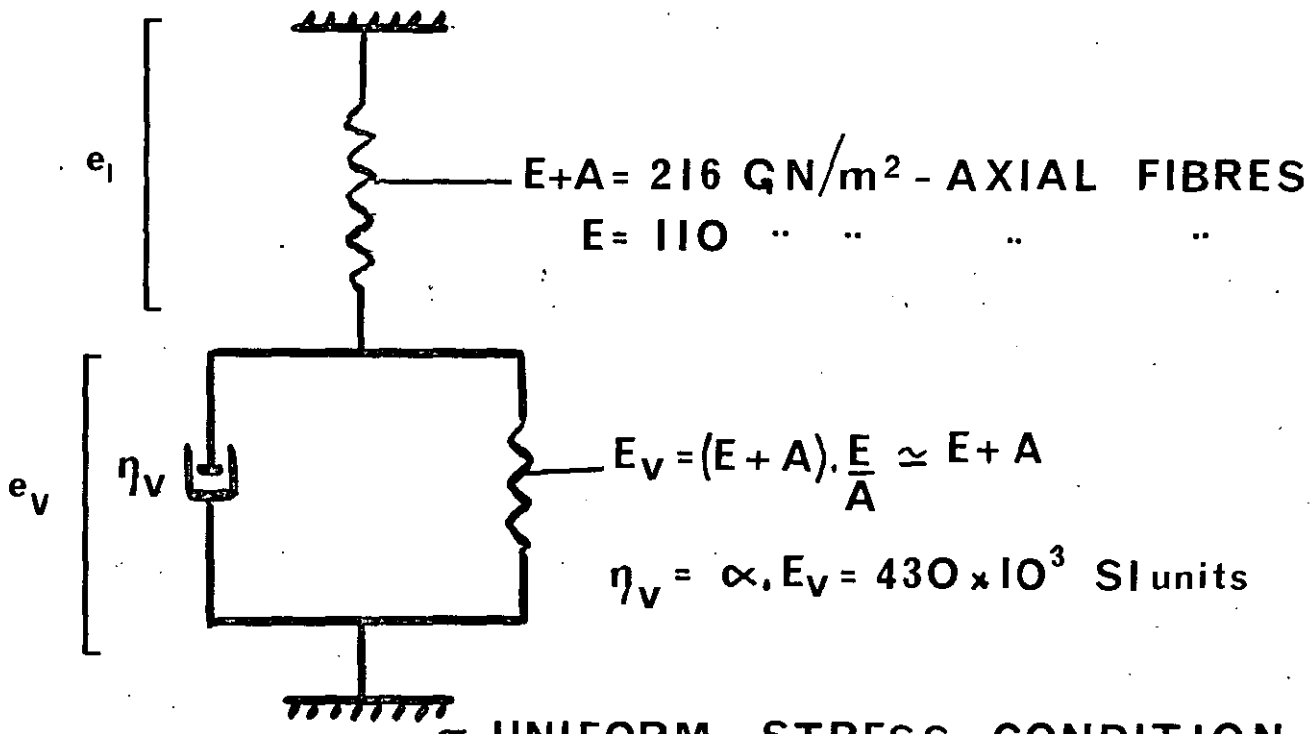

$$\sigma = (E+A).e_1 = E_v e_v + \eta_v \frac{de}{dt}_v \quad ; \quad e_1 + e_v = e$$

(σ : e) FORM -

$$(E+A+E_v).\sigma + \eta_v \frac{d\sigma}{dt} - \eta_v.(E+A) \frac{de}{dt} - (E+A).E_v . e = 0$$

STATIC MODULUS = E

$$\frac{1}{E} = \frac{1}{E_v} + \frac{1}{E+A}$$

response ($E\varepsilon$) and not as part of the memory function.

Strain rates used in the loading portion of the pulse were in the ranges 100 to 400 s^{-1} (axial fibres) and 150 to 550 s^{-1} (chordal fibres), and a strain rate dependence was assumed for these materials. The viscoelastic response of polymer systems has not yet been explained in terms of a physical model, although some theories are available which describe the strain rate dependence as an effect of the coiling and uncoiling of long chain molecules. These chain motions can be identified with the relaxation times of a viscous model; however, this is unlikely in the HR4C material since its cross-linked structure would prevent any large moledular movement between the crosslink sites.

Other work which is relevant to a viscoelastic analysis includes Tennyson, Ewert and Niranjan(1972) who considered the behaviour of bone samples under dynamic loading. Bone is known to be fibrous on a microscopic scale, but for the split pressure bar experiment the samples were taken to be transversely isotropic. A linear viscoelastic response was used to describe the dynamic behaviour with a Voigt model, and the elastic and viscous parameters were found to be strain rate dependent.

Lee and Morrison (1956) considered various viscoelastic models for longitudinal wave propagation; one conclusion was that the standard linear solid could be simplified as a Maxwell solid for short times after impact, and a Voigt solid for longer times.

Billington and Brissenden (1971 a) proposed an empirical relation for glass fibre composite behaviour in a Hopkinson bar experiment; the stress-strain response had a logarithmic form for strains less than a critical value, and then became linear for strains greater than this value. The form of this relation was similar in some respects to the memory function used above.

CHAPTER 9 CONCLUDING REMARKS

9.1 CONCLUSIONS FROM EXPERIMENTAL INVESTIGATIONS

In this work on carbon fibre composites the behaviour of the material at high rates of loading has been investigated and has been found to differ markedly from that measured under static loading conditions. The material properties which are of importance in determining the behaviour are:

(i) fibre orientation relative to the loading,

(ii) fibre volume fraction, particularly for axial fibre loading, and

(iii) the viscoelastic characteristics of the matrix material.

A strain rate dependent memory function may be used to describe the material response, and the fracture behaviour and dynamic response at elevated temperatures may be considered in qualitative terms as functions of the viscous properties of the matrix and the nature of the fibre-matrix interface.

The basic theoretical principles and experimental apparatus required in a study of stress wave behaviour in solid materials have been considered, and it has been shown that there are available many techniques for the measurement of dynamic behaviour. The Hopkinson pressure bar has been used extensively in this work since it is the only method to provide a plane stress situation which can be analysed to calculate the stress-strain response at a high rate of compressive loading. A number of limitations on the use of this method have been found. These limitations arise because of the anisotropic nature of fibre composites, which produces a non-uniform strain in the specimen.

An optical-shutter technique has been found to give a satisfactory measure of the particle displacement at each end of a short specimen, and certain other stress and strain measuring techniques have been used in special circumstances.

Wave velocity measurements in long bars of fibre composite have also been undertaken, and the relative value of these results in providing dynamic characteristics has been compared with the results of experiments with the Hopkinson pressure bar.

9.2 RECOMMENDATIONS FOR FUTURE WORK

It can be seen that this thesis forms the initial stage of a much larger project to determine the dynamic behaviour of fibre composite materials. Further developments on the split pressure bar experiment may be accomplished by replacing the bullet loading system with a variable impact velocity projectile, driven by a gas gun. The use of a projectile loading system would also extend the range and applicability of long bar experiments, provided that the measuring techniques and the theoretical analysis were suitable for such experimental work. The amplitude and duration of the stress pulse could then be varied over a larger range so that stain rate effects in the specimen would be more readily identified.

A direct impact device by means of flyer-plate missiles or shock wave loading on the specimen (in the form of a large rigidly clamped plate) would produce plane strain conditions in the centre of the specimen for short times after impact. Such a system would overcome the difficulties of fibre buckling and lateral inertia, since it would simulate an infinite medium condition in the initial stages. This type of plane strain experiment would be more appropriate for any determination of the stress wave response of the large plate-like structure of the RB211 fan blade, and would also provide more direct experimental data on the bulk material properties than the plane stress Hopkinson bar experiment.

Clearly thereneeds to be considerable work done on the theoretical interpretation of experimental data from high rates of loading studies. The resolution of the controversy over strain rate effects may be obtained only when a satisfactory model is available to describe the behaviour of those materials whose physical properties include plastic flow, delayed recovery and creep, viscoelasticity, dislocation movement and thermal effects. The separation of Hopkinson

bar data into strain rate sensitivity and lateral inertia effects also requires more analysis. A complete explanation of the dynamic behaviour of carbon fibre composites will require a mathematical model which involves the properties of the separate components and the fibre-matrix interface properties.

The problems of experimental and theoretical studies of non-linear and perhaps time-dependent material behaviour at high rates will cause controversy until an approach is available which brings together the experimental physicist, the applied mathematician and the materials scientist.

9.3 THE BIRD IMPACT PROBLEM

The work of this thesis arose from the problem of bird impact on the carbon fibre fan blades in the RB211 aero-engine. It is apparent that the features of stress wave propagation caused by a rapid impact loading are a function of the fibre and matrix properties and the rate of stress application. The design engineer, however, is more interested in the failure characteristics of his blade structure, and the fracture mechanisms are primarily determined by the fibre-matrix and interlaminar bonds. Interfacial shear between the fibres and matrix becomes important because of the different response of each component to the wave propagation. Reactions at the interface cause the faster travelling pulse in the fibre to be retarded to a speed appropriate to the average fibre content. Since the fibre-matrix bond is thought to be chemical in nature, a reduction of the failure mechanisms associated with interfacial shear may be obtained by changing the matrix properties to more closely resemble the fibre properties, or by treating the fibre surface chemically. (Although the feature of interfacial crack stopping may then be reduced). The viscoelastic material properties of the memory function at high rates of loading indicate that the matrix influences the composite behaviour much more than at quasi-static rates of loading.

REFERENCES

Achenbach & Herrmann (1968)
A.I.A.A. Journal Vol. 6 No. 10 p 1832

Aldridge & Lidington (1969)
"Ultrasonics for Industry" Conf. (London) p. 37

Alter & Curtis (1956)
J. App. Physics Vol. 27 p. 1079

American Soc. Metals. (1964)
"Fibre Composite Materials" Conf.

American Soc. Testing & Materials (1969)
"Interfaces in Composites" Conf. STP 452

Back & Campbell (1957)
"Properties of Materials at High Rates" Conf. p. 221

Barker (A.J.) (1971)
"Carbon Fibres, Composites & Applications" Conf. (London)

Barker (L.M.) (1971)
J. Composite Materials Vol. 5 p.140

Bell (1956)
J. Applied Physics Vol. 27 p. 1109

Bell (1966)
J. Mech. Phys. Solids Vol. 14 p. 309

Bell (1968)
"The Physics of large deformation in crystalline solids"
Pub: Springer-Verlag N.Y.

Berg & Rinsky (1971)
Fibre Science & Technology Vol. 3 p. 295

Billington & Brissenden (1971a)
J. Physics "D" - Applied Physics Vol. 4 p.272

Billington & Brissenden (1971b)
Int. J. Mech. Sci. Vol. 13 p. 531

Billington & Tate (1972)
Proc. Roy. Soc. (A) Vol. 327 p. 23

Campbell & Duby (1956)
Proc. Roy. Society (A) Vol. 236 p. 24

Campbell & Dowling (1970)
J. Mech. Phys. Solids Vol. 18 p. 43

Chiddister & Malvern (1963)
Experimental Mechanics Vol. 3 p. 81

Chiu & Neubert (1967)
J. Mech. Phys. Solids Vol. 15 p. 177

Chou & Wang (1970)
J. Composite Materials Vol. 4 p. 444

Chree (1889)
Tran. Cambridge Phil. Soc. Vol. 14 p. 250

Christensen, Swanson & Brown (1972)
Experimental Mechanics Vol. 12 p. 508

Conn (1965)
J. Mech. Phys, Solids Vol. 13 p. 311

Cook & Gordon (1964)
Proc. Roy. Soc. (A) Vol. 282 p. 508

Cristescu (1967)
"Dynamic Plasticity" Pub: North Holland

Cunningham & Goldsmith (1958)
Proc. Soc. Exp. Stress Analysis Vol. 16 (2) p. 153

Davies (R.M.) (1948)
Phil. Trans. Roy. Soc. (A) Vol. 240 p. 375

Davies (R,M.) (1956a)
"Surveys in Mechanics" p. 64 C.U.P.

Davies (R.M.) (1956b)
British J. of Applied Physics Vol. 7 p. 203

Davies (E.H.D.) & Hunter (1963)
J. Mech. Phys. Solids Vol. 11 p. 155

De Vault (1965)
J. Mech. Phys. Solids Vol. 13 p. 55

Dillon (1967)
J. Mech. Phys. Solids Vol. 15 p. 341

Dragnich & Calder (1973)
Experimental Mechanics Vol. 13 p. 199

Duffy, Campbell & Hawley (1971)
J. Applied Mech. Vol. 38 p. 83

Ensminger & Fyfe (1966)
J. Mech. Phys. Solids Vol. 14 p. 231

Goatham (1970)
Proc. Roy. Soc. (A) Vol. 319 p. 45

Griffith (1920)
Phil. Trans. Roy. Soc. (A) Vol. 221 p. 163

Hashin (1966)
A.I.A.A. Journal Vol. 4 p. 1411

Hashin & Rosen (1964)
J. Applied Mechanics Vol. 31 p. 223

Hauser, Simmons & Dorn (1961)
A.I.M.E. Conference, "Response of metals to High Velocity Deformation" p. 93

Hillier (1949)
Proc. Phys. Soc. (B) Vol. 62 p. 701

Hopkins (1963)
"Stress Waves in Anelastic Solids"
I.U.T.A.M. Symposium - Providence R.I.

Hopkinson (1914)
Phil. Trans. Roy. Soc. (A) Vol. 213 p. 437

Huffington (1965) ed.
A.S.M.E. Conference
"Behaviour of Materials under Dynamic Loading"

Hunter (1959)
Progress in Solid Mechanics Vol. 1. p.1

Jahsman (1971)
J. Applied Mechanics Vol. 38 p. 75

von Karman & Duwez (1950)
J. App. Phys. Vol 21 p.987

Karnes (1967) A.S.M.E. Conf. Mech. Behaviour p.270

Karnes & Ripperger (1966)
J. Mech. Phys. Solids Vol. 14 p. 75

Kelly (1967)
Contemporary Physics Vol. 8 p. 313

Knaus (1968)
J. Applied Mechanics Vol. 35 p. 1

Kolsky (1949)
Proc. Phys. Soc. (B) Vol. 62 p. 676

Kolsky (1953)
"Stress Waves in Solids" Pub: OUP

Kolsky (1960)
"Stress Wave Propagation in Materials" Conf.

Kolsky & Douch (1962)
J. Mech. Phys. Solids Vol. 10 p. 195

Krafft, Sullivan & Tipper (1954)
Proc. Royal Soc. (A) Vol. 221 p. 114

Lee & Morrison (1956)
J. Polymer Science Vol. 19 p. 93

Leknitskii (1963)
"Theory of Elasticity of an Anisotropic Body"
Pub: Holden-Day

Lindholm (1964)
J. Mech. Phys. Solids Vol. 12 p. 317

Lindholm & Yeakley (1965)
J. Mech. Phys. Solids Vol. 13 p. 41

Lindholm & Yeakley (1968)
Experimental Mechanics Vol. 8 p. 1

Love (1927)
"Mathematical theory of Elasticity" CUP

Mallinder (1970)
Polymer Age Vol. 1. p. 116

Malvern (1951)
J. Applied Mech. Vol. 18 p. 203

Manjoine & Nadai (1940)
A.S.T.M. Proc. Vol. 40 p. 822

Markham (1973)
AGARD Conference Proceedings No. 63

Mason (1958)
"Physical Acoustics & the properties of Solids"
Pub: Van Nostrand.

National Physical Laboratory Conf. (1971)
"The Properties of fibre Composites".

Nevill, Sierakowski, Ross & Jones (1972)
Experimental Mechanics Vol. 12 p. 278

Norris (1967)
Experimental Mechanics Vol. 7 p. 297

Ogorkiewicz (1973)
J. Strain Analysis Vol. 8 p. 132

Peck & Gurtman (1969)
J. Applied Mechanics. Vol. 36 p. 479

Percy & Meikle (1969)
"Science of Materials" Conf. (Auckland) p. 130

Phillips (1967)
RAE Technical Report 67088

Pochhammer (1876)
J. Reine Angew. Math. Vol. 81 p. 324

Rakhmatulin & Dem' Yanou (1966)
"Strength under high transient loads"
Pub: Oldbourne Press

Reed & Schuster (1970)
J. Composite Materials Vol. 4 p. 514

Reed & Munson (1972)
J. Composite Materials Vol. 6 p. 232

Ripperger & Watson (1968)
"Mechanical behaviour of materials under dynamic loads"
Conf. p. 294

Rosen (1964)
"Fibre Composite Materials" A.S.M. Conference

Sayers & Harris (1973)
J. Composite Materials Vol. 7 p.129

Schuster & Reed (1969)
J. Composite Materials Vol. 3 p. 562

Scop & Argon (1969)
J. Composite Materials Vol. 3 p. 30

Sharpe & Hoge (1972)
Experimental Mechanics Vol. 12 p. 570

Sierakowski, Nevill, Ross & Jones (1970)
A.I.A.A./A.S.M.E. Structures Conf. p. 164

Sternglass & Stuart (1953)
J. Applied Mech. Vol. 20 p. 427

Sun, Achenbach & Herrmann (1968)
J. Applied Mech. Vol. 35 p. 467

Tardiff & Marquis (1963)
Canadian J. Aero Space Vol. 9 p. 205

Tauchert & Moon (1970)
A.I.A.A./A.S.M.E. Structures Conf. p. 176

Tauchert & Guzelsu (1972)
J. Applied Mech. Vol. 39 p. 98

Taylor (1946)
J. Inst. Civil Engineers Vol. 26 p. 486

Tennyson, Ewert & Niranjan (1972)
Experimental Mechanics Vol. 12 p. 502

Tennyson, Zimcik & Tulk (1972)
Institute for Aerospace Studies, University of Toronto,
Report No. 159

Ting & Lee (1969)
J. Applied Mechanics Vol. 36 p. 1

Torvik (1970)
J. Composite Materials Vol. 4 p. 296

Tsai, Halpin & Pagano (1967) eds.
"Composite Materials Workshop" Pub: Technomic

Tsou & Chou (1969)
J. Composite Materials Vol. 3 p. 500

Tsou & Chou (1970)
J. Composite Materials Vol. 4 p. 526

Turner & Johnson (1969)
J. Applied Polymer Science Vol. 13 p. 2073

Voelker & Achenbach (1969)
J. Acoustical Soc. America Vol. 46 p. 1213

Wasley, Hoge & Cast (1969)
Rev. Sci. Inst. Vol. 40 p. 889

Watson (1970)
Int. J. of Solids & Structures Vol. 6 p. 1157

Whittier & Peck (1969)
J. Applied Mechanics Vol. 36 p. 485

Wright & Lyon (1957)
"Properties of Materials at High Rates" Conf.
(London - Inst. Mech. Engineers) p. 37